The University Of Sheffield.

DESIGN OF A NOVEL MICRO FEATURED POLY (GLYCEROL SEBACATE) METHACRYLATE (PGS-M) SCAFFOLD FOR CORNEAL REGENERATION

A thesis submitted in partial fulfilment of the requirements for the degree of Doctor of Philosophy

Iris Cristina Becerril Rodríguez

Department of Materials Science and Engineering

November 2020

ACKNOWLEDGMENTS

This has been a long road that has filled me with satisfaction and learning. Without a doubt, over and over again I would take this dream again.

I am grateful for the opportunity given to me and for all the support that I have received throughout these years.

I thank God, thus far He has helped me, illuminated my path, sustained me to this day and His love exceeds all my expectations.

I thank every person who was there to challenge me, to teach me, to support me, and to forge my character.

Mainly, I thank my advisors: Dr. Frederik Claeyssens, for his support at all times, his timely advice and for giving me the opportunity to work in his group. Every moment, I appreciate your patience and help on the path to being a researcher. To Dr. Ilida Ortega, for always being there and giving me her valuable advice and support.

I thank CONACyT and the Mexican government for their funding to support the completion of my PhD studies.

I especially thank each of my friends who were there to listen to me and share their dreams and projects, especially to Raji, Betül, Ana, and Valeria. You made this journey more enjoyable, and I learned so much through you. You have left a mark on my life and on my heart.

Agradezco a mi papá por su apoyo incondicional y por enseñarme a creer en mí, a ser perseverante y siempre esforzarme un poco más. A mi mamá por todo su cariño y por siempre creer en mis sueños por más locos o imposibles que parezcan y por haberme acompañado en cada uno de ellos, a mi hermano por su apoyo, sus palabras de aliento y por qué siempre ha creído en mí.

Y dedico esta tesis especialmente a mi compañero de viaje Ricardo

Quien bendice mi vida con su presencia, que trajo luz a cada día nublado y me ayudo a superar mis miedos. Amor mío gracias por tu apoyo y paciencia a cada momento, por tu sabio consejo y por estar junto a mi alcanzando cada estrella.

Este es apenas el comienzo…

No temeré aunque la tierra sea removida

por qué TÚ estarás conmigo

ABSTRACT

The cornea has limbal stem cells (LSC's) located in limbal crypts (niches). LSC's are responsible for corneal integrity, maintain a healthy equilibrium, and act as a proliferative barrier for the corneal epithelia, preventing invasion from the conjunctiva and its vascularization. Limbal stem cells deficiency (LSCD) causes this barrier to break down, leading to ingrowth from conjunctival cells and blood vessels. LSCD produce scar tissue, causing pain, blushing, and sometimes leading to blindness. Blindness is a worldwide problem which is caused by various conditions, such as blindness of the cornea. This is the 4th most common cause of loss of vision, with corneal defects impacting the lives of approximately 2 million people. Corneal transplants are the first proposed solution, though the risk of rejection and lack of donors make it an unsuitable option. Various strategies have been proposed to overcome the lack of donors and the rejection of allogeneic transplants.

Current treatments include the development cell carriers with biopolymers like collagen, fibrin, silk, fibronectin, and gelatin, among others. The cell carrier should be biocompatible and have the capacity to support both cell survival and proliferation to aid tissue regeneration. Despite the biocompatibility shown by biopolymers, some have presented acute inflammation and lacked the necessary mechanical properties for implantation and supporting tissue regeneration.

Recent research has been focused on the treatment of corneal defects with synthetic polymers, positioning them as an option for overcoming issues with biopolymers. Synthetic polymers have tuneable mechanical properties, but most are hydrophobic and lack of proper transparency.

Current reports of scaffolds have begun to include topography and microstructures that mimic the target tissue and influence cell behaviour. Numerous studies reported micro and nanostructures in the form of honeycombs,

microposts, grids, and parallel lines with promising results enhancing cell proliferation, migration, differentiation, and cell alignment. Later, Ortega et al. reported the creation of microenvironments to mimic the niches found in the corneal limbus, generating a new research area for the corneal replacements. The next challenge was the selection of a suitable synthetic polymer that met the necessary requirements for a corneal replacement, being able to achieve the characteristics found in the native cornea. Poly (glycerol sebacate) (PGS) was one of the polymers that stood out for its biocompatibility, transparency, elasticity, and biodegradability that resembled soft tissues, such as the cornea.

PGS was first reported by Wang et. al. in 2002 and has been used as scaffold and cell carrier due its characteristics as a conductive surface for cell adherence. In addition to being able to support cell growth, PGS is biocompatible, biodegradable, and has an elastomeric nature, making it highly suitable for soft tissue engineering. PGS has been used in biomedical applications as retinal graft, vascular tissue, cartilage, cardiac patch, nerve, and adhesive sutures.

However, PGS has rapid degradation rate *in vivo* and its crosslinking requires high temperatures and long processing times, which limit its application. Furthermore, PGS has some degree of cytotoxicity due to their non-reacted carboxylic acid groups from the sebacic acid.

To overcome these limitations, the production of photocurable PGS with the addition of acrylate groups was first proposed by Nijst et al. and Englemayr et al. This modification gives control over crosslinking process and provides more processing options. Nevertheless, acrylate groups are extremely reactive and unstable, making them susceptible to spontaneous crosslinking and producing a large amount of chlorine salts as resulting by-products, which require removal.

The addition of methacrylate groups as a different form to synthesize photocurable PGS was first reported by Singh et al. and Pashneh-Tala et al. in 2018. Methacrylate groups were added to the PGS molecule to give an additional

level of control of strength, degradation, crosslinking density, and elongation. These groups allow curing under UV light, avoiding the degradation of the polymer during heat crosslinking. Additionally, the reaction is more stable and cleaner in comparison to PGS acrylation. The addition of methacrylate groups is a new promising research area in the generation of a compatible tuneable biomaterial for application in cornea regeneration.

The main challenge was the development of an efficient carrier that delivers cells to specific sites and ensures their survival, mimicking the limbal stem cell niche structure, allowing the cell survival, and offering physical protection to stem cells. The research aim of this work is to develop a cell carrier that can re-establish the healthy balance in a damaged cornea with an anatomical structure that mimics the limbus to provide physical protection to the cells ensuring their survival. This cell carrier would be biocompatible, biodegradable, and with mechanical properties that match the target tissue. Additionally, the scaffold fabrication methodology should allow for the creation of precise microfeatures and dome shape that mimic both the morphology and curvature of native cornea. This scaffold is expected to produce more optimal results in survival and delivery of the stem cells in comparison to previous work.

In the current work, poly (glycerol sebacate) methacrylate (PGS-M) was synthesized with controlled conditions to obtain samples with different degrees of methacrylation (DM) (20-40%). Characterisation showed the DM with mechanical properties that better matched the native cornea and with the lower percentage of sol content was 40%. Through soft stereolithography, we achieved the development of a microfeatured dome shape scaffold that mimics the morphological characteristics of the cornea. We designed dome shape scaffolds with microfeatures (200 μm) and a reduced scaffold thickness (100 μm), which are much smaller and thinner than previously reported corneal substitute implants. This is the first time that a corneal substitute has achieved these

features, marking an important step towards the development of an artificial cornea replacement.

The biological evaluation of PGS-M scaffolds revealed problems with cell survival and proliferation using a variety of corneal cell lines, related with the scaffold composition. A series of physical, chemical, and biological modifications were proposed, which included extending the wash time to remove unreacted reagents, constant media changes during cell culture, modification of the substrate topography, immobilization of proteins, plasma coating, among others. However, no improvement in cell survival was observed with these changes.

We decided to combine crosslinking methodologies (heat and UV light) to assess whether there was a significant difference in the final scaffolds, based on the evidence that PGS is crosslinked with heat. We evaluated cell growth on scaffolds crosslinked with 1) heat, 2) UV, and 3) heat + UV (10, 20 and 30 seconds). Scaffolds with heat (120 ^{o}C/24 hours) + UV (30 seconds) considerably improved cell survival and proliferation, showing the formation of tissue (~10 layers of cells) after 14 days. ATR-FTIR analysis revealed a structural change in the PGS-M molecule crosslinked with heat + UV, resulting in a more crosslinked matrix. These results coincide with those previously reported regarding the cytotoxicity of PGS in matrices that were not completely cross-linked due to the COOH groups, acidifying the surrounding environment, and considerably affecting cell survival.

The results obtained in this work have not been previously reported. This data comprises the basis for future development of PGS-M scaffolds with better biocompatibility and mechanical properties close to the gold standard of a corneal scaffold.

TABLE OF CONTENTS

LIST OF FIGURES

Chapter 3

Chapter 5

Chapter 6

LIST OF TABLES

LIST OF EQUATIONS

Chapter 2

LIST OF ABBREVIATIONS

2D	Two dimensional	**DA**	Degree of acrylation
3D	Three dimensional	**DAPI**	4’,6-diamidino-2-phenylindole dihydrochloride
µl	Microlitres	**DCM**	Dichloromethane
µm	Micrometre	**DE**	Degree of esterification
ºC	Centigrade	**dH_2O**	Deionized water
ΔH_c	Enthalpy of crystallization	**DI**	Dispersity index
ΔH_m	Enthalpy of melting	**DM**	Degree of methacrylation
ADSC’s	Adipose-derived stem cells	**DMEM**	Dulbecco's Modified Eagle Media
ATR-FTIR	Attenuated total reflectance Fourier transform infrared spectroscopy	**DNA**	Deoxyribonucleic acid
BLCs	Bioengineered limbal crypts	**DRIE**	Deep reactive ion-etching
BSA	Bovine serum albumin	**DSC**	Differential scanning calorimetry
$CaCl_2$	Calcium chloride	**dsDNA**	Double-stranded DNA
CAD	Computer assisted design	**EBL**	Electron beam lithography
CDCl3	Deuterated chloroform	**ECM**	Extra cellular matrix
CLET	Cultured limbal epithelial transplantation	**EDTA**	Ethylenediaminetetraacetic acid
CO_2	Carbon dioxide	**EGF**	Epidermal growth factor
COOH	Carboxy	**FDA**	Food and Drug Administration
D#	Day number	**FITC**	Fluorescein isothiocyanate

GPC	Gel permeation chromatography	**MDF's**	Mouse dermal fibroblasts
H&E	Hematoxylin and Eosin	**MeHQ**	4-methoxyphenol
hAM	Human amniotic membrane	**mg**	Milligrams
HCE's	Human corneal epithelial cells	**ml**	Millilitres
HCl	Hydrochloric acid human	**mm**	Millimetre
hCSSC's	Human corneal stromal stem cells	**M_n**	Number average molecular weight
hDF's	Human dermal fibroblasts	**MPa**	Mega Pascals
hESC's	HUman embryonic stem cells	**mRPC's**	Murine retinal progenitor cells
HFF's	Human foreskin fibroblasts	**MSCs**	Mesenchymal stem cells
HIPEs	High internal phase emulsions	**MSC's**	Marrow stromal cells
hLEC's	Human limbal epithelial cells	**M_w**	Weight average molecular weight
HMDS	Hexamethyldisilazane	**N_2**	Nitrogen
hMSC's	Human mesenchymal stem cells	**NHS**	National Health Service
IMS	Industrial Methylated Spirit	**nm**	Nanometres
kPa	Kilo pascals	**NMR**	Nuclear magnetic resonance
LDH	Lactate dehydrogenase	**OH**	Hydroxy
LEC's	Limbal epithelial cells	**P**	P value
LESC's	Limbal epithelial stem cells	**P#**	Passage number
LSC's	Limbal stem cells	**PAA**	Polyacrylic acid
LSCD	Limbal stem cell deficiency	**PBS**	Phosphate buffer saline

PCL	Poly (ε-caprolactone)	**rLEC's**	Rabbit limbal epithelial cells
PDLLA	Poly- D , L - lactic acid	**rLF's**	Rabbit limbal fibroblasts
PDMS	Poly(dimethylsiloxane)	**SC's**	Stem cells
PED's	Persistent epithelial defects	**SD**	Standard deviation
PEGDA	Polyethylene glycol diacrylate	**SEM**	Scanning electron microscopy
PGS	Poly (glycol sebacate)	**SLA**	Soft stereolithography
PGSA	Poly (glycerol sebacate) acrylate	**SLET**	Simple limbal epithelial transplantation
PGS-M	Poly (glycerol sebacate) methacrylate	**SMC's**	Smooth muscle cells
pH	Potential of hydrogen	**T_{DI}**	Initial degradation temperature
PHEMA	Poly(2-hydroxyethyl methacrylate)	**T_{DP}**	Degradation temperature
PI	Photoinitiator	**T_c**	Recrystallization temperature
pLF's	Pig limbal fibroblasts	**T_g**	Glass transition temperature
PLGA	Poly (lactide-co-glycolide)	**TGA**	Thermogravimetric analysis
PLLA	Poly-L-lactic acid	**THF**	Tetrahydrofuran
PMAA	Poly(methacrylic acid)	**T_m**	Melting point
PMMA	Poly(methyl methacrylate)	**UTS**	Ultimate tensile strength
pPGS	Prepolymer poly (glycerol sebacate)	**UV**	Ultraviolet
PVA	Polyvinyl alcohol	**W**	Watts
RAFT	Real Architecture For 3D Tissue	**WHO**	World Health Organization
		W_i	Initial weight

W_d	Final weight		
W_s	Swollen weight		
(w/v)	Weight/volume		

DECLARATION

I confirm that the work presented here is completely mine.

CHAPTER 1. LITERATURE REVIEW

1.1 CLINICAL NEED

More than 10 million people are blind worldwide (according to the World Health Organization (WHO) [1]. Every year 7 million people go blind, and in total around 180 million people are blind or are visually disabled around the world. The main causes of blindness are cataracts, glaucoma, age-related macular degeneration, and corneal visual impairment. Inflammatory and infectious diseases wear down the corneal tissue, leading to the formation of scars and eventually loss of vision [2]. The loss of corneal function can be caused principally due to limbal stem cell deficiency (LSCD). LSCD can be triggered by illnesses such Aniridia or Steven Johnson´s syndrome, as well as thermal/chemical burns and radiation[3].

1.2 CORNEA

Corneal tissue plays an important role in vision (light transmission and light refraction). It is the outermost transparent and avascular central tissue [4]; its main function is eye's focusing and protecting the eye against UV radiation and bacteria [5] . The average thickness of the human cornea varies, with the centre and the periphery measuring ~500 μm and 750 μm, respectively [6].

The cornea is formed by six well-defined layers that are constituted in the following order (Figure 1.1):

1. Corneal epithelium (48 to 55 μm thickness)
   The external layer of the cornea is a squamous, stratified, and non-keratinized epithelial layer formed by 5 to 7 layers of epithelial cells. The tear film covers its surface, protects the corneal surface from physical, chemical, biological (bacterial) damage, which also softens the epithelium surface from micro-irregularities. It is formed by an outer layer of lipids, an

inner layer of water, and mucous membranes. The existence of cellular junctions makes it extremely impermeable and stable. The corneal epithelium is constantly repaired to preserve the corneal physiology. Homeostasis is fundamental to maintain ocular structural integrity, corneal transparency, and visual function [6,7].

2. Bowman's layer (10 to 12 µm thickness)
   It is a stiff extracellular collagenous membrane that limits the corneal epithelium. It contains the sub-basal nerves and helps the maintenance of the corneal shape [5,8,9].

3. Underlying stroma (480 to 510 µm thickness)
   Hydrated extracellular matrix, contributing to 90% of the corneal average thickness. It provides corneal integrity and consists primarily of collagen I with small amounts of collagen V. The collagen is a well-organized network and is responsible of corneal mechanical strength and transparency. It is also formed by proteoglycans that regulate hydration and keratocytes that maintain organization and function [7,10].

4. Dua's layer (about 15 µm thick)
   This layer is very resistant and impermeable to the air, standing up to 2 bar (200 kPa) of pressure [11].

5. Descemet's membrane (about 8 to 10 µm thick)
   A basement membrane for endothelial cells, its main constituent is collagen IV [12].

6. Corneal endothelial (about 5 µm thick) –

   This layer is formed by metabolically active cells that are in contact with the aqueous humour in the anterior chamber. The corneal transparency is maintained for its cells by moving the water out of the stroma [13,14].

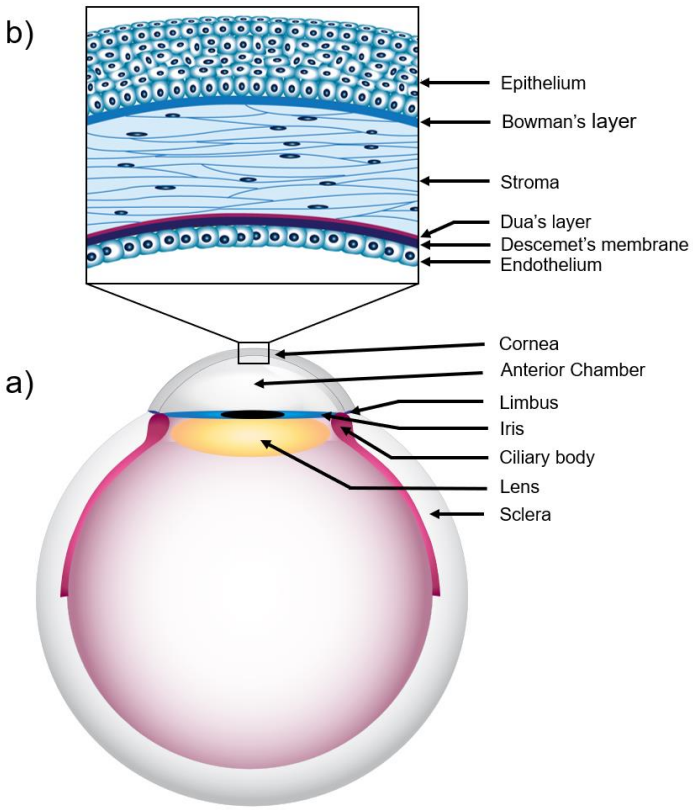

Figure 1.1 a) Sagittal plane of the eye b) Corneal layers.

1.3 LIMBAL STEM CELLS

Between the cornea and the sclera is the corneal limbus (1.5 µm wide) [13,15,16] . The cornea has limbal stem cells (LSC's) in niches in the limbus. LSC's maintain their self-renewal and are responsible for the corneal integrity and healthy balance, even after injury [17]. They act as a proliferative barrier between the corneal epithelia and the conjunctiva and its blood vessels (Figure 1.2) .

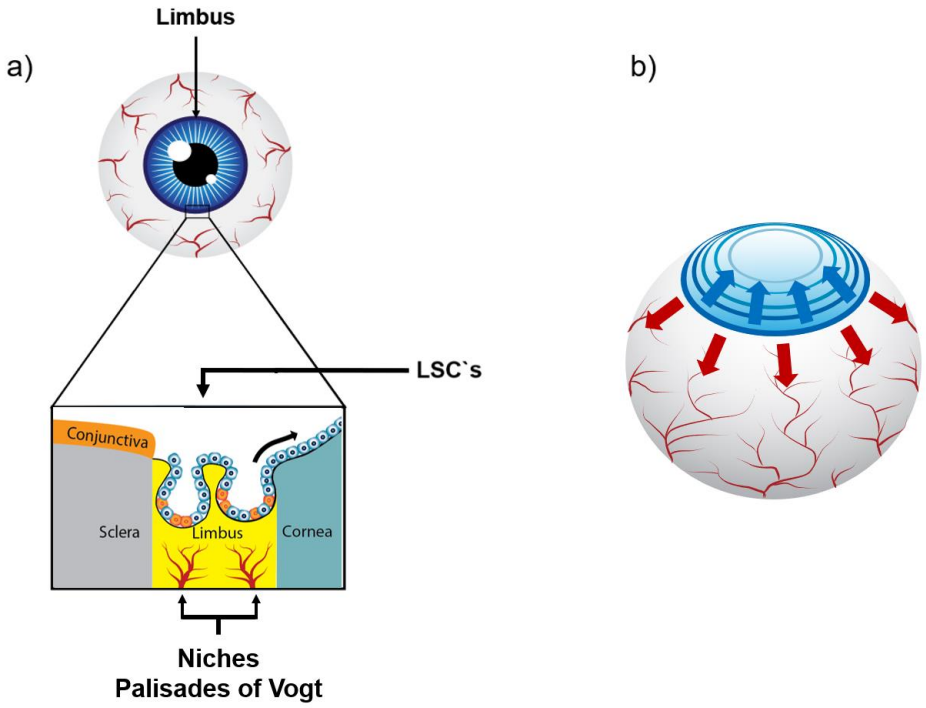

Figure 1.2 a) Corneal limbal stem cells (LSC's) in niches b) LSC's as a proliferative barrier between cornea and conjunctiva.

The main characteristics of LSC's are their behaviour as oligopotent stem cells, slow cell cycle, short S phase duration, high proliferative potential, proliferation free of genetic errors, high capacity of self-renewal by asymmetric division, poor differentiation, and small cell size (15.5 µm) [18]. Compared with differentiated cells, LSC's do not express the markers for terminal differentiation (cytokeratins 3 and 12, involucrin, and connexin 43) [13, 19–22].

The stem cells (SC's) located on corneal epithelium are in niches known as the Palisades of Vogt (with sizes between 120-150 µm) [23]. These are located in the limbus and are the repository of corneal epithelial stem cells [24]. The limbus is the transition zone between the conjunctiva and the cornea where transient amplification cells are produced, generating different epithelial cell groups of the cornea that undergo centripetal and vertical migration (Figure 1.3) [25].

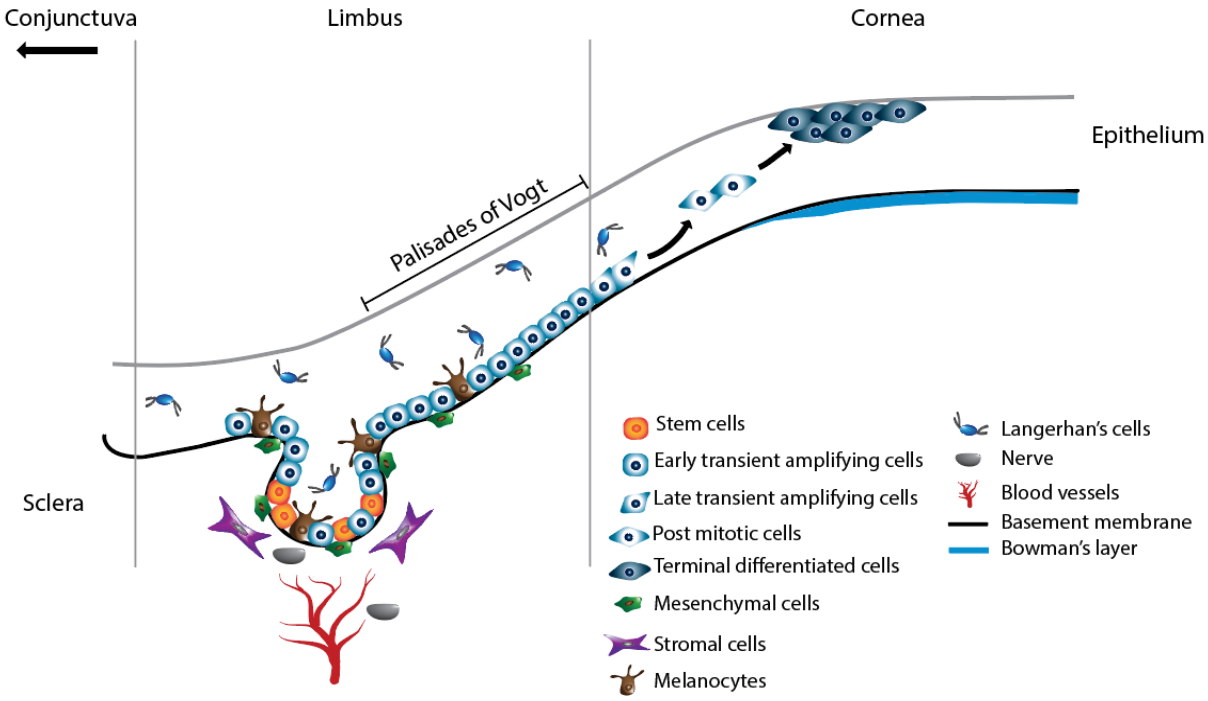

Figure 1.3 Limbus and Palisades of Vogt. It is an intermediate region between the cornea and the conjunctiva. LSC's centripetal-vertical migration and differentiation through the corneal epithelium.

The limbal basal epithelium is the only place where the limbal stem cells are located; this maintains the integrity and homeostasis of the corneal epithelium. The limbus is highly pigmented because of melanocytes [26,27]. The melanin pigmentation protects cells from potential damage by ultraviolet light and the subsequent generation of oxygen radicals [28]. In the limbus there are different cellular subpopulations: progenitors and amplifying cells (at different stages of differentiation), antigen-presenting melanocytes, and mesenchymal cells, vascular elements, and nerve endings that are part of the niche [13].

The niche is a special anatomically defined microenvironment with complex physicochemical and metabolic structural characteristics that provide physical protection for cells , from mechanical stress due to eye movement and intraocular

pressure and maintain the quiescence of SC's involved in corneal epithelial tissue homeostasis [23,29]. Other tissues with stem cell niches that can be found in the human body are: the hematopoietic stem niche in the bone marrow, the crypt of an intestinal villus, the rete ridges of the epidermis of the skin, the canals of Hering in the liver, and the bulge of the hair follicle, where stem cells are physically protected, surrounded by supporting mesenchymal cells [17].

As other epithelial surfaces, the corneal epithelium constantly loses cells from the surface [30]. The cells of the corneal epithelium are renewed every 7 - 10 days due to the differentiation of stem cells present in the limbus [7].

The maintenance and function of the LSC's are regulated by environmental factors like cell adhesion molecules, mesenchymal stem cells, blood capillaries, extracellular matrix components, and growth and survival factors secreted by stromal fibroblasts [31].

The basal limbus membrane is undulating with papillae, suggesting that epithelial stem cells of the limbus may interact closely with the cells in the subjacent limbal stroma. This means that limbal stem cells interact with unique extracellular components in the niche. The collagen chains in the limbal basement membrane could help to determine the SC's distribution in the niche (Figure 1.3) [20].

The limbus environment is very different from the rest of the cornea. The main difference is that the cornea is avascular, while the limbus has a blood supply which provides stem cell nutrition and growth factors [32]. Undulations in the Palisades of Vogt protect stem cells from the shear forces. These differences are important for the maintenance of the stem cell properties of the limbus and to protect them from external damage [16].

1.4 LIMBAL STEM CELL DEFICIENCY (LSCD)

The LSC's are a proliferative barrier between the epithelia of the cornea and the conjunctiva. Limbal stem cell deficiency (LSCD) causes this barrier to break down, allowing the migration of conjunctival cells towards the cornea. In turn, this causes vascularization of the region, producing scar tissue, ultimately leading to pain and blushing (Figure 1.4) [23].

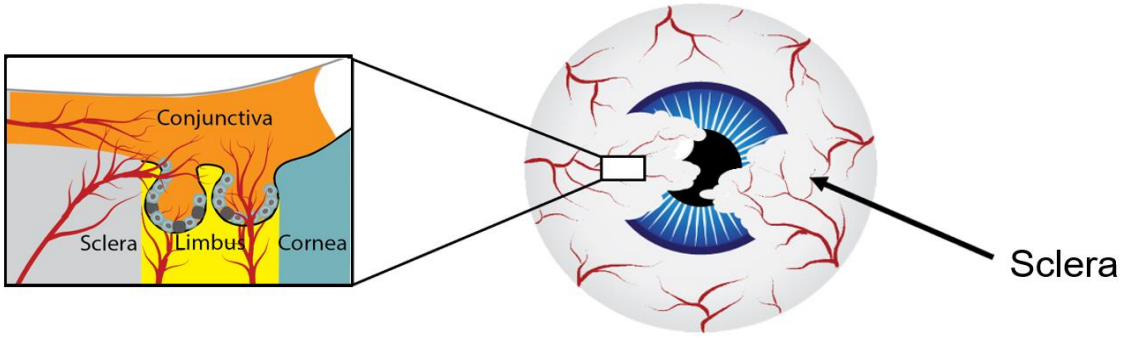

Figure. 1.4 Limbal stem cell deficiency (LSCD) causes corneal vascularization and conjuntivalization with loss of transparency.

Corneal injuries (trauma, infection, degeneration, immune disease) can lead to corneal stromal diseases and eventual tissue failure [33]. Opacity and corneal vascularization cause 10% of total blindness around the world each year [34].

1.4.1 CURRENT TREATMENT

Worldwide more than 10 million people are waiting for a corneal transplant. The lack of donors makes the development of corneal replacement overriding and urgent. Surgical techniques and different procedures have been developed for decades with the aim of regenerating damaged cornea replacing different tissue layers or the complete cornea [35–37] (Figure 1.5).

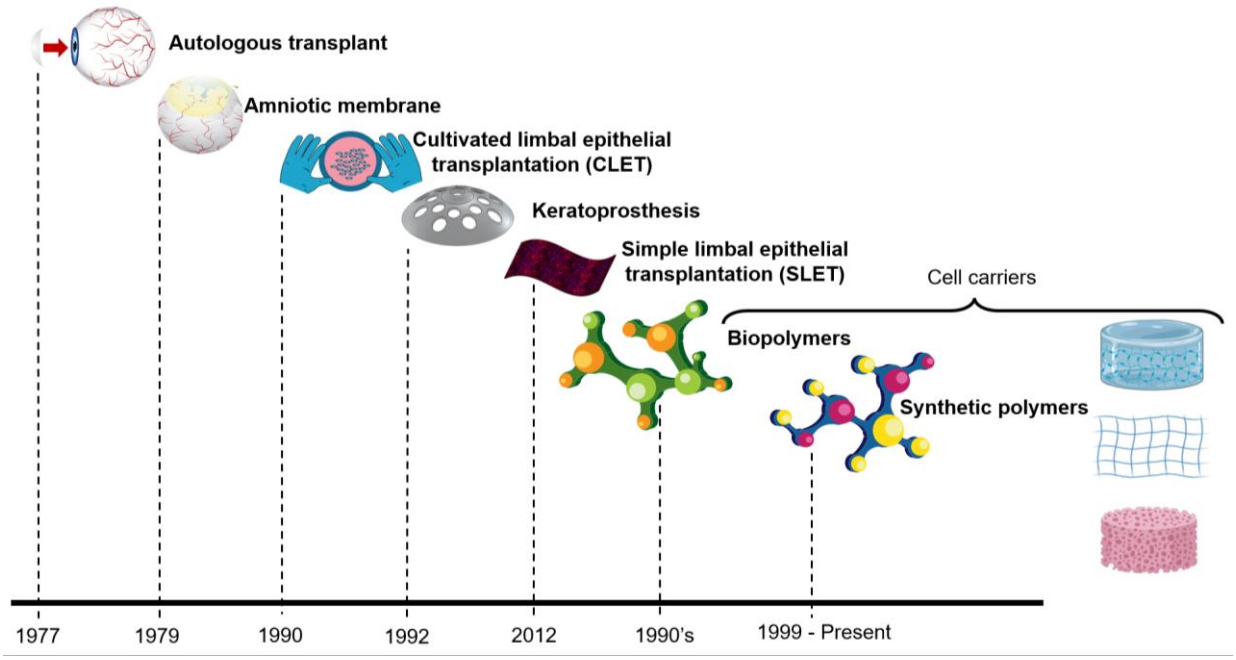

Figure 1.5 Development timeline of techniques for corneal regeneration.

Current studies have explored the development of materials with natural, synthetic polymers and the blend of both. However, mimic the well organize corneal tissue and its characteristic is still a challenge.

The optimal corneal replacement should be biocompatible, biodegradable, with optical, mechanical, and topographical properties that mimic the native cornea.

The treatment most widely used has been the corneal transplantation from allogeneic donors. The major disadvantages of this treatment lie in the biocompatibility with the host tissue and the adverse effects after implantation and tissue rejection [38]. Therefore, other treatment alternatives have been developed, being the most innovative the development of cell carriers. Natural and synthetic polymers have been outstanding in their use as cell carriers. Synthetic polymers have advantage due to their tuneable mechanical and chemical properties, offering an area of opportunity in the search for a better treatment for LSCD.

The gold standard for a full thickness corneal substitute (endothelial, epithelial and stromal layers) would be a biocompatible, biodegradable substrate, capable of mimicking the properties of soft tissue such as cornea, but mechanically capable of supporting tissue regeneration, and stable in physiological conditions [39].

Table 1.1 shows the comparison of the advantages and disadvantages in the treatments that are currently used for the limbal stem cell deficiency (LSCD).

Table 1.1 Current treatments for stem cell deficiency.

Treatments		Advantages	Disadvantages	Reference
Transplants	Cornea	- Rapid adhesion	- Donor dependent - Depend on the quality of the graft - Biocompatibility - Extensive serological screening - Success rate less than 35% - Rejection time ~24 months after implantation	[40–42]
Cultured limbal epithelial transplantation (CLET)		- A small sample of tissue is necessary - It is possible to carry out a self-explant	- The expansion of the stem cells obtained by biopsy is difficult - Risk of immune compatibility due to the presence of animal	[14,19,34,43–45]

	- It is possible to perform a biopsy of the tissue of the patient's oral mucosa	elements (used for the expansion) - Offers short-term effective results, but long-term results are inconsistent	
Keratoprosthesis		- Invasive method because debridement of the corneal connective tissue is required - Risk of infection or extrusion of the device - Can cause inflammation and glaucoma	[46]
Simple limbal epithelial transplantation (SLET)	- Rapid adhesion, does not require preparation and standardization of membranes,	- Possibility of detachment from the ocular surface in the	[47,48]

		Does not require sutures	early period after surgery	
Cell carriers	Human amniotic membrane (hAM) Degradation1 month after surgery	- Preserves the stemness of cells - Anti-inflammatory and antimicrobial properties - Disintegrates within 1 month after surgery - Provides growth factors and cytokines - Stimulates cell growth - Anti-inflammatory and anti-angiogenic properties - Correct elasticity	- Low availability - Structural variations - Inconsistent treatment effectiveness - Biocompatibility/ infections - Transmission of viral diseases - Biological variability - Success rate less than 45% - Can fail after 3-5 years - Limited transparency - Variable quality - Difficult storage and processing	[45,49,50]

		- Risk of disease transmission - Limited mechanical strength - Poor standardization	
Decellularized cornea	- Better biocompatibility compared with corneal transplant - Scaffold identical to original tissue	- Donor variability - If decellularization is incomplete a graft rejection could occur - Biocompatibility can be compromised depending on the origin of the tissue (human, porcine, bovine)	
Collagen based substrate	- Constitutes ≈70% of the dry weight of the cornea - Facilitates cell adhesion and proliferation - Biodegradable - Bioabsorbable	- Expensive - Variability (crosslink density, fibre size, trace impurities)	51–54

		- Biocompatible - Haemostatic	- Poor mechanical properties (Young's modulus ≈95–370 Pa) - Hydrophobicity - Variable degradation rate - Loses volume and shrinks when cells are seeded on the scaffold - Quickly degraded - Variable degradation rate	
	Silk fibrin	- Transparent - Good cell adhesion - Permeable and strong - High Young's modulus (6–8 GPa) - Flexible - No immune rejection	- Brittle - Some degree of cytotoxicity due to sericin (protein contained in silk)	[9,55–59]

Fibrin/ Fibronectin Slow degradation kinetics	- Facilitates cell adhesion and proliferation - Proper transparency - Bioabsorbable - Easy manipulation - Good mechanical strength - Elastic - Biodegradable - The possibility of viral transmission and prion infection is greatly reduced - Inexpensive	- Corneal inflammation- affects wound healing process - Acts as physical barrier delaying cell migration - Possibility of immune response - Risk of disease transmission - Gel shrinkage happen during the formation of flat sheets - Low mechanical stiffness - Rapid degradation before the proper formation of tissue engineered structures - Poor physical properties - Low mechanical strength - Rapid degradation rates	60–62

	Gelatin	- Biocompatibility - Inexpensive - Transparent - Permeable - Favourable mechanical properties	- Unstable above 37 ^{o} C - High degradation rate	[63–66]
	Chitosan	- Biocompatible - Anti-inflammatory properties - Biodegradable - Antimicrobial	- Poor mechanical properties - High degradation rate - Molecule with high degree of acidic groups	[67,68]
	Alginate	- Biocompatible	- Lack of cell adhesion - Poor mechanical properties - Unstable - Lack of binding sites	[9]
	Hyaluronic acid	- Part of extra cellular matrix (ECM)	- Can lead to lymphangiogenesis (lymphatic vessel	[69,70]

		- Regulates cell adhesion and motility - Mediates cell proliferation and differentiation - Modulates inflammation, - Stimulates angiogenesis	development) in the limbus, reducing transparency and visual acuity	
	Synthetic polymers	- Tuneable characteristics - Good transparency - High mechanical strength - Permeable - Flexible - Biocompatibility - Easy to use - Controlled shape and pore size	- In current polymers, lack of good degradability and limited elasticity	[9,48]

1.4.2 CURRENT SYNTHETIC POLYMERS USED FOR CORNEA REGENERATION

The development of biomaterials for corneal regeneration has been widely explored with synthetic polymers being used for the treatment of corneal defects. However, the current polymers have a lack of adequate transparency, biodegradability, and limited elasticity, making them unable to completely mimic the structure of the native cornea with its microfeatures.

Currently, there are no full thickness artificial corneas created by tissue engineering. The main challenge remains in the development of a biomaterial that mimics the native corneal structure with in-built artificial stem cell niches. The scaffolds should have the curvature (dome shape), architecture, transparency, and stiffness to ensure cell survival, proliferation, migration, and lead the regeneration of damaged tissue [71]. Therefore, the development of materials that mimic the microenvironment in the native cornea (known as microfeatured biomaterials) is an area of opportunity.

Table 1.2 shows in chronological order, from the oldest to the newest, the description of polymers that have been used as cell carriers in cell transplantation for damaged cornea regeneration, and the comparison between their advantages and disadvantage

Table 1.2 Polymer carriers in cell transplantation for corneal regeneration.

Polymer	Description	Advantages	Disadvantages	Reference
Poly(methyl methacrylate) PMMA contact lenses	A keratoprosthesis model based on a porous contact lenses Use: 20 – 34 years Tested on humans	- Transparent polymer - Mechanically stable	- Long term success is limited - Formation of erosive tissue, necrosis, leakage of aqueous humor, epithelization, infection, and extrusion of implant - Long term users present irregular corneal endothelium	[72,73]
Poly(dimethylsiloxane) (PDMS) contact lenses	Contact lenses that simplify the cell transplant application	- Promote cell attachment and growth in vitro - Nontoxic - High oxygen permeability	- Cause discomfort and excessive ocular deposits - Lead to reduced visual acuity - Mechanically weak	[74,75]

	~65% corneal epithelization was covered after 4 days. *In vitro* pig model	- Micropatterned (topography) - Highly transparent		
Poly(2-hydroxyethyl methacrylate) (PHEMA) /collagen hydrogels	PHEMA gels Keratoprosthesis or artificial cornea. Allow cellular invasion (in rabbits) – 6 months *In vivo* rabbit model	- Support corneal wound healing in animal models - Biocompatible	- Some scarring - Neovascularization - Calcium deposits	76
Poly- D , L - lactic acid (PDLLA)	Colourless and transparent membrane Evaluation of membrane: after 11 days	- Bioresorbable polymer	- Low hydrophilicity - Deposition of lactic acid - Degradation products acidify the surroundings	77

	In vivo rabbit model		(pH is unfavourable for cell proliferation and causes inflammation) - Neovascularization - Corneal ulceration - High amount of corneal epithelial defects - Conjunctival congestion - Mechanically stable	
(PDLLA/ Collagen)	Evaluation of membrane: after 11 days *In vivo* rabbit model	- Colourless and transparent membrane	- Proliferation and disordered collagen. - Corneal epithelial defects - Scar tissue formation	[77]
(PDLLA/chitosan) membranes	Yellowish and translucent membrane Evaluation membrane: after 11 days	- Chitosan enhances the hydrophilicity of PDLLA that promotes cell proliferation,	- Conjunctival discharge persists for long time	[77,78]

	In vivo rabbit model	biocompatibility, and cell adhesion		
Surface modified contact lens with acrylic acid	Commercial contact lenses model with surface modification Evaluation after 11 days *In vitro* rabbit model	- Formation of multiple cell layers, 11 days after application	- Poor cell transfer after culture cells onto contact lens for 5 days	[79]
Poly (lactide-co-glycolide) (PLGA) electrospum scaffolds	Scaffold substitute for hAM Degradation starts after two weeks. *In vitro* rabbit model	- Cells were well attached and organized on this scaffold	- After two weeks scaffolds were smaller, brittle, and opaque. - Mechanically instable	[80]
Silicone hydrogels	Soft silicone contact lens, ocular bandage	- Contact lens can deliver LEC's to the cornea and improve	- Cause dry eye syndrome	[81]

	20 days treatment Tested in humans	persistent epithelial defects (PED's) symptoms		
1 – 4 diaminobutane modified polymethacrylate hydrogel coated with collagen IV	Amine-modified polymethacrylate hydrogel implants coated with collagen IV. Full re-epithelization by corneal epithelial cells after 5 days *In vitro* bovine model	- Newly formed tissue grew on the hydrogel surface.	- Small pores sizes makes the implant opaque	[82]
Electrospun microfabricated 3D rings with microarchitecture	Design of artificial limbal stem cells niches with the fabrication of biodegradable rings made of polyethylene	- The rings support good cell proliferation - Scaffolds with topography that aims to	- Opaque scaffold which avoids the passage of light. - Irregular fibre formation on microfabricated substrates	[83]

	glycol diacrylate (PEGDA). *In vitro* rabbit model	recreate the 3D niche structure		
Alginate hydrogels	Alginate hydrogels comprised of blocks of mannuronic and guluronic acid cross-linked via carboxyl groups with multi-valent cations. After 7 days, 57% cells remained alive. *In vitro* bovine cornea model	- Influence stem cell differentiation of mesenchymal progenitor cells.	- Biocompatibility depends on the material structure. - Some cell types are only modestly viable in this material. - Mechanical properties influence cell differentiation. - Short-term preservation of corneal epithelial cells.	84

Biodegradable synthetic Poly D,L-lactide-co-glycolide (PLGA) membrane	Synthetic membrane Breakdown in 6 weeks *In vivo* rabbit eye model	- Supports LEC's growth and their transfer to the cornea	- Acid catalysed hydrolysis can be triggered by the accumulation of carbonic acid	85
Limbal crypts with 3D niche architecture	Cellular collagen constructs with BLCs (bioengineered limbal crypts) to mimic the native limbal epithelial stem cells (LESC's) niche. Multilayer after 2 weeks *In vitro* human limbal fibroblasts	- A mixed population of hLEC's can be maintained on the surface of the scaffold - Scaffolds with topography that aims to recreate the 3D niche structure	- Expensive - Loss of volume and shrinkage when cells are seeded - Quickly degrades	17

Microfabricated artificial limbus with micropockets made with Polyethylene glycol diacrylate (PEGDA)	Microfabricated niches coated with fibronectin in a PEGDA ring. 6 weeks to partial re-epithelialization of *In vivo* rabbit eye model	- Promote cell migration and re-epithelialization - Fibronectin promotes cell adhesion. - Scaffolds with topography (micropockets) that aims to recreate the 3D niche structure - Hydrophilic	- Poor cell-adhesion properties. - Poor protein adsorption	40
Microfabricated pockets in Poly $_{D,L}$-lactide-co-glycolide (PLGA) membranes	Fabrication of micropockets into microfabricated membranes 4 weeks for 50% cell migration	- The inclusion of micropockets provides explants with physical protection that enhances stem cell maintenance - Scaffolds with topography (micropockets) that aims	- More studies are necessary. - Acidic by products during degradation	3

	In vivo rabbit eye model	to recreate the 3D niche structure		
Fabrication of polyethylene glycol diacrylate (PEGDA) membranes with micropockets and electrospun with Poly $_{D,L}$-lactide-co-glycolide (PLGA)	Rings with microfabricated niches in a PEGDA using microstereolithograpy. Membrane was electrospun with PLGA fibres. Cell transfer after 4 weeks *In vitro* rabbit model	- Promote cell outgrowth and re-epithelialization - Scaffolds with topography (micropockets) that aims to recreate the 3D niche structure	- Poor cell-adhesion properties - Over curing of the PEGDA - Random alignment of fibres forming the membrane, which influences the degradation rate	[23]
Amine functional hydrogels	Synthetic hydrogel modified with alkyl amines as functional groups, adjusting the bulk	- Promote rabbit limbal ephitelial cells (rLEC's) growth and preventing	- High matrix density that inhibit epithelial outgrowth from explants even when modified with amines	[86]

	properties and varying the carbon chain length of the alkyl amine. 21% cell transfer after 7 days *In vitro* rabbit model	rabbit limbal fibroblast (rLF's) growth		
Poly (glycol sebacate)/ Poly (ε-caprolactone) PGS/PCL blend nanofibrous scaffolds	Membrane made by electrospinning of PGS/ PCL in different ratios.	- Biocompatible - Transparent - Nano fibrous-oriented scaffold	- Wettability (water uptake) - Biodegradability depends on the blend ratio of spinning solution - Evaluation of cytotoxicity and biocompatibility of this membrane is still necessary - Not widely investigated	[87]

The table above shows the early development of polymers that have been used as cell carriers in the treatment of corneal diseases. Most of these carriers have been tested only in vitro, and unfortunately, despite significant advances in biocompatibility, transparency, and cell attachment, there are still many challenges in terms of cell proliferation, hydrophilicity and in the design that mimics the limbal structure. Therefore, it is an area of opportunity that still offers possibilities in the development of new technologies to help with struggle against LSCD.

1.4.3 DISCUSSION OF DIFFERENT SOLUTIONS

The constant search for replacements for damaged cornea has mainly focused on the development of 3D printed, nanofibrous, and decellularized scaffolds to replace the epithelium, endothelium, stroma, and full thickness cornea. Main affords have been made to develop a replacement for the stromal layer since it represents ~90% of corneal thickness [88–91].

Current scaffolds are trying to replicate the features found in the native cornea as mechanical properties, substrate topography, and transparency. Mechanical properties have an influence in different corneal cells and cell lines, affecting cell behaviour and survival. Previous works have reported the influence of patterned scaffolds in cell migration, adhesion, proliferation, and alignment [92–94]. Transparency is one of the most difficult features to achieve due the employed techniques to synthetise the scaffolds (electrospinning, freeze drying, solvent casting, phase separation, etc) and in the native cornea is due to the cornea curvature, collagen alignment, and stromal cells [10,95,96].

Collagen is an important component of the cornea and has been used to replace all the corneal layers mentioned above. However, it has not been possible to design a microfeatured dome-shape scaffold due to its poor mechanical properties. Collagen is also not suitable for more complex manufacturing techniques for an aligned and thin material as structures are difficult to maintain and easily collapse [97,98]. Another material

that has received great interest due to its transparency and advantageous mechanical properties is silk. Despite these advantages, silk corneal scaffolds have only been synthesized with electrospinning. Although this technique allows control over the alignment and the size of fibres and pores between them, it cannot be used to fabricate a dome shape scaffold with defined microfeatures [99]. Agarose and fibrin also have remarkable optical properties, but the process used for their polymerization is complicated and often shows a certain degree of cytotoxicity [100,101]. Chitosan and gelatin are other natural polymers that have been used for the development of corneal materials, mainly synthesized by evaporation and with the use of crosslinking agents (Physical methods: dehydrothermal, UV radiation, Chemical agents: glutaraldehyde (GTA), carbodiimides, genipin (GP), Enzymes: transglutaminase, tyrosinases, and horseradish peroxidases)[102]. However, the impurities of other materials from their processing and poor mechanical properties have made the development of suitable materials complicated [39].

In summary, natural polymers have been widely used for the development of corneal substitutes due their biocompatibility, biodegradability, but most of them lack of appropriate transparency and mechanical properties and some works reported inflammatory responses [37,103].

The use of synthetic polymers has been explored to overcome the issues present in biopolymers. The polymers that have been most widely used for the synthesis of scaffolds are PHEMA, PEGDA, PLGA for epithelium replacement, PVA for epithelium and stroma replacement, PHBo, PHBV and PCL for endothelium replacement and combination of PEG / PAA and PHEMA / PAA for full thickness corneal replacements [39]. The polymer processing techniques that have been employed with these polymers are crosslinking and electrospinning. Although the problems with mechanical properties have been overcome, the processes involved during synthesis and manufacturing are complex and time consuming. The hydrophobic nature of some of the synthetic polymers often requires extra steps such as surface modification to increase biocompatibility with target cells and increase cell adhesion [104,105]. To date,

the creation of a corneal replacement that approaches the gold standard continues to be a challenge. This device should have the following characteristics: 1) mimic the optical and mechanical properties of the cornea, 2) possess the thickness necessary to be implanted in the patient ~150 µm (standard thickness for contact lenses [106]), 3) include in-built microenvironments (niches), and 4) have a dome shape that favours and influences cell behaviour, promoting cell migration and proliferation.

The tuneable mechanical properties, elasticity, and varied techniques for scaffold fabrication make synthetic polymers the most viable option to achieve the gold standard in corneal replacements. Furthermore, synthetic polymers have been used to overcome the drawbacks found in biopolymers, despite their lack of adequate transparency. Therefore, the development of a “smart” corneal biomaterial that can mimic the native cornea and lead to tissue regeneration is a key area of opportunity.

PGS has seen increasingly more research interest since its first report by Wang. *et. al*. in 2002 [107] due to its biocompatibility, biodegradability, inexpensiveness, transparency, and elastomeric nature, with tuneable mechanical properties useful for working with soft tissue [108–110].

PGS has been used in biomedical applications as a retinal graft, vascular tissue, cartilage, cardiac patch, and nerve applications. It has also been used as a biomedical adhesive instead of conventional sutures, and recently as a corneal epithelium replacement [111,112].

However, it has a rapid degradation rate *in vivo,* low mechanical strength, hydrophobicity, and requires high temperatures for an extended time to generate a crosslinked matrix. This limits the creation of precise features and restricts other applications based on PGS [109,111,113–115].

Recently, our research group reported the synthesis of poly (glycerol sebacate) methacrylate PGS-M, a novel photocurable material that has the advantages of PGS combined with the adaptability of fast crosslinking under UV light thanks to methacrylate groups [116,117]. It is possible to control the mechanical properties,

degradation rate, crosslinking density, and elongation through the degree of methacrylation. This makes PGS-M a promising biomaterial for the development of microfeatured scaffolds for corneal regeneration that could be able to mimic the characteristics of the native cornea.

1.5 DESIGN TARGETS

Design and manufacture an efficient cell carrier that can be able to re-establish the healthy balance in a damaged cornea. It should improve the delivery and survival of transplanted limbal epithelial stem cells (LESC's).

- Biocompatible
- Biodegradable
- Transparent
- Mechanical properties that mimic those of the native cornea (strength between 3 to 6 MPa and Young's modulus between 100 kPa to 57 MPa).
- This carrier should mimic the anatomical structure of the limbus to provide **physical protection** to the cells and **ensure their survival**

1.6 LITERATURE REVIEW REMARKS

The development of biomaterials for the regeneration of the cornea has reached a decisive point, as properties that mimic the native cornea and promote tissue regeneration become necessary.

Lack of donors, biocompatibility issues, and success rates less than 35% of corneal transplants, have led to the search of corneal substitutes. Synthetic and natural polymers such as collagen, fibrin, silk, alginate, PEGDA, PLGA, PCL, PDLLA, PHEMA, PMMA, PGS have been explored. However, despite the advantages they offer, have more disadvantages such as lack of biocompatibility, degradation,

inflammatory reactions, lack of transparency, poor mechanical properties, and instability after implantation.

On the other hand, the polymers developed to date have not completely mimicked the structure of the native cornea with its in-built niches and transparency. Therefore, the development of micro-featured materials for cornea is an area of opportunity for the improvement of proliferation and guiding migration of corneal cells.

The gold standard for a corneal substitute would be a biocompatible, biodegradable polymer, capable of mimicking the properties of soft tissue such as cornea, but mechanically capable of supporting tissue regeneration, biodegradable and stable in physiological conditions. In addition, this material should allow the design of an architecture that mimics the niches in the native cornea, promoting cell proliferation, migration, and differentiation, ultimately leading to tissue regeneration.

CHAPTER 2. PGS-M SYNTHESIS

2.1 INTRODUCTION

The previous studies listed in Chapter 1 (1.5) showed possible candidates developed for use as corneal replacements. However, a material capable of completely mimicking the native cornea and its physical-chemical properties has not been developed yet. Therefore, it is necessary to develop a material that mimics corneal dome-shape architecture with in-built niches, possesses similar mechanical properties, and has a chemical composition that promotes both cellular growth and tissue regeneration.

For this purpose, synthetic polymers seem to be the best choice due to their tuneable characteristics. It is necessary to choose a polymer that possesses the properties of soft tissues such as cornea, but with the mechanical properties that allow tissue regeneration without loss of architecture and stability. In addition to this, it should be biocompatible, biodegradable, and have transparency like cornea. The method of fabrication is also important, as it should allow the creation of micro-features that emulate the niches present in the cornea and its dome shape.

Our research has shown that poly glycerol sebacate (PGS) is an optimal candidate for use in soft tissue engineering, thanks to its mechanical properties, biocompatibility, biodegradability, elasticity and its wide use in soft tissue engineering in retina, cartilage, cardiac patch, etc. with promising results [108,111]. However, its high rate of degradation, low mechanical strength, and crosslinking methods have limited its applications and the creation of accurate geometries.

Therefore, based on previous results from our research group, I propose the addition of methacrylate groups in low percentages to optimize the properties of PGS as a biomaterial for soft tissue . The addition of methacrylate groups makes it possible to control the mechanical properties and the degradation rate through the degree of methacrylation. In addition, the creation of architectures with high precision is also possible as methacrylate groups allow photocuring of the material.

In this chapter, four low degrees of methacrylation (DM) (20,30,40 and 50%) are proposed, to characterize and select the candidate that presents physicochemical properties matching those of the native cornea. This will be considered as further biological characterization will be used to determine which material is best to regenerate corneal tissue.

2.1.2 PREPOLYMER POLY (GLYCEROL SEBACATE) (pPGS)

The synthesis of poly (glycerol sebacate) (PGS) was first reported by Wang. *et. al*. in 2002 [107]. Since then, different groups synthesized PGS under different temperatures and reaction times, resulting in polymers with distinct mechanical properties useful for a wide variety of applications (Table 2.1).

Table 2.1 PGS synthesis methodologies carried out by different research groups.

APPLICATION	MOLAR AMOUNT	PRE-POLYMERIZACION CONDITION	POLYMERIZATION CONDITIONS	MECHANICAL PROPERTIES	REFERENCE
Soft tissue	1:1	120 °C under argon for 24 h 1 torr to 40 mtorr over 5 h	40 mtorr and 120 °C for 48 h.	Rupture strain: 267 ± 59.4% Young's Modulus: 0.282 ± 0.0250 MPa UTS >0.5 MPa	[107]
Vascular tissue	1:1	150 ºC under nitrogen for 24 h	No information available	No information available	[118]

Soft tissue	1:1	120 °C under nitrogen for 24 h	40 mTorr 120 °C for 24 h	No information available	[119]
Myocardial tissue	1:1	110, 120, or 130 ºC under argon for 24 h 50mmHg over 5 h	110, 120, or 130 vacuum for 48 h.	Rupture strain:40-50% Young's Modulus: 0.040–1.2 MPa	[120]
Cartilage	3:4, 1:1, and 4:3	120 °C under nitrogen for 24 h	50 mTorr vacuum at 120 °C for 48 h	Young's Modulus: 0.25-4.5 MPa	[121]
Soft tissue	1:1	120 °C under nitrogen for 24 h	30 mTorr vacuum at 120 °C for 48 h	Young's Modulus: 0.3-2.5 MPa	[122]
Heart valve	1:1	nitrogen blanket to 120 °C 24 h	50 mTorr vacuum for 24 h	Young's Modulus: 1-2.75 MPa	[123]
Tissue engineering	1:1	nitrogen gas at either 130 °C for 24 h or 150 °C for 8 h.	No information available	Young's Modulus: 1.7-2.4 MPa	[110]
Skin	1:1	150 C for 12 h under the protection of N2	vacuum at 150 °C for 12 h.	No information available	[124]

Table 2.1 shows that the same reaction conditions have been carried out by different groups, but different results were obtained. This is due to the extent of esterification, the ratio of esterified secondary to primary alcohols, or in the monomer composition of the final polymer. Primary alcohols react faster with carboxylic groups and forming an unbranched polymer chain. Secondary alcohols are not very reactive and are responsible of crosslinking and are present in small quantities [110].

2.1.3 STANDARD SYNTHESIS

PGS is a polyester elastomer that is synthetized through a polycondensation/esterification reaction using 1:1 molar ratio of trifunctional glycerol [$HOCH_2CH(OH)CH_2OH$] and bifunctional sebacic acid [$(HOOC)(CH_2)_8(COOH)$] [110,125] (Figure 2.1). This reaction results in a transparent, almost colourless elastomer [107].

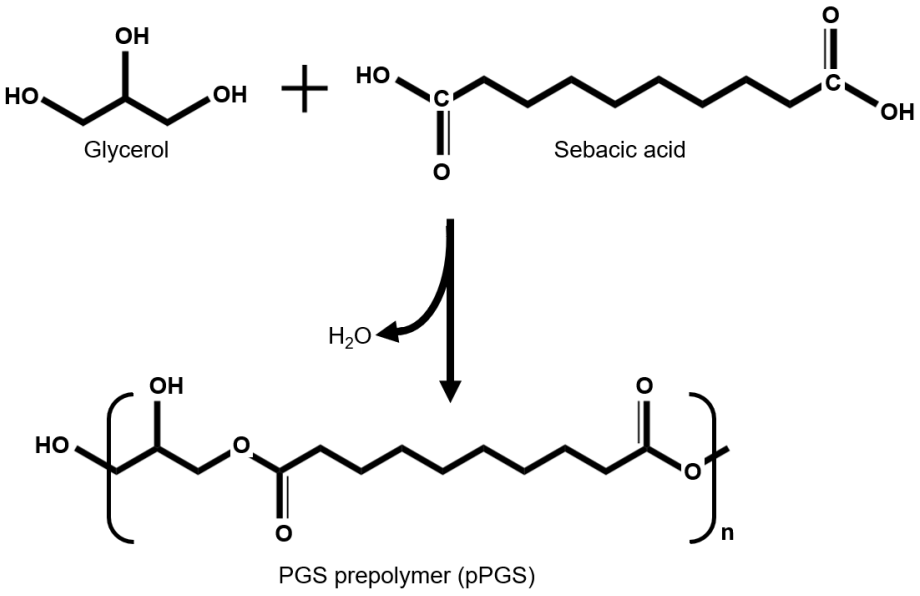

Figure 2.1 Polycondensation/ esterification of PGS.

Glycerol is a basic building block for lipids: it is a non-toxic, colourless, odourless, water soluble and hygroscopic simple polyol that is used in pharmaceutical formulations, as a humectant in food, and is approved by the United States Food and

Drug Administration (FDA) [126]. On the other hand, sebacic acid is derived from castor oil and is a metabolic intermediate in ω-oxidation of medium to long chain fatty acids. Similarly to glycerol, it is also non-toxic and approved by FDA, being used in drug delivery systems and as plasticizer in cosmetics [111,121,127].

A PGS film possesses a tensile Young's modulus of 0.01-1.5 MPa and its maximal elongation is 1.2 to 3 times its original length; for this reason, this polymer is suitable substitute material in soft tissue engineering [111].

PGS's Young's modulus values are higher as curing time and curing temperature are increased. Its physical properties are further modified by changing the molar concentration of reactants. Although the maximum strain at break decreased with longer curing times, the biocompatibility was improved [126]. Furthermore, the degree of esterification (DE) has been used to predict the Young's modulus, degradation rate and physical characteristics of PGS [111].

PGS has been used as scaffold and cell delivery vehicle as it provides a conductive surface allowing cell adherence. It is also capable of guiding and organizing cells in the required manner to support cell growth.

The physical characteristics (mechanical properties and elastic behaviour) of PGS are like common biological soft tissues. This polymer has high biocompatibility and elastomeric nature, making it able to recover after deformation as a result of its intrinsic elasticity [120]. PGS degrades by surface erosion, losing mass and strength during reabsorption in host tissue. It also has minimum water absorption and no detectable swelling [128].

Advantages

- Biocompatible, biodegradable, inexpensive, generally has soft and flexible mechanical properties useful for working with soft tissue [110].
- Bioresorbable in natural pathways [113].

- This polymer has a similar acute inflammatory response with PLGA, but with less fibrous capsule formation and the absence of chronic inflammation [129].

Disadvantages

- Rapid degradation rate *in vivo*, that limits the use of the scaffold. This can be improved with chemical modifications [113].
- Low mechanical strength (0.2 – 0.5 MPa), Young's modulus between 0.01 to 1.5 MPa and poor hydrophilicity (water retention capacity ~2%). This can be improved with chemical modifications, like modifying PGS with acrylates [109,111].
- A certain degree of cytotoxicity due to their non-reacted carboxylic acid groups or carboxylic acids produced by the aqueous hydrolysis of the PGS ester groups. This can decrease the extracellular pH (acidify) [120], and as such the degree of cytotoxicity is associated with crosslinking density, It is possible that a low crosslinked network with high degradation rate can decrease the pH to such an extent that the environment becomes cytotoxic [111].
- Requires high temperatures for extended periods of time to generate a crosslinked matrix. These conditions make the creation of accurate geometries difficult and limit its possible applications.

2.1.4 MICROWAVE ASSISTED SYNTHESIS

The conventional PGS synthesis requires long reaction times with high energy and inert atmosphere (flow of nitrogen or argon). In industry, microwave radiation is used in drying process and chemical reactions [125].

Advantages

- The non-contact nature of the process, instant and rapid heating, fast reaction, minimization of side reactions and better quality (purity) [125]
- Efficient reaction (time and energy) [130].

Disadvantages

- Lack of information in the reaction and difficulties of control [125]
- Heterogeneous energy transfer and intensive glycerol evaporation that causes distortion in the ratio of sebacic acid and glycerol. This results in a stiffer PGS when is cured [130].
- Yellowish pre-polymer [127].

This reaction can be carried out in a commercial microwave oven or an industrial microwave reactor. The synthesis in the microwave reactor is carried out in a controlled way. We have a constant nitrogen flow that prevents the oxidation of the polymer and constant vacuum that allows the removal of the by product (water) avoiding hydrolysis of the molecule. In addition, it is possible to maintain a continuous stirring that allows the reagents to be mixed during all the reaction. The disadvantage of this method is the limited amount that can be synthesized due to the size of the reactor. On the other hand, conventional microwave synthesis is faster and larger amounts of polymer can be synthesized. However, the synthesis is not carried out under controlled conditions, as result of this, the polymer is more yellow, and the molecule can be hydrolysed due to lack of removal of the by product.

The table 2.2 shows some of the protocols used for the synthesis of microwave PGS.

Table 2.2 Protocols used for the synthesis of microwave PGS.

Type of microwave	Reaction time	Intervals	Microwave power	Result	Reference
Domestic oven	3 minutes	10 seconds in every minute	650 W	Young's modulus 0.5 ± 0.02 MPa Tensile strength 0.27±0.06 MPa, Elongation 180%	[125]

Domestic oven	3 min (tested until 30 min reaction, with best results obtained at 3 min)	Every minute	600 W	Young's modulus 0.29 ± 0.10 MPa Elongation at break 2.44 ±0.17	[130]
Microwave reactor	1.5 h under continuous stirring at 180 °C. and an additional 30 min in vacuum to remove water.	-	-	2600 g/mol Degradation of 4.5 % in 16 weeks	[127]

2.1.5 POLY (GLYCEROL SEBACATE) ACRYLATE (PGSA)

The acrylation of Poly (glycerol sebacate) is the addition of acrylate groups in the backbone of PGS. It was firstly proposed by Nijst et al. [131] and Englemayr et al. [132]. (Figure 2.2).

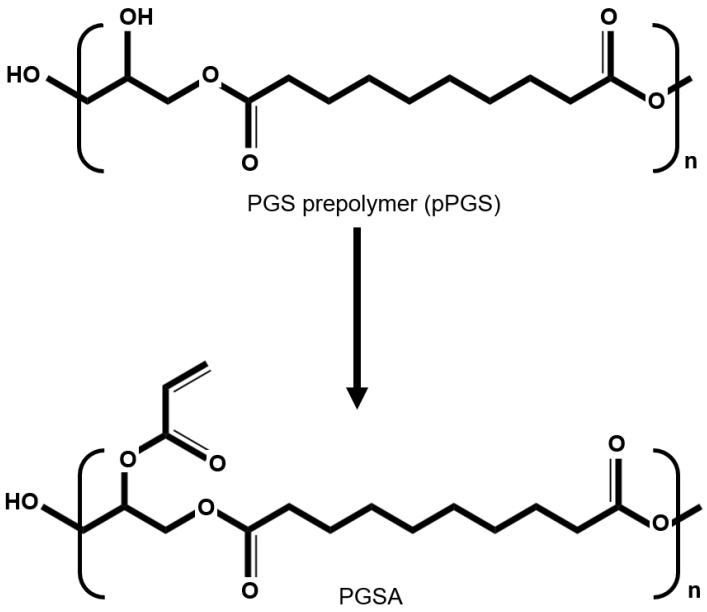

Figure 2.2 Diagram detailing PGS acrylation.

This modification gives control over crosslinking process and provides more processing options, as the crosslinking can occur via redox (useful for injectable polymers with applications in drug delivery, tissue adhesives, tissue barriers and scaffolds) and photoinitiation, which that can be controlled by changing the initiator concentration and light intensity [115]. The synthesis of PGS requires high temperatures and vacuum conditions, limiting its application since it makes crosslinking *in vivo* impossible [114].

Acrylated PGS can also be crosslinked under exposure of UV light, with the number of acrylate functional groups dictating the concentration of cross-links formed in the network. This modification allows it to overcome the limitation of the high temperature and vacuum requires to cure PGS [115]. Table 2.3 shows the comparison of the properties between the PGS and PGSA.

Table 2.3 Comparison of the properties between the PGS and PGSA.

	PGS	**PGSA**
REFERENCES	[115,129,131,133]	[115,129,131,133]
PROPERTIES		
Degree of acrylation (DA)	No information available	1 – 88 %
Ultimate tensile strength	0.2 – 0.7 MPa	0.01 to 0.6 MPa
Young's modulus	0.01 to 1.5 MPa	~30 KPa to 6.6 MPa
Elastic elongation	120 to 300 %	40% - 190%
Degradation rate	~ 21 d/mm thickness *in vivo* / after 6 weeks *in vivo*	10% *in vivo* after 10 weeks 37 % *in vivo* after 8 weeks ~20 – 100 % *in vivo* at 12 weeks (depends on DA)
Water retention	8% - 12%	8% - 12%

It has been observed that if the DA increases, Young's modulus, stiffness, tensile strength and crosslinking increase, but the % elongation at break decreases [115].

Advantages

- This modification gives an additional level of control with tunable mechanical properties [131,133].

- It can be cured rapidly at ambient temperatures, producing a material with a large range of mechanical properties. It showed *in vitro* enzymatic degradation and biocompatibility by sufficient cell adhesion with subsequent proliferation into a confluent monolayer [131].
- This polymer could also be combined with other acrylated molecules to extend additional control of its macromolecular properties: for example, the co-polymerization of PEGDA with PGSA enabled further control of characteristics such as mechanical strength, water swelling, hydrophobicity, and degradation rates [134].

Disadvantages

- It is not soluble in aqueous solutions, which may limit some of its applications [131].
- It can generate a mild inflammatory response *in vivo* [129].
- Difficult the removal of the by-product (mainly chlorine salts) [116].

2.1.6 POLY (GLYCEROL SEBACATE) METHACRYLATE (PGS-M)

Methacrylation of PGS was performed as reported before by Singh et al. in 2018[117] and Pashneh-Tala et al. in 2018 [116], both worked with higher degree of methacrylation because the application of their work was based in the development of a biomaterial for nerve conduits, that required stiffer materials. In this work the application of PGS-M is for soft tissue (cornea) for that reason why lower methacrylation degrees were investigated during this work The main difference is that PGS-M reacts more slowly compared to PGS-A, reducing spontaneous crosslinking of the molecules. Additionally, the use of methacrylate anhydride instead of acryloyl chloride makes the reaction much cleaner, as we avoid the formation of a large amount of salts during acrylation. These salts are difficult to remove from the final product. Therefore, it is a better option when modifying the PGS molecule compared with acrylate groups (Figure 2.3).

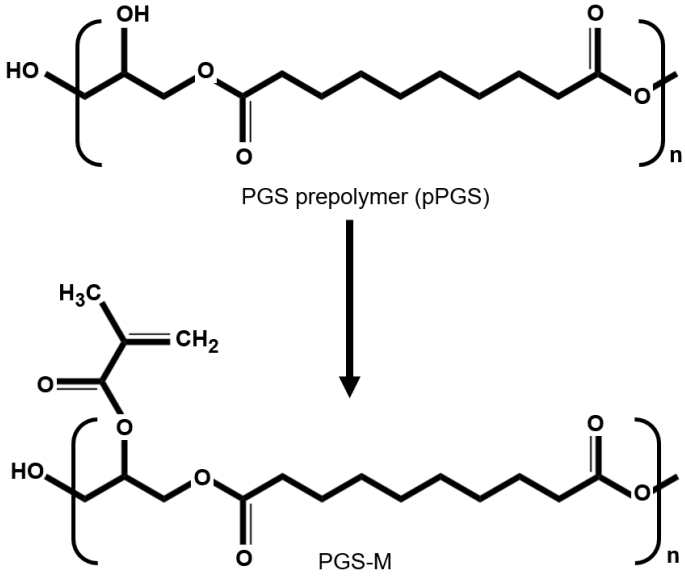

Figure 2.3. Diagram detailing PGS methacrylation. The PGS methacrylation was carried out by adding methacrylate groups from methacrylate anhydride to the hydroxyl groups of the PGS molecule.

2.2 OBJECTIVES

2.2.1 GENERAL OBJECTIVE

Synthesize and characterize a polymer suitable for use in tissue engineering. This polymer should be transparent, biocompatible, and biodegradable with mechanical properties that mimic the native cornea.

2.2.2 SPECIFIC OBJECTIVES

- To synthesize poly glycerol sebacate (PGS) prepolymer through microwave and standard synthesis.
- To synthesize poly glycerol sebacate methacrylate (PGS-M) polymer with different degrees of methacrylation (20%,30%, 40% and 50%) in order to develop a device with mechanical properties that mimics the native cornea.
- Characterize and evaluate the material to select the best PGS-M candidate (DM) for a material to regenerate cornea.

2.3 MATERIALS AND METHODS

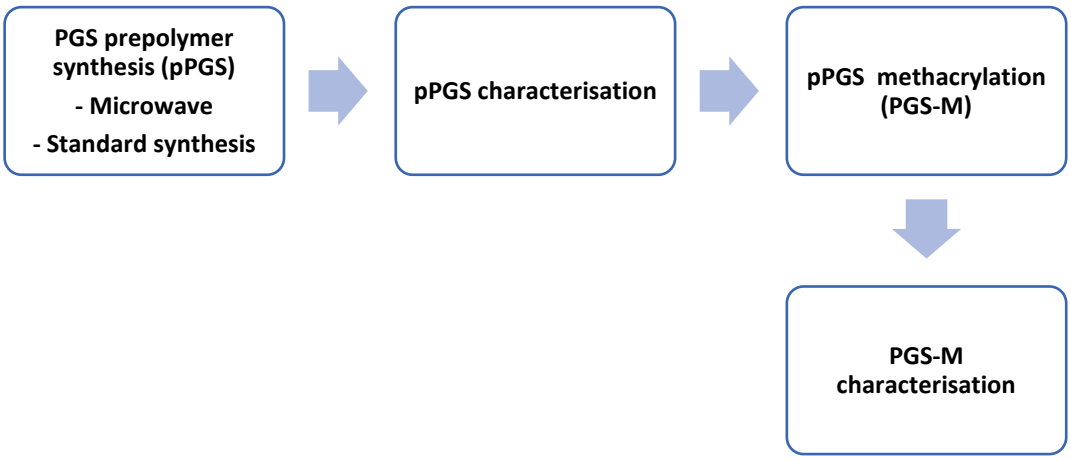

Figure 2.4 Methods diagram for PGS-M synthesis.

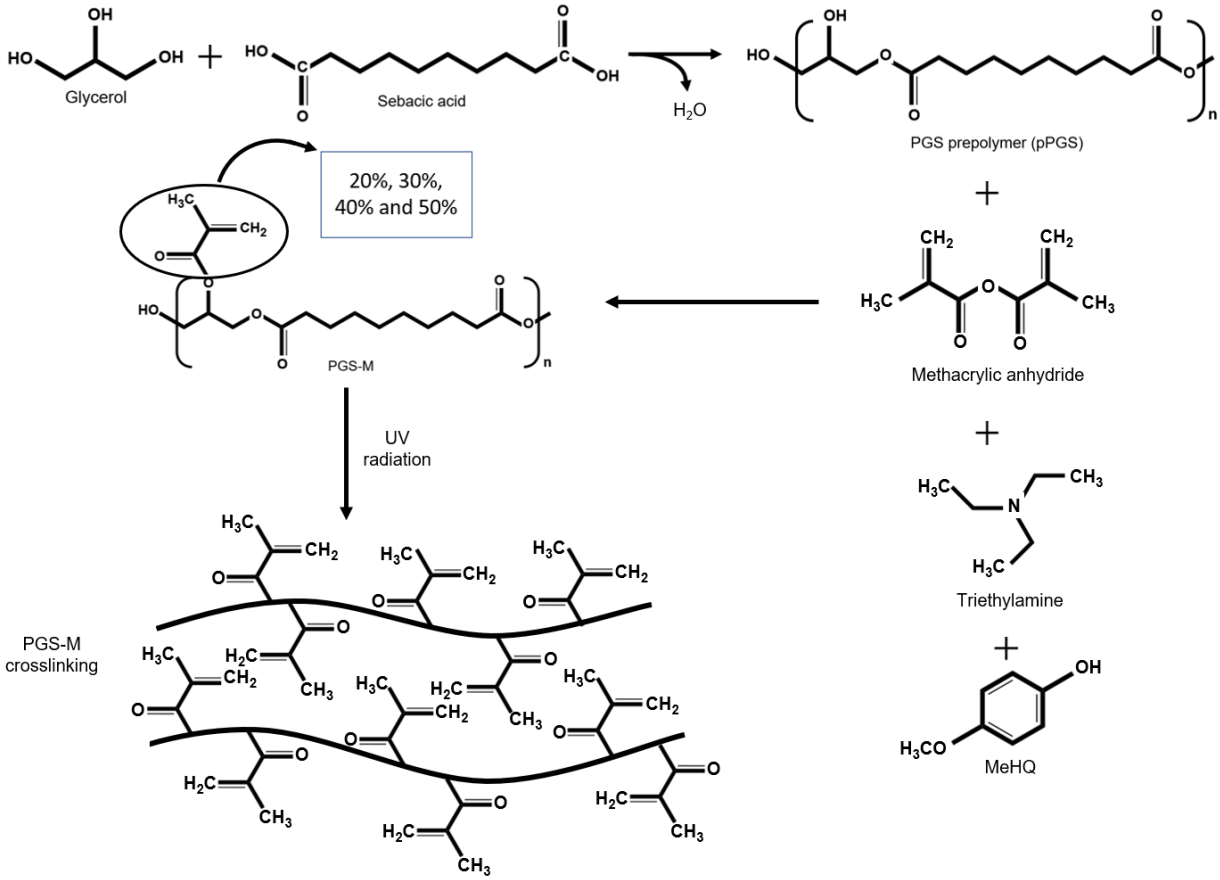

Figure 2.5 Chemical reactions for PGS-M synthesis and crosslinking.

METHODS

PGS PREPOLYMER (pPGS) STANDARD SYNTHESIS

PGS was synthesized through the polycondensation reaction of a 1:1 molar mixture of glycerol ($C_3H_8O_3$) (Sigma Aldrich) and sebacic acid ($C_{10}H_{18}O_4$) (Sigma Aldrich) added in two-neck round bottomed flask and reacted at 120 °C under a continuous flow of nitrogen for 24 h to avoid oxidation. This was heated for an additional 24 h under a continuous stirring and vacuum at 120 °C to remove water (reaction by-product, shown in Figures 2.5 and 2.6). The molar mass of the pPGS polymer unit (Glycerol-Sebacic acid) was 259.32 g/mol (Figure 2.6) (Figure 2.7).

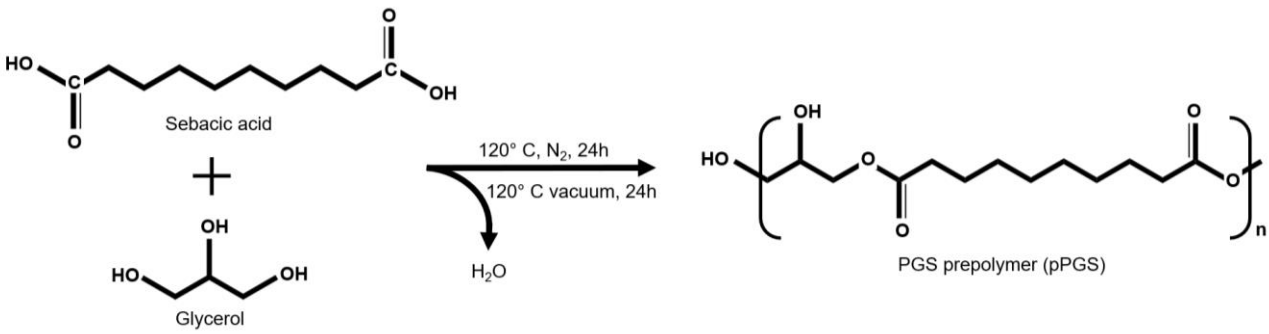

Figure 2.6 PGS prepolymer polycondensation reaction.

Figure 2.7 PGS synthesis standard method.

MICROWAVE ASSISTED SYNTHESIS

The polycondensation reaction of 1:1 molar of glycerol ($C_3H_8O_3$) (Sigma Aldrich) and sebacic acid ($C_{10}H_{18}O_4$) (Sigma Aldrich) was carried out using a CEM Discover SP microwave reactor to heat the mixture for different times (30 sec, 1 min, 2 min, 3 min, 4 min, 5 min, 10 min, 15 min, 30 min, 1 hr and 1.5 hr) (N=3, n=3). The reaction was done under continuous stirring at 180 °C with one initial nitrogen purge. The maximum pressure during polycondensation was 5 bar and the microwave maximum power was

set to 200 W. To remove the by-product (water) the samples were vacuumed at 150 °C by 30 additional minutes. The software used to analyse the sample's reaction was Synergy™ (Figure 2.8).

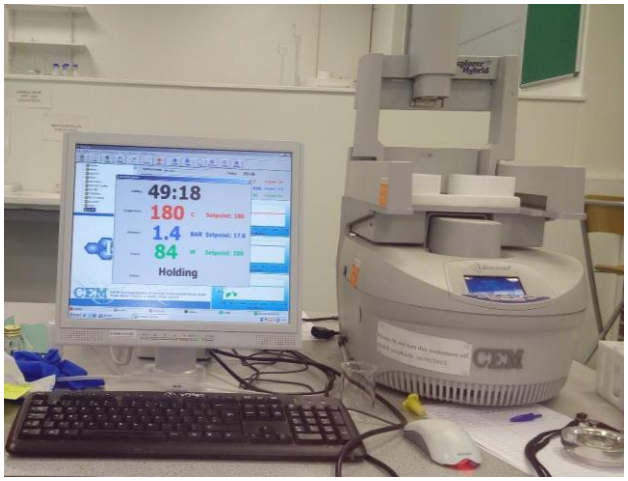

Figure 2.8 PGS synthesis in CEM Discover SP microwave reactor.

PGS-M SYNTHESIS

Methacrylation was carried out in the PGS samples obtained by the microwave assisted synthesis and the standard synthesis and was performed as reported before by Singh et al. in 2018 [117] and Pashneh-Tala et al. in 2018 [116].

Glycerol has three hydroxyl (OH) groups in its structure. It was assumed that only the two primary hydroxyls groups in glycerol reacted with sebacic acid during the PGS synthesis. Therefore, 3.856 mmol of OH are available for methacrylation [131,133]. The methacrylation was carried out by adding methacrylate groups from methacrylate anhydride to the hydroxyl groups of the PGS molecule. PGS was methacrylated in 4 degrees of methacrylation (DM) - 20, 30, 40 and 50%.

The methacrylation was carried out using dichloromethane (DCM) (CH_2Cl_2) (Fisher Scientific, UK) to dissolve the PGS prepolymer in a 1:4 (w/v) ratio synthetized by standard synthesis and microwave assisted synthesis. Then, triethylamine ($(C_2H_5)_3N$)

(Sigma Aldrich) was added (equimolar amount) as a neutralizing base for the acidic side products (Methacrylic acid) . After this, 4-methoxyphenol (MeHQ) ($C_7H_8O_2$) (Sigma Aldrich) (1mg/g of PGS prepolymer) was added as photo polymerisation inhibitor to avoid spontaneous crosslinking. Finally, methacrylic anhydride ([H2C=C(CH3)CO]2O) (Sigma Aldrich) was added dropwise, in four different concentrations related with the degree of methacrylation (DM) (20%, 30%, 40% and 50%).

The reaction was performed in the dark (24h) on ice and allowed to reach room temperature. Extra MeHQ was added at the end of the reaction (0.5 mg/g of PGS prepolymer) and the solution was washed four times with 30 mM hydrochloric acid solution (HCl) (Fisher scientific, UK) at 1:1 to remove unreacted reagents and impurities by changing their polarity and partitioning the solution in organic and inorganic layers. Water was removed from the washing solution using granular calcium chloride ($CaCl_2$) (Fisher scientific, UK) at 0.4 g/g of pPGS. The solution was filtered using a 6 µm pore cellulose filter (Whatman - Grade 3, GE Healthcare Life Sciences, UK). Finally, the DCM was removed through rotary evaporation under vacuum in an ice bath until the PGS-M prepolymer was a viscous liquid. To maintain PGS-M stable, the polymer was stored at -8 °C prior to use (Figure 2.9).

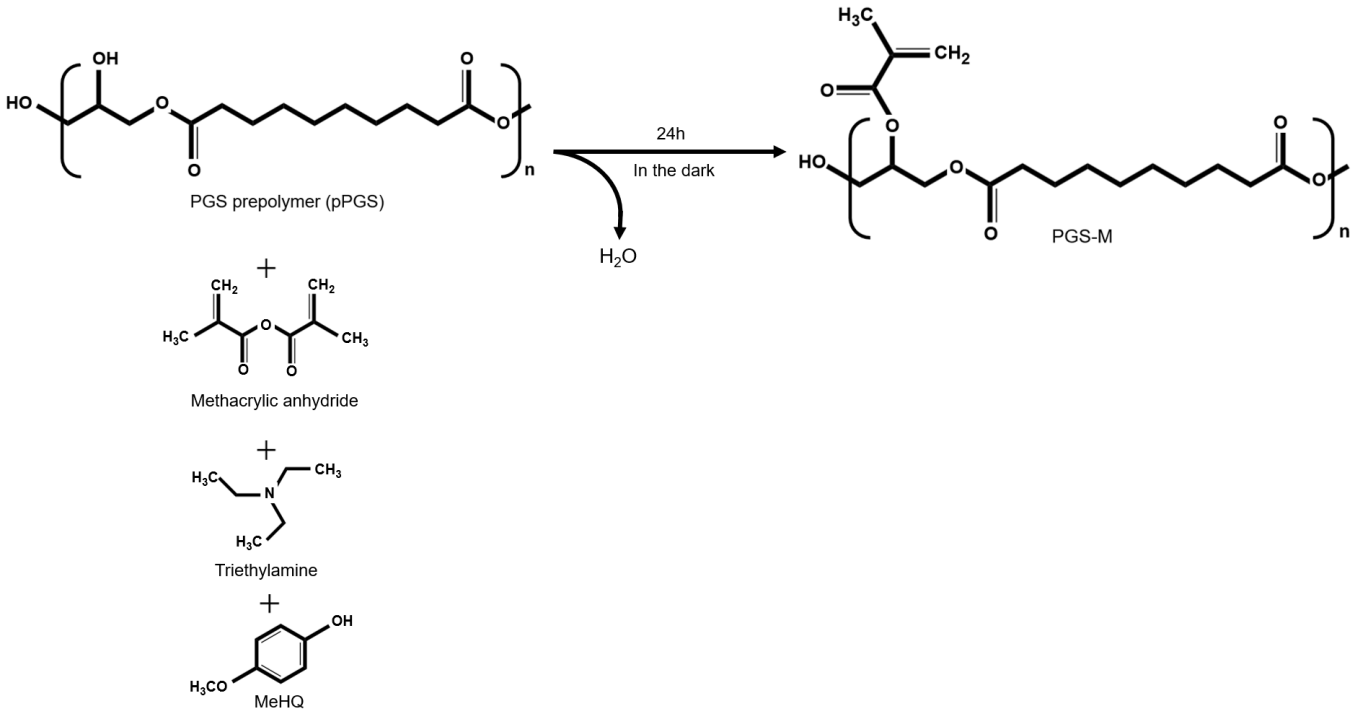

Figure 2.9 PGS-M synthesis reaction. Triethylamine ((C2H5)3N) was added as a neutralizing base for the acidic side products (Methacrylic acid) . 4-methoxyphenol (MeHQ) (C7H8O2) was added as photo polymerisation inhibitor to avoid spontaneous crosslinking. Finally, methacrylic anhydride ([H2C=C(CH3)CO]2O) was added dropwise, in four different concentrations related with the degree of methacrylation (DM) (20%, 30%, 40% and 50%).

MATERIAL CHARACTERIZATION

Methacrylation was carried out only in PGS synthesized by the standard method, because while the PGS yield from the microwave synthesis was 19.72 g, after purification only 2 g of highly viscous polymer remained, making methacrylation inefficient. PGS-M in four different degrees of methacrylation (20, 30, 40 and 50%) were analysed before and after crosslinking. The photoinitiator (PI) diphenyl(2,4,6-trimethylbenzoyl) phosphine oxide/2-hydroxy- 2-methylpropiophenone (Sigma Aldrich) 1% (w/w) was used to photocure the PGS-M polymer, it was mixed and exposed to UV light (200 W, OmniCure Series 2000 curing lamp) for 10 min to photocure. The samples obtained were photocured disks (1 mm thickness, 15 mm diameter). The samples were washed with methanol (CH_3OH) (Sigma Aldrich) 4

consecutive times (24 hours each). After this, the samples were dried in a vacuum oven at 70 ºC for 24 h.

2.3.1 GEL PERMEATION CHROMATOGRAPHY (GPC)

The theoretical number average molecular weight (M_n) and the weight average molecular weight (M_w) were determined through the data obtained from gel permeation chromatography (GPC) (Viscotek GPCmax VE2001 Cirrus with PLgel 3um mixed E column). Tetrahydrofuran was used for dissolving samples at 1% w/v. The samples synthesized in the microwave reaction were exposed to vacuum for 30 minutes at 150° C after the synthesis to remove water by product. The changes in number average molecular weight (M_n) and the weight average molecular weight (M_w) after vacuum exposition were also calculated.

The average molecular weights by number and by weight were calculated from the data obtained from GPC, using the following equations (equation 2.1 and 2.2).

$$Mw = \frac{\sum(NiMi^2)}{\sum NiMi}$$

Equation 2.1 Average molecular weight by number

$$Mn = \frac{\sum(NiMi)}{\sum Ni}$$

Equation 2.2 Average molecular weight by weight

Where Ni and Mi represent signal intensity in the peak area and mass for the oligomer containing i monomers, respectively [135–137].

The dispersity index (DI) was determined from the ratio of M_w to M_n (Equation 2.3).

$$PDI = \frac{Mw}{Mn}$$

Equation 2.3 Polydispersity index

2.3.2 SWELLING

Sol free samples were submerged in phosphate buffer saline (PBS), Dulbecco's Modified Eagle Media (DMEM) and methanol at 35 °C for 24h. The excess surface liquid was removed, and the swollen samples (W_s) were weighed. The degree of swelling and swelling ratio was calculated from the swollen weight (W_s), final weight (W_d), and initial weight (W_i) using Equations 2.4 and 2.5.

$$Degree\ of\ swelling\ (\%) = \frac{(Ws - Wd)}{Ws}\ x\ 100$$

Equation 2.4 Degree of swelling

$$Swelling\ ratio = \frac{Ws}{Wi}$$

Equation 2.5 Swelling ratio

2.3.3 GEL CONTENT (DEGREE OF CROSSLINKING)

Photocured PGS-M disks were dried at 70 °C 24 h under vacuum (W_i: initial weight) and submerged in methanol at 35 °C for 24h (N=3, n=3). Samples were dried at 70 °C 24 h under vacuum (W_d: final weight) to determine the degree of crosslinking (Equation 2.6).

$$Gel\ content\ (\%) = \frac{(Wd)}{Wi}\ x\ 100$$

Equation 2.6 Degree of crosslinking

2.3.4 SOL CONTENT

Soluble fractions were determined by washing photocured PGS-M disks in methanol to solubilise the unreacted prepolymer. The disks were dried at 70 °C 24 h under vacuum (W_i = initial weight) and re-weighed at 24 h (W_s = swollen weight after the first 24 hrs) intervals, until reaching a constant mass in approximately 3 days (N = 3, n = 3).

During the weighing, solvent on the surfaces of the samples was cleaned up, and samples were placed into sealed vials to reduce solvent evaporation. Controls were subjected to the same drying protocol, but without methanol washing. At the end of experiment samples were dried at 70 °C 24 h under vacuum (W_d = final weight) (Equation 2.7).

$$Sol(\%) = \frac{(Wi - Wd)}{Wi}\ x\ 100$$

Equation 2.7 Sol content

2.3.5 ATTENUATED TOTAL REFLECTANCE FOURIER TRANSFORM INFRARED SPECTROSCOPY (ATR-FTIR)

- PREPOLYMER

0.1 ml PGS prepolymer was analysed using attenuated total reflectance Fourier transform infrared spectroscopy (ATR-FTIR), with a Nicolet 380 spectrometer including an ATR device (Golden Gate, 45° single-bounce diamond anvil, Specac). Spectra were obtained between 4000 and 500 cm^{-1}, with a resolution of 4 cm^{-1} and 16 repeated scans. The data was analysed using OMNIC and Origin Pro software. The samples synthesized in microwave reaction were exposed to vacuum for 30 minutes at 150°C after the synthesis, to remove water by product. The ATR-FTIR spectra shows the changes after this processing.

- PGS-M

Sol free disks with 1 mm thickness of photocured PGS-M (DM) 20, 30, 40 and 50%, were washed with methanol (CH_3OH) (Sigma Aldrich) 4 consecutive times (24 hours each). After this, the samples were dried in a vacuum oven at 70 ºC for 24h. Afterwards, they were analysed by ATR-FTIR.

2.3.6 NUCLEAR MAGNETIC RESONANCE (NMR)

PGS and PGS-M with different DM were analysed by nuclear magnetic resonance (NMR) using a Bruker AVIIIHD spectrometer at 500 MHz. The polymer samples were dissolved in 1ml of deuterated chloroform (CDCl3) at 1% (w/v). The data was analysed using Origin Pro software.

2.3.7 MECHANICAL ANALYSIS

Sol free PGS-M samples with different DM (20, 30, 40 and 50%) were shaped and photocured into tensile test pieces (Type 4 dumb-bell, as specified in BS ISO 37:2011) using a silicone mould. Tensile testing was performed in Zwick Roell System at a crosshead speed of 500 mm/min, with samples elongated to failure to determine Young's modulus, ultimate tensile strength (UTS), rupture to strain, and maximum elongation.

2.3.8 THERMOGRAVIMETRIC ANALYSIS (TGA)

Sol free disks were cut in small pieces (~10 mg). The analysis was done using a Perkin-Elmer Pyris1 TGA with gas purge at 60mL/min. Samples were subjected to a heating cycle of 200°C to 600°C at a heating rate of 10°C min^{-1}. Initial degradation temperature (T_{DI}) and peak degradation temperature (T_{DP}) were determined using the first derivative curve to determine the onset of thermal degradation. Thermal stability was determined by calculating the remaining weight at 600°C. Degradation temperature and temperature range were determined from the first derivative curve (%weight loss/°C).

2.3.9 DIFFERENTIAL SCANNING CALORIMETRY (DSC)

Sol free disks were cut in small pieces (~5 mg). The analysis was done using Perkin-Elmer Pyris1 purged with nitrogen at 30mL/min. Samples were heated from −60 °C to 100 °C under N_2 at a rate of 10 °C min−1. Thermal properties melting point (T_m), glass transition temperature (T_g), enthalpy of melting (ΔH_m) and enthalpy of crystallization (ΔH_c) were calculated using the first cooling cycle and second heating cycle. The melting temperature (T_m) and glass transition temperature (T_g) were located at the peak of the process. Recrystallization temperature (T_c) was found in the valley point in the heat capacity curve.

2.3.10 IN VITRO DEGRADATION OF PHOTOCURED PGS-M

Sol free disks were weighed and incubated in PBS and media at 37°C. The samples were analysed at days 3, 7, 10, and 28, and dried at 70°C overnight under vacuum. Dried samples were weighed and the percentage of weight loss at specific time point was calculated from the initial (W_i) and final dried weight (W_d) using Equation 2.8. The surface degradation was analysed using scanning electron microscopy (SEM).

$$Weight\ loss\ (\%) = \frac{(Wi - Wd)}{Wi}\ x\ 100$$

Equation 2.8: Weight loss percentage.

2.3.11 SURFACE ANALYSIS

- SEM

Sol free disks were affixed to aluminium stubs, gold coated using a sputter coater (Edwards S150B) and examined by scanning electron microscopy (SEM) using TESCAN Vega 3 LMU SEM at an accelerating voltage of 20 kV.

- CONTACT ANGLE

PGS-M disk hydrophilicity was determined using a goniometer by the sessile drop method . A 3 µL drop of deionized water was placed onto a flat surface of PGS-M of different degrees of methacrylation using a 21-gauge flat needle. Optical images were collected after 10 seconds of contact. The contact angle of water was determined from the optical images with DSA3 software.

2.3.12 STATISTICS

The characterization was carried out with three independent experimental repeats (N=3) in triplicates per experiment (n = 3). The data was analysed with GraphPad Prism version 7.04 software. The data significance was calculated with one-way ANOVA with Tukey post-hoc pairwise multiple comparison analysis for experiments with one independent variable or factor (sample type or condition). Two-way ANOVA (paired samples) with Tukey post-hoc pairwise multiple comparison analysis was used for the experiments with two independent variables or factors (sample type or conditions). $P \leq 0.05$ was considered statistically significant (*) and $P > 0.05$ was considered non-significant (ns). Data was graphed as means ± SD (standard deviation).

2.4 RESULTS AND DISCUSSION

- Standard method

A slightly yellowish and viscous PGS prepolymer was obtained by the standard synthesis method as was reported by Rai et al. in 2012 [108]. The prepolymer colour is due to a small number of crosslinks and hydroxyl groups directly attached to the backbone as reported before by Cai and Liu [138].

THEORETICAL YIELD

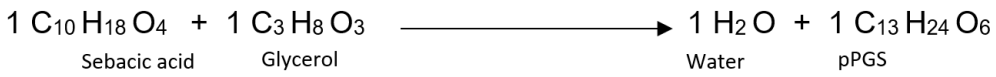

$$150\ g\ Sebacic\ acid\ \times \frac{1\ mol\ Sebacic\ acid}{202.25\ g\ Sebacic\ acid} = 0.741\ mol\ Sebacic\ acid$$

$$0.741\ mol\ Sebacic\ acid\ \times \frac{1\ mol\ pPGS}{1\ mol\ Sebacic\ acid} \times \frac{276.32\ g\ pPGS}{1\ mol\ pPGS}$$

$$= 204.93\ g\ pPGS\ (Theoretical\ yield)$$

$$\% = \frac{Real\ yield}{Theoretical\ yield}$$

$$\% = \frac{183.78}{204.93} \times 100 = 89.67\ \%$$

- Microwave method

The prepolymer synthesized by microwave was yellowish and viscous (Figure 2.10), the same features were reported before by Bodakhe *et. al.* in 2012 [114] and Yang *et. al.* in 2015 [139] during the microwave synthesis.

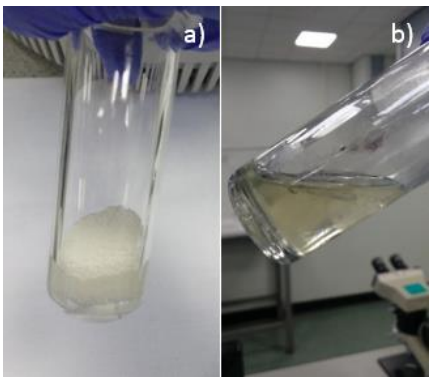

Figure 2.10 a) Sample before the placing it in the microwave reactor, b) Sample after the reaction.

The obtained polymer was more liquid and transparent as the reaction time increased. Figure 2.11 shows how the reaction time influences the resulting polymer. The change in colouration is due to sample oxidation in the absence of a constant N_2 flow during the reaction.

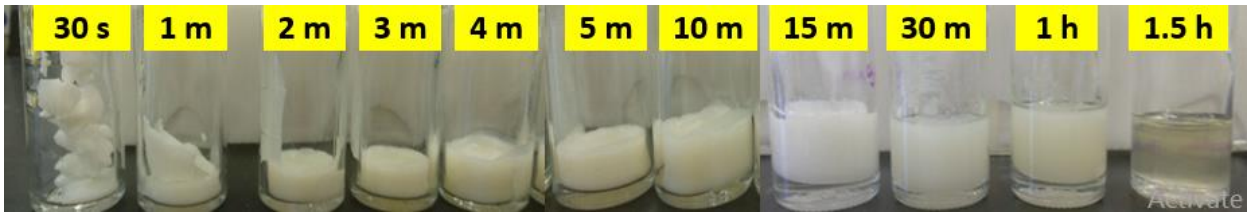

Figure 2.11 PGS prepolymer samples at different times.

THEORETICAL YIELD

$$15\ g\ Sebacic\ acid\ \times \frac{1\ mol\ Sebacic\ acid}{202.25\ g\ Sebacic\ acid} = 0.074\ mol\ Sebacic\ acid$$

$$0.074\ mol\ Sebacic\ acid\ \times \frac{1\ mol\ pPGS}{1\ mol\ Sebacic\ acid} \times \frac{276.32\ g\ pPGS}{1\ mol\ pPGS}$$

$$= 20.493\ g\ pPGS\ (Theoretical\ yield)$$

$$\% = \frac{Real\ yield}{Theoretical\ yield}$$

$$\% = \frac{19.72}{20.493} \times 100 = 96.22\ \%$$

According with the theoretical yield calculations, the microwave synthesis is more efficient compared to the standard synthesis. However, the maximum amount of polymer that can be synthesized in microwave is only ~19 g, limiting PGS synthesis. The reason for this is the small vials used in the microwave reactor. On the other hand, the standard synthesis has a lower yield, but it is possible to synthesize more than 500 g in a single reaction, making it much more useful. It is also important to mention that water is the by product in the PGS synthesis. During the standard synthesis, water is

removed through vacuum, but during microwave synthesis it is not possible to remove it. Water can affect the PGS causing hydrolysis of the molecules, another reason to choose the standard over the microwave synthesis.

2.4.1 GEL PERMEATION CHROMATOGRAPHY (GPC)

The average molecular weights (by number and by weight) of the synthesized samples (standard and microwave synthesis), were calculated from the data obtained in GPC analysis before and after vacuum, using the equations 2.1 and 2.2. The results are shown in table 2.4.

Table 2.4 Average molecular weights.

Sample (time)	**Molecular weight (M_w) g/mol**		**Molecular weight (M_n) g/mol**	
	Not dry	Dry in the oven	Not dry	Dry in the oven
30 seconds	717	650	508	468
1 minute	904	770	622	541
2 minutes	1,014	905	692	625
3 minutes	911	1,007	628	695
4 minutes	938	1,174	633	764
5 minutes	992	1,017	678	692
10 minutes	1,415	1,346	921	888
15 minutes	1,538	1,662	1,032	1,113
30 minutes	1,890	2,243	1,304	1,474

1 hour	2,116	2,226	1,384	1,480
1.5 hour	1,674	2,337	1,138	1,556
Standard	23,603		7,711	

Table 2.4 shows that molecular weight (M_w) increases proportionally with reaction time; this is due to polymer crosslinking [140]. M_w and M_n are higher in samples dried in the oven. Therefore, it is assumed that the time in the oven increased the crosslinking. In comparison, the samples obtained through standard synthesis have higher Mw and Mn.

Theoretical number average molecular weight (M_n) and weight average molecular weight (M_w) for standard synthesis were 7,711 g/mol and 23,600 g/mol, respectively. The results are comparable with other studies where PGS was synthesised under the same conditions (24 hr at 120 ºC). Nijst et al. obtained polymer with an average molecular weight (M_w) of 23 000 g/mol, a number average molecular weight (M_n) of 6500 g/mol and a dispersity index (DI) of 3.5 [131] .

Samples synthetized in microwave showed lower number average molecular weight (M_n) from 770 to 2,337 g/mol and weight average molecular weight (M_w) from 541 to 1556 g/mol which increased as the reaction time increased. The results obtained in the microwave synthesis are also comparable with previous studies carried out under the same conditions (1.5 hr at 180ºC). Mogosanu et al. reported an average molecular weight (M_w) of 3600 g/mol.

The index of heterogeneity or dispersity index (DI) is used to measure the amplitude of the molecular weight distribution of a polymer chain. The values of the dispersity index close to unity represent a great homogeneity of molecular weights (monodisperse polymer) [141]. A DI with a value of 1 means that all the chain lengths are equal and is only observed in proteins and nucleic acids. Polymers with a dispersity

index close to unity have better properties than those with an index much higher than unity. The best controlled synthetic polymers have a PDI of 1.02 to 1.10 [142].

The table 2.5 shows the dispersity for each sample synthesised in the microwave reactor and standard protocol.

Table 2.5 Dispersity Index for PGS prepolymer samples.

Samples	Not dry	Dry in the oven
30 seconds	1.41	1.39
1 minute	1.45	1.42
2 minutes	1.47	1.45
3 minutes	1.45	1.45
4 minutes	1.48	1.54
5 minutes	1.46	1.47
10 minutes	1.54	1.52
15 minutes	1.49	1.49
30 minutes	1.45	1.52
1 hour	1.53	1.50
1.5 hour	1.47	1.50
Standard	3.06	-

PGS synthesis is carried out with equimolar quantities of the monomer's reaction (sebacic acid and glycerol). Due to this, the reaction in theory should produce a linear

polymer. The maximum value of the DI is 2, which occurs at a monomer conversion of 100%. This is true for step-growth polymerization of linear polymers.

Dispersity index was 3.6 in the standard reaction compared to a range from 1.39 to 1.5 in the microwave reaction, which increased as the reaction time increased. Results obtained were comparable with other studies where PGS prepolymer was synthesized using a equimolar ratio of glycerol and sebacic acid [108,114,115,131,133,138,139]. However, there is not any report about DI in samples synthesized in the microwave. The equimolar amount of the glycerol and sebacic acid (1:1) favours polymer chain extension over chain branching as reaction duration increases, due to the increased reactivity of the two primary hydroxyl groups of the glycerol monomer compared to its secondary hydroxyl group [3]. Chain branching is undesirable in this study, as this has been shown to reduce the solubility of the prepolymer, limiting further functionalisation and processing.

2.4.2 SWELLING

Hydrophilicity in a material allows cell adhesion and proliferation, making it a crucial parameter for biomaterials and its use in tissue engineering[113,114]. Swelling by hydration was measured in the samples using PBS and media. There was no significant difference on swelling in media and PBS for each DM. PGS-M with different DM showed minimal water uptake between samples with over 30% DM (Figure 2.12).

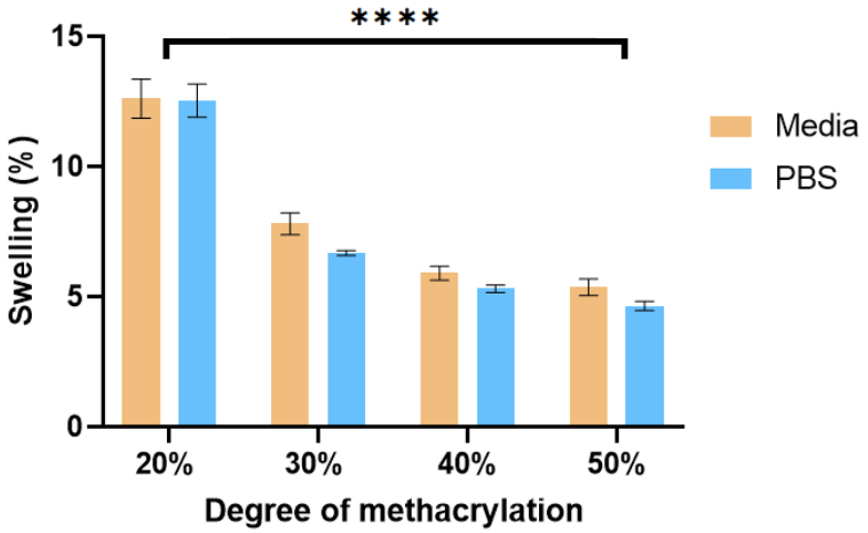

Figure 2.12 Effects of DM on swelling by hydration in media and PBS. Samples show means and error bars corresponding to ±SD (N=3, n=3), analysed by two-way ANOVA, Tukey's post-hoc pairwise comparison. P≤0.05 was considered significant.

There is no previous information about PGS-M swelling by hydration, but there is information about PGS. Liang et al. observed a water swelling of 0.36% while Yang et al. reported a swelling of 3.82% and 3.41% in water and PBS, respectively [143,144]. Some studies report that the modification of PGS with the addition of Bioglass or PEG may increase the swelling in water [126,143]. However, swelling significantly decreases from 13% ± 0.55% to 5% ± 0.19% as DM increases from 20% to 50% in PGS-M (P<0.0001).

The swelling properties in organic solvents are also important for the processing of PGS-M. The amount of sol and gel content in PGS-M scaffolds was determined by methanol swelling (Figure 2.13).

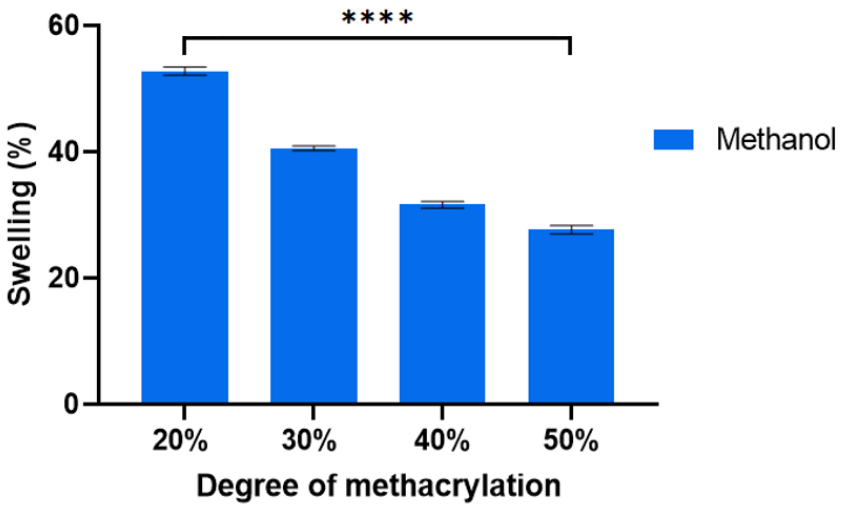

Figure 2.13 Effects of DM on swelling in methanol. Samples show means and error bars corresponding to ±SD (N=3, n=3), analysed by one-way ANOVA, Tukey's post-hoc pairwise comparison. P≤0.05 was considered significant.

Similarly, there is no previous information about PGS-M swelling in organic solvents or PGS in methanol. Although information regarding PGS swelling in methanol has not been reported yet, there is some data in swelling in THF (from 587 to 630%) [115,117]. The increase of DM results in a lower swelling degree, decreasing from 52.79% ± 0.57 (20% DM) to 27.64% ± 0.65 (50% DM) (P<0.0001).

2.4.3 GEL CONTENT (DEGREE OF CROSSLINKING)

The percentage of gel content shows the degree of the crosslinked network. The gel fraction increases as the DM rises from 60% ± 0.28% to 93% ± 0.41% for 20% DM to 50% DM, respectively. This is due the higher number of methacrylate groups attached at PGS molecule that increase the degree of crosslinking and the amount of ester bonds within the molecule, which make the polymer chains longer. In contrast, unbound chains can be found in PGS-M with low DM, resulting in a lower gel content.

The statistical analysis shows that all the samples are significantly different ($p<0.0001$) (Figure 2.14).

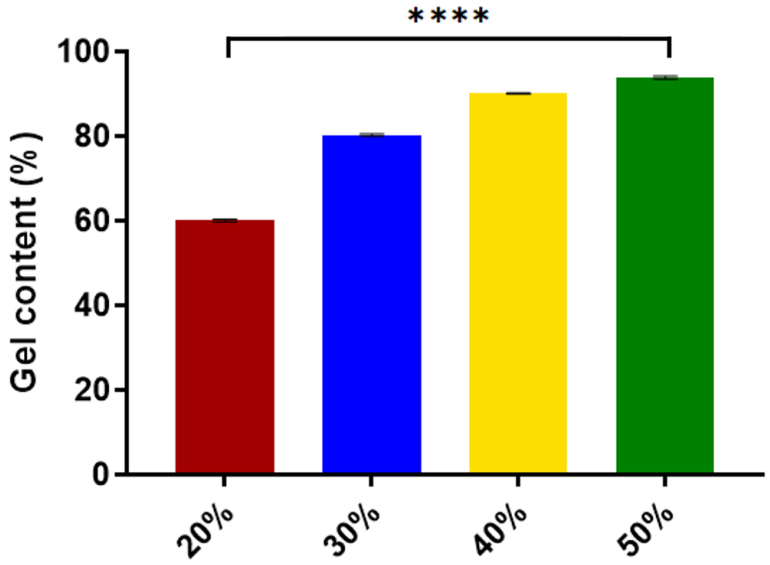

Figure 2.14 Effects of DM on the degree of gel content. Samples show means and error bars corresponding to ±SD (N=3, n=3), analysed by one-way ANOVA, Tukey's post-hoc pairwise comparison. P≤0.05 was considered significant.

A range of values have been reported for gel content (60.3% to 80.2%), but these are for thermally crosslinked polymers, not photopolymerised matrices like PGS-M [92,100,117]. The results in this study are comparable with the results obtained for Pashneh-Tala el al., who reported a gel content of 72.6% for PGS-M with a DM of 30%.

2.4.4 SOL CONTENT

The sol content is the un-crosslinked network in the scaffold. The sol content decreases as the DM increases from 39.95% ± 0.29% to 6.16% ± 0.41% for 20% DM to 50% DM, respectively. This is caused by the higher number of methacrylate groups attached to PGS molecule which increased the degree of crosslinking network, and the amount of ester bonds within the molecule that make the polymer chains longer. Therefore, unbound chains in low DM result in a higher sol content. The statistical analysis show that all the samples are significantly different ($P<0.0001$) (Figure 2.15).

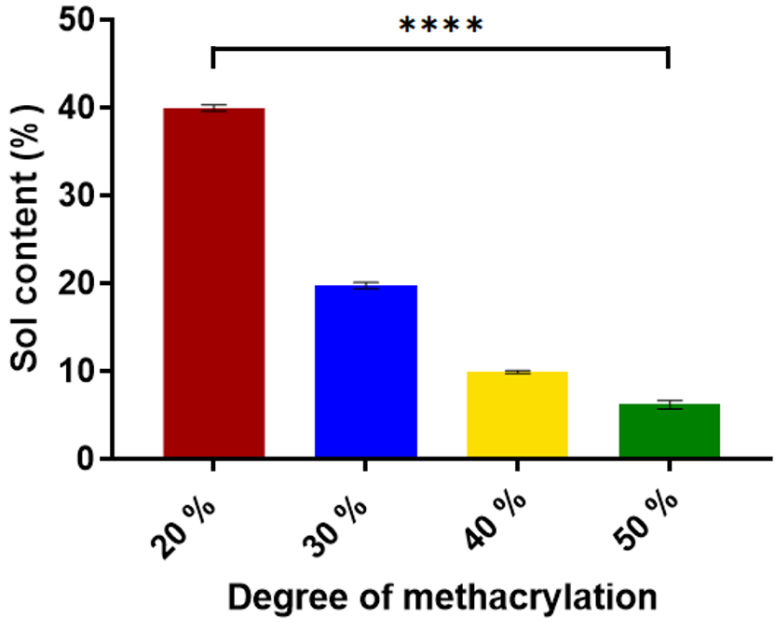

Figure 2.15 Effects of DM on the sol content percentage. Samples show means and error bars corresponding to ±SD (N=3, n=3), analysed by one-way ANOVA, Tukey's post-hoc pairwise comparison. P≤0.05 was considered significant.

These results are comparable with those reported by Pashneh-Tala el al., showing a sol content of 27.4% for DM of 30%.

2.4.5 ATTENUATED TOTAL REFLECTANCE FOURIER TRANSFORM INFRARED SPECTROSCOPY (ATR-FTIR)

- pPGS

PGS molecular structure and the effect of synthesis technique (standard/microwave) were analysed by ATR-FTIR. Intense OH stretching shows a broad peak in the range of 3480–3419 cm^{-1} [138]. Peaks related with alkane ($-CH_2$) groups were present at 2924 cm^{-1} and 2851 cm^{-1} and methyl ($-CH_3$) bending appeared at 1354–1456 cm^{-1} [138,145]. The intense C=O stretches appeared at 1730 cm^{-1} and confirmed the formation of ester bonds (Figure 2.10), which means that the resulting polymer is a polyester [5]. The peaks present around 1291-1050 cm^{-1} where associated with the stretch vibrations of COOH bonds [130], [138].

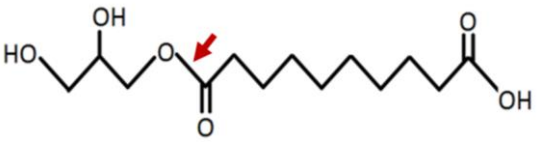

Figure 2.16 PGS prepolymer ester bonds.

The ATR-FTIR spectra were analysed to compare if there is a significant difference in the molecular structure of the PGS depending on the method of synthesis (standard/microwave). Figure 2.17 shows the spectra of PGS standard and microwave synthesis.

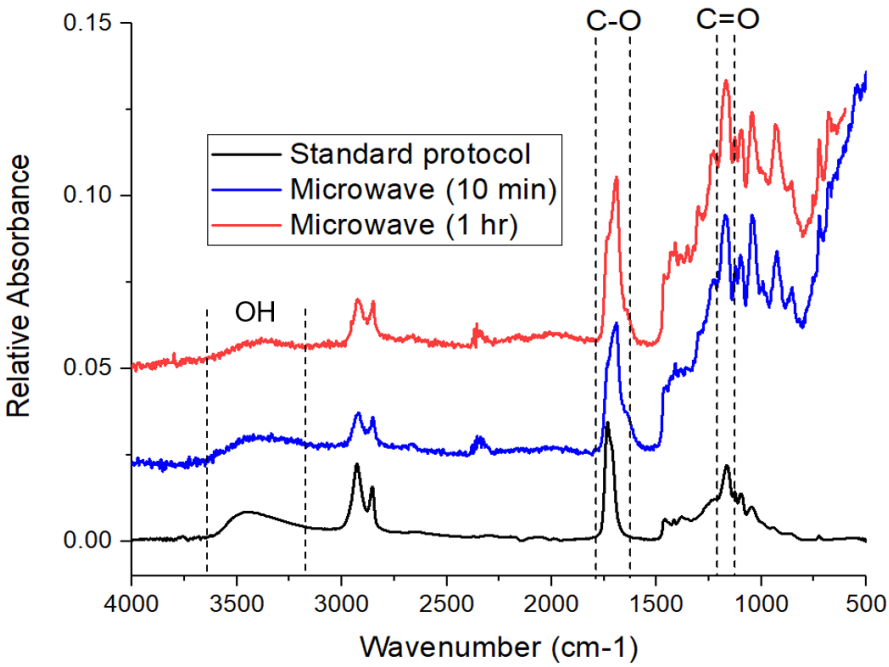

Figure 2.17 ATR-FTIR spectra of PGS polymer standard and microwave synthesis (10 min and 1 hr).

The absorption bands of hydroxyl groups become weak or disappear as reaction time increases (microwave). In turn, the peaks at 1170 cm^{-1} and 1700 cm^{-1} for ester bonds become stronger as a result from their formation [138].

Currently, there are few research articles that report PGS synthesis by microwave synthesis. Aydin et al. reported differences observed in the ATR-FTIR spectra at the

wavelengths of 1159 cm^{-1} and 1740 cm^{-1}, corresponding to the formation of C-O and C=O bonds. The observed differences were due to changes in the molar composition of the reagents from the starting molar composition sebacic acid: glycerol (100:100 to 78:22) [125]. In contrast, Li et al. reported that there were no significant differences in their ATR-FTIR spectra for microwave and standard synthesis, based on comparing samples with similar degrees of esterification. The degree of esterification (DE) increases the intensities of the C=O bond induced peaks, whereas peaks from O-H bonds decrease. This shows an increase in density of crosslinks and the formation of ester bonds [130]. Therefore, they concluded that the two polymerization methods did not induce a difference in molecular bonding.

The differences in the standard and microwave synthesis ATR-FTIR spectra is explained by the change in the molar composition of the reactants at the end of the reaction. The microwave polymerisation is faster than standard synthesis due to the higher temperatures used during the reaction. The boiling point of glycerol is 290°C, which contributes to its evaporation during synthesis in microwave and it has been shown that sebacic acid degradation starts at 180º C [146].

The results showed by Aydin et al. and Li et al. were carried out in a conventional microwave oven with short synthesis time. In contrast, the oven used in this project is a microwave reactor, where the synthesis conditions are more controlled. Due to the lack of data regarding this new synthesis methodology, it is necessary to carry out more analysis to corroborate if there is a significant difference between the synthesized PGS structures synthesized in the standard and the microwave reactor synthesis.

Figure 2.18 shows the spectra of samples obtained by microwave synthesis with the increment in reaction times from 30 seconds to 1.5 hours compared with the standard synthesis.

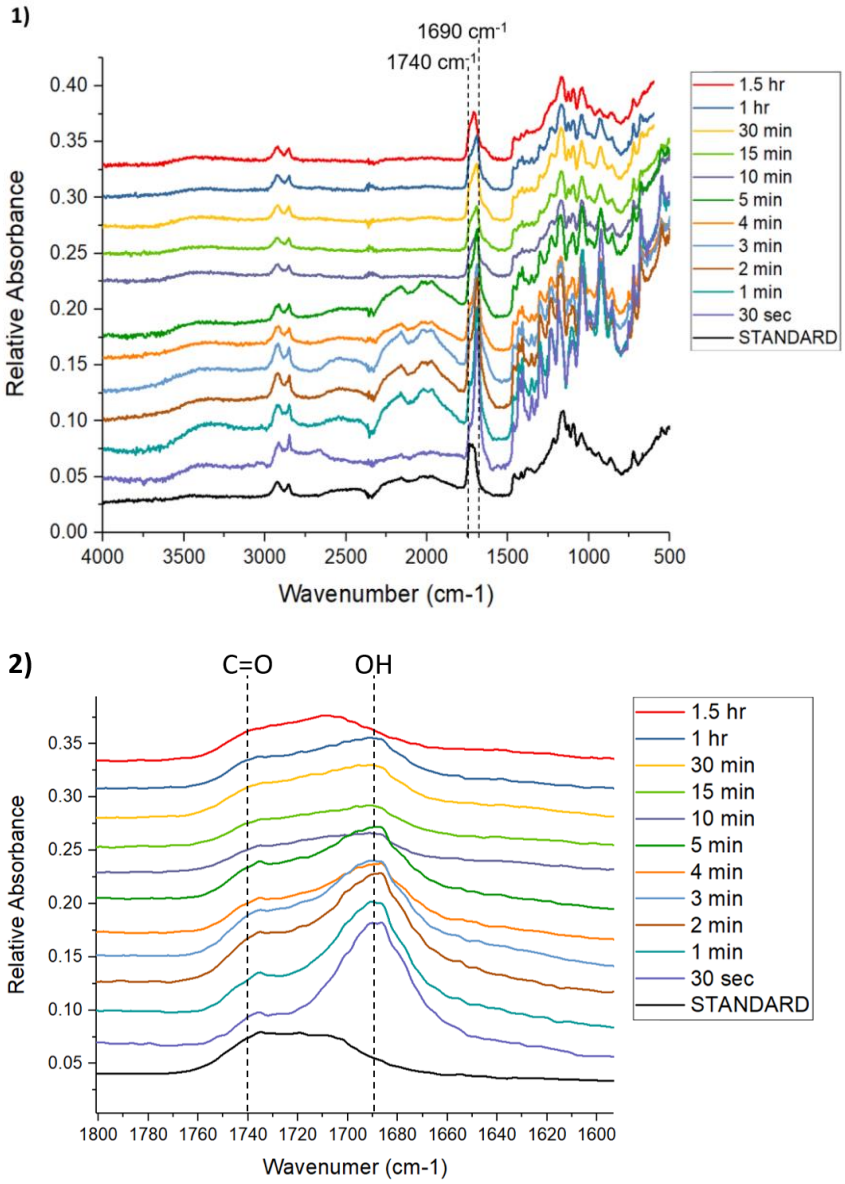

Figure 2.18 1) ATR-FTIR spectra for PGS samples synthesised in the microwave reactor for different time lengths compared with standard synthesis. 2) Zoom of the absorption of the esterified (1740 cm^{-1}) and non-esterified carboxyl groups (1690 cm^{-1}).

The figure 2.18 shows the peaks that change during the increase of reaction time. The main change is the increment of peaks at 1170 cm^{-1} and 1700 cm^{-1} for ester bonds. These changes result from formation of ester bonds[138] .

Peaks in 1740 and 1690 cm^{-1} are related with the absorption of the esterified and non-esterified carboxyl groups (carboxylic ester groups and the carboxylic acid) of the PGS molecule [147]. The degree of esterification was calculated using the area under these peaks (equation 2.9) [148].

$$DE = \frac{A_{1740}}{A_{1740} + A_{1690}} x\ 100$$

Equation 2.9 Degree of esterification

Table 2.6 shows the results of DE from the samples synthesised by standard and microwave synthesis.

Table 2.6 DE of samples synthesized in microwave in different times in comparison with standard synthesis (n=3).

SYNTHESIS METHOD	REACTION TIME	DEGREE OF ESTERIFICATION (%)
Microwave	1.5 hr	53.12 ± 1.61
Microwave	1 hr	52.93 ± 1.28
Microwave	30 min	52.55 ± 1.51
Microwave	15 min	52.15 ± 1.18
Microwave	10 min	52.03 ± 1.17
Microwave	5 min	51.25 ± 1.66
Microwave	4 min	49.86 ± 1.65
Microwave	3 min	49.55 ± 1.40
Microwave	2 min	48.21 ± 1.27
Microwave	1 min	42.15 ± 3.76
Microwave	30 sec	38.91 ± 1.31

Standard	24 hr	55.38 ± 1.36

The degree of esterification (DE) was calculated to track structural changes during the microwave reaction in comparison with the standard method. DE showed an increase as the reaction time in microwave increases, with higher DE obtained during microwave reaction (53.12 ± 1.61%) being close to the one obtained with the standard synthesis (55.38 ± 1.36%). Therefore, the microwave reaction is an efficient method for the ester bond formation in the PGS synthesis. There is no significant difference between the samples synthesized in the microwave from 3 to 90 minutes compared to the sample obtained with the standard synthesis.

The figure 2.19 shows the spectra of microwave samples after 30 minutes in vacuum at 150 °C to remove the by- product (water). The changes in the spectra were analysed by comparing the main peaks and DE.

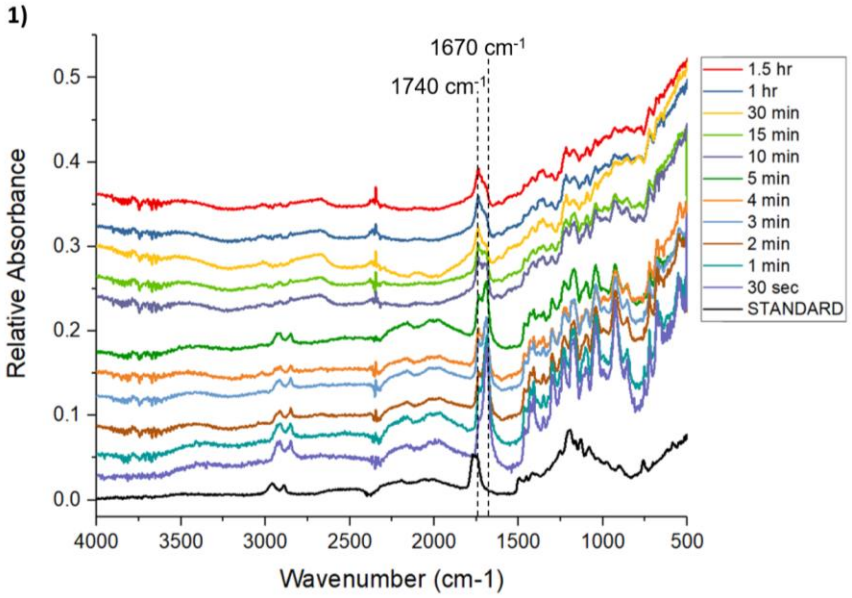

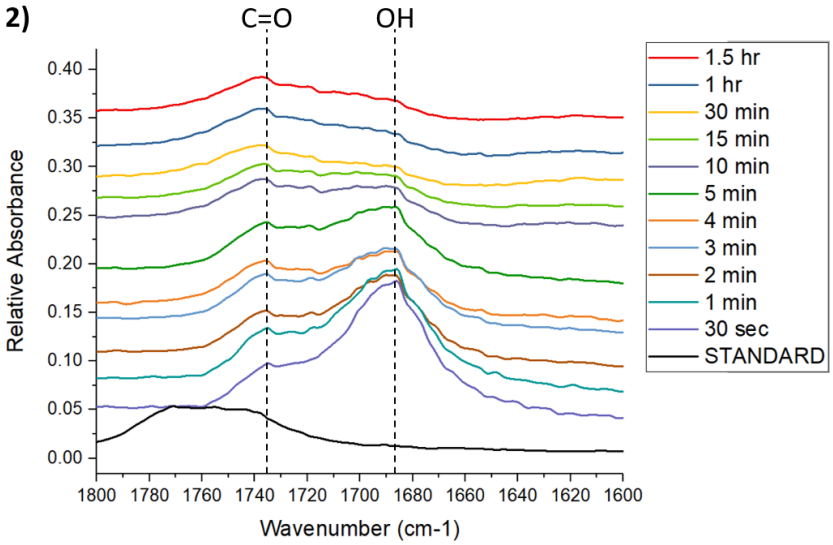

Figure 2.19 1) ATR-FTIR spectra for PGS samples synthesised in the microwave reactor after vacuum. 2) Zoom of the absorption of the esterified (1740 cm^{-1}) and non-esterified carboxyl groups (1670 cm^{-1}).

The main change in figure 2.19 lies mainly in the change in peak at 1740 cm^{-1}, which becomes higher while the peak at 1670 cm^{-1} weak or disappears. The peak at 1740 cm^{-1} is characteristic of the stretch of C=O, confirming the formation of ester bonds. Table 2.7 shows the DE calculated after vacuum.

Table 2.7 DE of samples synthesized in microwave after 30 min under vacuum at 150°C (n=3).

SYNTHESIS METHOD	REACTION TIME	DEGREE OF ESTERIFICATION (%)
Microwave	1.5 hr	56.42 ± 1.48
Microwave	1 hr	55.78 ± 1.16
Microwave	30 min	55.67 ± 1.24
Microwave	15 min	54.91 ± 1.06
Microwave	10 min	54.78 ± 1.15

Microwave	5 min	54.52 ± 1.28
Microwave	4 min	53.05 ± 1.63
Microwave	3 min	52.51 ± 1.37
Microwave	2 min	50.95 ± 1.22
Microwave	1 min	47.32 ± 2.58
Microwave	30 sec	41.42 ± 1.42

All the samples increased the DE in ~3% after the additional 30 minutes in the oven at 150°C. Therefore, we can conclude that extra time under 150°C triggers the ester bond formation. Through vacuum and high temperature, the water (by-product) is being removed from the reaction, which drives the esterification reaction via le Chatelier's principle [149]. . There is no significant difference between the samples synthesized in the microwave from 3 to 90 minutes.

- PGS-M

PGS-M molecular structure and the effect methacrylation degree were analysed by ATR-FTIR. Peaks related with methacrylate groups appear at 940 cm^{-1} (=C-H bending) and 1640 cm^{-1} (C=C stretching) [150]. These peaks were absent in pPGS. The DM was comparing with the area under these peaks (Figure 2.20) (Table 2.8).

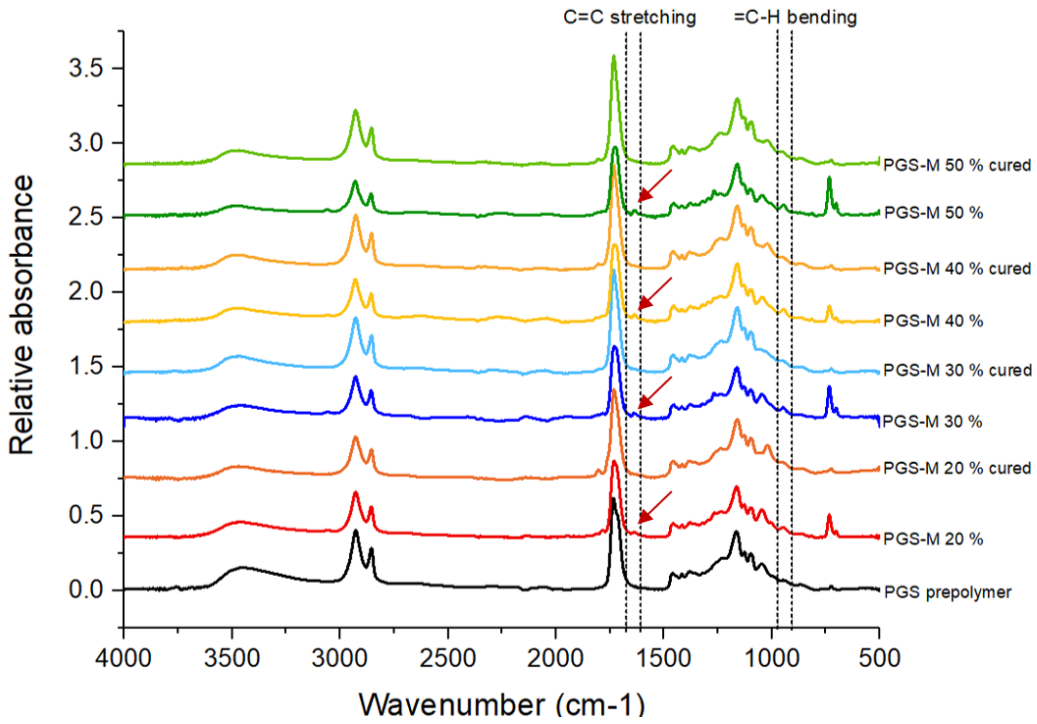

Figure 2.20 ATR-FTIR spectra of pPGS and PGS-M samples before and after curing.

Figure 2.20 shows the peaks related with methacrylate groups in PGS-M spectra in different DM (20%-50%). These peaks are absent in pPGS and they disappear after PGS-M photopolymerization.

Table 2.8 Area under the peaks related with methacrylate groups in different DM (n=3).

Degree of methacrylation	**Area**	
	Wavenumber (cm^{-1})	
	1640	**940**
pPGS	0.10	0.27
20	0.16	0.60
30	0.19	0.70
40	0.28	0.86
50	0.38	0.89

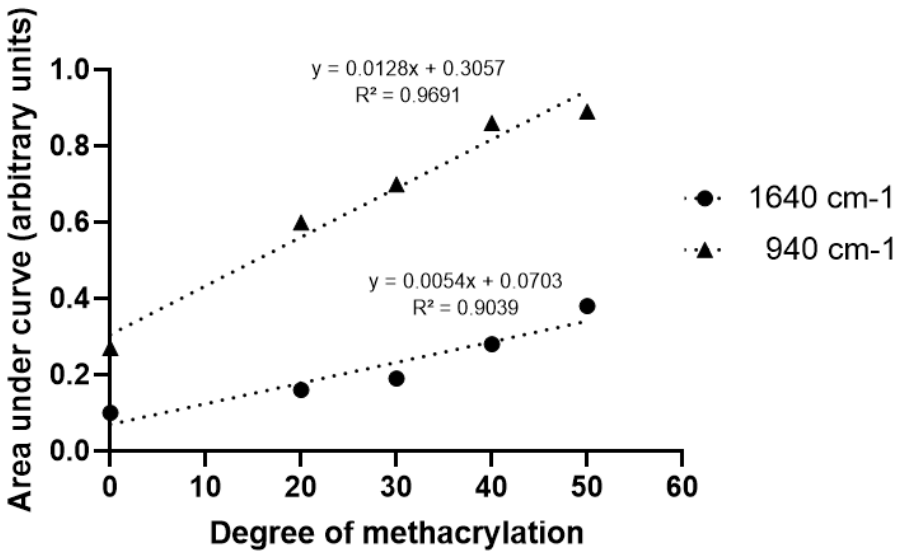

Figure 2.21 Comparison of DM with the area under the peaks related with methacrylate groups at 940 cm^{-1} and 1640 cm^{-1}. The data has a strong agreement for 940 cm^{-1} y=0.0128x+0.3057 and R^2 = 0.9691 and for 1640 cm-1 y=0.0054x+0.0703 and R^2 = 0.9039.

The area of these peaks is well correlated with the DM of the PGS-M samples, as can be observed in Table 2.8 and Figure 2.21.

2.4.6 NUCLEAR MAGNETIC RESONANCE (NMR)

pPGS and PGS-M chemical composition was estimated with NMR analysis. It was determined by calculating signal integrals of —$COCH_2CH_2CH_2$— at 1.2, 1.65, and 2.36 ppm for sebacic acid, —CH_2CH— at 3.75, 4.19, and 5.11 ppm for glycerol, and -CH_3,CH_2 at 1.97, 5.3, and 6.17 ppm for the addition of methacrylate group to the pPGS molecule. $CDCl_3$ was used as reference at 7.3 ppm. The integrals of the signal for the methacrylate groups (1.97, 5.3 and 6.17 ppm) were calculated with the software OriginPro 2017 and the obtained values correspond with the degree of methacrylation (DM) (Figure 2.22).

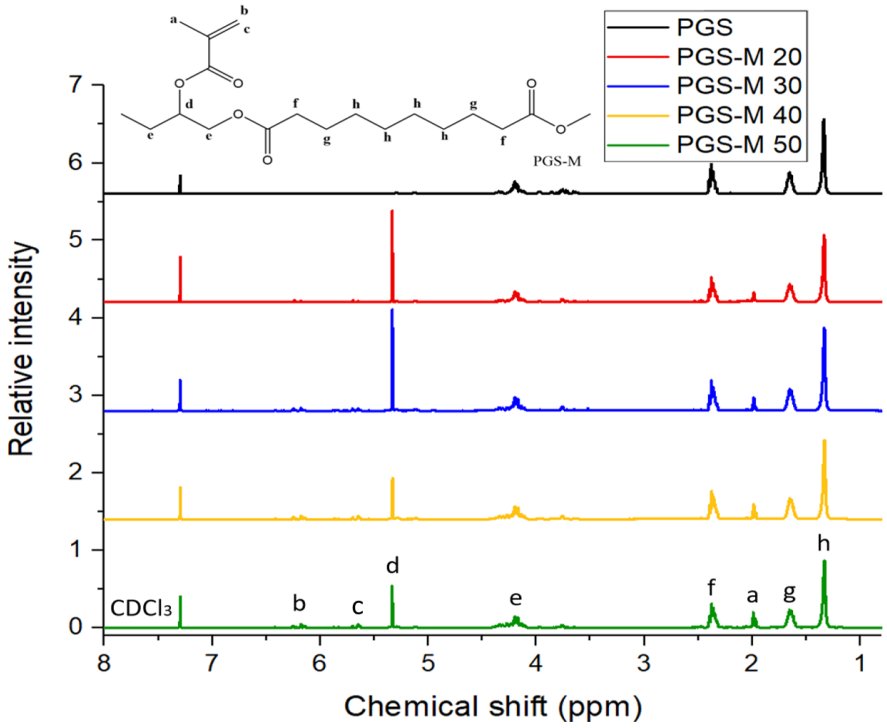

Figure 2.22 pPGS and PGS-M NMR spectra. PGS-M with different DM (20%, 30%, 40% and 50%). Hydrogen environment peaks of methacrylate groups appear at 1.97, 5.3, and 6.17 ppm, (“a”, “b” and “c”).

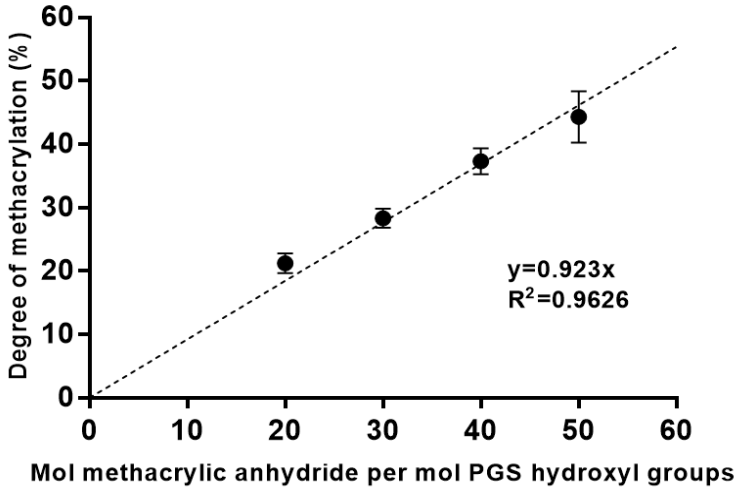

Figure 2.23 Comparison of PGS-M DM with the molar ratio of methacrylic anhydride per mol of pPGS hydroxyl groups. The data has a strong agreement y=0.923x and R^2 = 0.9626. Error bars are SD (*n* = 3).

The obtained DM has a linear relationship and is directly proportional to the molar ratio of methacrylic anhydride per mol of pPGS hydroxyl groups. The results show a correlation of y=0.923x and R^2 value of 0.9626. (Figure 2.23); from this data, we can conclude that all methacrylate groups added during the reaction are attached in the PGS-M molecule.

NMR analysis suggests that an effective pPGS methacrylation process was carried out, resulting in PGS-M with DM 20%, 30%, 40% and 50%. This can be confirmed with the appearance of peaks related with methacrylate groups that are absent in pPGS spectra. This result can be compared with the data reported by Pashneh-Tala et al. during the PGS methacrylation (DM 30%-80%). Even though the methacrylation in that study is higher, the relationship between the DM and the molar ratio of methacrylic anhydride per mol of pPGS hydroxyl groups is consistent [116].

2.4.7 MECHANICAL ANALYSIS

Tissue regeneration involves stress and load bearing in the surrounding tissue. Therefore, there should be an equilibrium between the scaffold's mechanical stability and degradation time until tissue regeneration is achieved [151,152].

Mechanical properties of scaffolds such as the degree of crosslinking and stiffness affect cell behaviour and biodegradability [153]. Ideally, scaffolds for corneal regeneration should have the transparency, elasticity, structural and functional requirements of the native cornea [39]. They should also support intraocular pressure, eyelid motion, intraocular pressure as well as external forces [154]. PGS-M mechanical analysis was carried out in order to select the degree of methacrylation that best matches the mechanical properties in the native cornea and provides appropriate mechanical signals to stimulate the production of corneal tissue [155] (Figure 2.24). The corneal scaffold should be strong enough to support deformation, but not too stiff that it stresses the surrounding tissue [9]. There is a considerable variation in the corneal tensile strength and Young's modulus reported before (strength between 3 to 6 MPa

and Young's modulus between 100 kPa to 57 MPa). These results depend on different testing mechanisms, tissue anisotropy, and donor variability [9,156,157] .

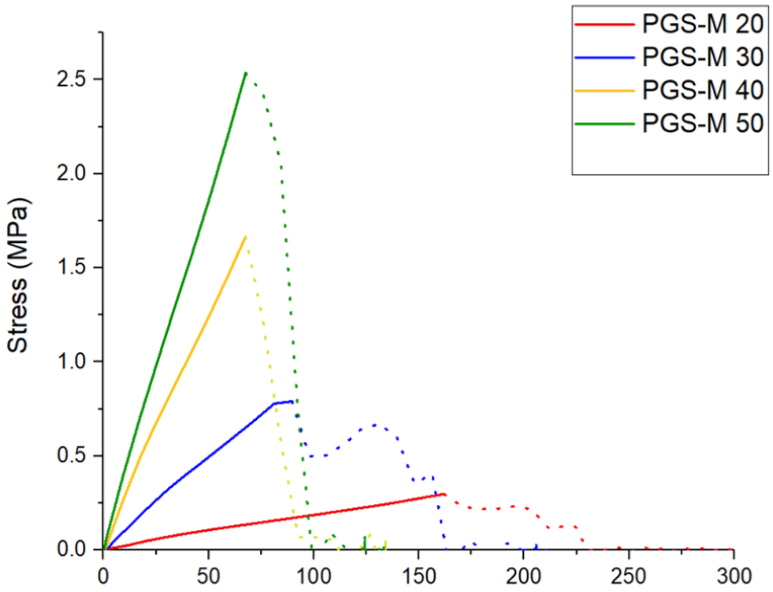

Methacrylation degree	Young`s Modulus (MPa)	Ultimate tensile strain (MPa)	Maximum elongation %
20	0.2083 ± 0.010	0.362 ± 0.025	192.54 ± 29.28
30	1.119 ± 0.179	1.145 ± 0.026	122.96 ± 15.10
40	3.109 ± 0.668	1.822 ± 0.110	75.75 ± 6.72
50	4.235 ± 0.170	2.874 ± 0.364	75.93 ± 6.58

Figure 2.24 PGS-M mechanical properties in different DM (20% - 50%). The graph is the mean of load deformation curves (n=3).

As can be seen in Figure 2.24, the Young's modulus and the ultimate tensile strain increase along with DM. However, the maximum elongation decreases as the DM increases. Therefore, PGS-M with higher DM is stiffer, which coincides with the Young's modulus increment, as it is a measurement of stiffness [158]. The ultimate tensile strain is the force applied to cause rupture; it makes sense that the values increase with the DM, because the last one is an indication that the polymer matrix is

more cross-linked [159]. The maximum elongation decreases as a result of the material being stiffer with more covalent bonds in the polymer matrix, making it more ductile [160]. From these data we can assume that the methacrylation of PGS-M enhances its mechanical properties compared with PGS (Young's Modulus of 0.17± 0.018 MPa, tensile strength of 0.264±0.025 MPa and rupture elongation of 292.8 ±14.1% [109]).

The data obtained is comparable with other studies for the development of corneal scaffolds. Duan et al. obtained a dendrimer crosslinked collagen-based scaffolds with a Young's modulus of 1.47 ± 0.1 MPa and ultimate tensile strength of 1.27 ± 0.17 N [53]. Similarly, Bakhshandeh et al. reported similar values for a poly (ε-caprolactone) (PCL) nanofibrous matrix (Young's modulus 7.5 MPa and ultimate tensile strength 2.53 ± 0.58 MPa) and polyvinyl alcohol (PVA) hydrogels (Young's modulus 5.3 MPa and ultimate tensile strength 0.85 ± 0.55MPa) [161].

2.4.8 THERMOGRAVIMETRY (TGA)

PGS-M thermal stability was determined by TGA analysis (Figure 2.25). Thermal behaviour is an important feature that determines polymer mechanical stability and degradation [162].

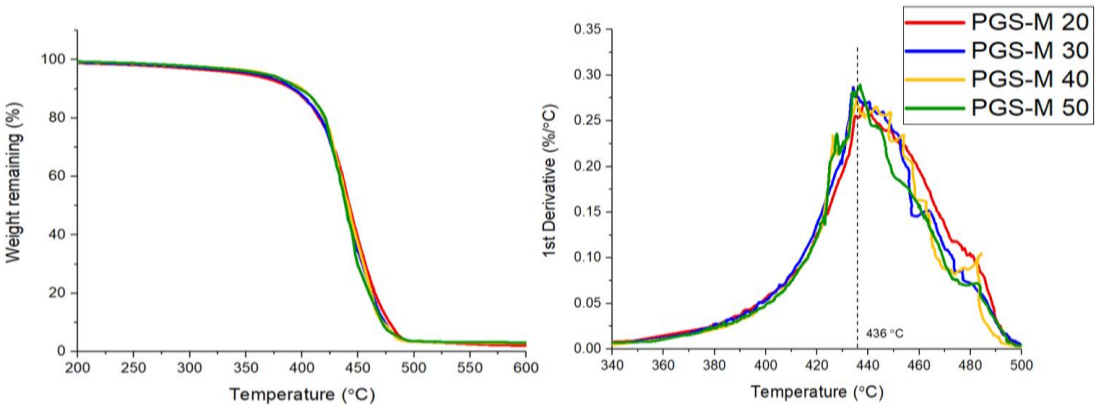

Figure 2.25 PGS-M thermal properties in different DM (20% - 50%).

Figure 2.25 shows that PGS-M started to degrade at 436º C. There is no significant difference in the degradation behaviour for the different DM. The degradation profile

of PGS-M is also comparable with the previously reported PGS profiles by Jiang et al. and Gaharwar et al. with a degradation temperature of 433 º C and 439 º C, respectively [162,163].

2.4.9 DIFFERENTIAL SCANNING CALORIMETER ANALYSIS (DSC)

PGS-M thermal transitions and crystalline behaviour were determined by DSC analysis (Figure 2.26).

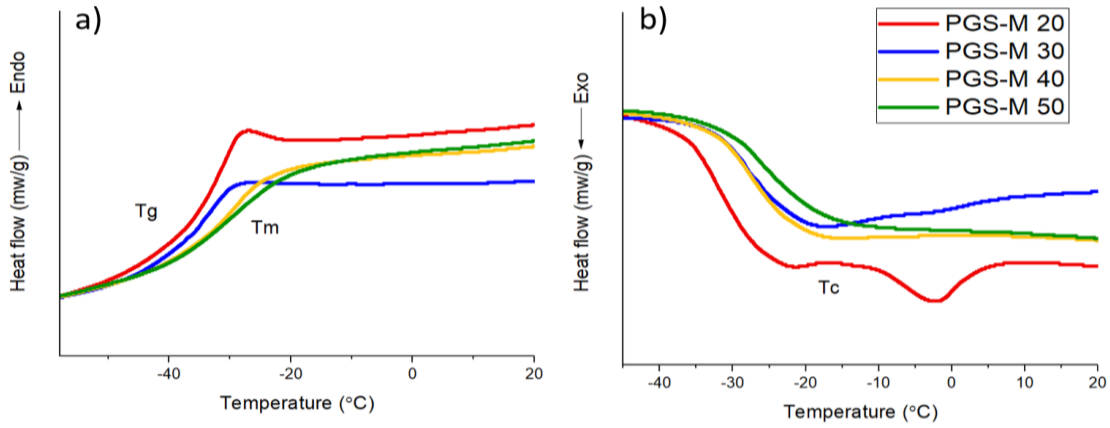

Figure 2.26 PGS-M thermal transitions and crystalline behaviour in different DM (20% - 50%) a) heating cycle and (b) cooling cycle.

Table 2.9 PGS-M thermal properties from TGA and DSC thermographs.

Sample	TDI (°C)	TDP (°C)	Tg (°C)	Tm1 (°C)	ΔHm (J/g)	Tc (°C)	ΔHc (J/g)
PGS-M 20	350	439.52	-37	-28.63	3.024	-22	1.36
PGS-M 30	360	438.71	-36.8	-28.35	2.183	-18.32	1.052
PGS-M 40	360	438.31	-34.54	-22.65	2.182	-15.79	0.936
PGS-M 50	360	433.86	-33.95	-21.10	2.048	-14.48	0.852

Figure 2.26 and Table 2.9 show the glass transition temperature (T_g) for PGS-M with different DM. The initial and peak thermal decomposition temperatures (T_{DI} and T_{DP}) were obtained from the TGA thermograph. The glass transition temperature (T_g), melting temperature (T_m), crystallization temperature (T_c), enthalpy of melting (ΔH_m) and enthalpy of crystallization (ΔH_c) were obtained from the DSC thermograph.

It was observed that Tg increases as DM increases, from -37 to -33.95 ºC. Melting points (T_m) showed a similar behaviour increasing as DM increases, from -28.63 to -21.10ºC . Enthalpy of melting decreases as DM increases from 3.024 to 2.048 (J/g). In the cooling cycle the crystallization temperature increases directly proportional with the DM from -22.00 to -14.48ºC. The enthalpy of crystallization decreases as DM increases from -1.36 to -0.852 (J/g). Similar results were reported by Singh et al. on PGS-M methacrylation with a DM of 75%, reporting a Tg of -30 ºC [117]. The low T_g (below 0 ºC) suggest that PGS-M is semicrystalline below its melting point and amorphous-elastomeric at physiological temperature. Likewise, similar results were previously reported for PGS [138,164,165,166].

2.4.10 *IN VITRO* DEGRADATION OF PHOTOCURED PGS-M

Polymeric materials used for tissue engineering should be biocompatible and bioresorbable with controlled degradation rates that match the tissue where they will be implanted [167,168]. Current polymers used for corneal regeneration have a lack of degradability and stability after implantation. The polymers for corneal regeneration are expected to be degradable biomaterials that support the wound healing processes [169]. PGS-M *in vitro* (PBS) degradation was evaluated through weight loss and SEM analysis (Figure 2.27-2.29).

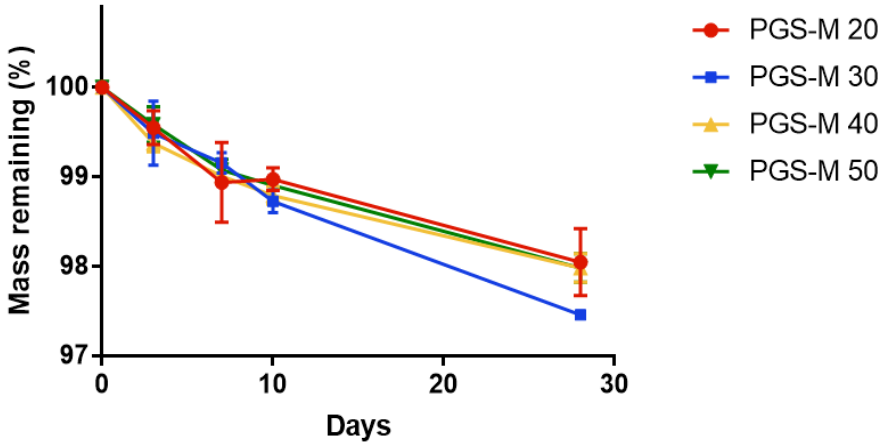

Figure 2.27 PGS-M weight loss in different DM (20%-50%).

PGS is a biocompatible polymer but has a fast degradation rate *in vivo* (around 21 days per mm thickness) and full resorption in 60 days, conditions which limit its applications [113,170]. Comparatively, PGS-M shows lower degradation rate, remaining stable *in vitro* for 30 days, and showing a degradation rate of ~3% throughout this time. It is possibly this is due to the higher degree of crosslinking in PGS-M compared with PGS. The increment in gel content indicated a higher degree of crosslinking and hence lower degradation rate [171]. Gel content for PGS has been reported around 70% [109,124,172], while gel content in PGS-M has been reported in this study as 60 to 93%, for 20% to 50% DM respectively.

PGS degradation in PBS occurs by hydrolysis, which breaks the ester bonds between glycerol and sebacic acid after extended period of time [120]. Degradation of PGS is caused by surface erosion with a linear loss of mass, which allows scaffold geometry and mechanical properties to be maintained [170,173]. In comparison, PGS-M is an amorphous polymer at physiological temperature. The amorphous region in the polymers are more susceptible to hydrolysis, but by increasing the DM, the degradation rate decreases, as it was reported by Singh et al. and Samand et al. [116,117,174]. Figures 2.28 and 2.29 show the SEM for PGS-M (20-50% DM) degradation in PBS for 0,3,7,10 and 28 days.

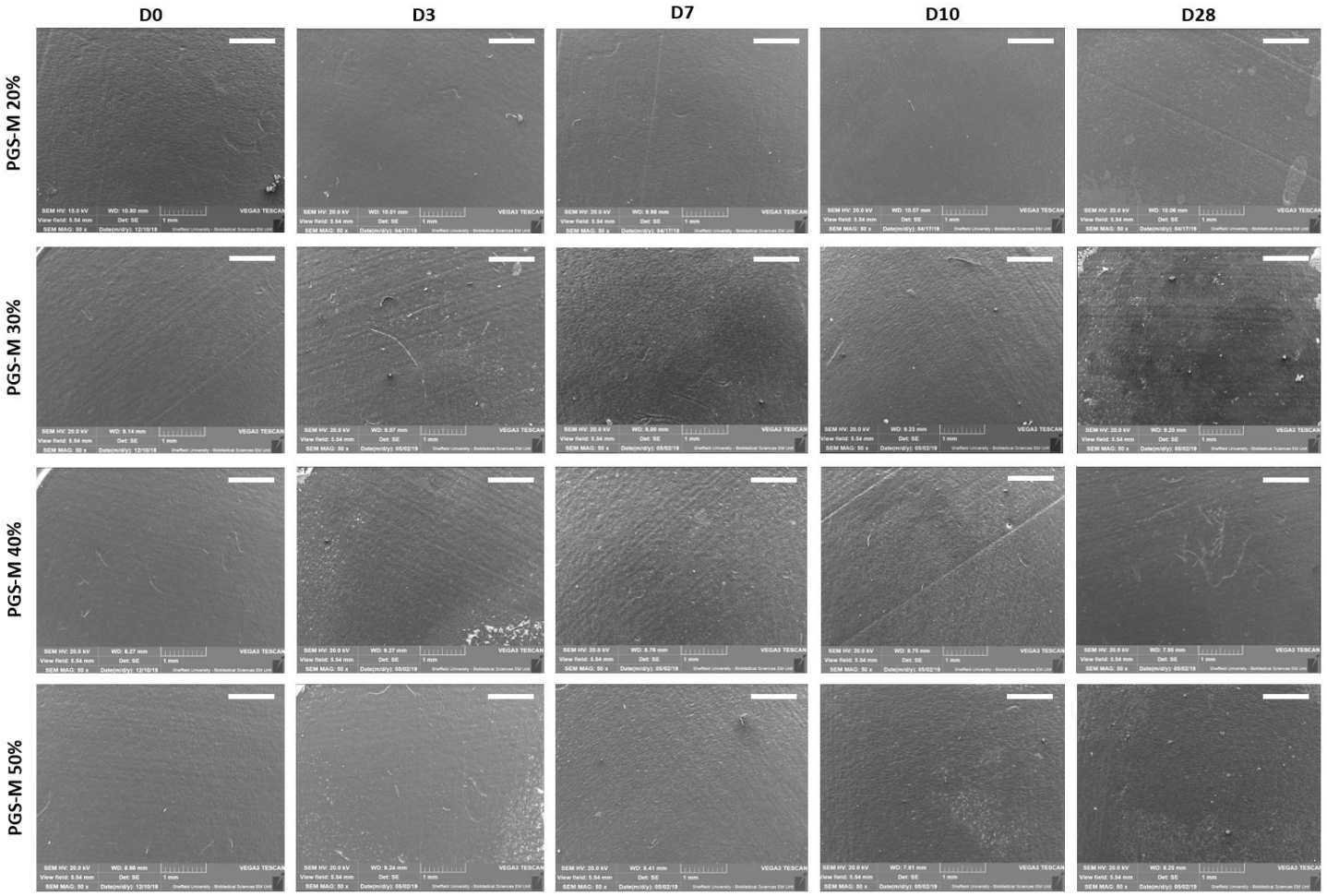

Figure 2.28 SEM for PGS-M (20-50% DM) degradation in PBS for 0,3,7,10 and 28 days (scale bar=1mm).

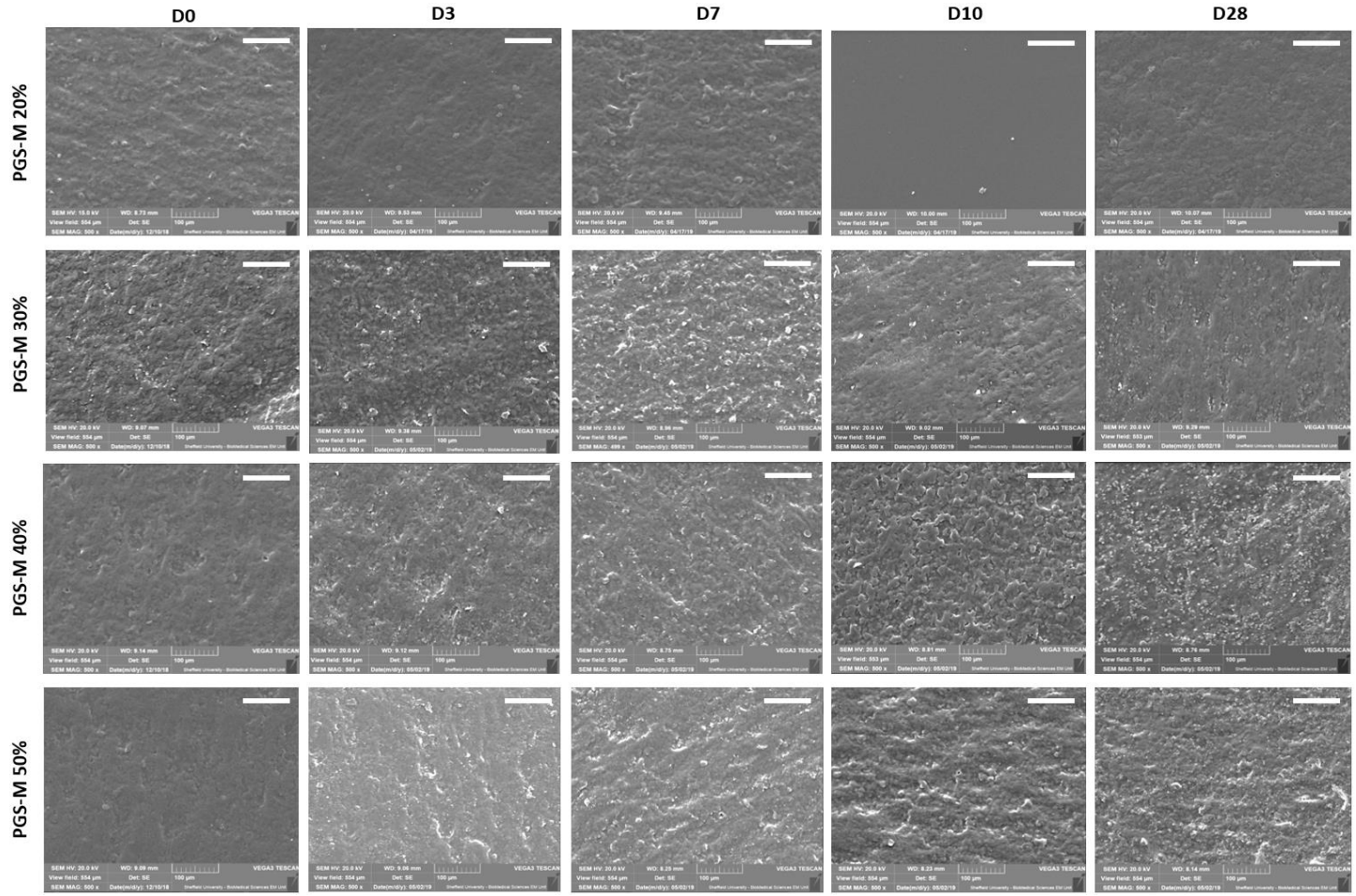

Figure 2.29 Magnification image. SEM analysis for PGS-M (20-50% DM) degradation in PBS for 0, 3, 7, 10 and 28 days (scale bar=100 μm).

In figure 2.28 and 2.29, it is possible to observe that PGS-M has no significant mass loss in PBS. The addition of methacrylate groups increases the degradation time compared with PGS, with PGS-M showing degradation by surface erosion. This results in a small reduction of strength and structure. Therefore, the PGS-M scaffold maintains its integrity throughout the degradation process. Similar degradation rates of PGS-M in PBS were reported before by Singh et al. and Pashneh-Tala et al. [116,117].

2.4.11 SURFACE ANALYSIS

- CONTACT ANGLE

PGS-M hydrophilicity was measure with sessile drop method method (Figure 2.30)

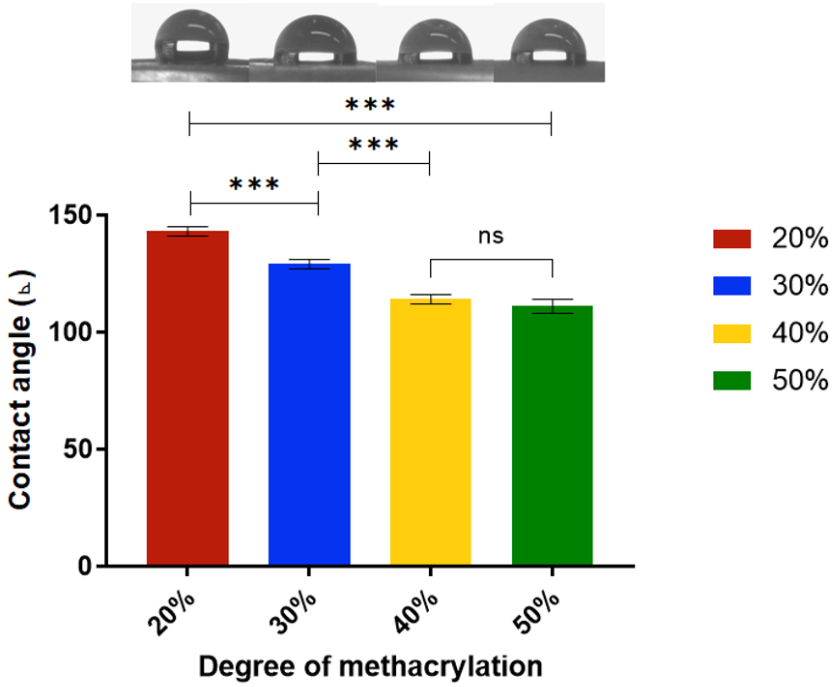

Figure 2.30 Contact angle measurements in deionized water of PGS-M (20-50%). Samples show means and error bars corresponding to ±SD (N=3, n=3), analysed by one-way ANOVA, Tukey's post-hoc pairwise comparison. P≤0.05 was considered significant.

Figure 2.30 shows that contact angle decreases as DM increases from 143 to 111° for 20 to 50% DM, respectively. PGS has previously been reported to have good hydrophilicity (~37°) [112,124]. This is due to the OH groups attached to its molecule. The methacrylation of PGS is carried out by adding methacrylate groups in the OH groups, which reduces their number. In addition, methacrylate groups promote matrix crosslinking, further reducing OH group exposure. Thus, PGS-M is more hydrophobic than PGS.

2.5 CONCLUSION

PGS was synthesized by microwave and standard reactions. The microwave synthesis was faster and a more monodisperse polymer was obtained (DI 1.5) compared to the polydisperse polymer obtained with the standard synthesis (DI 3.06). During the standard synthesis, it is possible to obtain a polymer with a higher Mn and Mw. In addition, the standard synthesis allows to scale PGS-M production, while the microwave reaction has a maximum yield of 20 g. Another disadvantage found during the microwave synthesis is that at the end of the purification only 2 g of PGS-M were obtained, which were impossible to cross-link them due to the high viscosity of the polymer. Therefore, the microwave synthesis was discarded in favour of the standard synthesis.

PGS-M with different degrees of methacrylation was successfully synthesized through the standard synthesis for evaluation as a biomaterial for corneal regeneration. The physicochemical properties of the polymer were analysed using different characterization techniques. Based on the data, the DM with mechanical properties that better matched the native cornea and with the lower percentage of sol content was 40%.

During chemical characterisation (FTIR and NMR analysis), the addition of methacrylate groups was confirmed.

The degradation of PGS-M was only carried out *in vitro* (PBS): further evaluation is still necessary under physiological conditions that resemble the physiological environment. The PGS-M low degradation rate has advantages for biomedical applications, such as stable long-term implants that keep their shape, low risk of uncontrollable degradation, and unvarying mechanical properties. The optimization of PGS-M degradation rate opens a new area of research for using different techniques that allow the synthesis of PGS-M scaffolds with different physical characteristics. In comparison to the bulk material which undergoes surface degradation, structures such as fibres and pores may allow a more uniform degradation both within and throughout the scaffold. In addition, the combination of PGS-M with other polymers with better biodegradability such as PLA, PGA, and PHB, could positively impact its degradation rate, and are certainly an area of interest that can be explored in further work.

Hydrophilic evaluation resulted in PGS-M being a more hydrophobic polymer than PGS, indicating its biocompatibility still needs to be studied to determine suitability as a material for soft tissue engineering such as cornea.

CHAPTER 3. MANUFACTURE OF PGS-M SCAFFOLDS

3.1 INTRODUCTION

The synthesis of PGS-M with low degrees of methacrylation and its physicochemical characterization was successful, as shown in Chapter 2. During characterization, 40% DM was the one with the best characteristics due to its low percentage of sol content and mechanical properties like those of the cornea.

As previously mentioned, the development of materials with micro features for the use in cornea regeneration remains an area of opportunity. In this Chapter, stereolithography and moulding will be explored as methods of creating highly modified niches and architectures that mimic the shape of the corneal dome. PGS-M with a DM of 40% will be used to manufacture transparent and porous scaffolds for further biological evaluation.

3.1.1 CORNEA STRUCTURE, CURVATURE AND STIFFNESS

The development of a biomaterial for cornea requires prior knowledge of the tissue. The biomaterial should mimic the corneal native structure, and this means the inclusion of in-built artificial stem cell niches. The scaffolds should have the appropriate curvature, architecture and stiffness to ensure cell survival, proliferation, migration, and lead the regeneration of damaged tissue [71].

Gouveia et al. reported the importance of surface curvature as the key element to promote corneal stromal cells alignment, phenotype, and induce ECM production. Cell migration through the cornea is centripetal and homogeneous from the bottom to the top [175]. This cell alignment contributes to the physicochemical properties of the cornea [176].

According to the work published by Foster et al., the differentiation, homeostasis, phenotype, and physiological maintenance of LESC's can be controlled by material

stiffness [177,178]. The physical stimuli surrounding the cell (such as the material-cell interaction) generates a biological response that is defined as mechanotransduction [179]. The mechanotransduction induces LESC's centripetal migration and differentiation [180,181]. At the base of the central cornea is Bowman's layer, a rigid substrate that is absent in the limbus [182,183]. Hjortdal et al. reported that central cornea (stiffer substrate) attracts basal limbal cells leading to cell differentiation and migration, while the cells in limbus (soft substrate) remain undifferentiated [184]. (Figure 3.1).

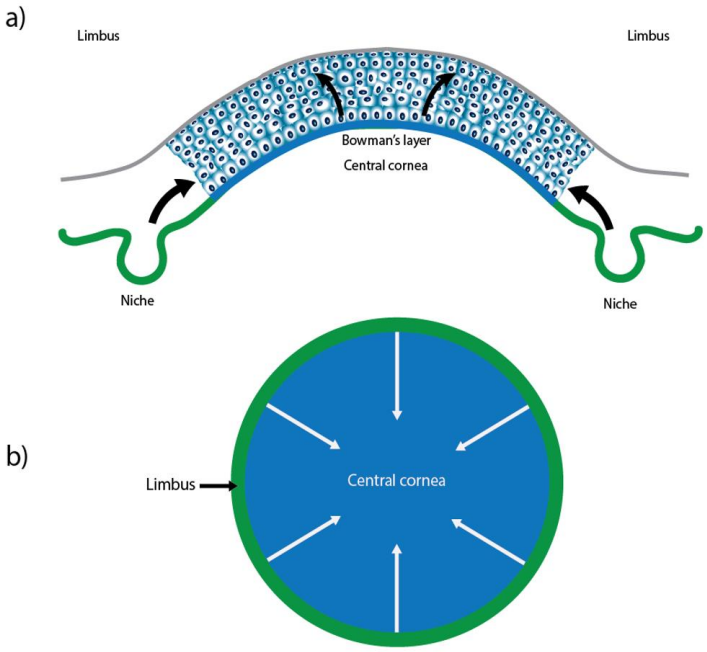

Figure 3.1 a) Limbus with undifferentiated cells (green) and central cornea (blue). The limbal cells migrate from limbus (soft substrate) to the central cornea (stiff substrate). b) Centripetal cell migration, starting from the outer limbus into the central cornea.

There have been attempts to replicate the microstructure of the corneal niches using different techniques and materials. Ortega el al. use microstereolithography and electrospining with PEGDA and PLGA achieving niches with 150–300 μm in diameter but without achieving high definition of the microstructures [3,23,40,83]. Likewise, Levis et. al. used Real Architecture For 3D Tissue (RAFT) with collagen generating scaffolds

with micro-ridges of ~100µm wide, however the structure was not defined [17,185]. Apart from these works, there have not been reports of highly defined microstructures that mimic corneal niches. Other works have reported the influence of various micro and nano structures in human mesenchymal stem cells (hMSC's) behaviour. Kawano et al reported how Polystyrene was cast to obtain honeycomb shaped scaffolds, the topography has influence on cell morphology and differentiation [186]. Fu et al reported how micropost arrays fabricated through high-resolution photolithography and deep reactive ion-etching (DRIE) influence cell morphology, migration, adhesion and differentiation [187]. On the other hand, Dalby et.al. report how PMMA nanotopographies (~10 nm) made with electron beam lithography (EBL) promoted cell adhesion and differentiation [188].

3.1.2 CORNEAL TRANSPARENCY

Transparency is a desirable characteristic when talking about the development of a biomaterial for the cornea. The transparency in the cornea is mainly due to the structure and organization of the parallel collagen fibrils, its lattice-like structure which reduces the scattering of light that passes through the cornea, the number of proteoglycans in the stroma, the space between the collagen fibrils, their diameter and packing, and is also age dependent [176,189–191].

Quantitative representation of the corneal transparency is an "insensitive" test according to Maurice (2001) due the inconsistent results that are obtained [192]. This is mainly due to the variability of the tissue and the sample processing when the analysis is performed (as the shape and tension in which the cornea is held when making the measurement). The experimental method also requires passing a defined beam of light through the tissue while subtracting the absorption and dispersion. In addition, the angle of the detector must be suitable for avoiding forward scattered light [191,193–195]. Therefore, the transparency in the cornea is multifactorial, making it difficult to quantify and establish a "standard" predetermined range or value for this tissue.

3.1.3 PGS-M VARIATIONS

- Transparent PGS-M

The main function of the cornea is the transmission and refraction of light, which is possible due to its structure and transparency [196]. One of the biggest challenges until now is the development of suitable transparent material for corneal regeneration.

Transparency is a key factor in corneal replacements, making it a feature to be sought during the manufacture of materials for corneal regeneration [37,197]. Previous reports for corneal replacements show results in transparency close the cornea, with the use of natural polymers like collagen, gelatin, silk, alginate, and their blends with synthetic polymers. However, there are no previous reports on corneal cell carriers with pure synthetic materials that present transparency similar with the native cornea [89,198–202].

- Polymers synthesized within high internal phase emulsions (PolyHIPES)

Porous materials are particularly interesting for tissue engineering due to their 3D architecture that mimics the ECM [203]. The porosity and architecture are related with the target tissue, cell type and environment. These features are able to generate a cell response (such as cell migration, vascularisation, and tissue growth) [151,204].

Porous scaffolds can improve scaffold performance and promote tissue regeneration. However, one of the main obstacles for porous materials is the lack of interconnectivity between pores. This challenge can be overcome with the use of highly interconnected porous structures with high internal phase emulsions (HIPEs), defined as PolyHIPEs [205]. The porosity in polyHIPEs is more than 74% of its volume (internal phase - water in oil (w/o)) and is dispersed in the external phase (monomers) [206,207,208]. The pore size distribution is in the range of 5 to 100 µm, based on the synthesis conditions and processing [209].

PolyHIPEs are synthesized through free radical polymerisation. The external phase is emulsified in water with a surfactant and the polymerization is carried out with a water-

soluble radical initiator. In this study, a photoinitiated polymerisation was carried out using a suitable photoinitiator [210].

3.2 OBJECTIVES

3.2.1 GENERAL OBJECTIVES

Design and manufacture a cell carrier with PGS-M based on a micro-fabricated biodegradable scaffold with in-built artificial microenvironments.

3.2.2 SPECIFIC OBJECTIVES

- Develop a transparent (that allows to see through it). PGS-M scaffold with tunable mechanical properties
- Develop a porous scaffold with PGS-M polyHIPEs with tunable mechanical properties
- Fabricate scaffolds with microenvironments (in-built niches) that mimic the niches in the limbus through the use stereolithography and moulding
- Design scaffolds with native corneal curvature that maintains its shape by itself without collapsing

3.3 MATERIALS AND METHODS

METHODS

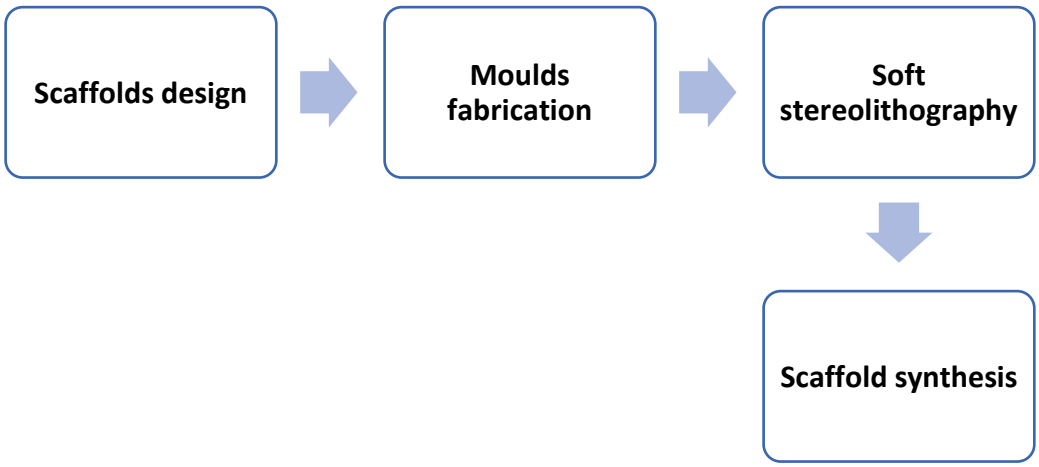

Figure 3.2 Methods diagram for PGS-M scaffold fabrication

3.3.1 SCAFFOLDS DESIGN

The design of the scaffolds was carried out considering the measurements of the cornea [211]. Design was done using 3D computer assisted design (CAD) design software (Solidworks 2019). Different scaffolds were designed with in-built artificial microenvironments . It has been reported that cell migration can be controlled by substrate stiffness (cells migrate from soft substrates to stiffer substrates) and promoted by patterned substrates [212]. Flat scaffolds were designed for *in vitro* biocompatibility studies and dome shape scaffolds for the study of cell alignment, migration, and proliferation affected by curvature.

3.3.2 SCAFFOLD TOPOGRAPHY

Scaffold architecture (micro and nano features) has been reported as a feature that can promote cell attachment, migration, and proliferation [213–216]. The influence on cell behaviour (homeostasis, migration, differentiation, proliferation, alignment), orientation and shape by the substrate topography has been defined as contact guidance [217–220]. Topography is the anchorage point for cell attachment and migration, this suggests that the architecture in the substrate increases cell adhesion that allow cell alignment and proliferation [221–223].

The scaffold design was inspired by nature (flowers, snowflakes), and they were developed to mimic the limbal niche structure. The channels were created as topography in my scaffolds to promote cell migration and differentiation from the outer part (niches) to the inner part (central cornea)(Figure 3.3).

Figure 3.3 Flat (left) and dome shape (right) scaffolds with in-built artificial cell niches moulded in Solidworks 2019. Scaffolds have 1 mm of thickness and 15 mm diameter.

3.3.3 SOFT STEREOLITHOGRAPHY (SLA)

The main technique that has been used in the elaboration of scaffolds with micro and nano structures with specific and highly defined dimensions is photolithography. Through the use of this technique it has been possible to create scaffolds with waves, pores, cylinders, ridges, groves and pits, steps and roughness among others [217] .

Soft stereolithography is a process where we combine stereolithography-produced templates with soft lithography to rapidly produce biomaterials based substrates [224]. The scaffolds were printed using the 3D printer Form Labs 2 with the resin grey V4 and photocured under UV light at 60ºC for 30 minutes. The mould was filled with polydimethylsiloxane (PDMS) (Sylgard-184) (Sigma Aldrich) and cross-linked at 60ºC overnight. The obtained mould had all the opposite features from the initial design from Solidworks (Figure 3.4).

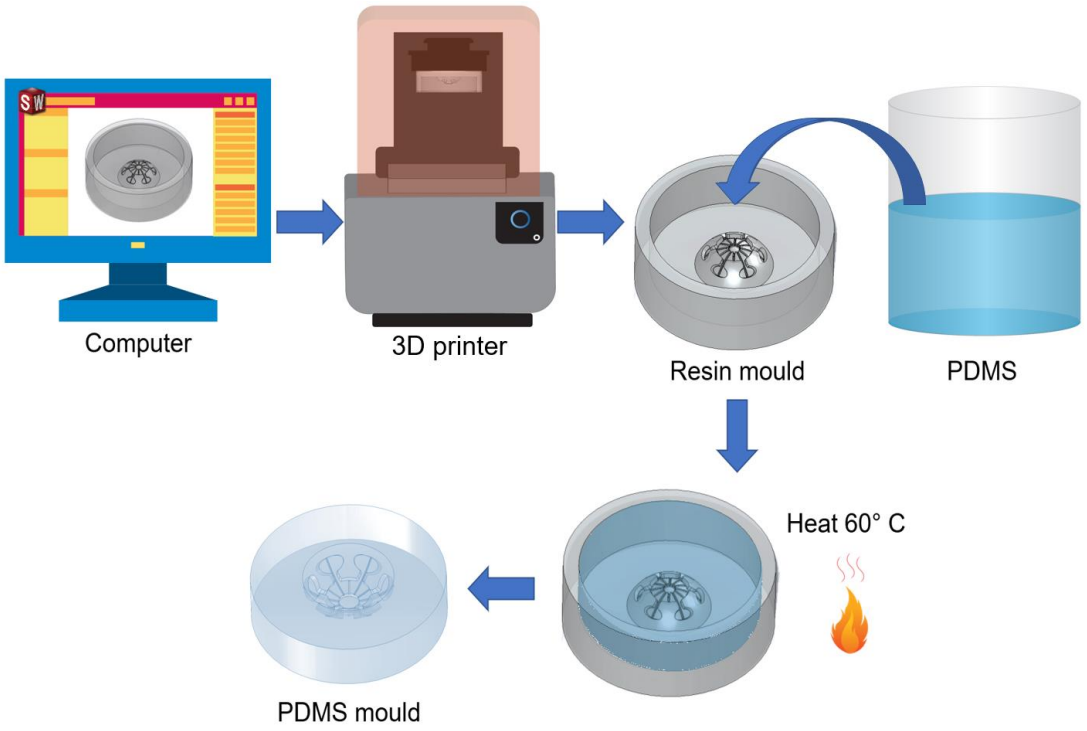

Figure 3.4 Soft stereolithography process.

3.3.4 SCAFFOLD SYNTHESIS AND FABRICATION

The scaffold synthesis was carried out using two PGS-M variants in order to choose the best one to be used in corneal applications.

- TRANSPARENT PGS-M SYNTHESIS

PGS-M in four different degrees of methacrylation (20, 30, 40, and 50%) were crosslinked with the photoinitiator diphenyl(2,4,6-trimethylbenzoyl) phosphine oxide/2-hydroxy- 2-methylpropiophenone (Sigma Aldrich) in three percentages: 1, 2, and 3% (w/w) (Figure 3.5). The mixture was poured into the silicone moulds and exposed to UV light (200W, OmniCure Series 2000 curing lamp) for 10 min to photocure (5 minutes each side). The samples obtained were photocured disks (1 mm thickness, 17 mm diameter). The samples were washed with methanol (CH_3OH) (Sigma Aldrich) four consecutive times (24 hours each). After this, the samples were dried in a vacuum

oven at 70ºC for 24h. Finally, samples were washed with water (dH_2O) four consecutive times (24 hours each), before their use in cell culture. The effect of the photoinitiator percentage was evaluated with ATR-FTIR, as described in Chapter 2.

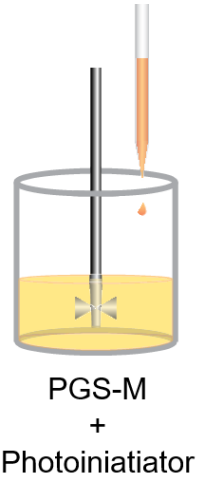

Figure 3.5 Transparent PGS-M synthesis.

- FLAT SCAFFOLDS FABRICATION

The flat scaffolds were fabricated using one PDMS mould with the printed design within its structure. The PGS-M was injected into the mould using a syringe filled with PGS-M and cured under UV light (200W, OmniCure Series 2000 curing lamp) for 10 min (5 minutes each side) (Figure 3.6). The transfer of micro features was evaluated with SEM analysis as described in Chapter 2.

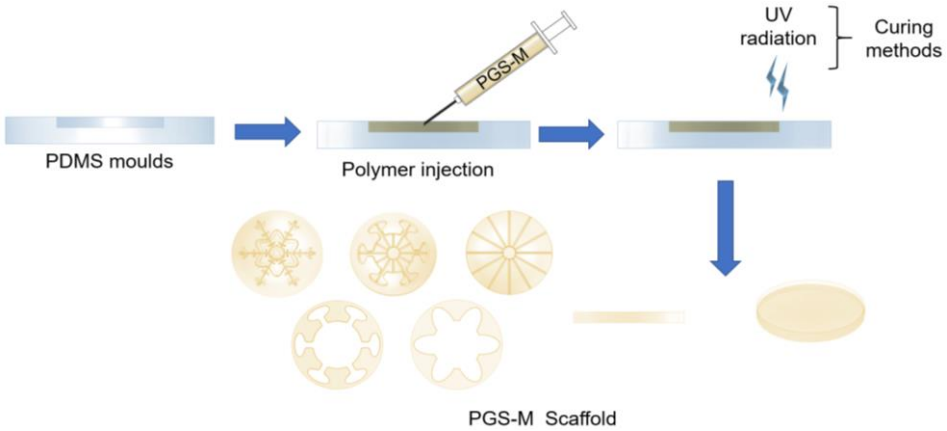

Figure 3.6 Flat PGS-M scaffolds fabrication with PDMS moulds.

- DOME SHAPE SCAFFOLDS FABRICATION

The dome shape scaffolds were synthetized assembling two silicone moulds: the bottom side (featureless dome) and the top side (corresponding dome shape with scaffold microfeatures). The PGS-M was injected into the gap between the moulds using a syringe filled with PGS-M and cured as previously detailed (Figure 3.7). The transfer of micro features was evaluated with SEM analysis as described in Chapter 2.

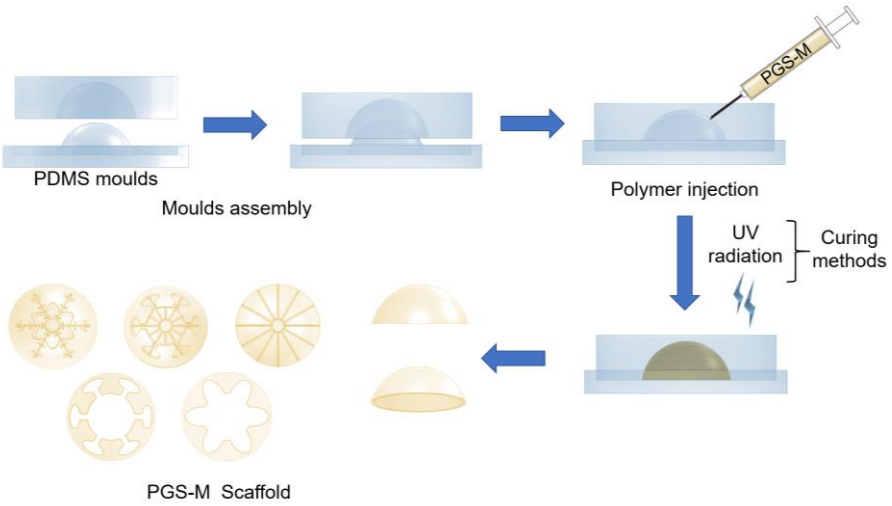

Figure 3.7 Dome shape PGS-M scaffolds fabrication with PDMS moulds.

- PGS-M PolyHIPEs SYNTHESIS

PGS-M PolyHIPEs in four different degrees of methacrylation (20, 30, 40, and 50%) were synthesized. The external phase is composed of PGS-M mixed with Toluene (C_7H_8) (Sigma Aldrich) 1:1 (w/w). To stabilize the reaction, the surfactant Hypermer B246 10% (w/w) was used at 10% (w/w). Crosslinking was initiated with the photoinitiator diphenyl(2,4,6-trimethylbenzoyl) phosphine oxide/2-hydroxy- 2-methylpropiophenone (Sigma Aldrich) at 20% (w/w) (Figure 3.8). A higher photoinitiator concentration was used as the organic phase (crosslinked polymer and surfactant) contains less than 10% PGS-M, while the aqueous phase (water and photo initiator) in PolyHIPES is ~90%, making crosslinking more efficient as PI % is increased [209,225–227]. The water (internal phase) was added dropwise (4 ml) under

continued stirring. The mixture was poured into the silicone moulds and exposed to UV light (200 W, OmniCure Series 2000 curing lamp) for 20 min to photocure (5 minutes each side). The samples obtained were photocured foams (1 mm thickness, 17 mm diameter). The samples were first washed with methanol (CH_3OH) (Sigma Aldrich) four consecutive times (24 hours each) and then washed four consecutive times with water (dH_2O) (24 hours each) before use in cell culture.

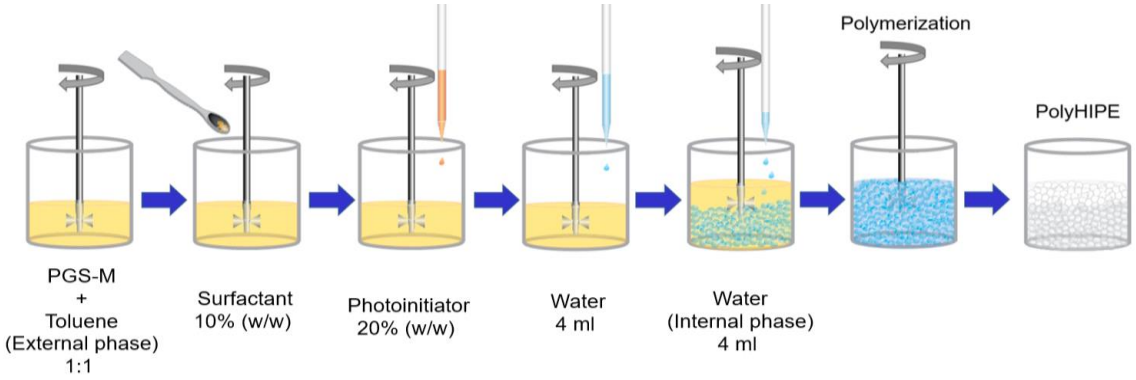

Figure 3.8 PGS-M polyHIPEs synthesis.

- FLAT POLYHIPE SCAFFOLDS FABRICATION

The flat scaffolds were synthetized using one PDMS mould with the design printed within its structure. The polyHIPE PGS-M was injected onto the mould using a syringe filled with HIPE and cured (as previously detailed Figure 3.6). The transfer of micro features was evaluated with SEM analysis as described in Chapter 2.

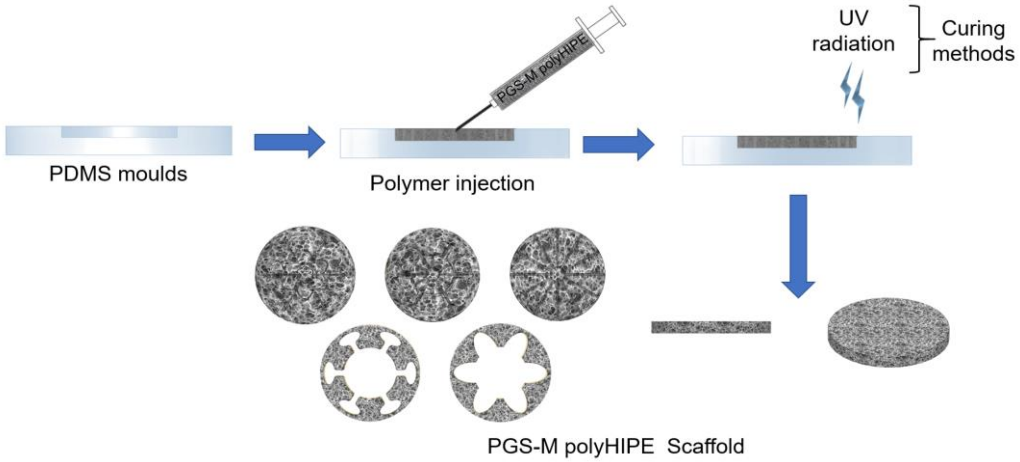

Figure 3.9 Flat PGS-M polyHIPE scaffolds fabrication with PDMS moulds.

- DOME SHAPE POLYHIPE SCAFFOLDS FABRICATION

The dome shape scaffolds were synthetized assembling two silicone moulds: one with the inner side and the other with the outer side of the scaffold. The PGS-M polyHIPE was injected into the gap between the moulds using a syringe filled with HIPE and cured as previously detailed (Figure 3.7). The transfer of micro features was evaluated with SEM analysis as described in chapter 2.

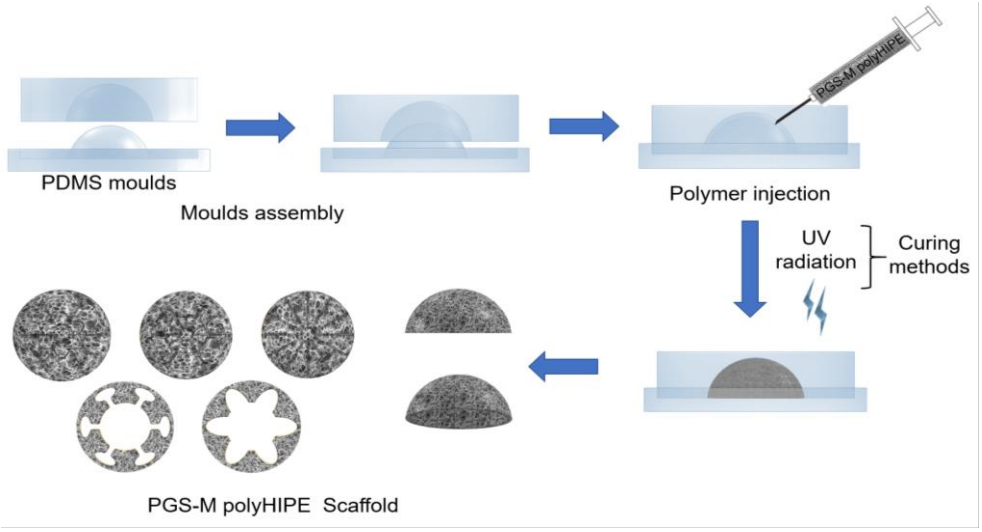

Figure 3.10 Dome shape PGS-M polyHIPE scaffolds fabrication with PDMS moulds.

3.4 RESULTS AND DISCUSSION

3.4.1 SCAFFOLDS DESIGN

The scaffold design was inspired in the corneal niche physiological morphology. The smallest features in the scaffold are the channels that connect the niches with the centre (300 x 250 μm, width and depth, respectively). The niche size for the flower design is 4.5 x 1.9 mm (width and length), and for the snowflake 2.41 x 0.86 mm (width and length) (Figure 3.11) . This is easily achieved using 3D printing: according to the manufacturer, the Formlabs2 has an XY resolution of 150 μm and Z resolution of 25 μm [228,229].

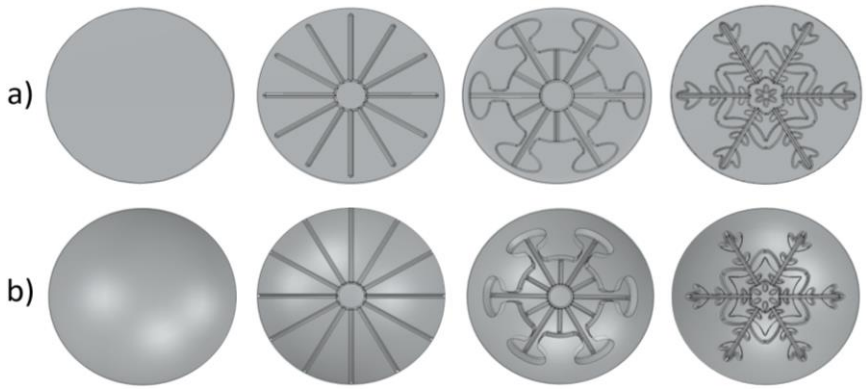

Figure 3.11 a) Flat and b) dome shape scaffolds with in-built artificial cell niches moulded in Solidworks 2019.

Previous studies reported that aligned featured scaffolds synthesized from natural polymers like collagen can lead cell migration, differentiation, and corneal tissue regeneration. However, there are no previous reports with synthetic, transparent polymers [230–234].

3.4.2 SOFT STEREOLITHOGRAPHY

Figure 3.12 shows the scaffolds printed in the Formlabs 2, the silicone moulds, and the scaffold after the curing under UV light. It is certain that soft stereolithography is an efficient method to generate scaffolds with highly defined microstructure as can be seen in figure 3.12, 3.13, and in SEM images (Figures 3.21, 3.23, and 3.24).

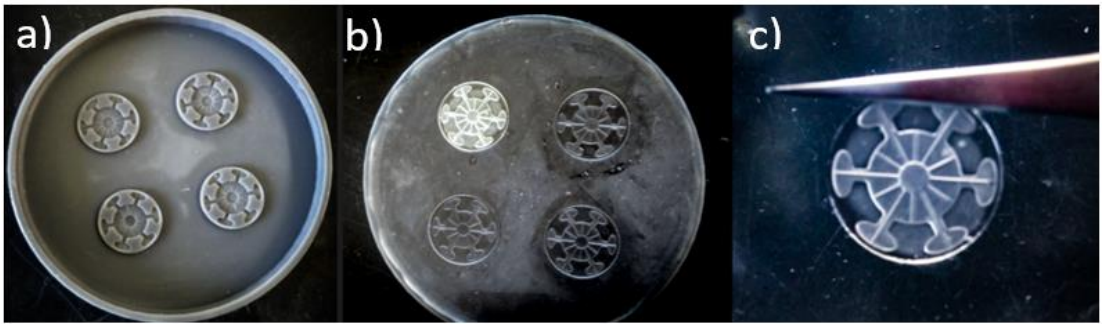

Figure 3.12 a) 3D printed moulds for flat scaffolds, b) silicone moulds (soft stereolithography) c) PGS-M scaffold

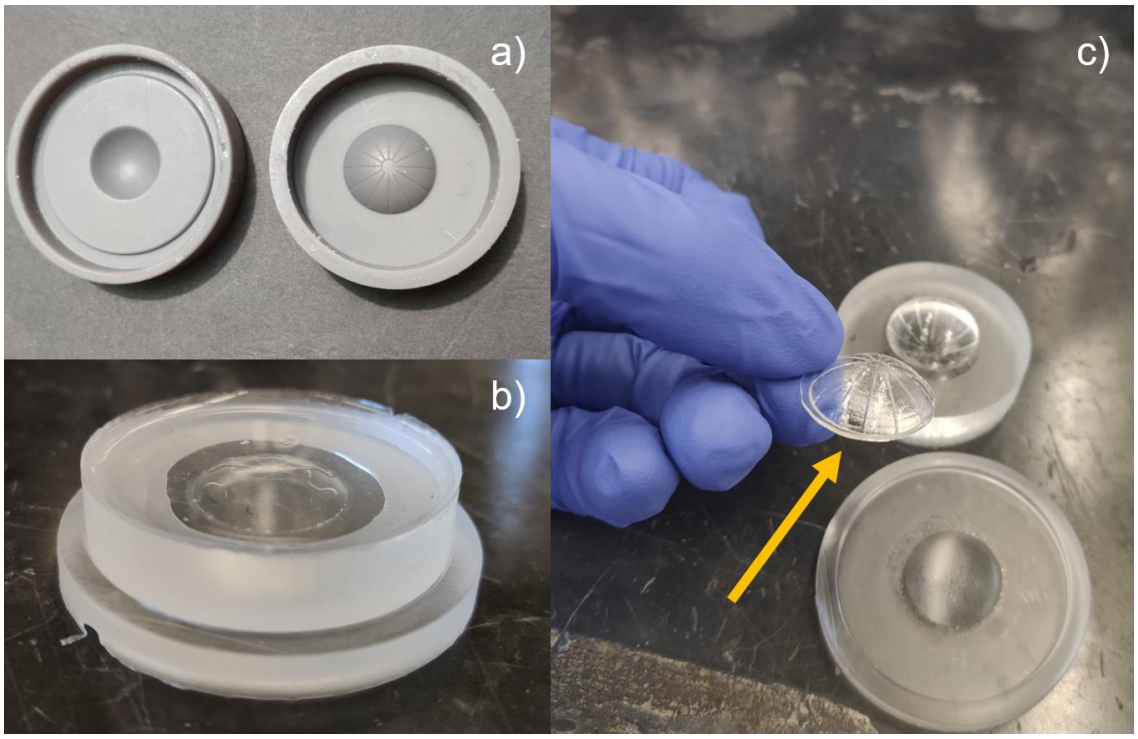

Figure 3.13 a) 3D printed moulds for dome shape scaffold, b) assembly of silicone moulds (soft stereolithography) c) PGS-M dome shape scaffold

3.4.3 SCAFFOLD SYNTHESIS AND FABRICATION

- TRANSPARENT PGS-M SYNTHESIS

The photoinitiator diphenyl(2,4,6-trimethylbenzoyl) phosphine oxide/2-hydroxy- 2-methylpropiophenone (Sigma Aldrich) was mixed with PGS-M in three separate percentages: 1, 2, and 3% (w/w) in order to study the effect of crosslinking (Figure 3.14).

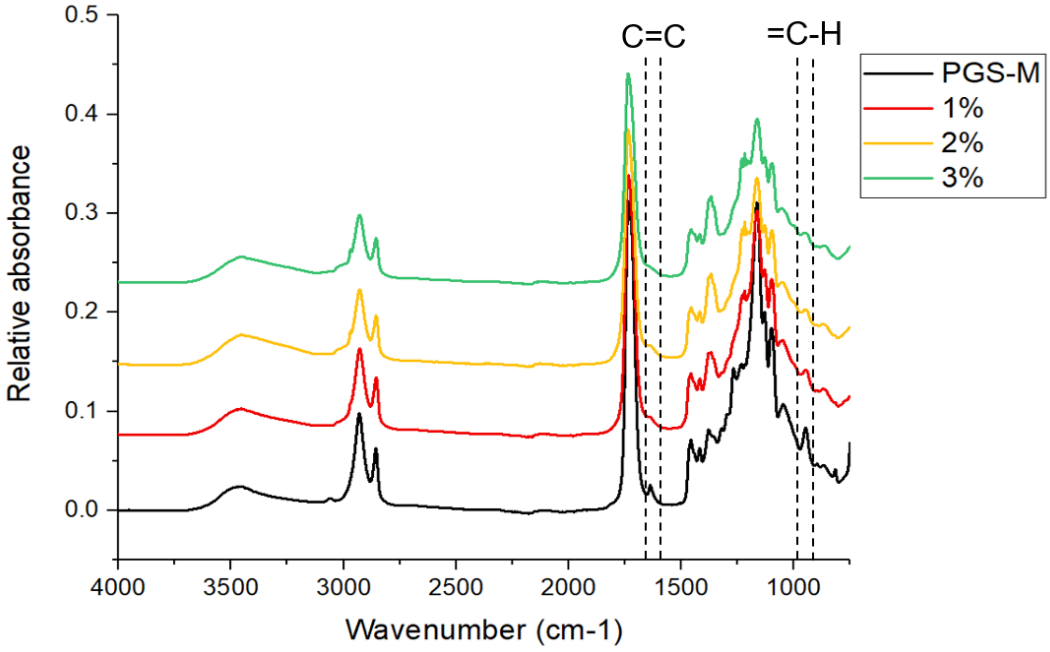

Figure 3.14 ATR-FTIR spectra for PGS-M and the effect of photoinitiator in the crosslinked matrix

Peaks related to methacrylate groups can be seen in the PGS-M spectra at 1640 cm-1 and 940 cm-1. These peaks are absent in pPGS and completely disappear after PGS-M photopolymerization.

Table 3.1 Area under the peaks related with methacrylate groups in different DM.

PGS-M			**AREA**	
			Wavenumber (cm^{-1})	
			1640	**940**
Not cured			0.209	0.55
Cured	Photoinitiator	1%	0.054	0.238
		2%	0.048	0.155
		3%	0.018	0.14

Table 3.1 shows the effect of photoinitiator (PI) in the PGS-M polymerisation. The peak at 1640 cm^{-1} decreases 75% with the addition of 1% PI, 78% with 2% PI, and 91.4% PI with 3%. Similarly, the peak at 940 cm^{-1} decreases 55% with the addition of 1% PI, 72% with 2% PI, and 75% PI with 3%. However, the scaffold was crosslinked from 1% PI, as PI percentage affects cell biocompatibility, 1% PI was the most suitable concentration for crosslinking the polymer.

- PGS-M PolyHIPEs SYNTHESIS

Pore size influences fibroblast and endothelial cell behaviour. Fibroblast growth has been shown to be better in pores with sizes between 5-90 μm, while endothelial cells prefer pore sizes closer with their own (36.6 μm for corneal superficial epithelial cells) [151,235,236]. The polyHIPE synthesis was carried out to achieve a pore size diameter close to 36.6 μm to ensure cell survival and proliferation (Figure 3.15).

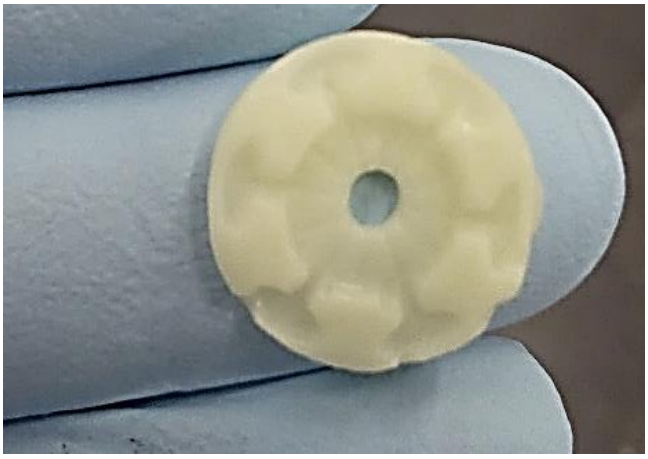

Figure 3.15 PolyHIPE scaffold.

- FLAT SCAFFOLD FABRICATION

The flat scaffold fabrication was successfully done with both transparent PGS-M and PGS-M polyHIPE. The obtained scaffold has all the features of the design moulded in Solidworks 2019 and transparency (Figure 3.16). According with the Oxford English dictionary, the definition of transparency is the quality of something that allows one to completely see through it, which was how I assessed scaffold transparency [237] .

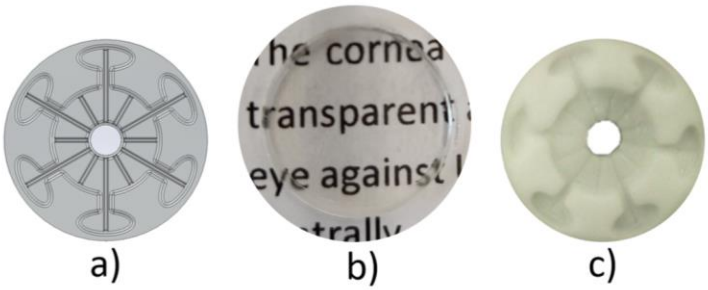

Figure 3.16 a) Scaffolds template design in Solidworks 2019, b) transparent PGS-M scaffold c) PGS-M polyHIPE scaffold.

Transparent PGS-M scaffolds with lower DM shrunk after the washes in methanol, the original size was 15 mm. This can be due to the high sol content in the lowest DM which is removed during the methanol washes (Figure 3.17 and Table 3.2).

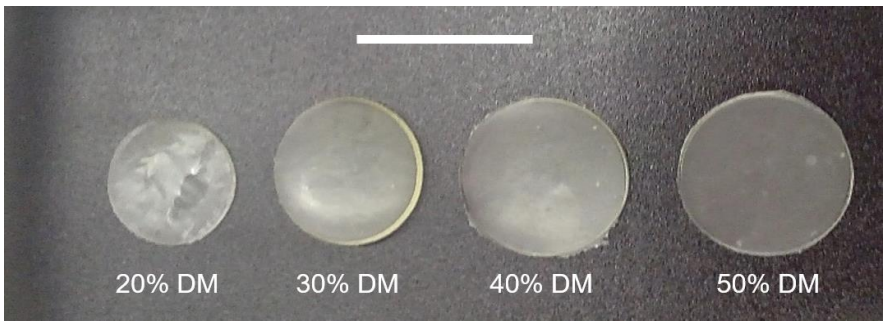

Figure 3.17 Scaffold shrinkage (different DM) after the methanol washes (Scale bar 15 mm).

Table 3.2 Shrinkage of PGS-M scaffolds after methanol washes (n=3)

DEGREE OF METHACRYLATION	SHRINKAGE (%)
20	26.16 ± 0.028
30	19.15 ± 0.009
40	6.10 ± 0.038
50	2.80 ± 0.032

It is possible to observe in Figure 3.17 and Table 3.2 that higher methacrylation degrees have a lower shrinkage percentage after methanol washes. This can be due the higher percentage of sol content found in lower DM as was reported in section 3.5.4, and their removal during the methanol washes which caused shrinkage in the final scaffolds. This is a characteristic that must be considered in the design of the final scaffold. Considering the percentage of shrinkage, it is possible to design a scaffold that meets the metric requirements even after washing.

- DOME SHAPE SCAFFOLD FABRICATION

The dome shape scaffold fabrication was done successfully in transparent PGS-M, though the PGS-M polyHIPE collapsed. The obtained scaffolds are flexible and have all the features (in-built niches and channels) of the design moulded in Solidworks 2019 (Figure 3.18 and 3.19).

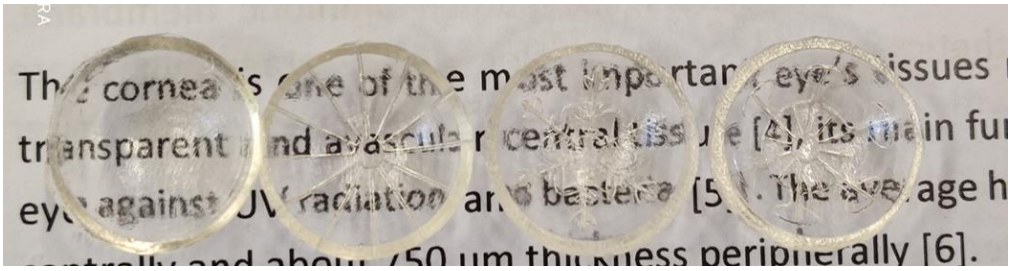

Figure 3.18 Dome shape PGS-M scaffold transparency.

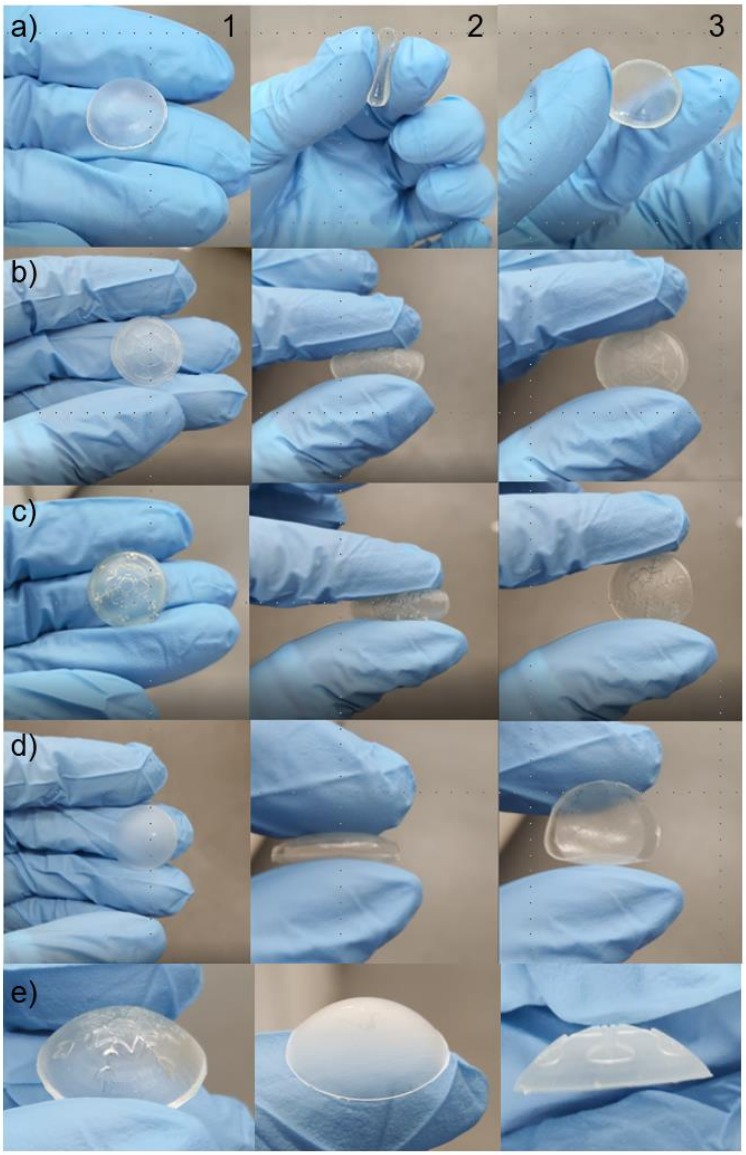

Figure 3.19 a) Planar scaffold, b) flower scaffold, c) snowflake scaffold, d) planar scaffold (100 µm) thickness, e) scaffold curvature. Scaffold elastic behaviour 1) Scaffold before compression, 2) scaffold with compression, 3) scaffold regains its original shape.

The average thickness of human cornea varies, with the centre and the periphery measuring ~500 µm and 750 µm, respectively [6]. In comparison, it has been reported that soft contact lenses have a thickness of 150 µm [106]. Previous works on corneal substitute implants have reported a thickness between 150 – 500 µm [238–241]. This is

the first time that an artificial corneal substitute has achieved dome shape scaffolds with 100 μm thickness (Figure 3.20).

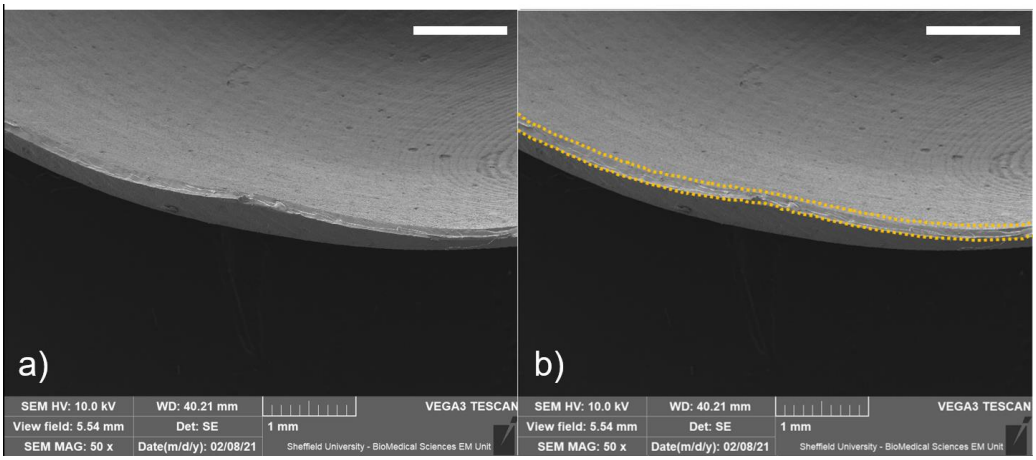

Figure 3.20 a) 50X magnification image of the thinner dome shape scaffold with 100 μm thickness (original image) b) Scaffold thickness shown using yellow dotted lines. Scale bars are 1mm.

- SEM

The transfer of micro features was evaluated with SEM analysis as described in Chapter 2 (Figures 3.21 – 3.24).

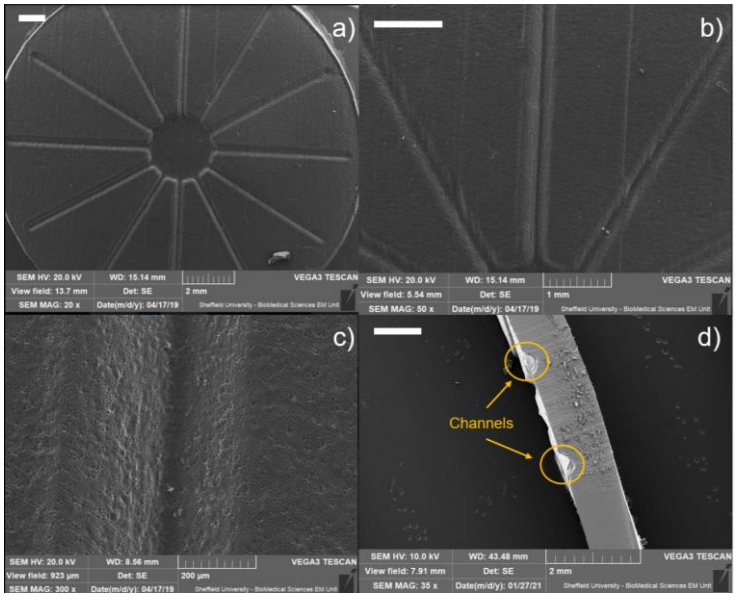

Figure 3.21 Flat scaffold with radial lines a) 20X magnification frontal view, b) 50X magnification focusing on the line patterns, c) 300X magnification showing an individual line/channel, d) 35X magnification showing the channel depth. Scale bars are 1mm.

The lines pattern has been transferred with high definition according with the original file. The smallest features in this scaffold are the lines with original measurements of: width of 200 µm, length of 6.5 mm, and depth of 250 µm. After washes of methanol and shrinkage (discussed in Table 3.2) the measurements were: width of 280 µm, length of 5.58 mm, and depth of 130 µm as can be seen in Figure 3.21 d). Patterned scaffolds with micro and nano topography have been reported to influence cell behaviour. Cells seeded on scaffolds with architecture that mimics the native tissue show higher interaction with the substrate. The substrate increased cell adhesion, alignment, showing changes in morphology, differentiation, and proliferation with the secretion of proteins similar to those found in the ECM [242–244].

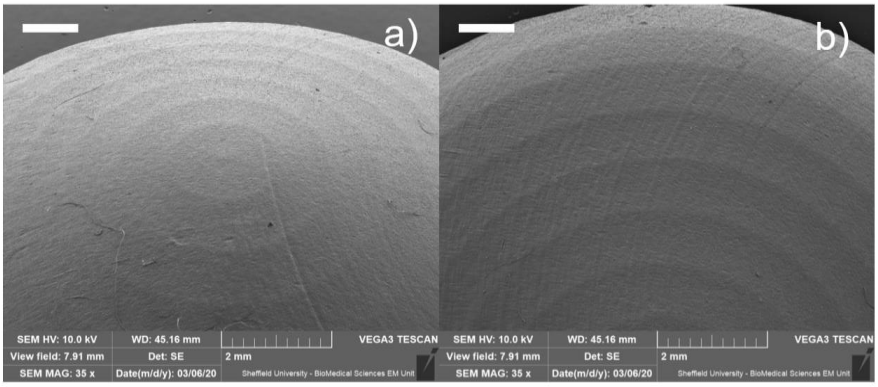

Figure 3.22 Dome shape scaffold a)tilted view (45º) and b) frontal view. Scale bars are 1mm.

Figure 3.22 shows the first scaffold that I fabricated with dome shape. The scaffold has 1 mm thickness, with the visible concentric circles being the result of both the fabrication technique and the moulds. There are few works that reported a successful 3D and dome shaped scaffold for corneal regeneration. The used techniques include 3D printing and electrospinning, limiting the materials that can be used and compromising the resolution and mechanical properties of the final scaffold. Therefore, these techniques are not the most suitable for fabricating scaffolds that require a solid and well defined structure [198,245].

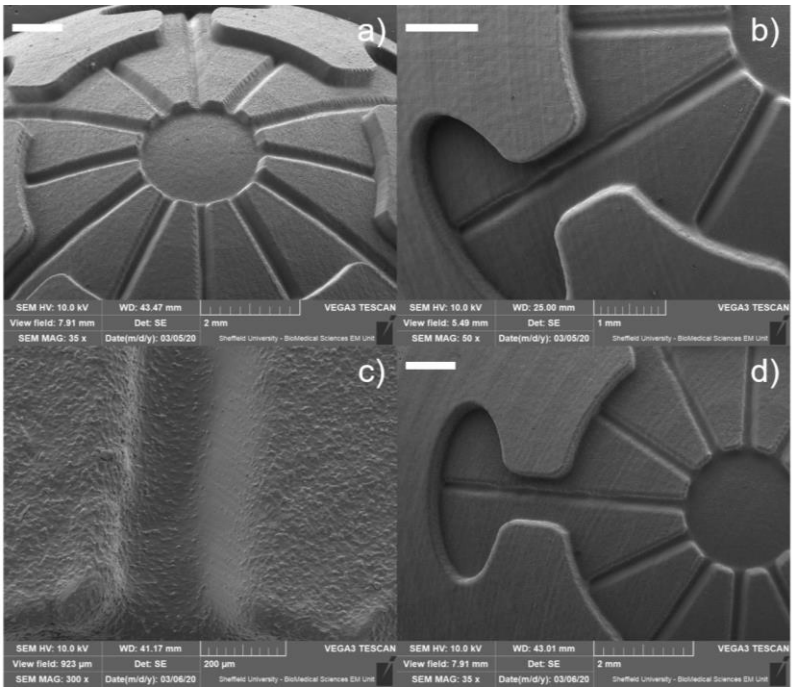

Figure 3.23 Dome shape scaffold with closed petal flower pattern. a) tilted view (45º), b) frontal view of the artificial microenvironment, c) 300X magnification to lines pattern, d) frontal view of the lines and the artificial microenvironment. Scale bars are 1mm.

Our scaffolds have a “closed petal” design, that can protect the cells and include channels that have the objective of promoting cell migration towards the centre of the scaffold.

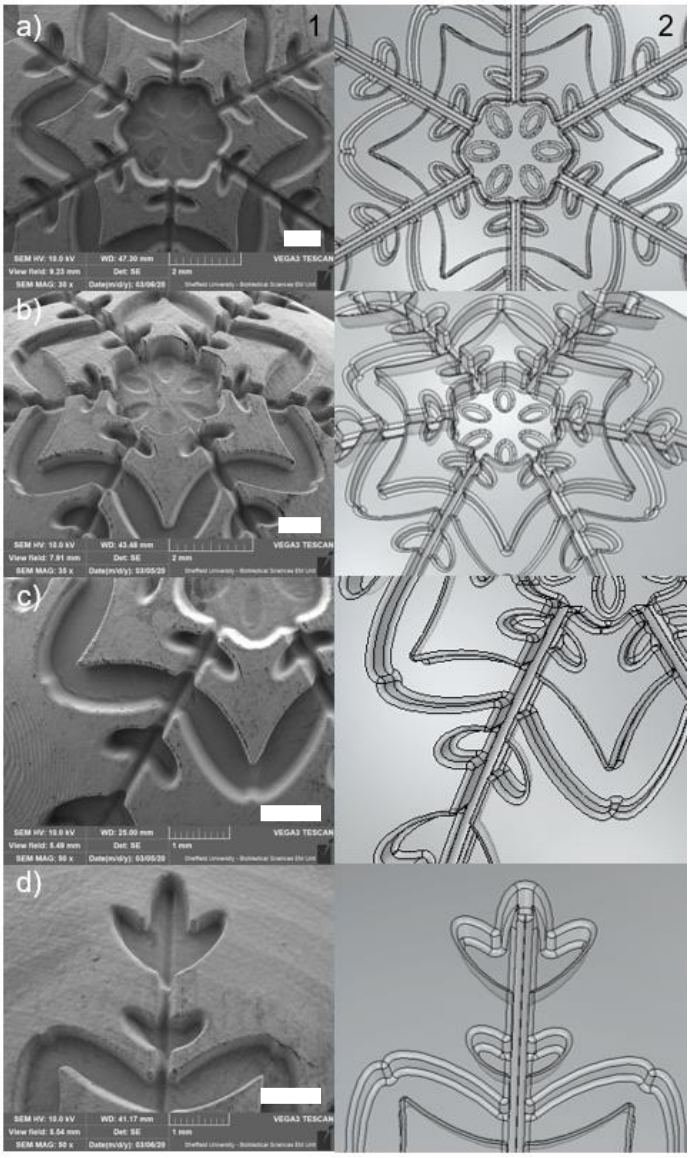

Figure 3.24 Dome shape scaffold with snowflake pattern. 1) SEM images, 2) Original file. a) 30X magnification on the frontal view, b) 35X magnification of tilted view (45º), c) 50X magnification to the artificial microenvironments and channels, d) 50X magnification to the artificial microenvironments and channels. Scale bars are 1mm.

One of the most elaborate designs we created was the snowflake, with artificial microenvironments that vary in sizes and shapes. This pattern has channels that join them and reach the centre. This design was thought to generate cell proliferation thanks to artificial microenvironments and promote cell migration with the channels. In

addition, the increase of surface area in the design could enhance cell proliferation. The smallest features in this scaffold are smallest artificial microenvironments, with width of 200 μm, length 250 μm and depth of 250 μm.

The evaluation of porous PGS-M with SEM was not possible as the drying processing (freeze drying) causes the scaffolds to collapse. This behaviour can be due to the low DM that does not support the structure and the small amount of polymer present in the scaffolds compared to the empty space from the water phase.

3. 5 CONCLUSIONS

Biomaterials for corneal application should have features like biocompatibility, biodegradability, mechanical properties, transparency, and optical properties that mimic the native cornea. Additionally, it is also important that the scaffold mimics the structure of the target tissue. These characteristics are important to select a suitable scaffold for corneal application as the two keys to the development of a corneal biomaterial are: the material used and the manufacturing technique.

The fabrication of cell carriers through soft stereolithography and moulding allows the creation of highly defined architectures that mimic the shape of the corneal dome. The creation of specific and highly defined topography is big step in the development of scaffolds for corneal regeneration. It has been suggested that scaffold topography improves the organization of new tissue, leading to increased tissue function [246]. This is very important in the case of the cornea since it is highly organized and owes many of its characteristics (such as transparency and mechanical properties) to this tissue organization. The development of scaffolds with highly defined structures with specific dimensions was successful with the use of moulding and soft stereolithography. In future work, I would focus on evaluating the impact of the different topographies on the growth, proliferation, differentiation, and migration of corneal cells. The continuation of this work would allow me to elucidate which pattern is the most suitable for corneal regeneration.

Due to its transparency, PGS-M is a potential suitable material for corneal regeneration. There are no previous reports that show the transparency and the high defined architecture and dome shape achieved in this study. In this chapter, the fabrication of transparent and porous scaffolds with in-built niches that mimics those in the native cornea was shown to be possible. Furthermore, scaffold thickness was reduced to 100 µm, which is much thinner than previously reported corneal substitute implants. This is the first time that a corneal substitute achieved these features, which is an important step in the development of an artificial cornea. However, the biocompatibility of these cell carriers still needs to be studied to determine suitability as a material corneal regeneration.

CHAPTER 4. CELL CULTURE ON PGS-M SURFACES

4.1 INTRODUCTION

Previously, transparent, and porous scaffolds were successfully fabricated with high define microstructures that mimic in built niches in the native cornea. In this chapter, the biological interaction of PGS-M scaffolds will be investigated using primary cells (epithelial cells and fibroblasts) isolated from pig and rabbit limbal explants as well as establish human epithelial corneal cells. Explants were used to reduce the time consumed during cell expansion and to improve the current isolation techniques. Explants were chosen as the cell source to approach the clinical setting of simple limbal epithelial transplantation (SLET), in which limbal explants are used directly from the patient's healthy eye [47]. The rabbit and pig models were selected as animal models due to their mechanical and physiological characteristics similar to those of the human cornea [247–253].

4.1.1 INTERACTION AND INFLUENCE OF PGS, PGSA AND PGS-M SUBSTRATES WITH DIFFERENT CELL TYPES

Since PGS was reported in 2002 by Wang et al, it has generated great research interest due to its characteristics as a biomaterial and use as a scaffold for countless tissues. High temperatures and long times are required to cross-link the molecule as a result of its nature. The poor mechanical properties that are obtained with this crosslinking methodology limit its use, which have been reported in a range of 0.01-2.5 MPa (Young's Modulus). PGS scaffolds support cell attachment, growth, differentiation and in general good proliferation. One of the main drawbacks that have been reported is the cytotoxicity of the PGS scaffolds cross-linked for shorter periods of time (less than 48 hours). This may be due to unreacted carboxylic acid groups of sebacic acid or the free sebacic acid produced by aqueous hydrolysis of PGS ester groups [110,143].

Mixtures of PGS with other polymers, such as PCL and PMMA, have been reported, notably improving their mechanical properties [87,254–257]. However, electrospinning as a main fabrication technique limits the type of materials and applications that can be tested. These mixtures have not had a negative effect on cell attachment, growth and proliferation.

Therefore, considering these disadvantages, the molecule was functionalized with acrylates (PGS-A) that allowed cross-linking under UV light for short periods of time and allowed the creation of 3D geometries in the scaffolds. However, the acrylation of PGS is unstable and generates high amounts of residues (mainly chlorine salts) that are difficult to remove. Nonetheless, its mechanical properties improve considerably, increasing to 0.6 - 13.2 MPa (Young's Modulus) [116]. Furthermore, acrylation has had a negative effect on cell attachment and biocompatibility in vivo and has a degree of cytotoxicity in bulk films [133].

Despite these downsides, PGS possesses properties that make it an excellent candidate for tissue engineering applications.

Our research group proposed PGS methacrylation as an alternative to overcome these issues. Neuronal Schwann cells, human dermal fibroblasts and human adipose-derived stem cells (ADSC's) have shown cell growth , migration, proliferation and alignment on PGS-M substrate [116,117].

Methacrylation, like acrylation, allows the crosslinking of the molecule under UV light and permits shorter crosslinking times, without the generation of residues and instability in the reaction. In addition, it enables the creation of more elaborate architectures and improves the mechanical properties of the molecule

Table 4.1 shows the interaction and influence of PGS, PGSA and PGS-M in different cells and cell lines and the mechanical properties achieved with different crosslinking and fabrication methods.

Table 4.1 Cell culture is influenced by synthesis methods and crosslinking conditions in PGS, PGSA and PGS.

MATERIAL	CROSSLINKING METHOD/ FABRICATION TECNIQUE	TARGET TISSUE	CELL TYPE	CELLULAR INFLUENCE	MECHANICAL PROPERTIES	REFERENCE
PGS	Heat (120, 135, 150 ^{o}C) 48, 72, 96 h	Soft tissue	No information available	No information available	Young's Modulus (MPa) 120 ^{o}C /48 h – 0.35 120 ^{o}C /72 h – 0.35 120 ^{o}C /96 h – 0.8 135 ^{o}C /48 h – 1.75 150 ^{o}C /48 h – 2.25	[122]

	Heat (110, 120, 130 ºC) 48 h	Cardiac tissue	Embryonic stem cell-derived cardiomyocytes	Biocompatible	Young's Modulus (MPa) 110 ºC/48 h – 0.0567± 0.011 120 ºC/48 h – 0.227 ± 0.03 130 ºC/48 h – 1.207 ± 0.08	[120]
	Heat (150 ºC) 24, 48 and 72 h	Cartilage	Chondrocytes	Morphology maintenance and cell differentiation	Young's Modulus (MPa) 150 ºC/24 h – 1.75 150 ºC/48 h – 2 150 ºC/72 h – 2.5	[121]
	Heat (150 ºC) 24 h	Bone	Rat bone marrow stromal cells (MSC's)	Differentiation but slow proliferation	Young's Modulus (MPa) 0.038 ± 0.08	[258]

	Heat (120 °C) 24 h	Nerve	Schwann cells	Cell adherence and proliferation	No information available	170
	Heat (140 °C) 8, 9, 10, 12 and 13 h	Skin	Mouse dermal fibroblasts (MDF's)	Cell proliferation dependent of pore size	No information available	124
	Heat (120 °C) 48 h	Retina	Murine retinal progenitor cells (mRPC's)	Cell adherence, proliferation and differentiation	No information available	259

	Heat (135 °C) 96 h	Cornea	Human corneal epithelial cells (HCE's)	Cell viability and proliferation.	No information available	[260]
PGS/PCL Functionalized with VEGF (2:1)	Electrospinning/ Evaporation	Cardiac tissue	Myoblast (C2C12) cells	Cell attachment, growth, and proliferation	Young's Modulus (MPa) 8 ± 2	[256]
PGS/εPCL (4:1, 3:1, 2:1 and 1:1, respectively)	Electrospinning/ Evaporation	Cornea	Human corneal endothelial cells (HCE's12)	Cell viability, proliferation, and cell elongation	No information available	[257]

PGS/PMMA -Gelatin (75:25, 50:50)	Electrospinning/ Evaporation	Nerve	Rat PC12 cells	Cell proliferation and elongation with neurite outgrowth	No information available	254
PGSA	Electrospinning/ UV light	Soft tissue	No information available	No information available	Young's Modulus (MPa) 10- 88% Degree of acrylation (DA): 0.15 – 30	115
	UV light (10 min)	Tissue engineering	Primary human foreskin fibroblasts (HFF's)	Cell adhesion and proliferation, with relatively normal morphology but not	Young's Modulus (MPa) 0.17 DA – 0.048 ± 0.005 0.20 DA – 0.148 ± 0.004 0.31 DA – 0.383 ± 0.028 0.34 DA – 0.568 ± 0.222	131

				adequate cell attachment	0.41 DA – 0.895 ± 0.052 0.54 DA – 1.375 ± 0.084	
	UV light (10 min)	Cell encapsulation and culture	Human embryonic stem cells (hESC's)	Cell proliferation and differentiation but *in vivo* caused acute inflammatory response	Young's Modulus (MPa) 0.568 ± 0.22	[261]
PGS-M	UV light (20 sec)	Nerve guide conduits	Neuronal Schwann (NG108-15) cells	Cell morphology maintenance and cell alignment	Young's Modulus (MPa) 3.2	[117]

	UV light (10 min)	Soft tissue and drug delivery	Human dermal fibroblasts and human adipose-derived stem cells (ADSC's)	Cell growth, spread and proliferation.	Young's Modulus (MPa) 0.5 – 6.8	[116]

4.2 OBJECTIVES

4.2.1 GENERAL OBJECTIVE

To evaluate the biocompatibility of the transparent and porous polyHIPE PGS-M scaffolds using human limbal epithelial cells (hLEC's) (established cell line) and rabbit and pig limbal fibroblasts (rLF's and pLF's) (primary cells).

4.2.2 SPECIFIC OBJECTIVES

- Isolate porcine and rabbit limbal explants
- Isolate porcine and rabbit limbal fibroblasts
- Fabricate PGS-M substrates for biological evaluation
- Evaluate the PGS-M biocompatibility with human limbal epithelial cells, human dermal fibroblasts, and rabbit and porcine limbal fibroblasts.

4.3 MATERIALS AND METHODS

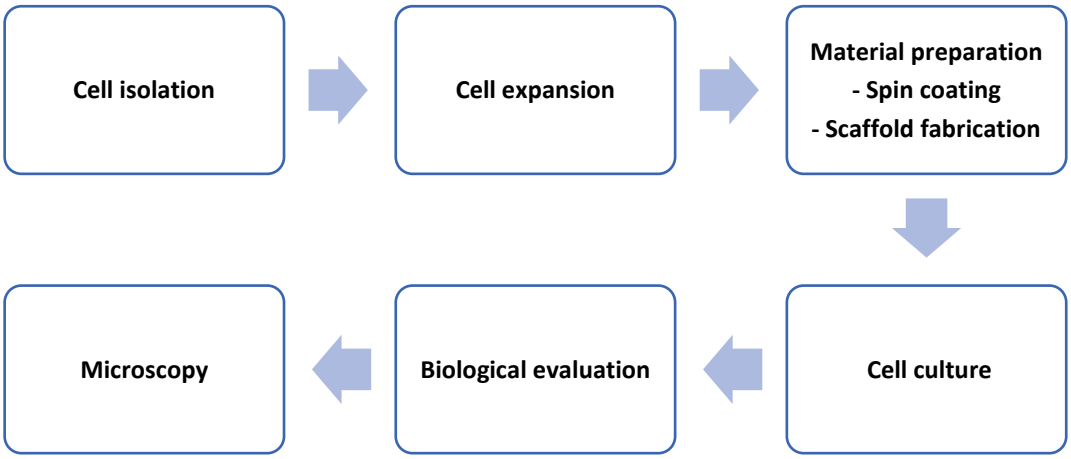

Figure 4.1 Methods diagram for cell culture on PGS-M surfaces

4.3.1 EXPLANT ISOLATION

Limbal explants were isolated from rabbit and porcine eyes (obtained from abattoirs: “The wild meat company” and “R B Elliot and sons limited”, respectively). The eyes were cleaned in PBS for one hour and immersed twice in an antiseptic solution: the first wash with 3% iodine in PBS (v/v) for 2 minutes, followed by a PBS rinse for 5 minutes. The second wash was carried out using 1.5% iodine in PBS (v/v) for 2 minutes, followed by a PBS rinse for 5 minutes.

The limbus was isolated from the eyes by removing the cornea and the sclera using a dissection microscope and a scalpel blade. The limbus (ring-like shape) was cut in small pieces (explants) of ~1 mm in length. The explants were cleaned in 1.5% iodine in PBS (v/v) 2 minutes and followed by a PBS wash. They were then directly used in culture with PGS-M scaffolds or for limbal fibroblast isolation (Figure 4.1).

4.3.2 ISOLATION OF PRIMARY LIMBAL FIBROBLASTS

The explants were left in a 12 well plate for 2 hours at room temperature in sterile conditions for attachment. Once the explants were attached, two millilitres of media culture were added. The culture media was composed of DMEM+Glutamax and HAM’s 12 in a 1:1 ratio, supplemented with penicillin/streptomycin (PS) 100 IU/ml, amphotericin 0.625 µg/ml, EGF 10 ng/ml, insulin 5 µg/ml, and fetal calf serum 10% (v/v). The limbal fibroblasts migrated from the explant after 4 weeks in culture conditions. These fibroblasts were then cultured and expanded until passage 3 (P3). Then, cells were frozen and stored prior to use. The isolated cells were used in culture with PGS-M scaffolds (Figure 4.2).

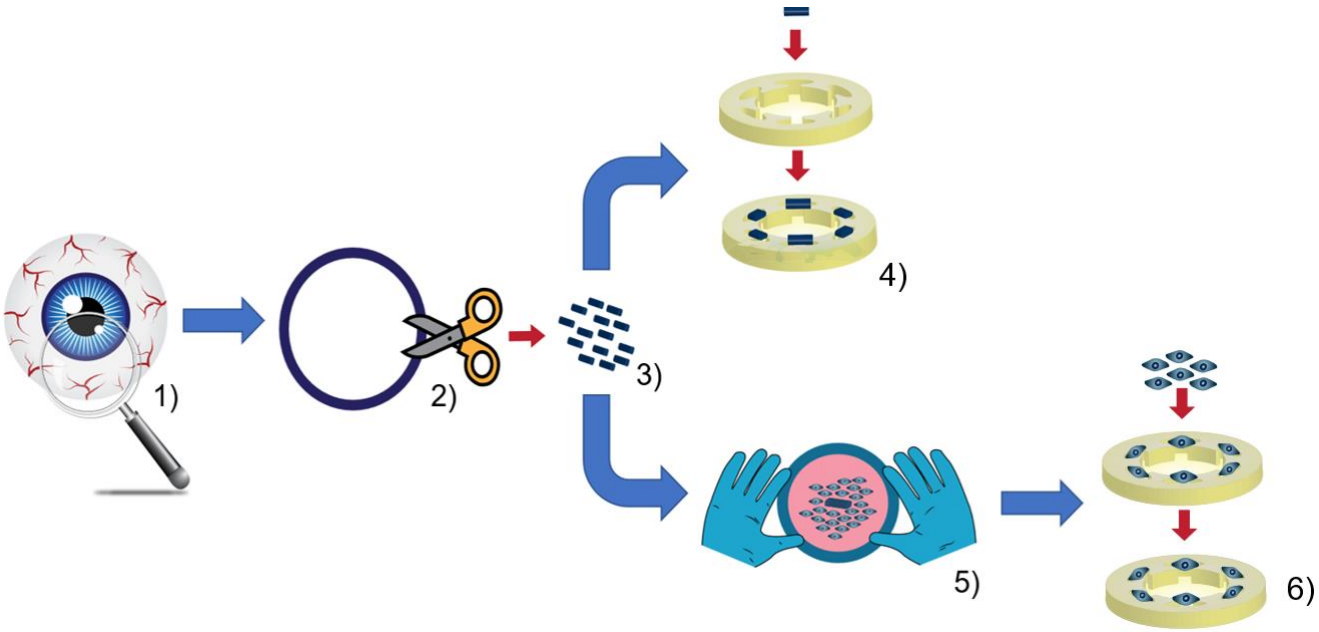

Figure 4.2 1) Limbus from healthy eye, 2) limbus isolation and division, 3) explants, 4) explant culture on micro-featured PGS-M scaffold, 5) limbal cells expansion , 6) limbal cell culture on micro-featured PGS-M scaffold.

4.3.3 CORNEAL HUMAN LIMBAL EPITHELIAL CELL (hLEC's) CULTURE

The cell line HCE-2 was obtained from ATTC in the P27. The cells were cultured according with the protocols provided by the company (see details below) [262,263].

FLASK COATING SOLUTION

T75 culture flask were pre-coated overnight with 4.5 ml solution of fibronectin 0.01mg/ml, bovine collagen type I 0.03 mg/ml, and bovine serum albumin (BSA) 0.01 mg/ml.

- Preparation of BSA solution

100 mg of BSA (Sigma 8806) were dissolved in 100 ml of sterile serum-free EMEM (ATCC 30-2003) and filtered slowly through a 0.22-micron syringe filter.

- Preparation of fibronectin solution

2ml of sterile serum-free EMEM media was mixed with a vial of 2mg fibronectin (Sigma F2006). The vial was placed in a water bath at 37^{o} C for one hour.

- Preparation of fibronectin-BSA-collagen solution

485 ml of sterile serum free media (Gibco) were mixed with 5ml BSA solution, 5 ml fibronectin solution, and 5 ml collagen (Purecol, Advanced Biomatrix 5005-B). The coating solution was aspirated 15 minutes before cell culture. Cells were cultured at 37 °C, 5% CO_2.

CELL CULTURE MEDIA

The media culture was composed of Keratinocyte-serum free medium (Gibco 17005-042) supplemented with bovine pituitary extract (BPE) (Gibco 17005-042) 0.05 mg/ml, epidermal growth factor (EGF) (Gibco 17005-042) 5 ng/ml, hydrocortisone (Sigma H0396) 500 ng/ml, and insulin (Sigma 91077-C) 0.005mg/ml.

4.3.4 HUMAN DERMAL FIBROBLASTS (hDF's) CULTURE

hDF's were obtained from primary tissue with informed consent from the NHS (National Health Service) for the donation of waste surgical tissue for research purposes (ethics reference: 15/YH/0177). The fibroblasts were culture in DMEM supplemented with PS 100 IU/ml, amphotericin 0.625 µg/ml, l-glutamine 2.5 mM, and FCS 10% (v/v). Cells were cultured at 37 °C, 5% CO_2.

4.3.5 SURFACE COATING OF GLASS COVERSLIPS WITH PGS-M

Borosilicate glass coverslips (13 mm diameter, No. 2 thickness) (Scientific Laboratory Supplies, UK) were treated with piranha solution for 1 hour and then washed five times in dH2O followed by three washes of methanol. Piranha solution was used as a hydroxylation agent to clean the glass surface and generate

additional silanol groups to allow further surface coating [264,265]. Piranha solution is made of sulphuric acid (H_2SO_4) (98%) (Sigma Aldrich) with hydrogen peroxide (H_2O_2) (30% wt in dH_2O) (Sigma Aldrich) (3:1 v/v). The coverslips were immersed in 10% (w/v) solution of 3-methacryloxypropyltrimethoxysilane in toluene for 24 hrs in the dark, then were washed three times with methanol and dried at room temperature. 3-methacryloxypropyltrimethoxysilane is a silane coupling agent that promotes the adhesion between the glass surface and PGS-M molecule [266,267].

Approximately 50 µl of low methacrylation PGS-M (20, 30, 40 and 50%) with 1% PI (w/w) were deposited in the centre of the coverslip previously treated with piranha solution. The spin coating was carried out at 4,000 rpm for 40 seconds (Laurell Technologies WS-400B-6NPP/Lite). The thin layer of polymer was photocured under UV light for 5 minutes (200W, OmniCure Series 2000 curing lamp). Unreacted reagents were removed from the coated coverslips by washing them four times in methanol (24 hours each) followed by four washes in dH_2O (24 hours each).

4.3.6 CELL CULTURE ON PGS-M SURFACES

PGS-M spin coated coverslips and bulk transparent and porous scaffolds were sterilised in the autoclave at 121°C for 30 minutes before the cell seeding. Cells (hLEC's, rLF's and pLF's) were harvested at confluence of 90% between the P3 and P9 with trypsin (0.025%)/EDTA (0.01%), centrifuged at 1,000 rpm for 5 minutes (Hettich Zentrifugen Rotofix 32A with 131 mm rotor radius), re-suspended in fresh media, and counted. The PGS-M scaffolds and spin coated coverslips were placed in a 12 well plate and 50,000 cells were seeded in each scaffold and coverslip. Uncoated glass coverslips seeded with cells were used as the positive control, and unseeded coated coverslips were designated as the negative control. The cells were left to attach for 6 hours. After that time, the scaffolds and spin coated coverslips were transferred to a new 12 well plate to ensure that only attached cells were included in future analysis. The cells were cultured with 2 ml

of media, which was changed every two days. Cell growth was evaluated after incubating scaffolds at 37.5 °C, 5% CO_2 for 14 days.

4.3.7 RESAZURIN REDUCTION ASSAY

Resazurin reduction assay (also known as AlamarBlue®) is a common assay used as an indicator of cell viability and cytocompatibility. The blue resazurin dye (nonfluorescent) is reduced by the mitochondrial reductase to pink resorufin (highly fluorescent). The output data has been shown to be proportional with the number of viable cells [268–270]. The resazurin working solution was prepared with 1mM resazurin salt (Scientific Laboratory Supplies) dissolved in dH_2O and filtered through 0.22 µm filter. In days 1, 3, and 7, the growth media was changed prior resazurin assay and mixed with resazurin solution 10% (v/v). The samples were incubated at 37 °C, 5% CO_2 in the dark, using media with resazurin solution as a blank. After 4 hours in incubation, the samples were taken out and 200 µl of each sample were placed in a 96 well plate in triplicate. The resorufin fluorescence was read at 540 nm excitation and 635 nm emission (Biotek instruments FLX800). The blank was subtracted from the samples before analysing the data.

4.3.8 PICOGREEN® DNA QUANTIFICATION ASSAY

- STANDARD CURVE FOR THE PICOGREEN® DNA QUANTIFICATION ASSAY

PicoGreen® is a fluorochrome that binds selectively to double-stranded DNA (dsDNA) and exponentially increases its fluorescence compared to its unbound state [271,272]. The DNA in the sample is measured by the output fluorescence. The Quant-iT™ PicoGreen® reagent was dissolved in TE buffer (10 mM Tris-HCl, 1 mM EDTA, pH 7.5). The stock working solution was prepared to obtain a final concentration of 0.5% PicoGreen®. Dilutions of the stock solution in dH_2O were made to obtain concentrations of 0, 200, 400, 600, 800 and 1,000 ng/ml dsDNA.

100 µl of the dilutions were placed in triplicate in a 96 well plate, with dH_2O used as a blank. The fluorescence (Bio-tek instruments FLX800) was read at 480 nm excitation and 520 nm emission. Before analysing the data, the blank was subtracted from the samples. The obtained data was analysed to plot a linear regression between the fluorescence and the amount of dsDNA.

- PICOGREEN® DNA QUANTIFICATION ASSAY

The PicoGreen® assay can be used to infer the number of cells present in the sample based on total DNA concentration. The number of cells in PGS-M surfaces was evaluated as follows: the cell seeding and controls were described in section 4.3.6. In days 1,3, and 7, the growth media was removed; samples were washed three times in PBS to remove the remaining media. The samples were incubated in the refrigerator with 500 µl of dH_2O at 4°C for 12 hours. Then, they were subjected to a freeze-thaw regime, passing from -80°C to 37°C three times, with time intervals of 30 min freeze, 30 min thaw, with the purpose of lysing the cells and releasing the DNA for quantification. After the final thawing, each solution was removed and placed in a 1 ml microcentrifuge tube. The tubes were vortexed for 15 seconds and centrifuged at 10,000 rpm for 5 minutes (Sanyo MSE Micro Centaur MSB010.CX2.5 with 64 mm rotor). 180 µl were taken from each sample and mixed with 180 µl of stock working solution (0.5% PicoGreen® in TE buffer 10mM). 180 µl of the stock solution mixed with 180 µl of dH_2O was used as a blank. The samples were covered with foil, vortexed for 5 seconds and incubated for 10 minutes at room temperature. 100 µl were taken from each sample and were placed in triplicates in a 96 well plate. The PicoGreen® fluorescence was read at 480 nm excitation and 520 nm emission (Bio-tek instruments FLX800), before analysing the data, the blank was subtracted from the samples.

4.3.9 LDH RELEASE ASSAY

Lactate dehydrogenase (LDH) is an enzyme that works as an indicator of cellular toxicity [273]. The enzyme reacts with the tetrazolium salt, forming formazan (a red-coloured product) that is measured by fluorescence. LDH assay is typically carried out to analyse the material compatibility with the target cells [274]. The cytotoxicity of PGS-M surfaces was evaluated as follows: the cell seeding, and controls were described in section 4.3.6. In days 1, 3, and 7, 50 µl of the growth media were taken and placed in a 96 well plate in triplicate along with 50 µl LDH working solution in each well. The samples were incubated in room temperature in the dark for 30 minutes. Afterwards, 50 µl LDH stop solutions were added to finalise the reaction. Absorbance for each well was read at 490 nm excitation and 680 nm emission (Biotek Instruments ELx800). LDH values on days 4 and 7 correspond to the cumulative LDH release of previous days.

4.3.10 F-ACTIN STAINING

The actin cytoskeleton was stained with phalloidin–fluorescein isothiocyanate (FITC). In addition, the nuclei were stained with 4',6-diamidino-2-phenylindole dihydrochloride (DAPI) as follow. Between days 7 and 14, the growth media was removed from the samples, and were washed gently with PBS. Samples were incubated at room temperature for 30 minutes with paraformaldehyde 3.7%. Then, the samples were washed with PBS and subsequently to permeabilize the cell membrane the samples were covered with Triton-X-100 0.1% in PBS for 5 minutes at 4^{o} C. Following this, samples were washed three times in PBS. The staining was carried out by covering the samples with a dilution of phalloidin-FITC and DAPI in PBS (1:1000 (v/v)). The samples were incubated 30 min in the darkness at room temperature, followed by washing three times with PBS. All samples were stored with fresh PBS prior to imaging.

4.3.11 MICROSCOPY

The visualisation of cell growth was carried out by fluorescence microscopy for spin coated samples and confocal microscopy for bulk samples.

- FLUORESCENCE MICROSCOPY

Spin coated samples were placed on an inverted epifluorescent microscope (Olympus IX73) and acquired with a Micro-Manager 1.4.22 software (University of California). The light source used was a mercury lamp: Phalloidin-FITC at 495 nm excitation and 520 nm emission and DAPI at 405 nm excitation and 450 nm emission.

- CONFOCAL MICROSCOPY

Bulk scaffolds were placed in a two-photon confocal microscope (Zeiss LSM510 Meta) with a Ti-Sapphire laser. Images were obtained using 488 nm (10%) laser line and an Achroplan 40×/0.75 N.A. water immersion objective. The image size was set at 210.4 ×210.4 × 7.2 μm area.

4.3.12 STATISTICS

The characterization was carried out with three independent experimental repeats (N=3) in triplicates per experiment (n = 3). The data was analysed with GraphPad Prism version 7.04 software. The data significance was calculated with two-way ANOVA (paired samples) with Tukey post-hoc pairwise multiple comparison analysis was used for the experiments with two independent variables or factors (sample type or conditions). $P \leq 0.05$ was considered statistically significant (*) and $P > 0.05$ was considered non-significant (ns). Data was graphed as means ± SD (standard deviation).

4.4 RESULTS AND DISCUSSION

4.4.1 EXPLANT ISOLATION

Because access to rabbit eyes was limited, only pig eyes were used. Pig eyes are more prone to develop infections during culture. Therefore, tissue handling, and aseptic techniques used during eyes processing were exhaustively carried out (Figure 4.3).

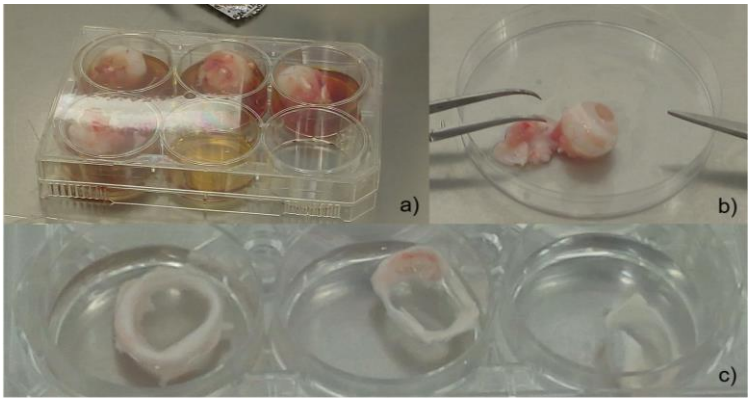

Figure 4.3 Processing of pig eyes. a) eyes cleaning in iodine solution, b) eye tissue removal, c) cleaning of corneal tissue.

Explant isolation was successfully carried out using a dissection microscope, (Figure 4.4). The limbus was isolated from the rest of the tissue, avoiding the sclera to prevent expansion of its cells.

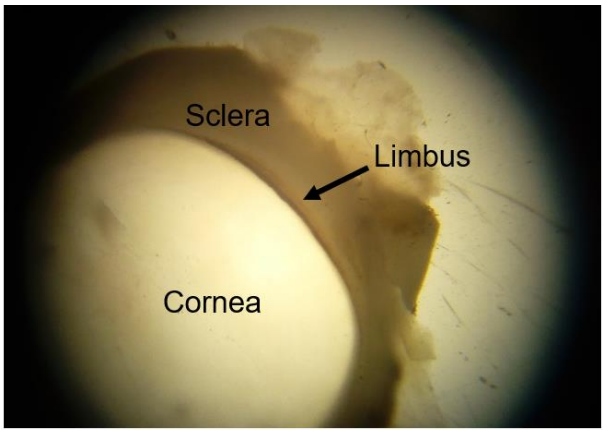

Figure 4.4 Limbus isolation in a dissection microscope

Explants were used directly in culture with PGS-M transparent scaffolds but did not attach in the substrate even after testing different attachment times (30 minutes, 1 hour, 4 hours, 6 hours, 12 hours, 24 hours). Therefore, explants were just used for limbal fibroblast isolation.

4.4.2 ISOLATION OF PRIMARY LIMBAL FIBROBLAST

Fibroblasts take over 4 weeks to grow and expand outside the explant. The cells were grown until passage 3 and then frozen down prior to use. pLF's were used between passage 3 to 9 in culture with PGS-M substrates to analyse the material cytotoxicity.

4.4.3 CORNEAL HUMAN LIMBAL EPITHELIAL CELLS (hLEC's) CULTURE ON PGS-M SURFACES

PGS-M scaffolds (transparent and polyHIPE) were tested with hLEC's, as they are a cell line which can be used as a standard for ocular biomaterial applications.

In Chapter 2, we determined that the DM with mechanical properties that better matched the native cornea and with lower percentage of sol content was 40% DM. However, hLECs were cultured on PGS-M transparent scaffolds in 20, 30, 40, and 50% DM to evaluate the PGS-M biological performance in different DMs and observe differences in proliferation.

The cell expansion protocols from the manufacturer were followed, changing only the collagen from Purecol (Advanced Biomatrix 5005-B) for collagen from Sigma-Aldrich (804592). The biocompatibility and cell viability of hLECs were evaluated with resazurin reduction assay on PGS-M surfaces (transparent and polyHIPE) with 1 mm thickness (Figure 4.5).

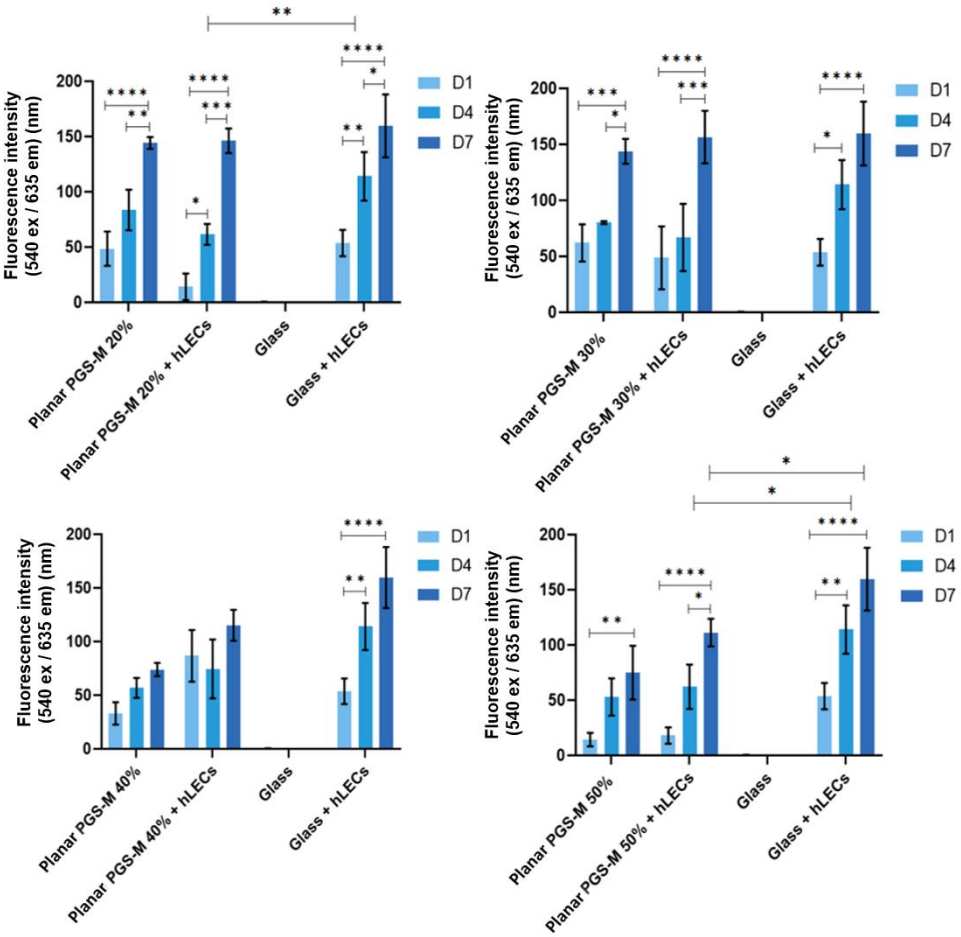

Figure 4.5 Resazurin reduction assay of hLEC's culture on planar PGS-M transparent scaffolds (20 - 50 % DM with 1 mm thickness). Positive controls were hLEC's culture on uncoated borosilicate glass. Negative controls were PGS-M substrates (20 - 50 % DM) and coated borosilicate glass without cells. The assay was carried out in days 1,4 and 7. Samples show means and error bars corresponding to ±SD (N=3, n=3), analysed by two-way ANOVA, Tukey's post-hoc pairwise comparison. P≤0.05 was considered significant (*).

Figure 4.5 shows that the fluorescence signal is very low in all the samples. The signal appears to increase in samples with cells, but also increases in samples of the planar PGS-M scaffolds without cells. There is no significant difference in cell growth in the different DMs. However, PGS-M with 20 and 50% DM shows a

significant difference in cell growth between PGS-M and glass (P=0.0057 for 20% day 4 and P=0.0189 and P=0.0339 day 4 and 7 for 50% DM respectively).

Initially, it was planned to culture hLEC's on PGS-M polyHIPEs in 20, 30, 40, and 50% DM. Nevertheless, the polyHIPEs with lowest DM (20 and 30%) folded on themselves after the methanol washes, making it impossible to unfold them for use in cell culture. For this reason, only PGS-M polyHIPEs in 40 and 50% DM were evaluated in cell culture (Figure 4.6).

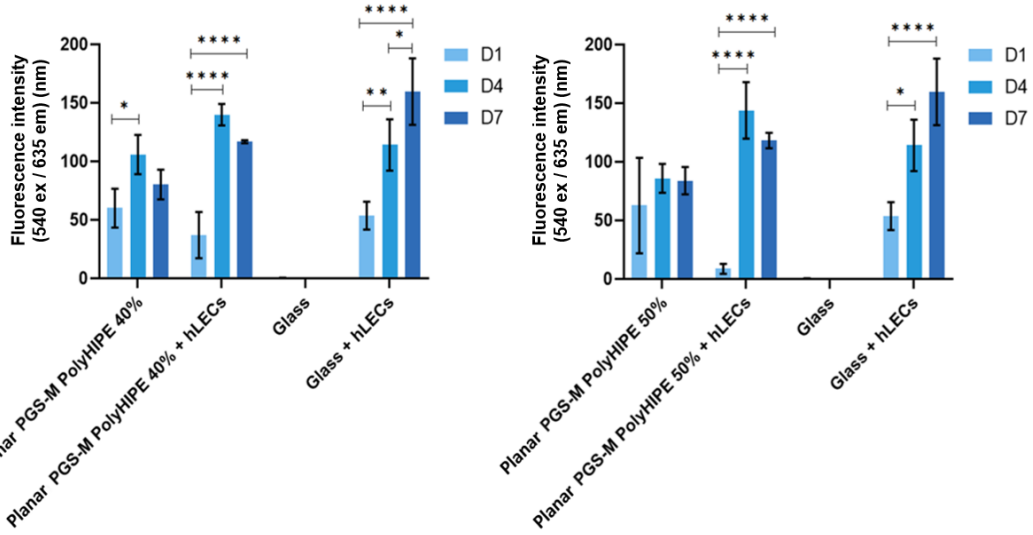

Figure 4.6 Resazurin reduction assay of hLEC's culture on planar PGS-M polyHIPE scaffolds (40 and 50 % DM with 1 mm thickness). Positive controls were hLEC's culture on uncoated borosilicate glass. Negative controls were PGS-M substrates (40 and 50 % DM with 1 mm thickness) and coated borosilicate glass without cells. The assay was carried out in days 1,4 and 7. Samples show means and error bars corresponding to ±SD (N=3, n=3), analysed by two-way ANOVA, Tukey's post-hoc pairwise comparison. P≤0.05 was considered significant (*).

In Figure 4.6 it is possible to observe that the fluorescence signal is also very low in all the samples. The signal increases in samples with cells in day 4 but in day 7 decreases; the same can be observed in PGS-M samples without cells. There is no significant difference in cell growth between 40 and 50% DM and between PGS-M and glass.

Figures 4.5 and 4.6 showed a low fluorescence signal even after several days of proliferation: the reason for this is unclear. This cell line was sent by the manufacturer with a high passage number (P26) which makes their handling and expansion difficult as we seek to avoid senescence after several passages. Additionally, the cell culture reagents used for hLEC's are significantly more expensive than those needed for the other mentioned cells (pLF.s), making it too costly to maintain. Therefore, we decided to postpone the use of hLEC's for evaluating PGS-M cytotoxicity until cell culture conditions could be optimised for their use.

4.4.4 PORCINE LIMBAL FIBROBLAST (pLF's) CULTURE ON PLANAR PGS-M SURFACES

Due to the previously mentioned difficulties associated with hLEC's culture, pLF's were used as second choice of cells for the evaluation of biocompatibility, cell viability, and cytotoxicity on PGS-M surfaces. Cell proliferation was evaluated with resazurin reduction assay and PicoGreen® DNA quantification assay (Figures 4.7 and 4.9). pLF's were cultured on PGS-M transparent scaffold with 40% DM and 1 mm of thickness.

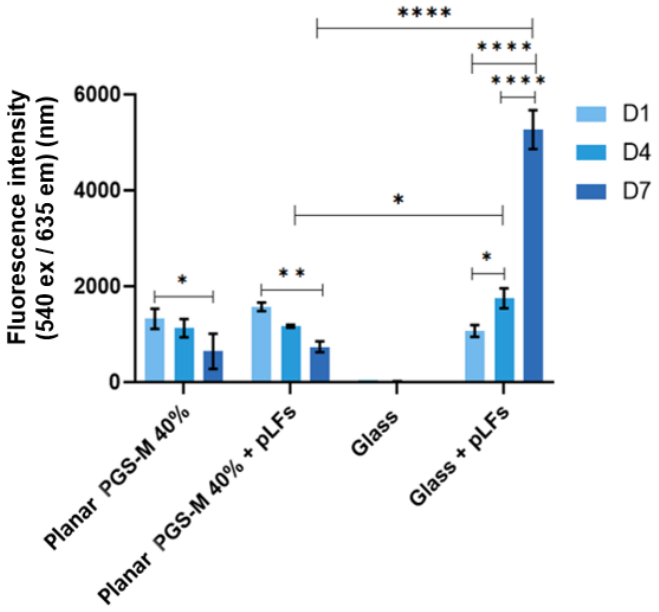

Figure 4.7 Resazurin reduction assay of hLEC's culture on planar PGS-M transparent scaffolds 40 % DM with 1 mm thickness. Positive controls were hLEC's culture on uncoated borosilicate glass. Negative controls were PGS-M substrate 40 % DM and coated borosilicate glass without cells. The assay was carried out in days 1,4 and 7. Samples show means and error bars corresponding to ±SD (N=3, n=3), analysed by two-way ANOVA, Tukey's post-hoc pairwise comparison. P≤0.05 was considered statistically significant (*).

Unlike hLEC's, pLF's culture showed a higher fluorescence signal. Nevertheless, samples without cells also showed a high signal. This will be further discussed in Chapter 5. It was possible to observe that cells were dying even after several days of culture on PGS-M substrate, while cells continued growing on the glass. There is a significant difference between the PGS-M and glass in days4 and 7(P≤0.05 day 4 and P≤0.0001 day 7 respectively).

The PicoGreen® standard curve can be used to infer the number of cells in the samples (seen in Figure 4.8). The standard curve has a linear tendency with a correlation of y= 45.705x and R^2 value of 0.9989.

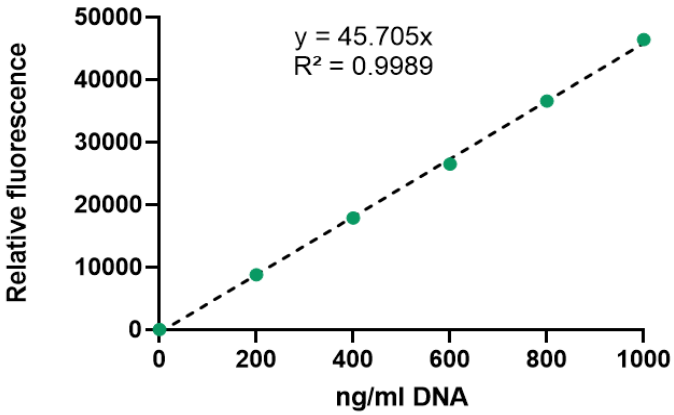

Figure 4.8 PicoGreen® standard calibration curve plotted with known concentrations of DNA (n = 3).

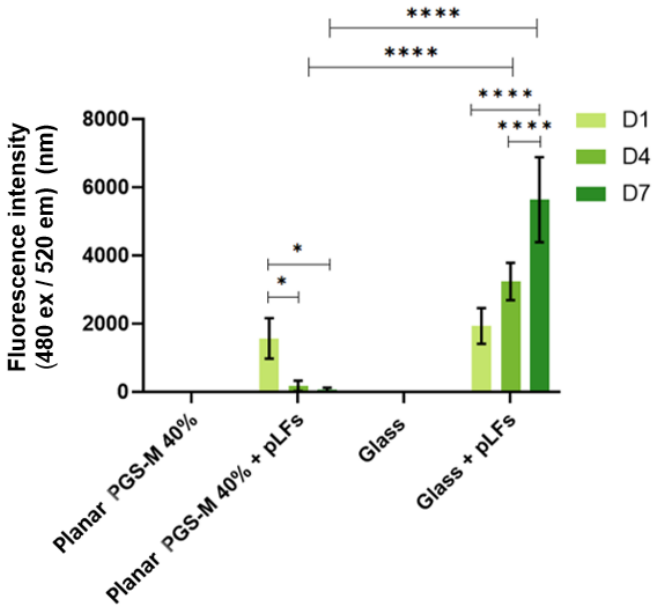

Figure 4.9 PicoGreen® DNA quantification assay of pLF's cultured on planar PGS-M transparent scaffold (40 % DM with 1 mm thickness). Positive controls were pLF's cultured on uncoated borosilicate glass. Negative controls were PGS-M substrate (40 % DM with 1 mm thickness) and coated borosilicate glass without cells. The assay was carried out in days 1,4 and 7. Samples show means and error bars corresponding to ±SD (N=3, n=3), analysed by two-way ANOVA, Tukey's post-hoc pairwise comparison. P≤0.05 was considered statistically significant (*).

In Figure 4.9 it is possible to observe that the PicoGreen® DNA quantification assay corroborates with data obtained with resazurin reduction assay: pLFs were dying on PGS-M substrate and growing on glass. There is a significant difference between the PGS-M and glass in days 4 and 7 ($P<0.0001$ for days 4 and 7 respectively).

There are no previous reports of cell growth on PGS-M surfaces thicker than 350 µm, though Pashneh-Tala et al. reported positive results with the culture of fibroblasts, adipose-derived stem cells (ADSC's), and smooth muscle cells (SMC's) on spin coated PGS-M 30% DM. Likewise, Singh et al. reported positive results with the culture of neuronal cells and primary Schwann cells seeded in PGS-M tubes produced by stereolithography (25 - 100% DM) with 350 µm wall [116,117]. In contrast, the results obtained in this study with cell culture on 1 mm thickness PGS-M substrates are not positive even after 7 days of growth. It is unclear if the material or cells that are used are having a negative effect on proliferation. Therefore, the use of human dermal fibroblasts and spin coated surfaces was proposed to elucidate why cells are dying after several days of culture on the material.

4.4.5. SPIN COATED BOROSILICATE GLASS WITH PGS-M

Spin coating is a widely used technique to produce thin and uniform films with controllable thickness [275,276]. The layer thickness depends on the angular velocity and the polymer viscosity [277]. As thick PGS-M substrates (1 mm thickness) seem to affect cell growth and proliferation, it was decided to test thinner surfaces to clarify the reason of cell death.

4.4.6 PORCINE LIMBAL FIBROBLAST (pLF's) CULTURE ON SPIN COATED PGS-M SURFACES

pLF's were seeded on PGS-M spin coated substrates with 20, 30, 40, and 50% DM to evaluate material cytotoxicity and observe if thinner surfaces promote

proliferation. Cell proliferation and cytotoxicity were evaluated with resazurin reduction assay and LDH release assay in spin coated PGS-M 20 - 50 %.(Figures 4.10 and 4.11). PicoGreen® DNA quantification assay was evaluated only in spin coated PGS-M 40% DM (Figure 4.12).

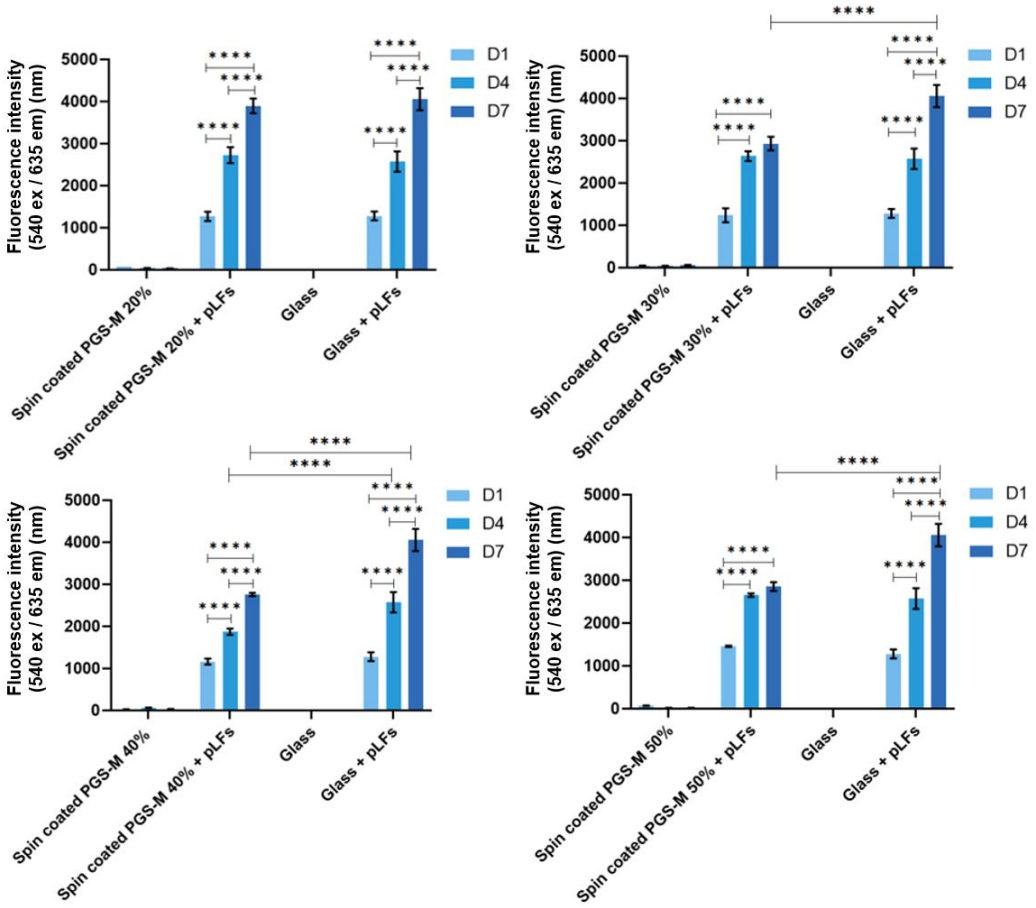

Figure 4.10 Resazurin reduction assay of pLFs cultured on spin coated PGS-M (20 - 50 % DM). Positive controls were pLFs cultured on uncoated borosilicate glass. Negative controls were PGS-M spin coated substrates (20 - 50 % DM) and coated borosilicate glass without cells. The assay was carried out in days 1,4 and 7. Samples show means and error bars corresponding to ±SD (N=3, n=3), analysed by two-way ANOVA, Tukey's post-hoc pairwise comparison. P≤0.05 was considered statistically significant (*).

Figure 4.10 shows pLF's grow on PGS-M spin coated surfaces, unlike cells seeded on thick PGS-M substrates (1 mm thickness). It is clear that the thin layer of

polymer spin coated on glass allows the cell growth in all the DMs. Additionally, cells seemed to grow better on lower DM. The most likely cause of high proliferation is the low amount of gel fraction in lower DM: around 60% gel in 20% DM which increases up to 80% gel in 50% DM (Chapter 2). If the polymer itself is affecting cell growth, the low percentage of crosslinked polymer in 20% DM explains the increased cell growth compared to 50% DM.

There is no significant difference between pLF's seeded on 20% DM and pLF's seeded on glass at all time points, showing an improvement compared with thick scaffolds. In contrast, there is a significant difference between pLF's seeded on 30% DM and pLF's seeded on glass in day 7 ($P \leq 0.0001$), between pLF's seeded on 40% DM and pLF's seeded on glass in days 4 and 7 ($P \leq 0.0001$ in both cases), and between pLF's seeded on 50% DM and pLF's seeded on glass in day 7 ($P \leq 0.0001$). The spontaneous LDH release in positive controls (pLF's culture on borosilicate glass) were compared with spontaneous LDH release in pLF's culture on spin coated PGS-M (Figure 4.11).

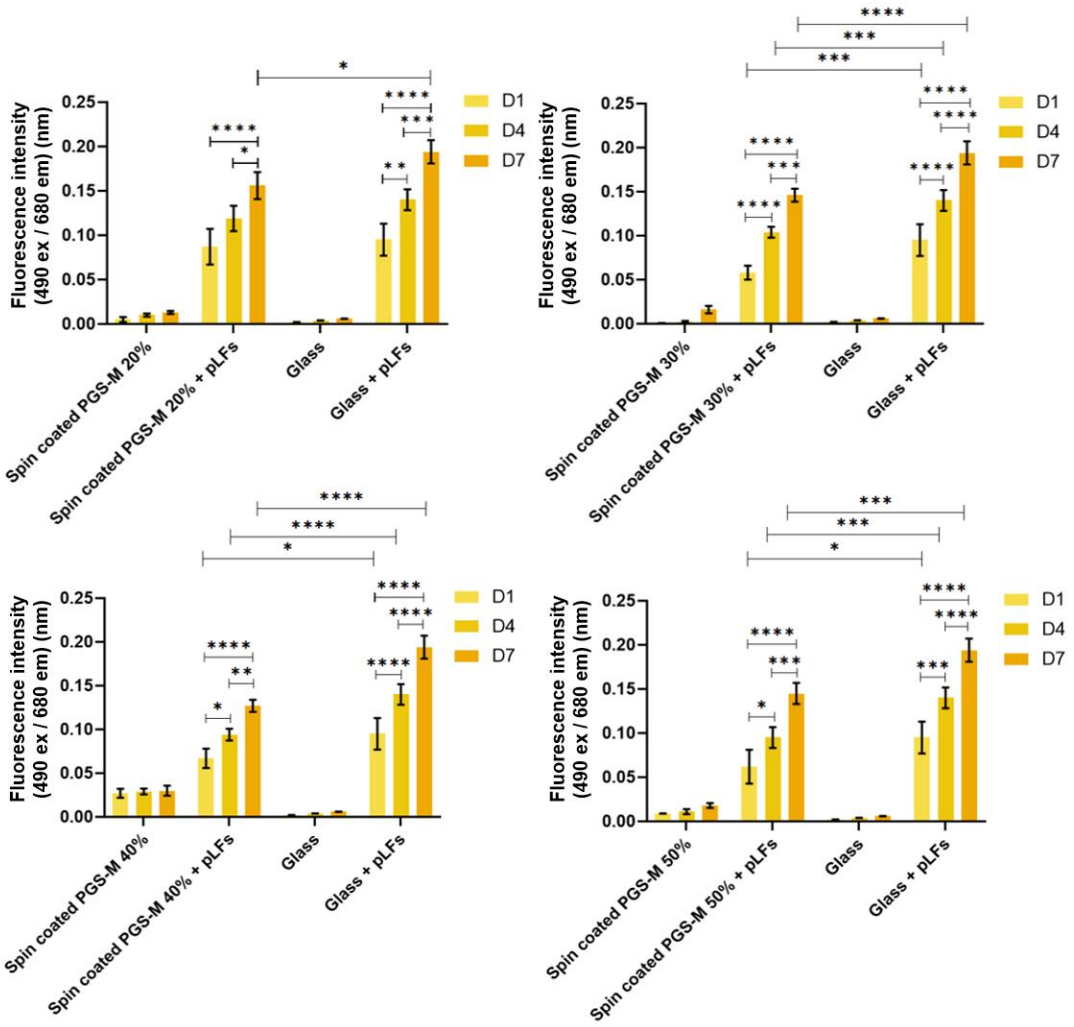

Figure 4.11 LDH release assay of pLF's culture on spin coated PGS-M (20 - 50 % DM). Positive controls were pLF's culture on uncoated borosilicate glass. Negative controls were PGS-M spin coated substrates (20 - 50 % DM) and coated borosilicate glass without cells. The assay was carried out in days 1,4 and 7(N=3). Samples show means and error bars corresponding to ±SD (N=3, n=3), analysed by two-way ANOVA, Tukey's post-hoc pairwise comparison. P≤0.05 was considered statistically significant (*).

Spontaneous LDH release of pLF's seeded on spin coated PGS-M is comparable with the one obtained in the positive control. There is a significant difference between pLF's seeded on PGS-M 20% and pLF's seeded on glass in day 7 (P≤0.05). For PGS-M 30% the difference increases from day 1, 4 and 7 (P≤0.001, P≤0.001 and P≤0.0001, respectively). pLF's seeded on PGS-M 40% show

significant difference on days 1, 4 and 7 (P≤0.05, P≤0.0001 and P≤0.0001, respectively). Lastly, pLF's seeded on PGS-M 50% the results on days 1,4 and 7 were also significantly different (P≤0.05, P≤0.001 and P≤0.001, respectively). Based on these results, we can infer that spin coated PGS-M substrates do not cause significant cytotoxicity regardless of DMs

It was decided to test PicoGreen® DNA quantification assay only on PGS-M 40% as it is the DM with mechanical properties that better matched the native cornea and with lower percentage of sol content (Chapter 2). It is planned to use only this DM in the elaboration of the corneal device, making its optimization a crucial part of this study.

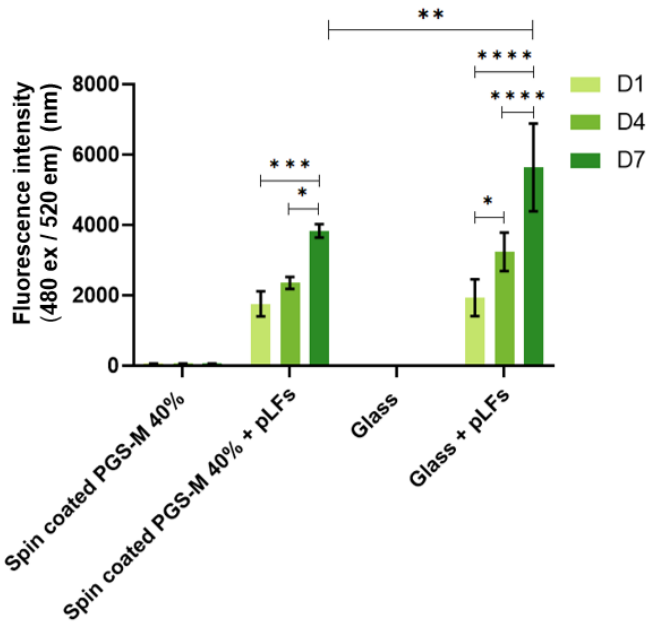

Figure 4.12 PicoGreen® DNA quantification assay of pLF's culture on spin coated PGS-M (40 % DM). Positive controls were pLF's culture on uncoated borosilicate glass. Negative controls were PGS-M spin coated substrates (40 % DM) and coated borosilicate glass without cells. The assay was carried out in days 1,4 and 7 (N=3). Samples show means and error bars corresponding to ±SD (N=3, n=3), analysed by two-way ANOVA, Tukey's post-hoc pairwise comparison. P≤0.05 was considered statistically significant (*).

In Figure 4.12 it is possible to observe that the PicoGreen® DNA quantification assay corroborates with data obtained with resazurin reduction assay: pLF's are growing on PGS-M spin coated substrates. There is no significant difference between pLF's seeded on PGS-M and pLF's seeded on glass in days 1 and 4, but there is a significant difference in day 7 ($P \leq 0.01$).

Cell morphology on spin coated PGS-M substrates was also analysed with fluorescence microscopy. Image acquisition was carried out only with phalloidin-FITC (495 nm excitation and 520 nm emission) because PGS-M was found to show fluorescence at 405 nm excitation and 450 nm emission (which overlaps with DAPI) (Figure 4.13).

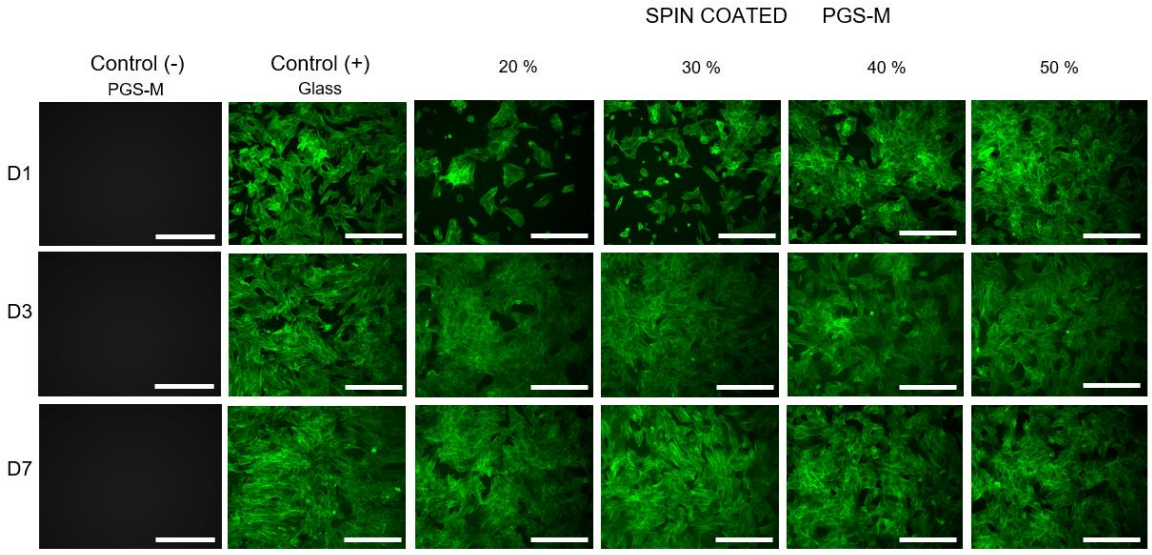

Figure 4.13 Fluorescence microscopy images of pLF's culture on spin coated PGS-M (20 - 50 % DM). Positive controls were pLF's culture on uncoated borosilicate glass. Negative controls were PGS-M spin coated substrates. The images were taken in days 1,4 and 7. All images were acquired using the same exposure and display settings. Scale bars are 200 μm.

Despite those previous results show pLF's growing and proliferating on PGS-M spin coated surfaces after 7 days of culture, the cell morphology is not as expected on PGS-M substrates in comparison with pLF's grown on glass. Morphology is an

important feature that can tell us about cell behaviour, stability and stress response to a variety of conditions [278,279]. Spindle-shaped fibroblasts are observed on glass surfaces while more rounded cells with pseudopodia retraction are observed on PGS-M substrates. Interestingly, lower DMs seem to affect pLF's morphology more than higher DMs. This can be caused by the lower stiffness in lower DMs, as was reported before by Yeung et al., where it was shown that fibroblasts grew better on stiffer substrates. Also, Jones et al. demonstrated that stiffer collagen gels promote cell differentiation using hLEC's [280]. Cells grown on softer substrates presented a rounded shape like pLF's on PGS-M surfaces in this present work [281]. Also, the high amount of sol fraction in lower DMs can be affecting cell growth as was shown in Resazurin assays. Previous reports show that cell morphology can be a response of the interaction with a material (mechanical, biochemical and architectural features) [212,282,283]. Nonetheless, more analyses are still required to elucidate what is causing this cell behaviour.

4.4.7 HUMAN DERMAL FIBROBLASTS (hDF's) CULTURE ON SPIN COATED PGS-M SURFACES

Fibroblasts from human skin, oral mucosa, periodontal membrane, or embryonic lung have been widely used in studies for the evaluation of material cytotoxicity [284,285]. Fibroblasts are useful in studies of adhesion to surfaces, replication, and cellular integrity due to their characteristics [286]. However, cytotoxicity studies are more reliable when carried out with the cells present in the target tissue. Biocompatibility, cell viability and cytotoxicity of hDF's in PGS-M surfaces were evaluated with resazurin reduction assay, PicoGreen® DNA quantification assay, LDH release assay and F-actin staining. Due to the low availability of human and pig cells, the continuous failure in cell culture, and previous reports that show positive results of fibroblasts seeded on spin coated PGS-M substrates, it was decided to use hDF's for cell proliferation studies on PGS-M.

hDF's were seeded on PGS-M spin coated substrates with 20, 30, 40, and 50% DM to evaluate material cytotoxicity and observe differences of culture compared with pLF's. Cell proliferation and cytotoxicity were evaluated with resazurin reduction assay and LDH release assay in spin coated PGS-M 20 - 50 %.(Figures 4.14 and 4.15). PicoGreen® DNA quantification assay was evaluated only in spin coated PGS-M 40% DM (Figure 4.16).

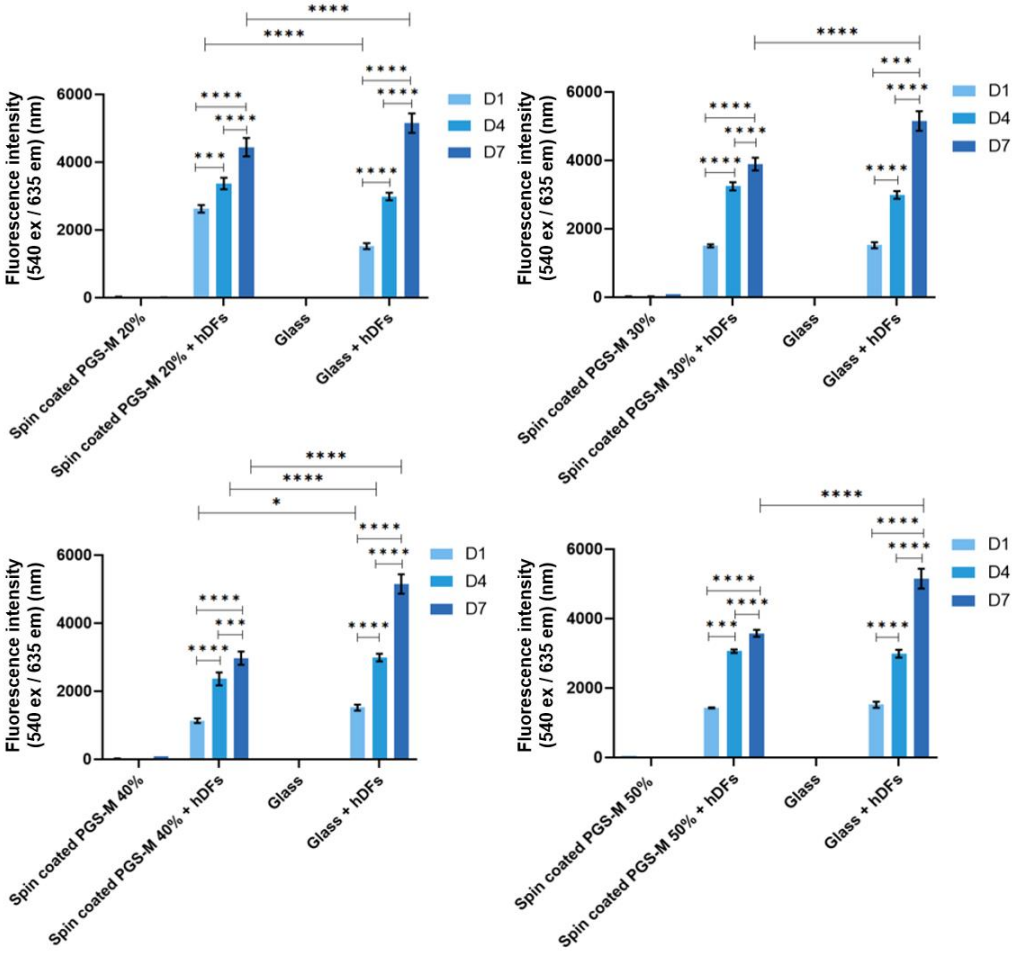

Figure 4.14 Resazurin reduction assay of hDF's culture on spin coated PGS-M (20 - 50 % DM). Positive controls were hDF's culture on uncoated borosilicate glass. Negative controls were PGS-M spin coated substrates (20 - 50 % DM) and coated borosilicate glass without cells. The assay was carried out in days 1,4 and 7 (N=3). Samples show means and error bars corresponding to ±SD (N=3, n=3), analysed by two-way ANOVA, Tukey's post-hoc pairwise comparison. P≤0.05 was considered statistically significant (*).

In figure 4.14 is possible to observe that hDF's showed similar behaviour growing on PGS-M spin coated substrates, as cells grew better on lower DM. This suggests that our hypothesis regarding the amount of gel fraction affecting cell growth is correct.

There is a significant difference between hDF's seeded on 20% DM and hDF's seeded on glass in days 1 and 7 ($P \leq 0.0001$). For hDF's seeded on 30% and hDF's seeded on glass, there is a difference on day 7 ($P \leq 0.0001$). hDF's seeded on 40% DM and hDF's seeded on glass were significantly different at all timepoints ($P \leq 0.05$, $P \leq 0.0001$ and $P \leq 0.0001$, respectively) and between hDF's seeded on 50% DM and hDF's seeded on glass in day 7 ($P \leq 0.0001$).
The spontaneous LDH release in positive controls (hDF's culture on borosilicate glass) were compared with spontaneous LDH release in hDF's culture on spin coated PGS-M (Figure 4.15).

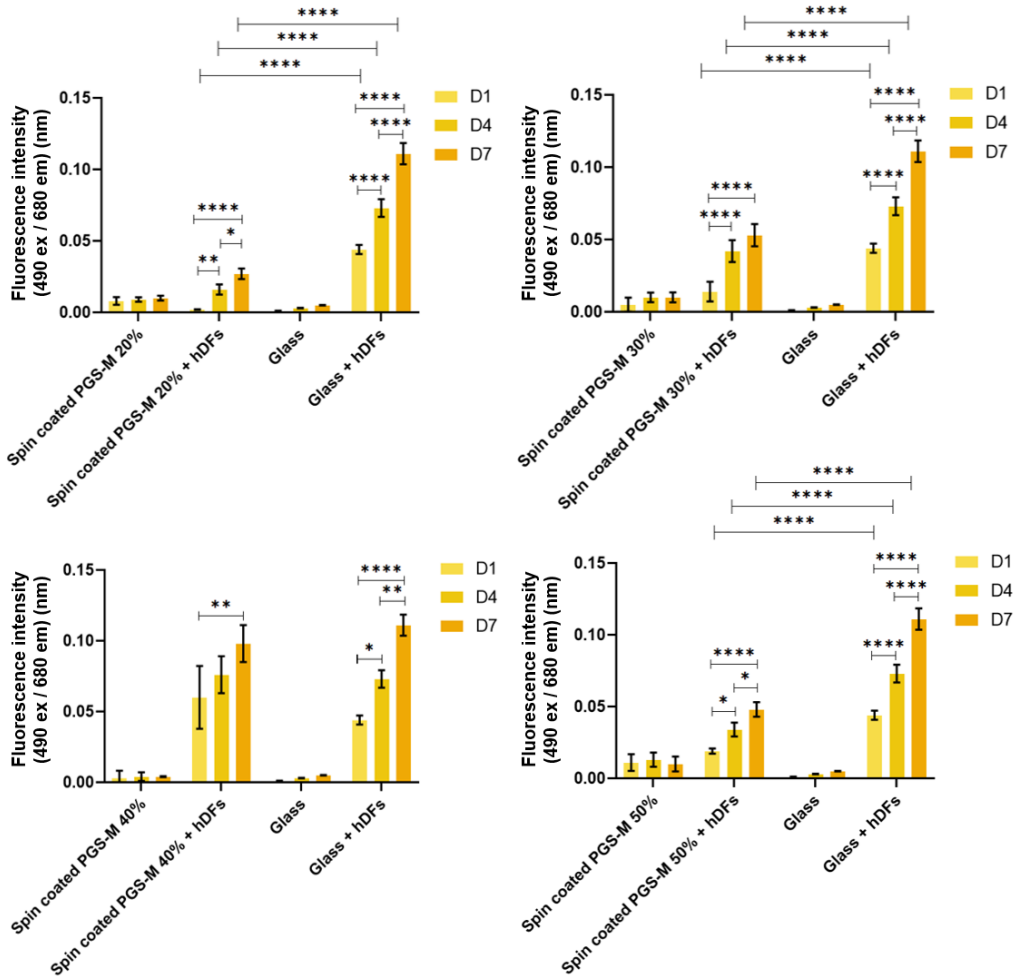

Figure 4.15 LDH release assay of hDF's culture on spin coated PGS-M (20 - 50 % DM). Positive controls were hDF's cultured on uncoated borosilicate glass. Negative controls were PGS-M spin coated substrates (20 - 50 % DM) and coated borosilicate glass without cells. The assay was carried out in days 1,4 and 7. Samples show means and error bars corresponding to ±SD (N=3, n=3), analysed by two-way ANOVA, Tukey's post-hoc pairwise comparison. P≤0.05 was considered statistically significant (*).

Spontaneous LDH release of hDF's seeded on spin coated PGS-M is lower for 20, 30 and 50% DM compared with the positive control. There is a significant difference between hDF's seeded on PGS-M 20, 30, and 50% DM, and hDF's seeded on glass in all time points (P≤0.0001 for all of them). On the other hand, there is no significant difference between LDH for hDF's seeded on 40% DM and glass.

Therefore, we can infer that there is no significant cytotoxicity proceeding from spin coated PGS-M substrates for hDF's as it is lower compared with control.

PicoGreen® DNA quantification assay was carried out only on PGS-M 40% due to it being the DM with mechanical properties that better matched the native cornea and with the lower percentage of sol content (Chapter 2).

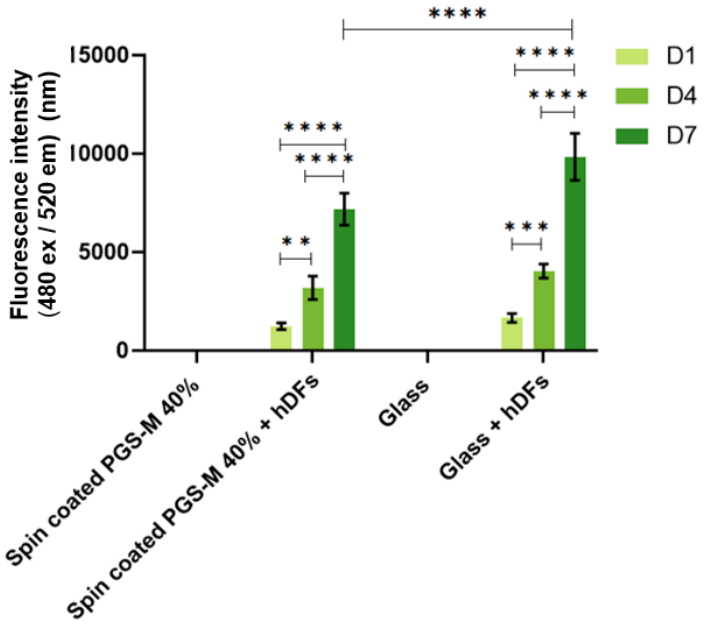

Figure 4.16 PicoGreen® DNA quantification assay of hDF's cultured on spin coated PGS-M (40 % DM). Positive controls were hDF's cultured on uncoated borosilicate glass. Negative controls were PGS-M spin coated substrates (40 % DM) and coated borosilicate glass without cells. The assay was carried out in days 1,4 and 7. Samples show means and error bars corresponding to ±SD (N=3, n=3), analysed by two-way ANOVA, Tukey's post-hoc pairwise comparison. P≤0.05 was considered statistically significant (*).

Figure 4.16 shows that the PicoGreen® DNA quantification assay is well correlated with data obtained with resazurin reduction assay: hDF's are growing on PGS-M spin coated substrates. There is no significant difference between pLF's seeded on PGS-M and pLF's seeded on glass in days 1 and 4, but there is a significant difference in day 7 ($P \leq 0.0001$).

Cell morphology was evaluated and compared with control. Cells were stained with phalloidin-FITC (495 nm excitation and 520 nm emission) (Figure 4.17).

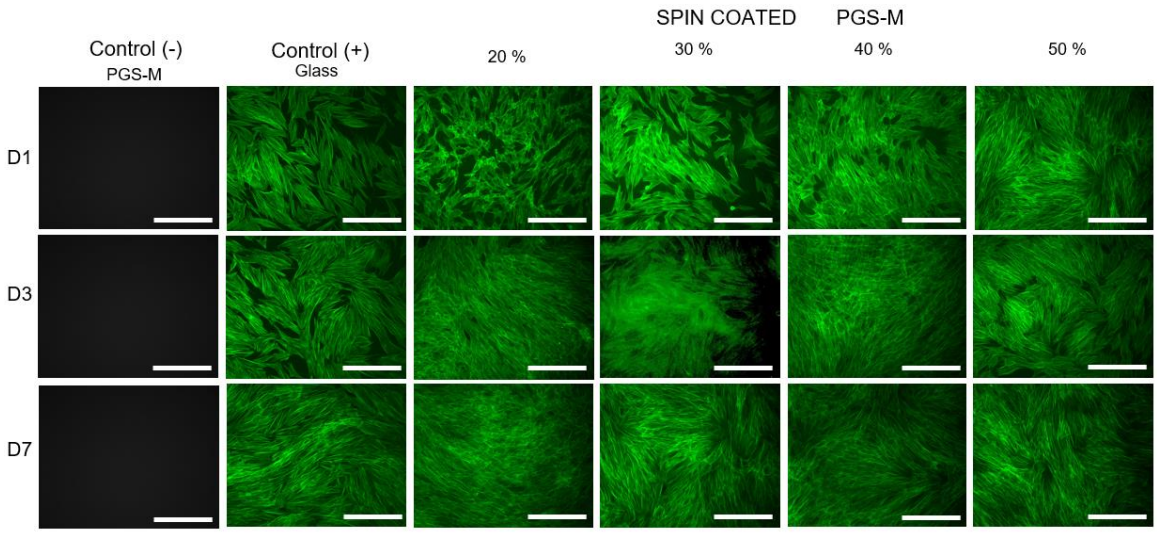

Figure 4.17 Fluorescence microscopy images of hDF's culture on spin coated PGS-M (20 - 50 % DM). Positive controls were hDF's culture on uncoated borosilicate glass. Negative controls were PGS-M spin coated substrates. The images were taken in days 1,4 and 7. Scale bars are 200 µm. All images were acquired using the same exposure and display settings.

hDF's seem to grow better than pLF's on spin coated PGS-M substrates which can be due cell adhesion, proliferation, and protein production change depending on the cells and substrate, as was shown by Tamada et al., who worked with fibroblasts grown on different polymer surfaces, and Tokiwa at al., who worked with human hepatoblastoma and hepatoma cells seeded on collagen type I, type IV, fibronectin, and laminin [278,287]. It is possible to observe that cell morphology on lower DM (20 and 50%) is more rounded, with cells presenting pseudopodia retraction, while cells on higher DM 40 and 50% are spindle-shaped since day 1. This suggests that lower stiffness in lower DMs is also affecting hDF's as was observed with pLF's. Also, the high amount of sol fraction in lower DMs can be affecting cell growth, as was shown in the Resazurin assays. Therefore, more

analyses are still required to elucidate what is causing this cell behaviour and how we can improve PGS-M as a material for corneal regeneration.

4. 5 CONCLUSIONS

This chapter explored the culture of three cell types on spin coated and bulk PGS-M substrates. In Chapter 2, it was established that the DM with mechanical properties that better matched the native cornea and with lower percentage of sol content was 40%. However, this was subject to further biological evaluation. In this chapter, bulk flat PGS-M scaffolds with 1 mm thickness were used to evaluate PGS-M biological performance on 20-50% DM (cell proliferation and cytotoxicity).

hLEC's were used as the standard for ocular biomaterial applications and seeded on bulk PGS-M substrates. However, due to the problems presented during cell culture and the low fluorescence signal from the resazurin reduction assay, their culture was postponed until conditions could be optimized for their use.

pLF's were seeded on PGS-M substrates as the second choice of cells for the evaluation of biocompatibility, cell viability, and cytotoxicity on PGS-M surfaces, with cells showing a higher fluorescence signal compared to hLEC's. Nonetheless, samples without cells also showed a high signal. It was unclear if the material or cells are having a negative effect on proliferation. Likewise, the reason for fluorescence in samples without cells is yet unknown, which will be further discussed in Chapter 5.

Both cell types shown similarities in attachment at day 1 after seeding compared to the control. However, cells on PGS-M substrates began dying on day 4 and 7 regardless of DM. Therefore, the use of human dermal fibroblasts and spin coated surfaces was proposed to elucidate the cause of cell death after several days of culture on the material, due to previous positive results in culture on spin coated PGS-M substrates with 25-100% DM.

pLF’s and hDF’s were seeded on PGS-M spin coated substrates and showed positive results on cell growth. However, cell morphology was not as expected on PGS-M substrates in comparison with pLF’s grown on glass. Cell morphology is an important feature that can tell us about cell behaviour, stability, and stress response to a variety of conditions. Cells seeded on lower DMs showed a rounded shape with pseudopodia retraction in comparison with cells seeded on higher DM and glass, which showed a spindle shape. Our hypothesis is that lower stiffness and higher percentages of sol fraction in lower DMs affect cell growth.

More analyses are still required to elucidate the reason for cell death and morphological change after attachment on the substrates. As shown in Chapter 2, PGS-M has excellent tuneable physicochemical properties, which are highly advantageous for tissue engineering. It also has the optical properties (transparency) which have not yet been found in any other synthetic polymer, making it an ideal candidate for the fabrication of corneal devices. However, there are no reports of successful cell proliferation on PGS-M substrates thicker than 350 µm. This is the most significant challenge that needs to be overcome to improve PGS-M as a material for corneal regeneration.

CHAPTER 5. IMPROVEMENT OF PGS-M SCAFFOLDS FOR CELL CULTURE

5.1 INTRODUCTION

In the previous chapter, we observed the interaction of 3 cell types (limbal epithelial cells (hLEC's), human dermal fibroblasts (hDF's) and pig limbal fibroblasts (pLF's)) with spin coated and bulk PGS-M surfaces. It was shown that animal and human cells grow better on spin coated surfaces, but cell morphology is affected in lower DMs. On the other hand, bulk surfaces present a certain degree of cytotoxicity, mainly in the ocular cells. In this chapter, strategies to overcome the cytotoxicity issue found in the transparent PGS-M will be explored. The cytotoxicity for *in vitro* culture is defined as a factor that affects morphology, cell attachment, and growth rate or leads to cell death[1,2].

5.2 OBJECTIVES

5.2.1 GENERAL OBJECTIVES

Develop strategies that allow the Improvement of PGS-M for its use in corneal cell culture.

5.2.2 SPECIFIC OBJECTIVES

- Implement of physical modifications of PGS-M substrate to improve it biocompatibility
- Evaluate biological modifications of PGS-M scaffolds to increase the interaction cell-substrate
- Develop chemical modifications to reduce cytotoxicity

5.3 MATERIALS AND METHODS

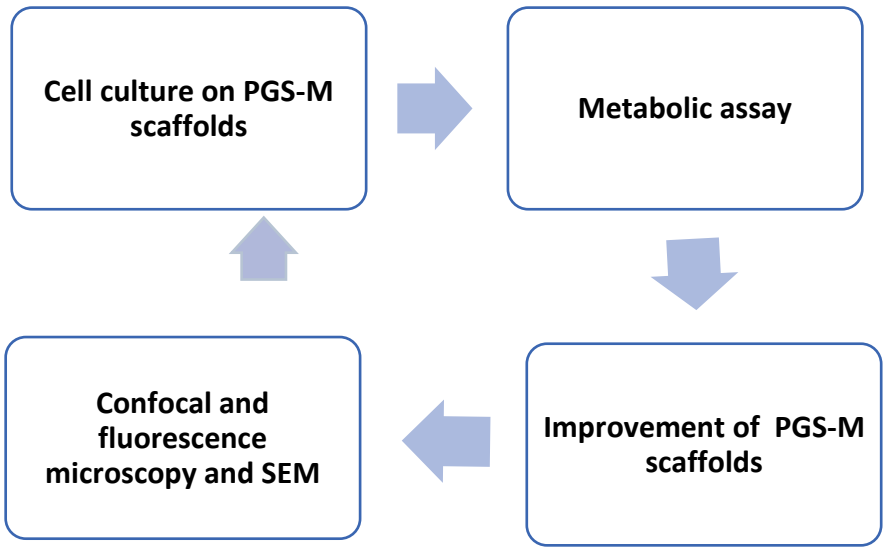

Figure 5.1 Methods diagram for the improvement of PGS-M scaffolds for cell culture

5.4 SCAFFOLD MODIFICATIONS

Physical, biological, and chemical modifications were proposed to improve PGS-M biocompatibility.

5.4.1 PHYSICAL MODIFICATIONS

5.4.1.1 SCAFFOLD THICKNESS

The native human cornea has an approximate thickness of ~500 μm [288]. Therefore, we decided to evaluate the reduction of thickness of scaffolds as a method to improve biocompatibility. New moulds were fabricated as described in section 3.3.2 with 15 mm diameter and 500 μm thickness (this modification was carried out only in this physical modification) (Figure 5.2). The scaffolds were

washed as described in section 3.3.3 and sterilized as described in section 4.4.5 prior cell culture.

Figure 5.2 Scaffold thickness reduction from 1 mm to 500 μm

5.4.1.2 MEDIA WASHES (pH)

Sterile PGS-M scaffolds (1 mm thickness) were placed in 6 well plates and incubated at 37.5 °C, 5% CO_2 in growth media (composition was described in section 4.3.2) and dH_2O for 5 days with a media/dH_2O change each 24 hours (Figure 5.3).

Figure 5.3 Scaffold media washes

5.4.1.3 SOXHLET EXTRACTION

Another method proposed to remove the sol fraction was Soxhlet extraction. Soxhlet extraction was carried out using methanol as the organic phase, washing for 24 hours to remove unreacted monomers. Then, PGS-M scaffolds (1 mm thickness) were dried 24 hours under vacuum. Afterwards, scaffolds were subjected to Soxhlet extraction with dH_2O for 24 hrs to remove both unreacted monomers and remaining solvent (Figure 5.4).

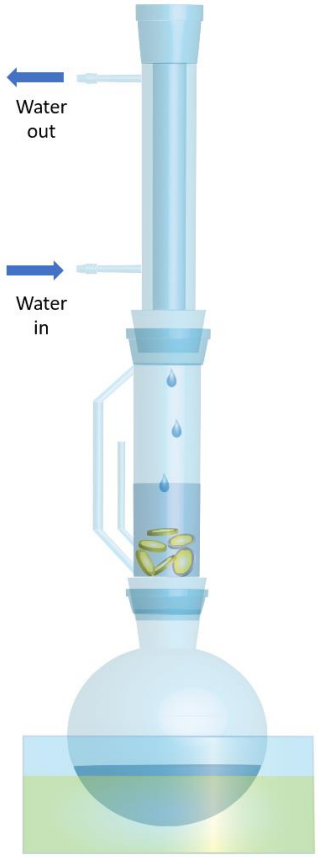

Figure 5.4 Soxhlet extraction. First wash under vacuum with methanol (24 hr), second wash under vacuum with dH_2O (24 hr).

5.4.1.4 SCAFFOLD ARCHITECTURE

Scaffold architecture has been reported as a feature that can promote cell attachment, migration, and proliferation. As was described in Chapter 3, the scaffolds designed with microfeatures in this work are proposed to increase cell survival and proliferation. The chosen scaffold is one with micro pockets, symmetric patterns, and concentric channels reaching the centre (Figure 5.5).

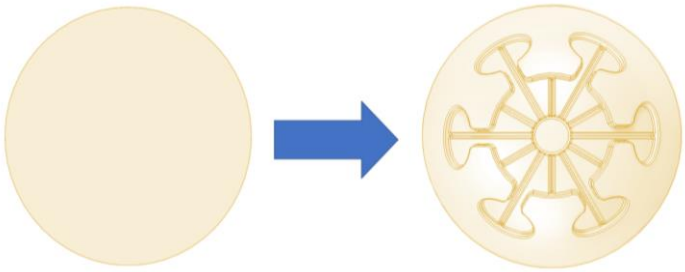

Figure 5.5 Scaffold architecture with flower pattern with niches and channels

5.4.2 BIOLOGICAL MODIFICATIONS

5.4.2.1 CELL SEEDING

Different seeding techniques are applied to guarantee cell attachment, and the most widely used is passive seeding [289]. This technique consists in adding a cell suspension on the scaffold surface for a predetermined time which allows attachment, then the scaffold is placed in a new petri dish. PGS-M disks (1 mm thickness) were placed in 6 well dishes. The pLF's were seeded with passive seeding. Drop seeding in the limbal artificial niches (developed in this work, Chapter 3) was carried out as described by Ortega et al [3] (Figure 5.6). In passive seeding, 50,000 cells were seeded in each plate in 2 ml of media. For seeding in niches, 20,000 cells were seeded within each niche in 5 µl of media. It has been reported that ~90% of endothelial cell and fibroblast attach on TCP after 6 hours. Thus, cell attachment was carried out for 6 hours with each seeding technique.

Afterwards, scaffolds were placed in a new petri dish to only allow attached cells to proliferate.

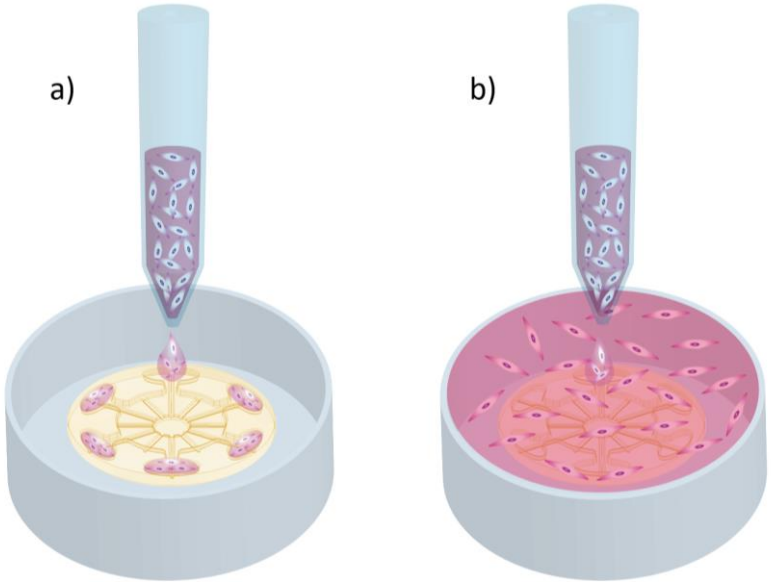

Figure 5.6 Cell seeding technique. a) Cell seeded in the scaffold niches in droplets. b) Passive seeding technique

5.4.2.2 GELATIN COATING

Gelatin (Sigma-Aldrich) solution was prepared at 0.1 % (w/v) concentration. After Soxhlet washes and sterilisation, PGS-M disks (1 mm thickness) were incubated in gelatin solution overnight before cell culture (Figure 5.7).

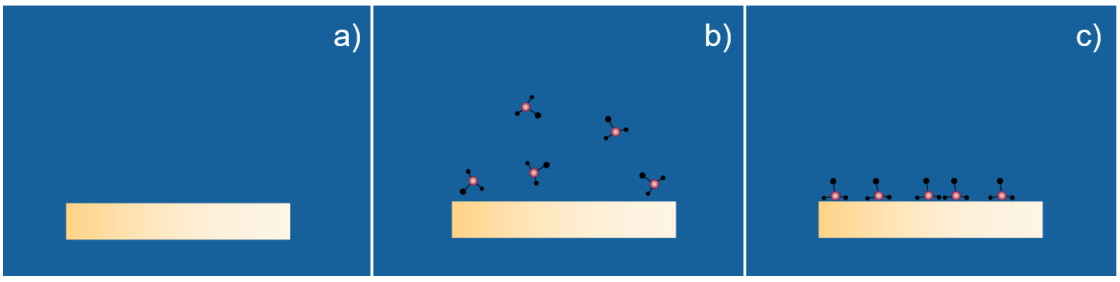

Figure 5.7 a) PGS-M scaffold before gelatin coating, b) PGS-M scaffold during gelatin coating, c) PGS-M scaffold after gelatin coating

5.4.2.3 PROTEIN IMMOBILIZATION

Covalent gelatin immobilization was adapted from the protocol reported by Ma et al. for poly-L-lactic acid (PLLA), poly(hydroxyethyl methacrylate) (PHEMA) and poly(methacrylic acid) (PMAA) films [290] (Figure 5.8) . The -OH free reactive groups from PGS-M were grafted with sulfonate groups, and then functionalized with gelatin. PGS-M disks (1mm thickness) were incubated at 20 ºC for 2 hours in a solution of 2 ml methyl sulfonyl chloride and 20 ml diethyl ether. Afterwards, the disks were washed with Soxhlet extraction as described in section 5.4.1.3. Then, PGS-M disks were incubated at 30 ºC for 24 hours immersed in a gelatin solution (2 mg/ml). Prior to cell culture, the disks were sterilized in the autoclave at 121°C for 30 minutes.

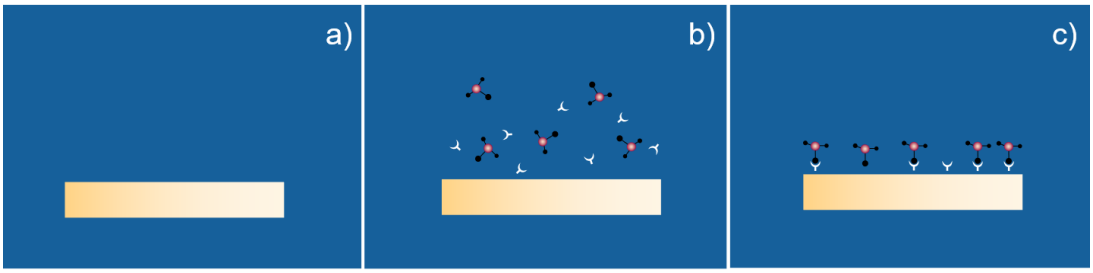

Figure 5.8 a) PGS-M scaffold before protein immobilisation, b) PGS-M scaffold during protein immobilisation, c) PGS-M scaffold after protein immobilisation

5.4.3 CHEMICAL MODIFICATIONS

5.4.3.1 PLASMA COATING

PGS-M disks (1 mm thickness) were treated with a Zepto LF air plasma system for 1 minute and then sterilized in the autoclave at 121°C for 30 minutes for use in cell culture (Figure 5.9).

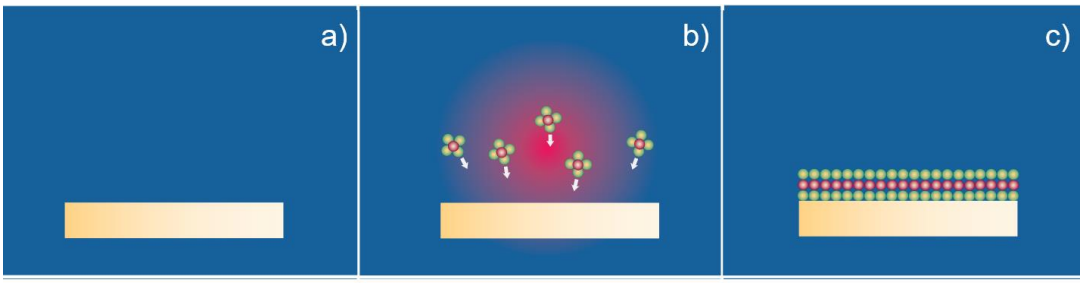

Figure 5.9 a) PGS-M scaffold before plasma coating, b) PGS-M scaffold during plasma coating, c) PGS-M scaffold after plasma coating

5.4.3.2 HEAT CROSSLINKING

PGS-M disks (1 mm thickness) were crosslinked at 120 ºC under vacuum for 24 hours (Figure 5.10). Then, disks were washed with Soxhlet as described in section 5.4.1.3. Before cell culture, the disks were sterilized in the autoclave at 121°C for 30 minutes.

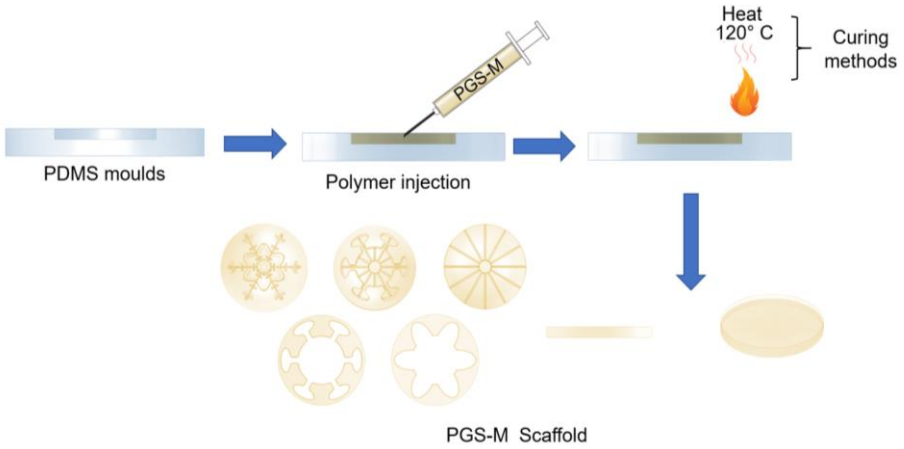

Figure 5.10 Flat PGS-M scaffolds fabrication with PDMS moulds and crosslinked with heat.

5.4.3.3 HEAT-UV CROSSLINKING

PGS-M disks (1 mm thickness) were crosslinked under UV light (200 W, OmniCure Series 2000 curing lamp) at different times (2.5 min, 10 sec, 20 sec, and 30 sec) and followed by crosslinking at 120 ºC under vacuum for 24 hours (Figure 5.11).

Afterwards, disks were washed with Soxhlet extraction as described in section 5.4.3.1. Before cell culture, disks were sterilized in the autoclave at 121°C for 30 minutes.

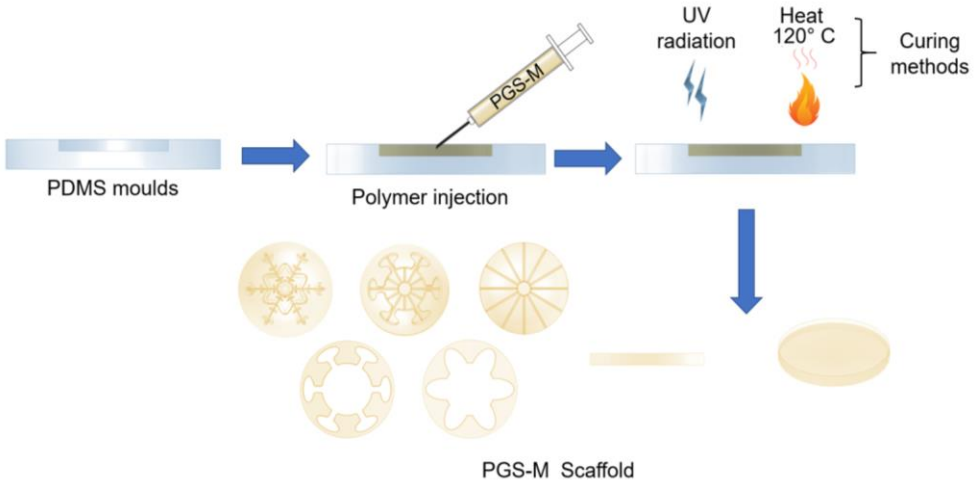

Figure 5.11 Flat PGS-M scaffolds fabrication with PDMS moulds and crosslinked with combination of UV and heat.

5.5 CHARACTERISATION

The biological evaluation was done by seeding pLF's on PGS-M scaffolds. Resazurin reduction was carried out as described in Chapter 4.3.7. In case that was considered necessary because of inconsistent results, cell proliferation was evaluated through F-actin staining, with microscopy as described in Chapter 4.3.10 and 4.3.11, respectively. The material that showed cell growth was characterised using the following techniques.

ATR-FTIR as was described in Chapter 2.4.5 and mechanical testing as was described in Chapter 2.4.7. SEM evaluation was done as follows: on day 14, the growth medium was removed from the samples, followed by gentle washes with PBS (three times). Samples were fixed by incubating at room temperature for 1 hour with 2.5% glutaraldehyde (in PBS). Then, samples were washed with PBS three times (15 minutes each) followed by one wash with dH_2O (5 minutes). To

dehydrate the samples, they were washed with methanol in dH_2O at different concentrations (35%, 60%, 80%, 90%, and 100%, 15 min each). Afterwards, the scaffolds were dried with HMDS/ethanol (1:1 w/w) for 1 hour and 100% HMDS for 5 minutes before air drying. Samples were affixed to aluminium stubs, gold coated using a sputter coater (Edwards S150B) and examined with a TESCAN Vega 3 LMU at an accelerating voltage of 10 kV. Histology was carried out as follows: on day 14, growth media was removed, and samples were washed with PBS (3 times). To fix the samples, they were incubated at room temperature for 30 minutes with paraformaldehyde 3.7%. Then, samples were dehydrated and embedded in wax, followed by demoulding. Using a microtome, sections were cut in 10 µm sections. The sections were placed on glass slides and stained with haematoxylin for 1.5 minutes and eosin for 5 minutes. Staining steps are given in table 5.1.

Table 5.1 H&E staining steps

STEP	**TIME**
Xylene	2 minutes
Xylene	2 minutes
100% IMS	2 minutes
70% IMS	2 minutes
Distilled water	2 minutes
Haematoxylin	1.5 minutes
Eosin	5 minutes
Tap water	1 minute
70% IMS	1 minute
100% IMS	1 minute

Xylene	2 minutes
Xylene	2 minutes

5.6 STATISTICS

The characterization was carried out with three independent experimental repeats (N=3) in triplicates per experiment (n = 3). The data was analysed with GraphPad Prism version 7.04 software. The data significance was calculated with one-way ANOVA with Tukey post-hoc pairwise multiple comparison analysis for experiments with one independent variable or factor (sample type or condition). Two-way ANOVA (paired samples) with Tukey post-hoc pairwise multiple comparison analysis was used for the experiments with two independent variables or factors (sample type or conditions). $P \leq 0.05$ was considered statistically significant (*) and $P > 0.05$ was considered non-significant (ns). Data was graphed as means ± SD (standard deviation).

5.7 RESULTS AND DISCUSION

5.7.1 PHYSICAL MODIFICATIONS

5.7.1.1 SCAFFOLD THICKNESS

It has been reported that scaffold thickness has an impact in cell growth and proliferation [291,292]. In Chapter 4, pLF's seeded on PGS-M scaffolds (1 mm thickness) showed attachment but start dying from day 3. The human cornea has a thickness around 500 µm [288]. Thus, this is the thickness that was proposed to clarify if it is the main cause of cell cytotoxicity. Resazurin reduction was carried out as was described on Chapter 4.3.8. to evaluate cell viability and proliferation (Figure 5.12).

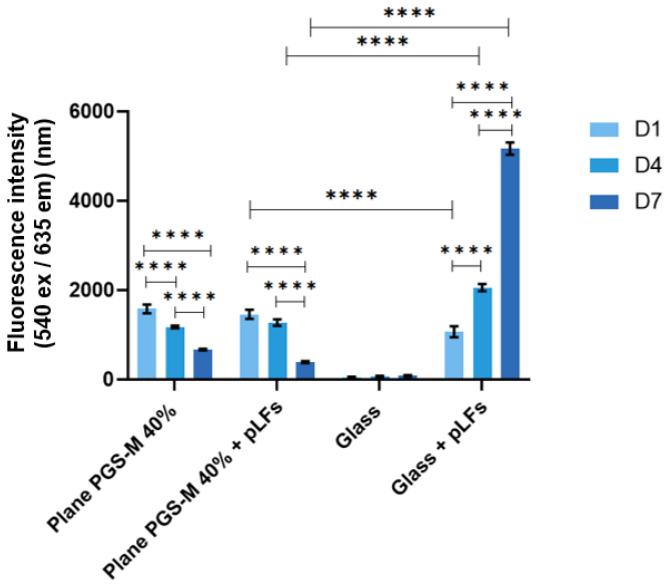

Figure 5.12 Resazurin reduction assay of pLF's culture on planar PGS-M transparent scaffolds 40 % DM with 500 µm thickness. Positive controls were pLF's cultured on borosilicate glass. Negative controls were PGS-M substrate 40 % DM and borosilicate glass without cells. The assay was carried out in days 1,4 and 7. Samples show means and error bars corresponding to ±SD (N=3, n=3), analysed by two-way ANOVA, Tukey's post-hoc pairwise comparison. P≤0.05 was considered significant (*).

It can be observed in Figure 5.12 that pLF's showed similar behaviour as previous results: cells attach on day 1 but start to die from day 3. Conversely, cells seeded on glass do not suffer from decreased growth. There is a significant difference between pLF's seeded on PGS-M in all time points, indicating a cytotoxic effect from PGS-M scaffolds during the initial days of growth (P≤0.0001).

Cell growth was also analysed with F-actin staining and microscopy in days 1, 3, and 7 to confirm results from metabolic activity evaluation (Figure 5.13).

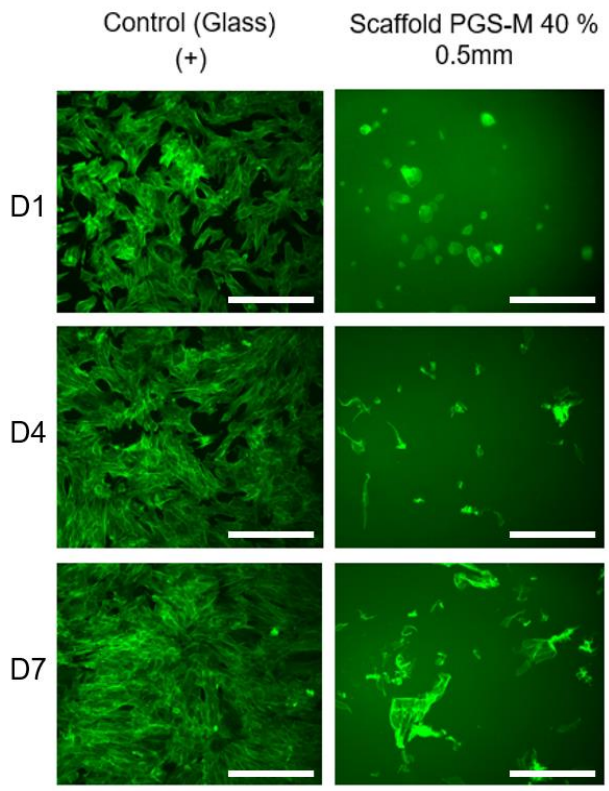

Figure 5.13 Fluorescence microscopy images of pLF's culture on PGS-M 40 % DM with 500 µm thickness. Positive controls were pLF's cultured on borosilicate glass. The images were taken in days 1,4 and 7 (D1, D4 and D7). All images were acquired using the same exposure and display settings. Scale bars are 200 µm.

Figure 5.13 shows that cells seeded on PGS-M scaffold died from day 1. According to the observed morphology, we can infer that the cell went through apoptosis after attachment on the substrate. Images from day 4 and 7 show cell debris, which most likely corresponds to the remains of cytoskeleton as F-actin staining was used.

The influence of the scaffold thickness on the cell growth has not been widely explored. However, it is well known that the nature of the material triggers a biological response in the surrounding tissue after application. This suggests that the volume of the material in the scaffold influences cell behaviour and growth in a certain way. Uygun et al. reported how thickness in chitosan membranes influenced mesenchymal stem cells (MSCs), enhancing cell growth and

proliferation as the membrane thickness was increased from 30 to 170 µm [291]. However, there appears to be an upper limit to the benefits obtained from thicker scaffolds. Haifei et al. reported that a skin grafts fabricated from a collagen–chitosan porous scaffolds lead to skin necrosis if the scaffold exceeds 2 mm of thickness [292]. This could be due to the lack of cell infiltration, slow degradation, or cytotoxicity from unreacted compounds within the structure.

The results from resazurin reduction, F-actin staining, and microscopy evaluations indicate that the reduction of thickness does not (by itself) improve cell survival and proliferation. Thus, additional modifications to the substrate are needed to overcome this issue.

5.7.1.2 MEDIA WASHES (pH)

Cell behaviour and viability is affected by crosslinked material and sol fraction (unreacted macromers) that leach out during cell culture [293]. Therefore, we decided to incubate the scaffolds in growth media one week prior cell culture to remove the non-crosslinked polymer and allow protein adsorption, increasing hydrophilicity and improving cell attachment [294].

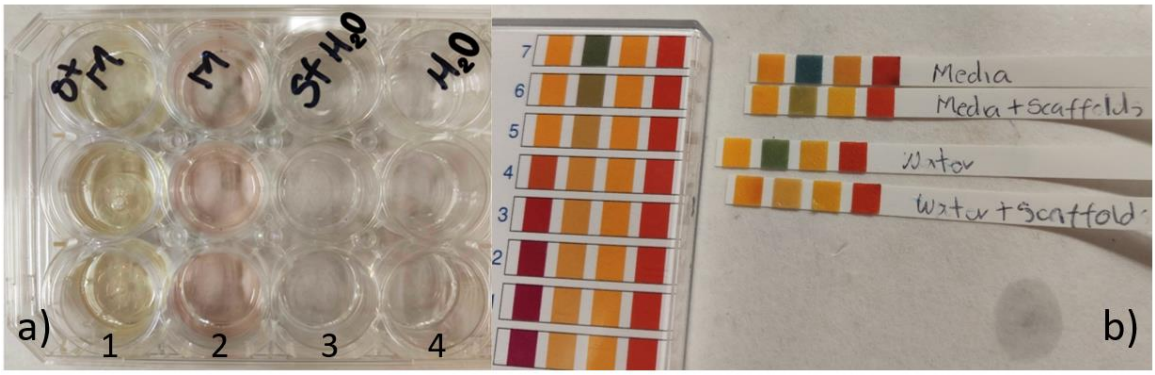

Figure 5.14 a) Scaffold washes (day 5) and b) the corresponding pH measurements with pH strips. The following conditions were tested: 1. Scaffold in media, 2. Media (control), 3. Scaffold in deionized water, 4. deionized water (control).

Figure 5.14 shows that scaffolds after 5 days culture still change the media pH (indicated by a change in colour). The media contains phenol red, a dye used as a colour indicator of media acidity [295]. Sample acidity was measured using pH strips in the absence of a pH meter. The pH drops in samples with the scaffold in media from pH 7 to pH 5.5, and from pH 7 to pH 3 for samples in deionized water. This difference can be explained by the presence of buffers in the media. While media changes did substantially reduce the pH drops compared to deionized water, they remain too acidic compared to optimum cell culture conditions. The pH in the media for cell culture should be stable to ensure cell growth and survival. pH drops below the optimal pH for an specific cell type will kill the cell culture. This is due to pH is a logarithmic scale, then a change in one unit in the pH scale corresponds to a tenfold increase of proton concentration.

Our hypothesis is that the unreacted carboxylic acid groups or the free carboxylic acid groups from the sebacic acid generated by aqueous hydrolysis of PGS-M ester groups acidify the media affecting the cell survival and causing cytotoxicity [110 143]. Wang et al. reported that high sol fraction-low gel fraction in poly(propylene fumarate) decreases metabolic activity in four cell types (human mesenchymal stem cells, fibroblasts, preosteoblasts, and mesenchymal stem cells) [296]. These results demonstrate that media washes are not enough to improve the cell growth on PGS-M substrates.

5.7.1.3 WASHES/SOXHLET EXTRACTION

Soxhlet is a technique that has been widely used to remove sol fractions in different synthetic and natural polymers, using solvents as methanol, hexane, toluene, ethanol, and dH_2O [297–301]. In comparison with the actual washing method (washing in methanol four consecutive times (24 hours each) followed by washing in dH_2O four consecutive times (24 hours each)), Soxhlet extraction is faster and can be used to wash the scaffold more consecutive times. This can considerably decrease the amount of unreacted reagents remaining in the material. However, results did

not show any improvement in cell culture. This suggests that there is another issue aside from unreacted reagents in PGS-M substrates which is causing cytotoxicity, likely associated to the pH drops that were previously observed.

5.7.1.4 SCAFFOLD ARCHITECTURE

The influence on cell behaviour (homeostasis, migration, differentiation, proliferation, alignment) by the substrate topography has been defined as contact guidance [218,219]. Substrate topographies have been previously developed with micro and nano scales [213]. Aligned and symmetrical patterns show more effect on cell alignment and filopodial guidance. On the other hand, cell seeded on random patterns have similar behaviour that the ones seeded on flat substrates [223,302–304]. Based on this evidence, we decided to seed the pLF's on the scaffolds with one of the architectures proposed in Chapter 3.

Figure 5.16 shows the resazurin reduction assay of pLF's seeded on flat and microfeatured PGS-M scaffolds (1 mm thickness).

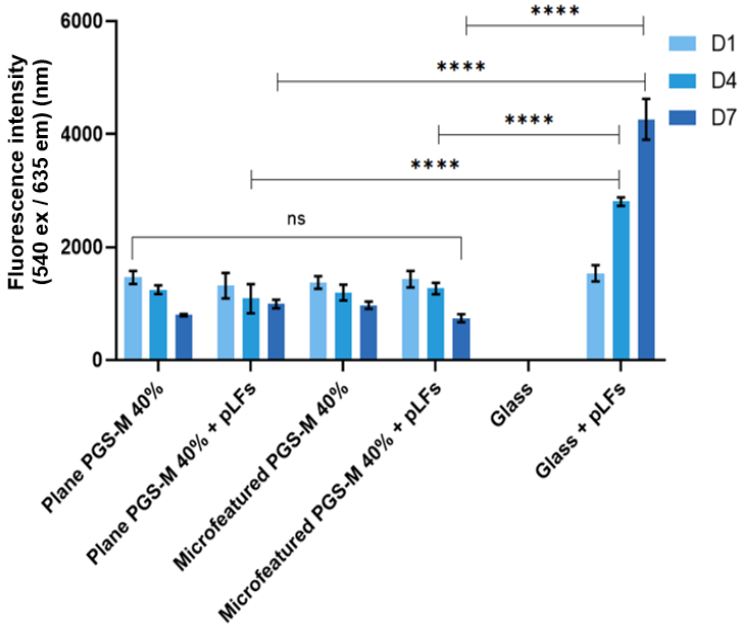

Figure 5.15 Resazurin reduction assay of pLF's culture on planar and microfeatured PGS-M transparent scaffolds 40 % DM with 1 mm thickness. Positive controls were

pLF's cultured on borosilicate glass. Negative controls were microfeatured PGS-M substrate 40 % DM and borosilicate glass without cells. The assay was carried out in days 1,4 and 7. Samples show means and error bars corresponding to ±SD (N=3, n=3), analysed by two-way ANOVA, Tukey's post-hoc pairwise comparison. P≤0.05 was considered significant (*).

Figure 5.15 shows that there is no significant difference in cell growth between flat and microfeatured PGS-M scaffolds. There is a significant difference in cell growth between PGS-M substrates and control in days 4 and 7 (P≤0.0001).

Cell growth on microfeatured PGS-M scaffolds was also analysed using fluorescence microscopy (Figure 5.16).

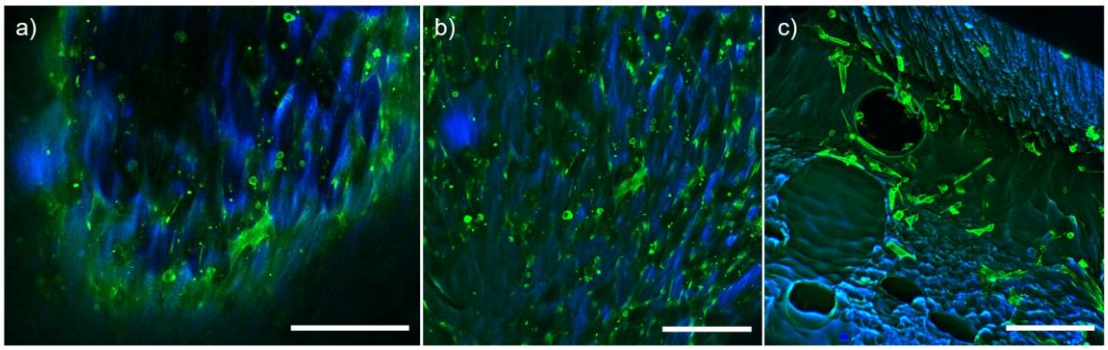

Figure 5.16 Fluorescence microscopy images of pLF's culture on microfeatured PGS-M 40 % DM: a) artificial niche, b) centre of the artificial niche, c) channel. Green colour: phalloidin-FITC staining, blue colour DAPI staining. The images were taken in Day 7. All images were acquired using the same exposure and display settings. Scale bars are 200 µm.

In figure 5.16, is possible to observe that most of the cells in the niches and channels are dead (cells with round shape). Previous reports indicate that cell adhesion and migration can be promoted by micro and nano topographies [212,305,306]. This suggests that the architecture in the substrate increases cell adhesive interactions that allow cell alignment and proliferation [222,223].

Lawrence et al. developed a silk pattern scaffolds for hLEC's, showing that architecture promotes cell attachment, migration, and actin-cell alignment [214]. In

addition, Kang et al. and Wu et al. reported that LEC's and human corneal stromal stem cells (hCSSC's) also show an increase in proliferation on patterned silk films [215,216]. However, there are no previous reports on microfeatured PGS-M substrates to compare the obtained results.

Teixeira et al. reported low hLEC's alignment in silicon oxide surface, while 3T3 fibroblast showed cell alignment [223]. This suggests that the material and the cell type also affect cell migration even in patterned substrates.

From the obtained results, we can conclude that microfeatured PGS-M scaffolds are not enough to promote cell proliferation. Further analyses and modifications are still required to improve cell survival on PGS-M substrates.

5.7.2 BIOLOGICAL MODIFICATIONS

5.7.2.1 CELL SEEDING

It is important to apply an efficient seeding technique to ensure cell attachment and proliferation, both on and within the substrate. The seeding techniques proposed in this section were the passive and the direct seeding in the niches. One of the main disadvantages of the passive seeding technique is that it is difficult for cells to form an uniform layer on the surface of the substrate [307,308]. For that reason, specific seeding in the niches was also explored. The seeding techniques for corneal substrates with 3D niches include cell encapsulation in gels [309–311] and seeding on top of mainly hydrogels, porous, and fibrous materials [26,253–256]. Seeding in the artificial niches has only been proposed by Ortega et al., who reported rabbit limbal epithelial cells(rLEC's) seeded in the limbal artificial niches and showed positive results in the promotion of cell migration [3]. This correlates well with previous reports on microfeatured scaffolds that increase cell attachment, proliferation, and alignment [316]. As there are not many reports on the direct seeding of corneal cells in 3D artificial niches, we believe that it is an area of opportunity that should be explored.

Seeding the cells on niches and passive seeding did not have any effect on cell survival. It is important to highlight that not only the seeding technique is an important factor for cell attachment, but also the material and the cell type are involved [317,318]. The previous modifications based on seeding strategy and scaffold architecture have been shown to not be related to proliferation. Our hypothesis is that the material itself is having a negative effect on cell survival. Further modifications are still required to improve the material for cell culture.

5.7.2.2 GELATIN COATING

Gelatin has been used as scaffold coating due to its properties. It is cheap, biocompatible, biodegradable, water soluble, and can be applied in thin layer to promote cell biocompatibility [319,320]. Gelatin has several advantages over collagen, it has more functional groups to allow adhesion and has less risk of generate an immune response as it is a denaturalized protein [321]. Gelatin also promotes hydrophilicity, cell attachment, and proliferation [322,323].

Figure 5.17 shows the resazurin reduction assay of pLF's seeded on PGS-M scaffolds coated with gelatin (0.1% w/v).

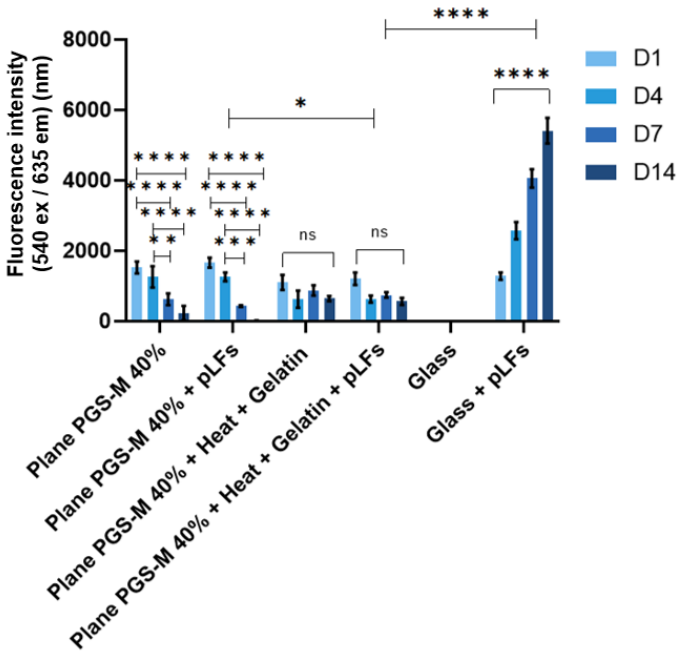

Figure 5.17 Resazurin reduction assay of pLF's culture on planar PGS-M transparent scaffolds 40 % DM with 1 mm thickness coated with gelatin (1% w/v) . Positive controls were pLF's cultured on borosilicate glass. Negative controls were microfeatured PGS-M substrate 40 % DM coated with gelatin (1% w/v) and borosilicate glass without cells. The assay was carried out in days 1,4,7 and 14. Samples show means and error bars corresponding to ±SD (N=3, n=3), analysed by two-way ANOVA, Tukey's post-hoc pairwise comparison. P≤0.05 was considered significant (*).

Results showed that cell attachment was higher in the uncoated PGS-M substrates compared with coated ones (38% and 26%, respectively). However, cell survival did not improve, as after day 1 cells started to die in coated and uncoated scaffolds. There is a significant difference between cells seeded on coated scaffolds and uncoated scaffolds on day 4 (P≤0.05). We can infer from the results that coating with gelatin did not improve cell survival and proliferation.

5.7.2.3 PROTEIN IMMOBILIZATION

Gelatin immobilization was proposed as an alternative to improve cell survival due to the failure of gelatin coating. Cell growth was evaluated with the resazurin reduction assay (Figure 5.18).

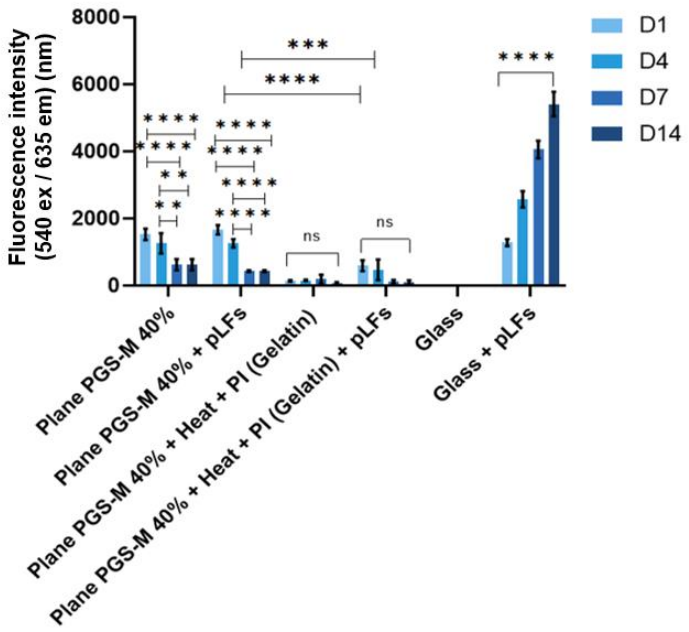

Figure 5.18 Resazurin reduction assay of pLF's culture on planar PGS-M transparent scaffolds 40 % DM with 1 mm thickness with gelatin immobilization (PI) . Positive controls were pLF's cultured on borosilicate glass. Negative controls were microfeatured PGS-M substrate 40 % DM with gelatin immobilization (PI) and borosilicate glass without cells. The assay was carried out in days 1,4,7 and 14. Samples show means and error bars corresponding to ±SD (N=3, n=3), analysed by two-way ANOVA, Tukey's post-hoc pairwise comparison. P≤0.05 was considered significant (*).

It can be observed in Figure 5.18 that protein immobilization showed a negative effect on cell survival, which was opposite of what was expected. It has been previously reported that gelatin immobilization can generate some degree of cytotoxicity due to the reagents used during the process [320]. It is important to mention that the protocol that was used did not mention a purification step to "clean" the scaffolds. While Soxhlet extraction washes proposed in this work were used for these gelatin immobilized scaffolds, we can conclude that it was not enough to remove the remaining reagents, causing cytotoxicity in pLF's.

5.7.3 CHEMICAL MODIFICATIONS

5.7.3.1 PLASMA TREATMENT

Plasma treatment is a surface modification that has been used to improve cell adhesion and proliferation without change the material bulk properties [324–327]. This treatment generates reactive sites on the substrate surface that increase the polymer energy and promote adhesive properties, resulting in the improvement of biocompatibility and hydrophilicity [328–330]. It has been reported that cornea cell growth and survival is improved on plasma treated substrates [331]. Therefore, PGS-M substrates were treated with air plasma and cell growth was evaluated with the resazurin reduction assay (Figure 5.19).

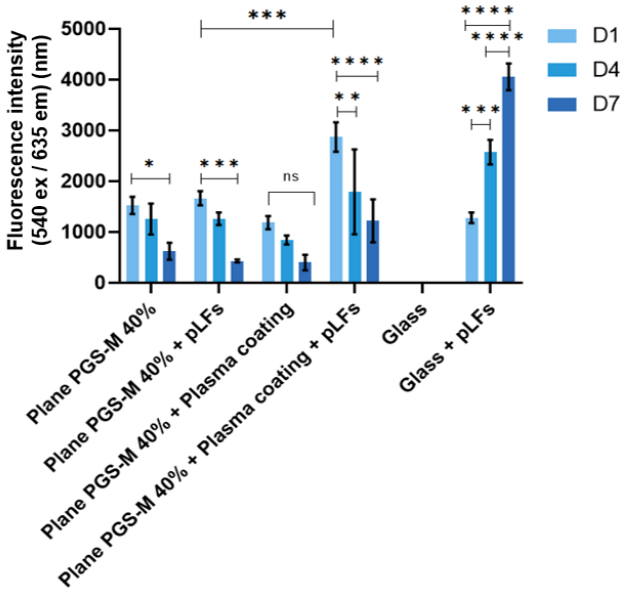

Figure 5.19 Resazurin reduction assay of pLF's culture on planar PGS-M transparent scaffolds 40 % DM with 1 mm thickness with plasma coating . Positive controls were pLF's cultured on borosilicate glass. Negative controls were microfeatured PGS-M substrate 40 % DM with plasma coating and borosilicate glass without cells. The assay was carried out in days 1,4,7 and 14. Samples show means and error bars corresponding to ±SD (N=3, n=3), analysed by two-way ANOVA, Tukey's post-hoc pairwise comparison. P≤0.05 was considered significant (*).

It can be observed in Figure 5.19 that cell attachment was improved with plasma coating from 25% in uncoated PGS-M substrates to 42% in plasma coated substrates. However, even with this modification and the improvement in cell attachment in day 1, cells started to die in day 3. There was only a significant difference between PGS-M and plasma coated PGS-M on day 1 ($P \leq 0.001$). Thus, further PGS-M modifications are still needed to allow cell survival on the substrate.

5.7.3.2 HEAT CROSSLINKING

PGS has been widely used as a biomaterial for different biological applications. Fibrous materials, films, porous membranes, and scaffolds have been synthesized under vacuum at different times and temperatures to align mechanical properties with the target tissue. The temperature range has been explored between 120 to 160 ^{o}C, with 120 ^{o}C being the most used for this application [118,123,124,170,254,332,333]. Due to the methacrylate groups added in the PGS molecule, crosslinked was carried out under UV light (previously explained in section 2.4). However, because of the constant failure in cell survival seeded on PGS-M substrates, crosslinking with heat at 120 ^{o}C was proposed. pLF's growth on PGS-M substrates crosslinked with heat was evaluated with resazurin reduction assay (Figure 5.20).

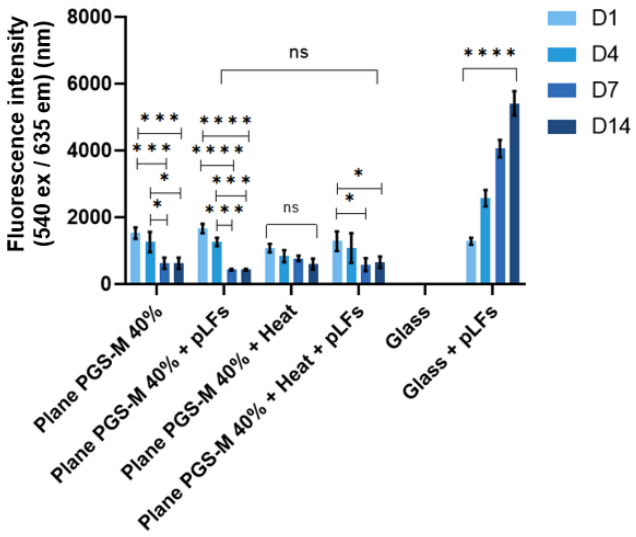

Figure 5.20 Resazurin reduction assay of pLF's culture on planar PGS-M transparent scaffolds 40 % DM with 1 mm thickness crosslinked with heat (120 ºC) . Positive controls were pLF's cultured on borosilicate glass. Negative controls were microfeatured PGS-M substrate 40 % DM crosslinked with heat (120 ºC) and borosilicate glass without cells. The assay was carried out in days 1,4,7 and 14. Samples show means and error bars corresponding to ±SD (N=3, n=3), analysed by two-way ANOVA, Tukey's post-hoc pairwise comparison. P≤0.05 was considered significant (*).

Cells seeded on crosslinked PGS-M substrates did not have any improvement in cell attachment or proliferation. There was no significant difference in cell growth between PGS-M crosslinked with heat and the one crosslinked with UV (normal crosslinked proposed in section 2.4) Cell proliferation was also evaluated with fluorescence microscopy (Figure 5.21).

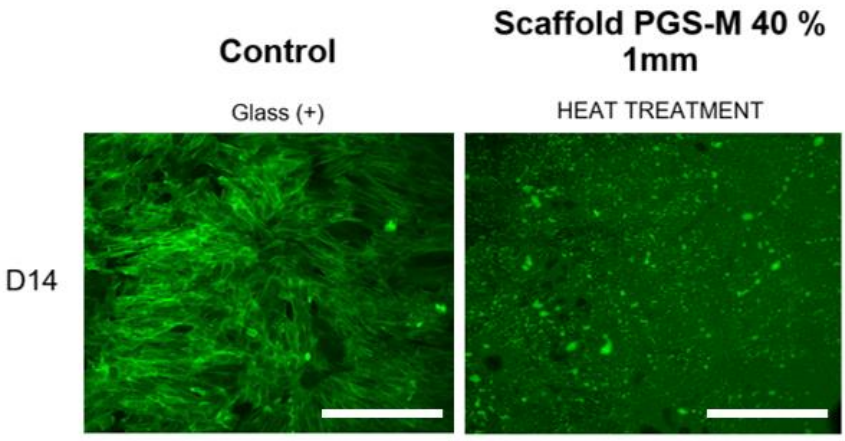

Figure 5.21 Fluorescence microscopy images of pLF's culture on PGS-M 40 % DM crosslinked with heat (120 °C). Positive controls were pLF's cultured on borosilicate glass. The images were taken on day 14 (D14) . All images were acquired using the same exposure and display settings. Scale bars are 200 µm.

It can be observed in Figure 5.21 that cells on heat crosslinked PGS-M are dead. The round morphology suggests that the cell went through apoptosis after attachment on the substrate. However, in comparison with results obtained after the reduction in scaffold thickness (section 5.5.1.1), here we can observe higher cell attachment. These results suggest that crosslinking with heat improves the cell attachment over time. Nevertheless, something remaining within the polymer matrix still causes cytotoxicity.

Our hypothesis is that during heat crosslinking the carboxyl groups are reacting with hydroxyl groups, forming the ester bonds [145]. This leaves the methacrylic groups free, which have been reported to cause some degree of cytotoxicity [334,335]. Matrices crosslinked with UV have been shown to contain more unreacted monomers that are leaching out in comparison with those that were heat cured [336]. Therefore, heat crosslinking was proposed as a possible solution with the drawbacks in cell culture. However, this modification did not improve cell survival.

5.7.3.3 HEAT-UV CROSSLINKING

We hypothesized that the combination of crosslinking methods (heat and UV) can improve cell proliferation. There are no previous reports on the formation of crosslinked PGS-M networks with heat and UV.

As was previously discussed, PGS is crosslinked under heat at 120 ºC, which allows carboxyl groups to react with hydroxyl groups, forming ester bonds [145]. Have been reported PGS scaffolds cross-linked for shorter periods of time (less than 48 hours) present some degree of cytotoxicity, due to the molecule was not completely cross-linked. This causes that the unreacted carboxylic acid groups of sebacic acid or the free sebacic acid produced by aqueous hydrolysis of PGS ester groups acidify the surroundings [110] [143].

On the other hand, PGS-M can be crosslinked under UV light via free radical polymerization among C=C groups, generating a bond between chains [116]. The addition of methacrylate groups leads them to be crosslinked, leaving OH groups free. This generates cytotoxicity as a result of the acidification of the media [337]. Therefore, we hypothesized that the combination of crosslinking methods can produce a polymer matrix with the appropriate degree of crosslinking between the OH and methacrylate groups, significantly improving cell growth.

However, it is still needed to optimise the time of crosslinking for each process. Firstly, we decided to crosslink PGS-M substrates under UV for 2.5 minutes (a quarter of the proposed initial time) and 24 hours with heat at 120 ºC under vacuum. The figure 5.22 shows the resazurin assay reduction from this initial approach.

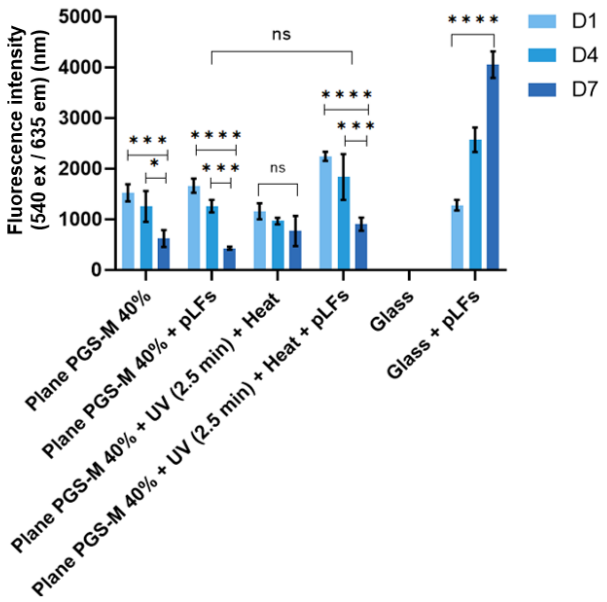

Figure 5.22 Resazurin reduction assay of pLF's culture on planar PGS-M transparent scaffolds 40 % DM with 1 mm thickness crosslinked with UV (2.5 minutes) and heat (120 ºC) . Positive controls were pLF's cultured on borosilicate glass. Negative controls were microfeatured PGS-M substrate 40 % DM crosslinked with UV (2.5 minutes) and heat (120 ºC) and borosilicate glass without cells. The assay was carried out in days 1,4,7 and 14. Samples show means and error bars corresponding to ±SD (N=3, n=3), analysed by two-way ANOVA, Tukey's post-hoc pairwise comparison. P≤0.05 was considered significant (*).

It can be observed in Figure 5.22 that cell attachment in PGS-M substrates crosslinked with UV and heat was significantly higher in comparation with the untreated substrates (70% UV-heat in comparison with 43% untreated). This has been the highest cell attachment reported so far with the modifications proposed in this chapter. However, there was no significant difference in cell growth on PGS-M (crosslinked in the standard method) and PGS-M crosslinked with UV and heat at all time points.

Thus, we proposed to decrease the UV light exposure from 2.5 minutes to 30 seconds. The cell growth was evaluated with resazurin reduction assay (Figure 5.23).

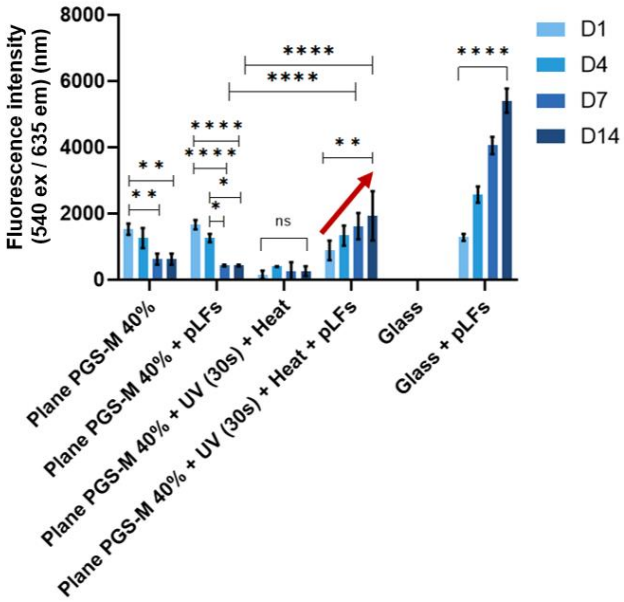

Figure 5.23 Resazurin reduction assay of pLF's culture on planar PGS-M transparent scaffolds 40 % DM with 1 mm thickness crosslinked with UV (30 seconds) and heat (120 ºC) . Positive controls were pLF's cultured on borosilicate glass. Negative controls were microfeatured PGS-M substrate 40 % DM crosslinked with UV (30 seconds) and heat (120 ºC) and borosilicate glass without cells. The assay was carried out in days 1,4,7 and 14. Samples show means and error bars corresponding to ±SD (N=3, n=3), analysed by two-way ANOVA, Tukey's post-hoc pairwise comparison. P≤0.05 was considered significant (*).

It can be observed in Figure 5.23 that pLF's finally showed a positive and constant cell growth throughout the 14-day culture period. Interestingly, cell attachment was lower (33%) in comparison with the previously obtained UV (2.5 minutes) heat crosslinking, though in this new sample cells survived. There was a significant difference between PGS-M crosslinked with the standard method and PGS-M crosslinked with UV (30 seconds) and heat on days 7 and 14 (P≤0.0001).

These positive results led us to propose exploring different crosslinking times under UV light (10, 20 and 30 seconds). The cell growth was evaluated with resazurin reduction assay (Figure 5.24).

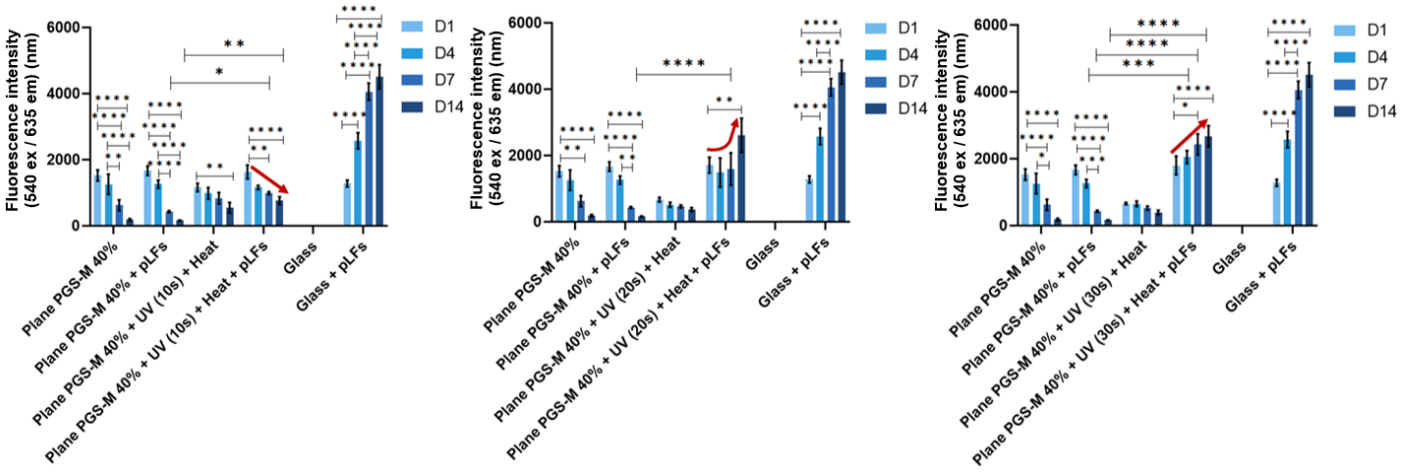

Figure 5.24 Resazurin reduction assay of pLFs culture on planar PGS-M transparent scaffolds 40 % DM with 1 mm thickness crosslinked with UV (10,20 and 30 seconds) and heat (120 ºC) . Positive controls were pLFs cultured on borosilicate glass. Negative controls were microfeatured PGS-M substrate 40 % DM crosslinked with UV (10,20 and 30 seconds) and heat (120 ºC) and borosilicate glass without cells. The assay was carried out in days 1,4,7 and 14. Samples show means and error bars corresponding to ±SD (N=3, n=3), analysed by two-way ANOVA, Tukey's post-hoc pairwise comparison. P≤0.05 was considered significant (*).

In figure 5.24 we can observe that cell growth is only consistently achieved in the substrates crosslinked with 30 seconds under UV light and heat. This indicates that lower times did not allow the appropriate degree of crosslinking between the OH and methacrylate groups.

pLF's seeded on PGS-M substrates crosslinked with UV (30 seconds) and heat were analysed with fluorescence microscopy (Figure 5.25).

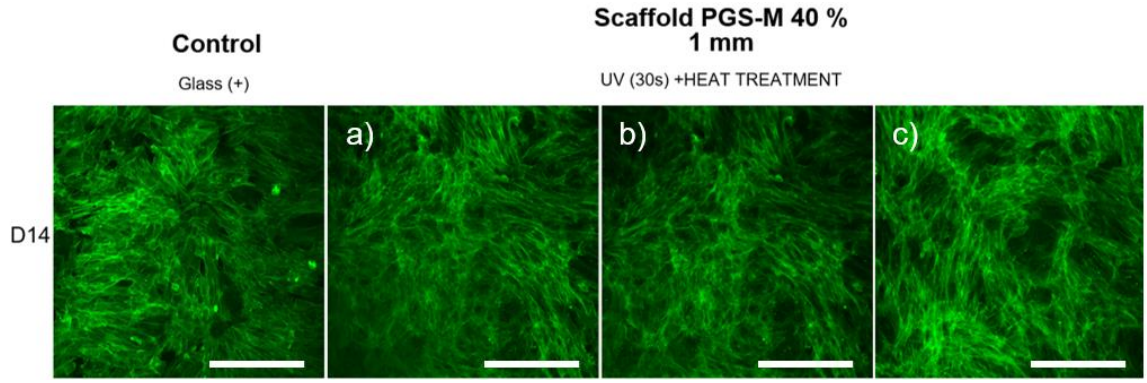

Figure 5.25 Fluorescence microscopy images of pLF's culture on PGS-M 40 % DM crosslinked with UV (30seconds) and heat (120 ºC). Positive controls were pLF's cultured on borosilicate glass. The images were taken on day 14 (D14) . a),b) and c) are different angles of the cell growth. All images were acquired using the same exposure and display settings. Scale bars are 200 µm.

It can be observed in figure 5.25 that cell morphology in cells seeded on PGS-M substrates crosslinked with UV (30 seconds) and heat is comparable with the control. It is also possible to observe that cells are growing in layers and forming tissue (Fig 5.26 a-c). Cell morphology was also analysed at higher magnification using confocal microscopy (Figure 5.26).

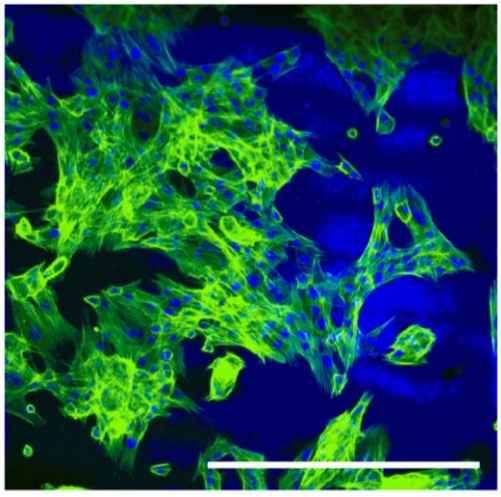

Figure 5.26 Confocal laser scanning microscopy images of pLF's culture on PGS-M 40 % DM crosslinked with UV (30seconds) and heat (120 ºC) (D14). The image was acquired using the same exposure and display settings. Scale bars is 50 µm.

Cell morphology observed in Figure 5.26 is very similar to standard fibroblasts as there is no pseudopodia retraction observed, which was seen before on PGS-M substrates (section 4.4.6). The observed morphology indicates that cells are stable and growing well on the modified PGS-M substrates.

Cell proliferation and morphology on PGS-M substrates crosslinked with UV (30 seconds) and heat was also analysed with SEM (Figures 5.27 and 5.28)

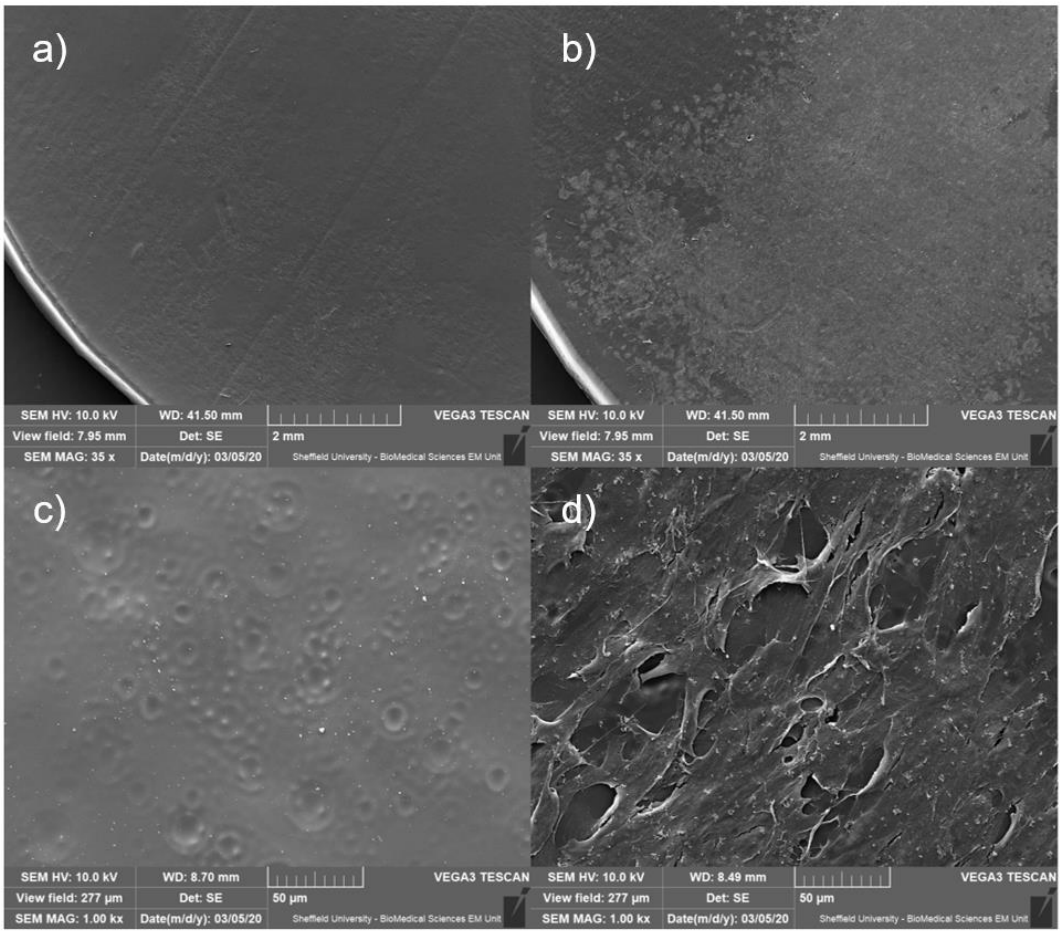

Figure 5.27 SEM images of pLF's seeded on PGS-M 40 % DM crosslinked with UV (30 seconds) and heat (120 ^{o}C). Images were taken on day 14.

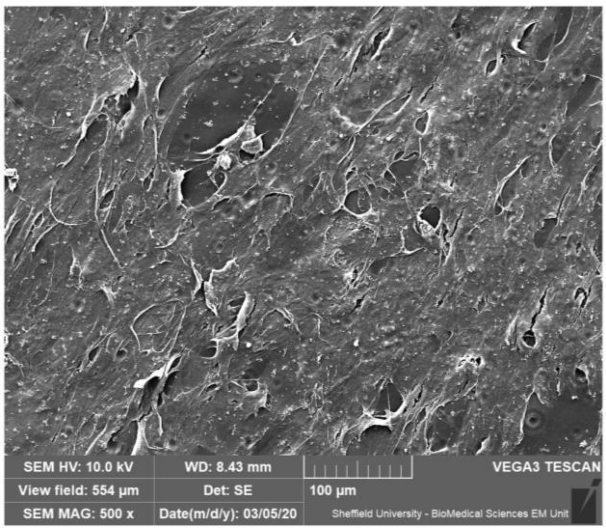

Figure 5.28 SEM images of pLF's seeded on PGS-M 40 % DM crosslinked with UV (30seconds) and heat (120 ºC). Image was taken on day 14.

According with the observed in figures 5.27 and 5.28, it is possible to observe that cells are growing well and forming tissue layers. To corroborate this, a histological analysis was carried out with the scaffolds by fixing and staining with H&E (Figure 5.29)

Figure 5.29 H&E stain of a section PGS-M 40 % DM crosslinked with UV (30 seconds) and heat (120 ºC) after 14 days in culture.

The images obtained from the H&E staining verify that cells were forming tissue, with the average tissue thickness being 86 μm, roughly corresponding to ~10 layers of cells.

PGS-M substrates crosslinked under UV (10, 20, and 30 seconds) and heat were analysed with ATR-FTIR as described in section 2.4.5 to determine the specific changes in the polymer matrix which allow cell growth. As was discussed previously in section 2.5.5, the addition of methacrylate groups is accompanied by the appearance of peaks around 945 cm^{-1} (=C-H bending) and 1640 cm^{-1} (C=C stretching) (Figure 5.30). These peaks disappear after polymerisation.

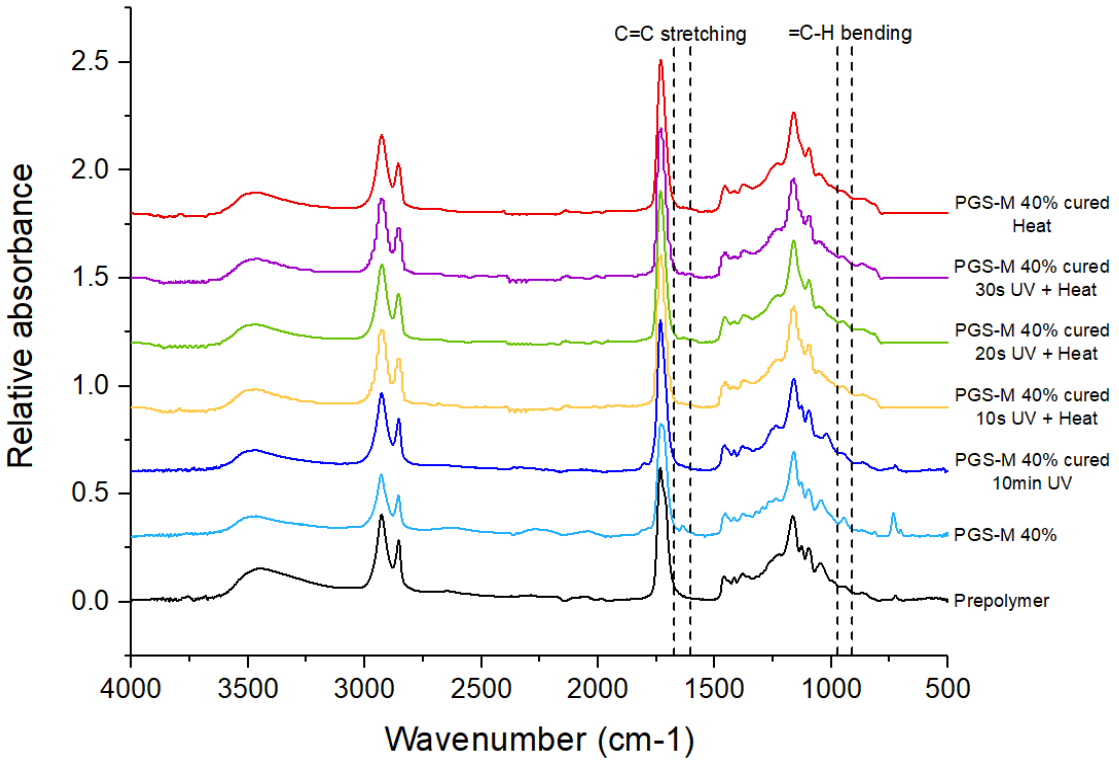

Figure 5.30 ATR-FTIR spectra of pPGS and PGS-M samples before and after curing. Peaks related with methacrylate groups appear at 940 cm^{-1} (=C-H bending) and 1640 cm^{-1} (C=C stretching).

There is no significant difference between the scaffolds exposed to different crosslinking times under UV (10, 20, and 30 seconds). However, both -OH and -COOH groups are implicated in PGS crosslinking, while C=C groups are implicated in PGS-M crosslinking. Therefore, we decided to analyse the wavenumber where these peaks appear in ATR-FTIR spectra (Figures 5.31 and 5.32)

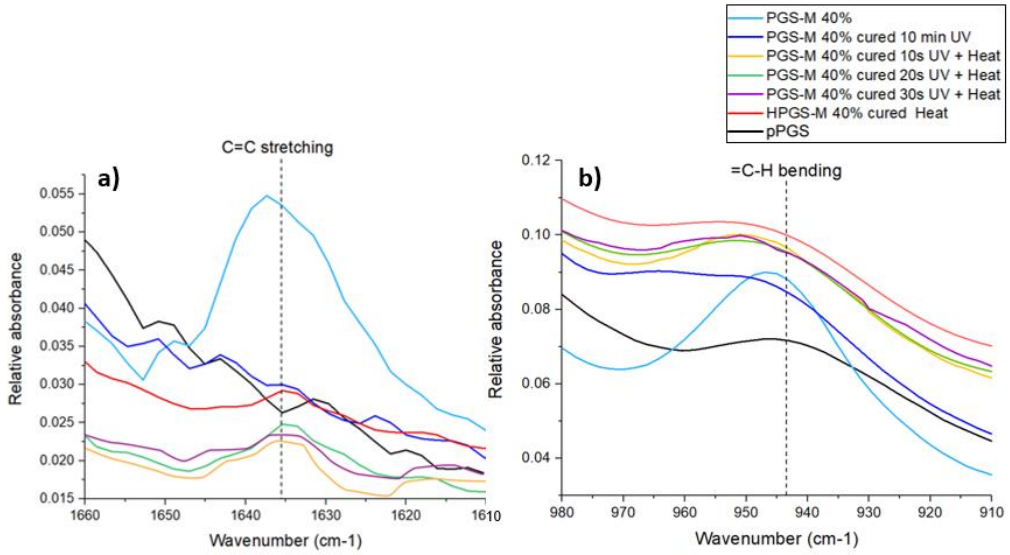

Figure 5.31 ATR-FTIR spectra of pPGS and PGS-M samples before and after curing. Peaks related with methacrylate groups appear at 940 cm^{-1} (=C-H bending) and 1640 cm^{-1} (C=C stretching).

The crosslinking methodologies compared in Figure 5.31 did not have any difference in the peaks related with methacrylate groups. In all cases, these peaks disappear after crosslinking.

The peaks related with PGS appear at 1330 cm^{-1} and 1418 cm^{-1} for carboxy groups and at 3450 cm^{-1} and 1100 cm^{-1} for hydroxy groups. These peaks decrease during thermal crosslinking, generating an increase in the peak related with the formation of ester bonds (COO) at 1150 cm^{-1}. These peaks have been shown to increase as crosslinking time and temperature are increased [126,145].

The effect of crosslinking processing for COOH, OH and COO groups was analysed with ATR-FTIR (Figure 5.32).

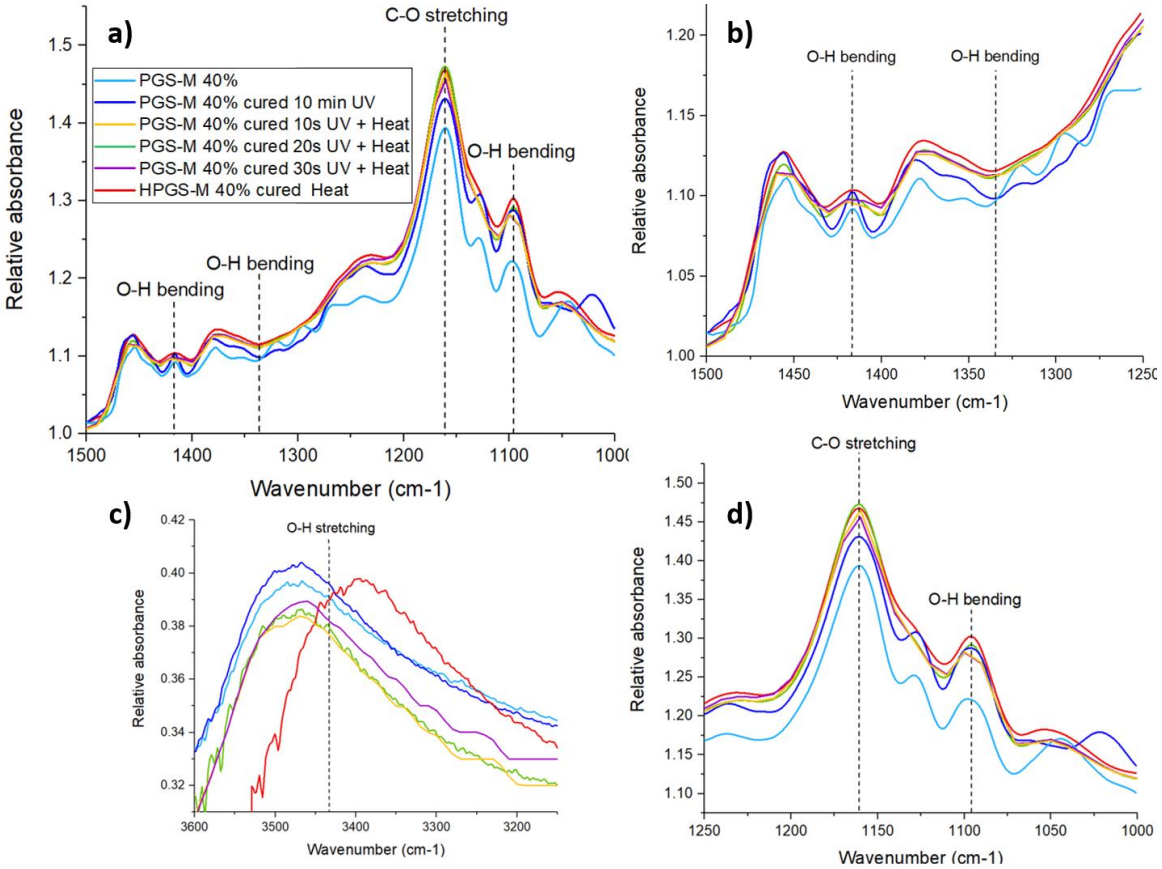

Figure 5.32 ATR-FTIR spectra of pPGS and PGS-M samples before and after curing. b) Peaks related -COOH groups appear at 1330 cm^{-1} (OH bending) and at 1418 cm^{-1} (OH bending), c) and d) peaks related with OH groups appear at 3450 cm^{-1} (OH stretching) and at 1100 cm^{-1} (OH bending) and d) peaks related with the formation of ester bonds (COO) appear at 1150 cm^{-1} (CO stretching).

We can observe that the main difference between the crosslinking methods lies in the decreasing of COOH groups in the samples crosslinked with the UV-heat combination (Figure 5.32 b). It has been reported that surface chemical composition and electrical charges have an influence in cell adhesion, proliferation, and migration [294,338–340]. Endothelial cells and fibroblasts proliferate more on positive and negative-positive charged copolymers [341]. It has been shown that COOH groups have negative charge and acid nature, affecting cell attachment, proliferation, differentiation and cell growth [342 343344]. It is also important to note that during polymer degradation, COOH is leaching through carboxylic acid

degradation, which release protons and leads to pH drop, acidifying the surrounding environment [169]. Hydrogen is a reducing agent that can trigger the Resazurin reduction, therefore I hypothesised that this generate the small signal in some Resazurin reduction assay analysed in Chapter 4 in samples without cells (Figure 4.5 and 4.6). This is the first work which has proposed and demonstrated the effectiveness of the combination of UV and heat to crosslink PGS-M substrates. This modification was able to reduce the material cytotoxicity and finally fabricate a PGS-M substrate which can allow seeded cells to effectively survive and grow. We can conclude from the analysis of ATR-FTIR spectra that this is due to the reduction of COOH groups.

The surface of PGS-M substrates was also analysed through the measurement of contact angle (Figure 5.33)

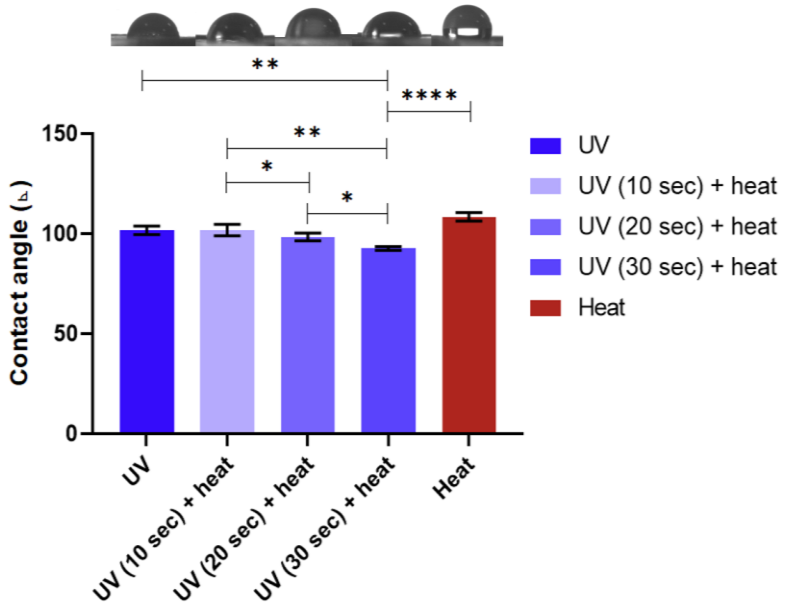

Figure 5.33 Contact angle measurements in deionized water of PGS-M crosslinked with heat and UV . Samples show means and error bars corresponding to ±SD (N=3, n=3), analysed by one-way ANOVA, Tukey's post-hoc pairwise comparison. P≤0.05 was considered significant (*).

Figure 5.33 show that PGS-M 40% DM crosslinked with UV has a contact angle of 101.7º, the substrate crosslinked with heat shows 108.4 º, and samples crosslinked with the combination of UV and heat have 101.8, 98.4 and 92.6 º for 10, 20 and 30 seconds, respectively. These results coincide with those from the biological evaluation as the sample with lower contact angle (UV 30 seconds + heat) showed the best performance. Despite the improvement of contact angle with heat + UV crosslinking method , the substrate surface is still hydrophobic.

The influence of the crosslinking method in mechanical properties was also evaluated as described in 2.4.7 (Figure 5.34).

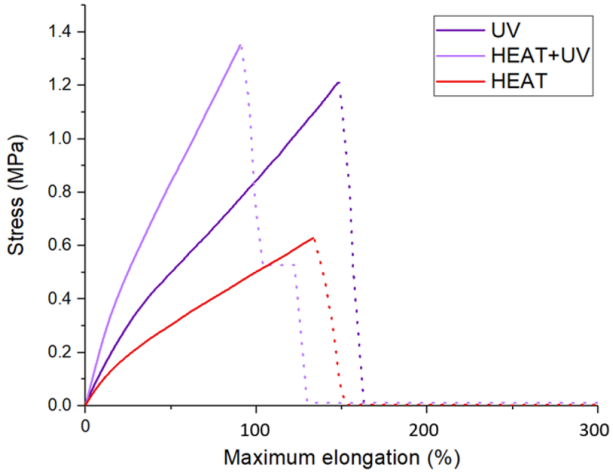

Crosslinking method	Young's Modulus (MPa)	Ultimate tensile strain (MPa)	Maximum elongation (%)
UV	1.275 ± 0.15	1.205 ± 0.06	147.83 ± 12.62
Heat + UV	2.247 ± 0.22	1.351 ± 0.01	134.65 ± 8.95
Heat	0.769 ± 0.08	0.627 ± 0.05	132.78 ± 17.75

Figure 5.34 Mechanical properties in different crosslinked method (UV, heat + UV and heat) . SD (*n* = 3). (Samples were stored 6 months before analysis)

As can be seen in Figure 5.34, the Young's modulus and the ultimate tensile strain are higher in the samples crosslinked with heat + UV. This means that the polymer matrix is stiffer and more crosslinked, but still flexible. Previous works reported cytotoxicity in materials which were not completely cross-linked, thus we can

conclude that UV crosslinking by itself is not enough to completely crosslink PGS-M [110] [143]. This data agrees with the improvement of cell survival observed in this chapter using heat + UV crosslinking. It is interesting to note that heat crosslinked substrates are more brittle, but at the same time retain their flexibility, as can be seen at maximum elongation value. On the other hand, UV crosslinked samples are flexible, but have poor mechanical properties in comparison with heat and heat + UV crosslinked scaffolds.

This data comprises the basis for future development of PGS-M scaffolds with better biocompatibility and mechanical properties close to the gold standard of a corneal scaffold.

5.8 CONCLUSIONS

Figure 5.35 shows the summary of all modifications carried out to improve PGS-M substrates.

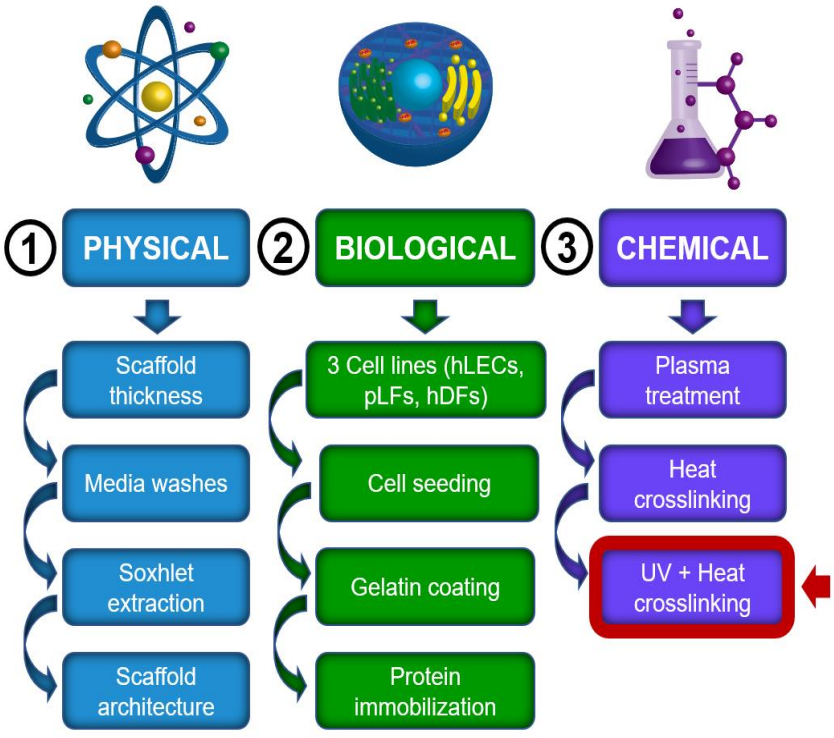

Figure 5.35 Scheme PGS-M scaffold modifications carried out to achieve cell survival and improve cell growth and proliferation.

In Chapter 4, we found problems with cell survival and morphology from the beginning of the biological evaluation with transparent PGS-M substrates (tested with human limbal epithelial cells (hLEC's), human dermal fibroblasts (hDF's) and rabbit and pig limbal fibroblasts (pLF's)). This led us to propose and explore a wide range of modifications for these substrates in Chapter 5, starting with the most common methods for improving material biocompatibility.

Physical modifications were proposed to adjust the external PGS-M features (thickness, sol fraction, and topography). Biological modifications were planned with the aim of increasing the cell-substrate interaction (the cell contact with the scaffold surface and attachment proteins). Chemical modifications were based on molecule modification, increasing reacting sites in the polymer surface, and combining crosslinking methods (UV and heat).

Finally, we improved PGS-M transparent surfaces for cell culture, overcoming the limitation of thickness and cytotoxicity. This is the first report of cell culture on thick transparent PGS-M scaffolds (more than 350 μm), which was achieved with the combination of UV and heat for crosslinking. We demonstrated that material cytotoxicity was reduced after this modification and pLF's seeded on PGS-M substrates survive and grow, eventually forming tissue.

This work is the first step in the development of next generation scaffolds for corneal regeneration.

We demonstrated that PGS-M is a tuneable biomaterial able to be moulded with microfeatures and a dome shape that mimic the structure in the native cornea, keeping transparency and mechanical properties found *in vivo*. There are no works that have reported the characteristics achieved in this work for corneal replacements. This places our development a step forward, approaching the gold standard of biomaterials for corneal regeneration Therefore, it is important to explore more this polymer and its modifications to achieve the development of an artificial cornea replacement.

CHAPTER 6. FUTURE WORK: TOWARDS PGS-M ARTIFICIAL CORNEA DEVELOPMENT

PGS-M is a novel biomaterial that has been reported firstly by our research group. However, the range of possibilities for its application in soft tissue engineering have not been explored. Previous reports for PGS-M have focused in the development of porous materials (polyHIPEs) and thin materials for tissue engineered blood vessels [116,117]. Nonetheless, this work is the first report of a thick transparent non-porous PGS-M. Without a doubt, it is worthy to explore the possible uses for transparent PGS-M, mainly for corneal applications.

The use of this material opens an interesting direction for the improvement and optimization of current biomaterials for corneal illness. This is the first step in development of an artificial corneal substitute based on PGS-M, which presents a window into new possibilities and challenges as we seek to achieve a “perfect” biomaterial that generates the adequate biological response without creating any adverse reaction.

Several strategies have been proposed throughout this work to improve the cell-substrate interaction between corneal cells and PGS-M, each with promising results. The present work highlights clear advantages to the use of PGS-M compared to other polymers currently used for corneal applications due to its tuneable mechanical and optical properties that have not been reported previously. For that reason, we propose to continue with the improvement of the PGS-M based scaffold materials.

The gold standard for a full thickness corneal substitute (endothelial, epithelial and stromal layers) would be a biocompatible, biodegradable substrate, capable of mimicking the properties of soft tissue such as cornea, while being mechanically capable of supporting tissue regeneration, biodegradation, and stable in

physiological conditions. Currently, there are no full thickness artificial corneas synthetized with artificial polymers.

For future work in the improvement of PGS-M molecule and the development of artificial cornea based on this material, we propose the follow strategies:

- MICROFEATURED SCAFFOLDS

We consider important to test the microfeatured patterns proposed in Chapter 3, since due to the time consumed during the PGS-M improvement we did not have enough time to test the influence of the topography on corneal cell behaviour (Figure 6.1).

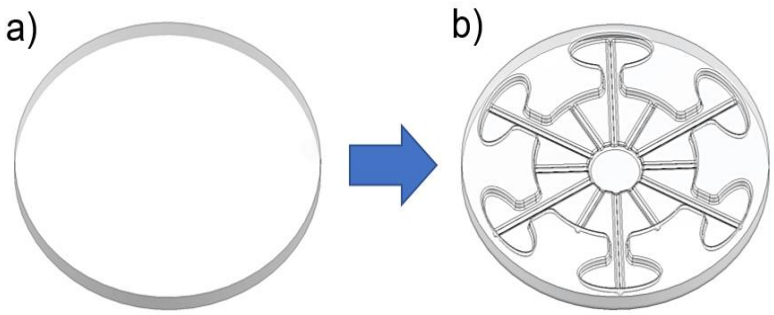

Figure 6.1 a) Flat scaffold and b) Microfeatured scaffolds

The influence of micropatterns has been widely discussed in Chapter 5, and we believe that is worthy to test the influence of micropatterns and niches on corneal cells behaviour. Our study highlighted the production of patterns with a resolution of 200 μm by using soft stereolithography. Another important feature to test is the addition of nanopatterns, as the designs developed in this work have explored only the addition of micropatterns. It has been reported that the addition of nanopatterns has more influence on cell performance.

- DOME SHAPED SCAFFOLDS

We propose to test the influence of the dome shape corneal substitute on proliferation, migration, and differentiation of corneal cells. Scaffolds with dome

shape have not been widely explored and synthetized. Current techniques used to produce dome scaffolds are based on 3D printing, limiting the materials used for fabrication [199,245,345,346]. The resulting scaffolds lack adequate transparency, biodegradability, elasticity, resolution, thickness, and the addition of microfeatures.

In this work, we proposed a versatile fabrication technique, using soft stereolithography and moulding that allowed the “printing” of dome shaped scaffolds with high defined microfeatures and tuneable thickness that mimic the structure of the native cornea (Chapter 3) (Figure 6.2).

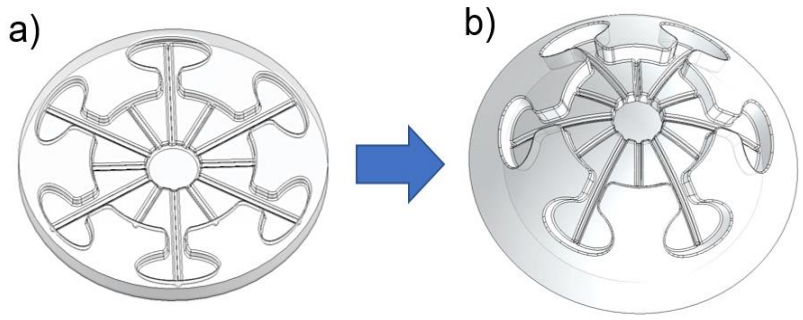

Figure 6.2 a) Flat patterned scaffold, b) dome shape patterned scaffold

- TUNEABLE STIFFNESS

Also, we consider important the development of corneal substrate that mimics the stiffness in the native cornea: softer in the limbus and stiffer in the central cornea that promote cell differentiation and migration [177,178,183,184,280]. Based on the manufacturing technique (soft stereolithography and moulding) used to synthetize the scaffolds and in the tuneable mechanical properties of PGS-M, we know that is possible to develop a scaffold with different stiffness within the same substrate (Figure 6.3).

Figure 6.3 Dome shaped scaffold with stiffness gradient, softer in the base and stiffer in the centre.

- SURFACE CHEMISTRY

The next step will be the improvement of the polymer matrix and its biocompatibility, which can be achieved with the addition of active groups in the PGS-M molecule. It has been reported that functionalizing surfaces with different groups and active molecules using a wide range of techniques can influence cell behaviour [53,347]. Previous works reported the use of OH groups that can increase cell growth and adhesion [348,349]. On the other hand, NH_2 groups influence cell growth, proliferation, and differentiation [350–353]. The addition of dendrimers in the collagen substrate has been shown to improve mechanical and optical properties while increasing biological interaction between cells-substrate [53]. Additionally, the grafting of molecules such as hyaluronic acid have been reported to improve cell adhesion [354] (Figure 6.4).

However, it is also important to consider the interaction, biofunctionality, and biocompatibility of the molecules with the cell type and the kind of response that we are expecting to develop a material.

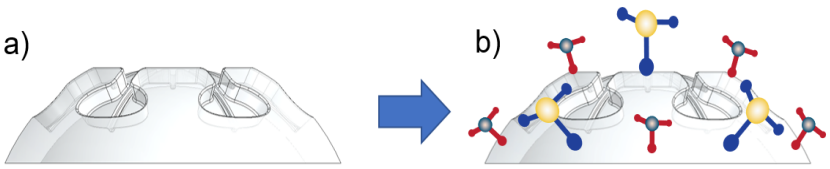

Figure 6.4 a) Scaffold without grafted molecules, b) Scaffold with active molecules grafted to improve cell interactions and biocompatibility.

- POLYMER BLENDS

Another important approach will be the blending of PGS-M with other polymers that can increase the biocompatibility and cell attachment.

Previous works on polymer blends have reported an improvement in the materials biocompatibility and hydrophilicity through a combination of the material's properties [355,356]. However, some drawbacks in mechanical properties, cell growth and substrate stability have been reported [357]. It is important to use the correct concentration and molecule in the blend to overcome these limitations.

Previous works reported PGS blends with poly (lactic acid) and Poly(ε-caprolactone) for cardiac tissue increased hydrophilicity, biocompatibility, and mechanical properties, improved cell attachment, proliferation, and distribution [256,358,359]. Another material blended with PGS has been Polyvinylpyrrolidone for skin application, improving mechanical properties and degradability [311]. The most recent work has reported the blend of PGS with silk and chitosan for skin tissue engineering enhancing crosslinking density, hydrophilicity and cell attachment [312]. Nevertheless, it is important to note that there are no reports on PGS-M blends, making this another area of opportunity (Figure 6.5).

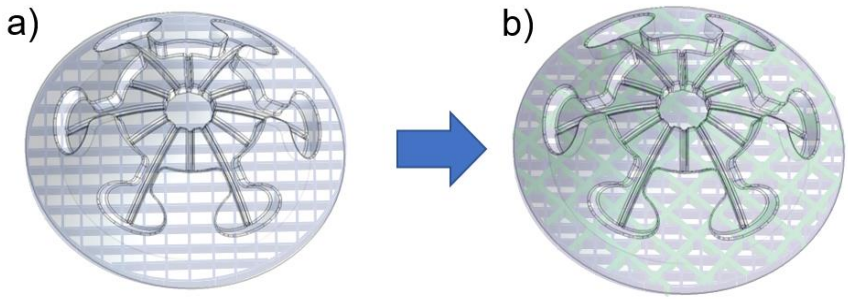

Figure 6.5 a) Pure PGS-M dome shaped scaffold, b) PGS-M/Blend polymer dome shaped scaffold.

- CORNEAL LAYER APPLICATION

This work has explored the development of PGS-M scaffolds that mimic the limbus and its microstructures. We consider interesting to test the biocompatibility and the effect of PGS-M on different corneal layers. Stroma is ~90% of the cornea, corresponding to the stroma layer, constituted by an unique composition of uniform collagen fibrils that give the cornea its characteristic transparency and mechanical properties [33,245]. The development of biomaterials for the stroma layer is still a challenge due its aligned structure, mechanical properties, and transparency. We have been able to produce a scaffold to support multilayer cell growth of limbal epithelial cells and relying on cellular self-assembly in combination with surface functionalisation and stiffness modulated scaffolds we might be able to produce a corneal mimic tissue. We expect PGS-M to replicate the stromal characteristics as it is a biomaterial with tuneable mechanical properties and transparency (Figure 6.6).

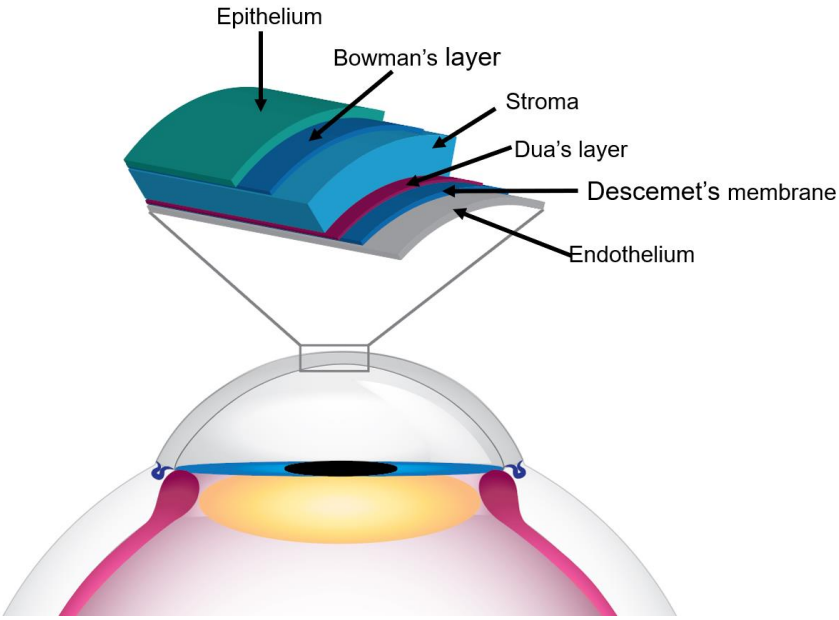

Figure 6.6 Corneal layers

SUMMARY OF KEY FINDINGS

- PGS-M was successfully synthesized with low degrees of methacrylation (DM) (20 - 50%). 40% DM was selected as it was the best match for the corneal mechanical properties.

- Moulding and soft stereolithography were used to design and synthetize a scaffold with topography that mimics the structure of the limbal niches. This dome shaped scaffold is transparent, and its thickness was reduced to 100 µm, which is thinner than any reported work. All these characteristics have not been previously reported in scaffolds for corneal regeneration.

- Different modifications were proposed to overcome PGS-M cytotoxicity with corneal cells:
    - Physical (thickness, scaffold washes, Soxhlet extraction, and modifications to scaffold architecture)
    - Biological (cell seeding, gelatin coating, and protein immobilization)
    - Chemical (plasma coating, heat crosslinking, and heat + UV crosslinking)

- The cytotoxicity issues of PGS-M 40% DM scaffolds were overcome by combining two crosslinking techniques (UV + heat) and significantly improved cell growth and proliferation. This was confirmed by the growth of multiple cell layers (~10 cells) on top of the PGS-M surface.

PGS-M is a relatively new material that provides unique characteristics for the development of a corneal replacement such as transparency, tunable mechanical properties, and elasticity. The work presented in this thesis further improves the potential of PGS-M for tissue engineering.

REFERENCES

1. (WHO), W. H. O. Prevention of Blindness and Visual Impairment. (2017). Available at: http://www.who.int/blindness/causes/priority/en/index8.html.

2. Burton, M. J. Prevention, treatment and rehabilitation. *Community eye Heal.* **22**, 33–5 (2009).

3. Ortega, I., McKean, R., Ryan, A. J., MacNeil, S. & Claeyssens, F. Characterisation and evaluation of the impact of microfabricated pockets on the performance of limbal epithelial stem cells in biodegradable PLGA membranes for corneal regeneration. *Biomater. Sci.* **2**, 723 (2014).

4. May Griffith, Rosemarie Osborne, R. M., Xiaojuan Xiong, Charles J. Doillon, N. L. C. L. & Malik Hakim, Ying Song, M. A. W. Functional Human Corneal Equivalents Constructed from Cell Lines. *Science (80-.).* **286**, 723-734. (1999).

5. Levis, H. *et al.* Tissue Engineering the Cornea: The Evolution of RAFT. *J. Funct. Biomater.* **6**, 50–65 (2015).

6. May Griffith, Per Fagerholm, Neil Lagali, Malcolm A. Latorre, Joanne Hackett, H. S. Chapter 49 – Regenerative Medicine in the Cornea. *Elsevier* 911-924. (2011).

7. Willoughby, C. E. *et al.* Anatomy and physiology of the human eye: Effects of mucopolysaccharidoses disease on structure and function - a review. *Clin. Exp. Ophthalmol.* **38**, 2–11 (2010).

8. Derek W. DelMonte, T. K. Anatomy and physiology of the cornea and related structures. *J Cataract Refract Surg* **37**, 588–598 (2011).

9. Ahearne, M., Fernández-Pérez, J., Masterton, S., Madden, P. W. & Bhattacharjee, P. Designing Scaffolds for Corneal Regeneration. *Adv. Funct. Mater.* **1908996**, (2020).

10. Hassell, J. R. & Birk, D. E. The molecular basis of corneal transparency. *Exp. Eye Res.* **91**, 326–335 (2010).

11. Dua, H. S. & Faraj, L. A. Dua's Layer: its discovery , characteristics and applications. *J. Emmetropia* **5**, 211–223 (2014).

12. Qazi, Y., Wong, G., Monson, B., Stringham, J. & Ambati, B. K. Corneal transparency : Genesis , maintenance and dysfunction. **81**, 198–210 (2010).

13. Casaroli-Marano, R., Nieto-Nicolau, N., Martínez-Conesa, E., Edel, M. & B.Álvarez-Palomo, A. Potential Role of Induced Pluripotent Stem Cells (IPSCs) for Cell-Based Therapy of the Ocular Surface. *J. Clin. Med.* **4**, 318–342 (2015).

14. Tseng, S. C. G., He, H., Zhang, S. & Chen, S. Y. Niche Regulation of Limbal Epithelial Stem Cells: Relationship between Inflammation and Regeneration. *Ocul. Surf.* **14**, 100–112 (2016).

15. Schlötzer-Schrehardt, U. & Kruse, F. E. Identification and characterization of limbal stem cells. *Exp. Eye Res.* **81**, 247–264 (2005).

16. Chee, K., Kicic, A. & Wiffen, S. Perspective Limbal stem cells : the search for a marker. *Clin. Exp. Ophthalmol.* **34**, 64–73 (2006).

17. Levis, H. J., Massie, I., Dziasko, M. A., Kaasi, A. & Daniels, J. T. Rapid tissue engineering of biomimetic human corneal limbal crypts with 3D niche architecture. *Biomaterials* **34**, 8860–8868 (2013).

18. Eric H Chan, Luxia Chen, Jian Yu Rao, Fei Yu, 5and Sophie X. Deng1. Limbal Basal Cell Density Decreases in Limbal Stem Cell Deficiency. *Am J Ophthalmol* **13**, 1478–1486 (2016).

19. Dua, H. S. & Azuara-Blanco, A. Autologous limbal transplantation in patients with unilateral corneal stem cell deficiency. *Br. J. Ophthalmol.* **84**, 273–8 (2000).

20. Li, W., Hayashida, Y., Chen, Y. T. & Tseng, S. C. Niche regulation of corneal epithelial stem cells at the limbus. *Cell Res.* **17**, 26–36 (2007).

21. Dua, H. S., Shanmuganathan, V. A., Powell-Richards, A. O., Tighe, P. J. & Joseph, A. Limbal epithelial crypts: a novel anatomical structure and a putative limbal stem cell niche. *Br. J. Ophthalmol.* **89**, 529–32 (2005).

22. Tissuetech, T. Concept and application of limbal stem cells. (2016). doi:10.1038/eye.1989.22

23. Ortega, I. *et al.* Combination of microstereolithography and electrospinning to produce membranes equipped with niches for corneal regeneration. *J. Vis. Exp.* 51826 (2014). doi:10.3791/51826

24. Dua, H. S., Miri, A., Alomar, T., Yeung, A. M. & Said, D. G. The Role of Limbal Stem Cells in Corneal Epithelial Maintenance. Testing the Dogma. *Ophthalmology* **116**, 856–863 (2009).

25. Kayama, M., Kurokawa, M. S., Ueno, H. & Suzuki, N. Recent advances in corneal regeneration and possible application of embryonic stem cell-derived corneal epithelial cells. *Clin. Ophthalmol.* **1**, 373–382 (2007).

26. Davanger, M. & Evensen, A. © 1971 Nature Publishing Group. *Nat. Phys. Sci.* **231**, 154–155 (1971).

27. Higa, K., Shimmura, S., Miyashita, H., Shimazaki, J. & Tsubota, K. Melanocytes in the corneal limbus interact with K19-positive basal epithelial cells. *Exp. Eye Res.* **81**, 218–223 (2005).

28. Daniels, J. T., Dart, J. K., Tuft, S. J. & Khaw, P. T. Corneal stem cells in review. *Wound Repair Regen.* **9**, 483–94 (2001).

29. Scleral structure and biomechanics.pdf.

30. Shortt, A. J. *et al.* Ex Vivo Expansion and Transplantation of Limbal Epithelial Stem Cells. *Ophthalmology* **115**, 1989–1997 (2008).

31. Dua, H. S. & Azuara-Blanco, A. Limbal stem cells of the corneal epithelium. *Surv. Ophthalmol.* **44**, 415–425 (2000).

32. Lim, P., Fuchsluger, T. A. & Jurkunas, U. V. Seminars in Ophthalmology Limbal Stem Cell Deficiency and Corneal Neovascularization Limbal Stem Cell Deficiency and Corneal Neovascularization. *Semin. Ophthalmol.* **243**, 139–148 (2009).

33. Yam, G. H. F. *et al.* Safety and feasibility of intrastromal injection of cultivated human corneal stromal keratocytes as cell-based therapy for corneal opacities. *Investig. Ophthalmol. Vis. Sci.* **59**, 3340–3354 (2018).

34. Kolli, S., Ahmad, S., Lako, M. & Figueiredo, F. Successful Clinical Implementation of Corneal Epithelial Stem Cell Therapy for Treatment of Unilateral Limbal Stem Cell Deficiency. *Stem Cells* **28**, 597–610 (2009).

35. Nakamura, T., Inatomi, T., Sotozono, C., Koizumi, N. & Kinoshita, S. Ocular surface reconstruction using stem cell and tissue engineering. *Prog. Retin. Eye Res.* **51**, 187–207 (2016).

36. Ghezzi, C. E., Rnjak-Kovacina, J. & Kaplan, D. L. Corneal Tissue Engineering: Recent Advances and Future Perspectives. *Tissue Engineering - Part B: Reviews* **21**, 278–287 (2015).

37. S. Sharareh Mahdavi, Mohammad J. Adbekhodaie, Shohreh Mashayekhan, Alireza Baradaran-Rafii, A. R. D. Bioengineering Approaches for Corneal Regenerative Medicine. *Tissue Engine Regen. Med.* (2020).

38. Panda, A., Vanathi, M., Kumar, A., Dash, Y. & Priya, S. Corneal Graft Rejection. *Surv. Ophthalmol.* **52**, 375–396 (2007).

39. Chen, Z. *et al.* Biomaterials for corneal bioengineering. *Biomed. Mater.* **13**, (2018).

40. Ortega, Í., Deshpande, P., Gill, A. a, MacNeil, S. & Claeyssens, F. Development of a microfabricated artificial limbus with micropockets for cell delivery to the cornea. *Biofabrication* **5**, 025008 (2013).

41. Borderie, V. M. *et al.* Predicted Long-term Outcome of Corneal Transplantation. *Ophthalmology* **116**, 2354–2360 (2009).

42. Grueterich, M., Espana, E. M., Touhami, A., Ti, S. E. & Tseng, S. C. G. Phenotypic study of a case with successful transplantation of ex vivo expanded human limbal epithelium for unilateral total limbal stem cell deficiency. *Ophthalmology* **109**, 1547–1552 (2002).

43. Ahmad, S. Concise Review : Limbal Stem Cell Deficiency , Dysfunction , and Distress. *Stem Cells Transl. Med.* **1**, 110–115 (2012).

44. Menzel-Severing, J., Kruse, F. E. & Schlötzer-Schrehardt, U. Stem cell-based therapy for

corneal epithelial reconstruction: present and future. *Can. J. Ophthalmol. Can. d'ophtalmologie* **48**, 13 (2013).

45. Sefat, F. *et al.* An 'off-the shelf' synthetic membrane to simplify regeneration of damaged corneas. *Middle East Conf. Biomed. Eng. MECBME* **5004**, 59–62 (2014).

46. Utheim, T. P. *Corneal Regenerative Medicine*. **1014**, (2013).

47. Sangwan, V. S., Basu, S., MacNeil, S. & Balasubramanian, D. Simple limbal epithelial transplantation (SLET): a novel surgical technique for the treatment of unilateral limbal stem cell deficiency. *Br. J. Ophthalmol.* **96**, 931–4 (2012).

48. Sehic, A., Utheim, Ø. A., Ommundsen, K. & Utheim, T. P. Pre-Clinical Cell-Based Therapy for Limbal Stem Cell Deficiency. *J. Funct. Biomater.* **6**, 863–88 (2015).

49. Niknejad H1, Peirovi H, Jorjani M, Ahmadiani A, Ghanavi J, S. A. Properties of the amniotic membrane for potential use in tissue engineering. *Eur Cell Mater.* **15**, 88–89 (2008).

50. Bryant-Greenwood, G. D. The extracellular matrix of the human fetal membranes: Structure and function. *Placenta* **19**, 1–11 (1998).

51. Lee, C. H., Singla, A. & Lee, Y. Biomedical applications of collagen. *Int. J. Pharm.* **221**, 1–22 (2001).

52. Orwin, E. J., Hubel, A. & Ph, D. In Vitro Culture Characteristics of Corneal Epithelial, Endothelial, and Keratocyte Cells in a Native Collagen Matrix. *Tissue Eng.* **6**, 307–319 (2000).

53. Duan, X. & Sheardown, H. Dendrimer crosslinked collagen as a corneal tissue engineering scaffold: Mechanical properties and corneal epithelial cell interactions. *Biomaterials* **27**, 4608–4617 (2006).

54. Borene, M. L., Barocas, V. H. & Hubel, A. Mechanical and cellular changes during compaction of a collagen-sponge- based corneal stromal equivalent. *Ann. Biomed. Eng.* **32**, 274–283 (2004).

55. Hogerheyde, T. A. *et al.* Assessment of freestanding membranes prepared from Antheraea pernyi silk fibroin as a potential vehicle for corneal epithelial cell transplantation. *Biomed. Mater.* **9**, (2014).

56. Darshan, G. H., Kong, D., Gautrot, J. & Vootla, S. Physico-chemical characterization of Antheraea mylitta silk mats for wound healing applications. *Sci. Rep.* **7**, 1–11 (2017).

57. Jiang, C. *et al.* Mechanical properties of robust ultrathin silk fibroin films. *Adv. Funct. Mater.* **17**, 2229–2237 (2007).

58. Vázquez, N. *et al.* Silk fibroin films for corneal endothelial regeneration: Transplant in a rabbit descemet membrane endothelial keratoplasty. *Investig. Ophthalmol. Vis. Sci.* **58**, 3357–3365 (2017).

59. Aramwit, P., Kanokpanont, S., Nakpheng, T. & Srichana, T. The effect of sericin from various extraction methods on cell viability and collagen production. *Int. J. Mol. Sci.* **11**, 2200–2211 (2010).

60. Ahmed, T. A. E., Dare, E. V. & Hincke, M. Fibrin: A Versatile Scaffold for Tissue Engineering Applications. *Tissue Eng. Part B Rev.* **14**, 199–215 (2008).

61. Han, B., Schwab, I. R., Madsen, T. K. & Isseroff, R. R. A fibrin-based bioengineered ocular surface with human corneal epithelial stem cells. *Cornea* **21**, 505–10 (2002).

62. Yeung, A. M., Faraj, L. A., McIntosh, O. D., Dhillon, V. K. & Dua, H. S. Fibrin glue inhibits migration of ocular surface epithelial cells. *Eye* **30**, 1389–1394 (2016).

63. Rose, J. B. *et al.* Gelatin-based materials in ocular tissue engineering. *Materials (Basel).* **7**, 3106–3135 (2014).

64. Sun, M. *et al.* Synthesis and properties of gelatin methacryloyl (GelMA) hydrogels and their recent applications in load-bearing tissue. *Polymers (Basel).* **10**, (2018).

65. Watanabe, R. *et al.* A novel gelatin hydrogel carrier sheet for corneal endothelial transplantation. *Tissue Eng. - Part A* **17**, 2213–2219 (2011).

66. Dranca, I. & Vyazovkin, S. Thermal stability of gelatin gels: Effect of preparation conditions on the activation energy barrier to melting. *Polymer (Guildf).* **50**, 4859–4867 (2009).

67. Croisier, F. & Jérôme, C. Chitosan-based biomaterials for tissue engineering. *Eur. Polym. J.* **49**, 780–792 (2013).

68. Kumar, P., Dehiya, B. S. & Sindhu, A. Comparative study of chitosan and chitosan–gelatin scaffold for tissue engineering. *Int. Nano Lett.* **7**, 285–290 (2017).

69. Sun, M. *et al.* Hyaluronan derived from the limbus is a key regulator of corneal lymphangiogenesis. *Investig. Ophthalmol. Vis. Sci.* **60**, 1050–1062 (2019).

70. Kirker, K. R., Luo, Y., Nielson, J. H., Shelby, J. & Prestwich, G. D. Glycosaminoglycan hydrogel films as bio-interactive dressings for wound healing. *Biomaterials* **23**, 3661–3671 (2002).

71. Chan, B. P. & Leong, K. W. Scaffolding in tissue engineering: General approaches and tissue-specific considerations. *Eur. Spine J.* **17**, (2008).

72. Macrae, S. M., Matsuda, M. & Phillips, D. S. The Long-Term Effects of Polymethylmethacrylate Contact-Lens Wear on the Corneal Endothelium. *Ophthalmology* **101**, 365–370 (1994).

73. Lai, J. Y. & Hsiue, G. H. Functional biomedical polymers for corneal regenerative medicine. *React. Funct. Polym.* **67**, 1284–1291 (2007).

74. Pino, C. J., Haselton, F. R. & Chang, M. S. Seeding of corneal wounds by epithelial cell

transfer from\nmicropatterned PDMS contact lenses. *Cell Transplant.* **14**, 565–571 (2005).

75. Lin, C. H., Yeh, Y. H., Lin, W. C. & Yang, M. C. Novel silicone hydrogel based on PDMS and PEGMA for contact lens application. *Colloids Surfaces B Biointerfaces* **123**, 986–994 (2014).

76. Crawford, G. J., Constable, I. J., Chirila, T. V, Vijayasekaran, S. & Thompson, D. E. Tissue interaction with hydrogel sponges implanted in the rabbit cornea. *Cornea* **12**, 348–357 (1993).

77. Du, L. Q., Wu, X. Y., Li, M. C., Wang, S. G. & Pang, K. P. Effect of different biomedical membranes on alkali-burned cornea. *Ophthalmic Res.* **40**, 282–290 (2008).

78. Cao, Y. *et al.* Poly(N-isopropylacrylamide)-chitosan as thermosensitive in situ gel-forming system for ocular drug delivery. *J. Control. Release* **120**, 186–194 (2007).

79. Deshpande, P. *et al.* Development of a surface modified contact lens for transfer of cultured limbal epithelial cells for ocular surface diseases. *Tissue Eng. Part A* **15**, (2009).

80. Pallavi Deshpande , Rob McKean , Keith A Blackwood , Richard A Senior , Adekemi Ogunbanjo, A. J. R. & S. M. Using poly(lactide-co-glycolide) electrospun scaffolds to deliver cultured epithelial cells to the cornea. *Regen. Med.* **5**, 395–401 (2010).

81. Choi, J. A. & Chung, S.-H. Combined application of autologous serum eye drops and silicone hydrogel lenses for the treatment of persistent epithelial defects. *Eye Contact Lens* **37**, 370–373 (2011).

82. Ma, A. *et al.* Corneal epithelialisation on surface-modified hydrogel implants: Artificial cornea. *J. Mater. Sci. Mater. Med.* **22**, 663–670 (2011).

83. Ortega, Í., Ryan, A. J., Deshpande, P., MacNeil, S. & Claeyssens, F. Combined microfabrication and electrospinning to produce 3-D architectures for corneal repair. *Acta Biomater.* **9**, 5511–5520 (2013).

84. Wright, B. *et al.* Enhanced viability of corneal epithelial cells for efficient transport/storage using a structurally modified calcium alginate hydrogel. *Regen. Med.* **7**, 295–307 (2012).

85. Deshpande, P. *et al.* Simplifying corneal surface regeneration using a biodegradable synthetic membrane and limbal tissue explants. *Biomaterials* **34**, 5088–5106 (2013).

86. Hassan, E., Deshpande, P., Claeyssens, F., Rimmer, S. & Macneil, S. Amine functional hydrogels as selective substrates for corneal epithelialization. *Acta Biomater.* **10**, 3029–3037 (2014).

87. Salehi, S. *et al.* Generation of PGS/PCL blend nanofibrous scaffolds mimicking corneal stroma structure. *Macromol. Mater. Eng.* **299**, 455–469 (2014).

88. Isidan, A. *et al.* Decellularization methods for developing porcine corneal xenografts and

future perspectives. *Xenotransplantation* **26**, 1–8 (2019).

89. Matthyssen, S., Van den Bogerd, B., Dhubhghaill, S. N., Koppen, C. & Zakaria, N. Corneal regeneration: A review of stromal replacements. *Acta Biomater.* **69**, 31–41 (2018).

90. Zhang, B. *et al.* 3D bioprinting for artificial cornea: Challenges and perspectives. *Med. Eng. Phys.* **71**, 68–78 (2019).

91. Wicklein, V. J., Singer, B. B., Scheibel, T. & Salehi, S. *Nanoengineered biomaterials for corneal regeneration*. *Nanoengineered Biomaterials for Regenerative Medicine* (Elsevier Inc., 2018). doi:10.1016/B978-0-12-813355-2.00017-X

92. Yang, C. Y. *et al.* Neural tissue engineering: The influence of scaffold surface topography and extracellular matrix microenvironment. *J. Mater. Chem. B* **9**, 567–584 (2021).

93. Jung, Y. L. & Donahue, H. J. Cell sensing and response to micro- and nanostructured surfaces produced by chemical and topographic patterning. *Tissue Eng.* **13**, 1879–1891 (2007).

94. Raghunathan, V. *et al.* Influence of extracellular matrix proteins and substratum topography on corneal epithelial cell alignment and migration. *Tissue Eng. - Part A* **19**, 1713–1722 (2013).

95. O'Donnell, C. & Wolffsohn, J. S. Grading of corneal transparency. *Contact Lens Anterior Eye* **27**, 161–170 (2004).

96. Abdalla Eltom , Gaoyan Zhong, and A. M. Scaffold Techniques and Designs in Tissue EngineeringFunctions and Purposes A Review. *Adv. Mater. Sci. Eng.* (2019).

97. Rafat, M. *et al.* PEG-stabilized carbodiimide crosslinked collagen-chitosan hydrogels for corneal tissue engineering. *Biomaterials* **29**, 3960–3972 (2008).

98. Levis, H. J. *et al.* Plastic Compressed Collagen as a Novel Carrier for Expanded Human Corneal Endothelial Cells for Transplantation. *PLoS One* **7**, (2012).

99. Vepari, C. & Kaplan, D. L. Silk as a biomaterial. *Prog. Polym. Sci.* **32**, 991–1007 (2007).

100. De La Cruz Cardona, J. *et al.* Transparency in a fibrin and fibrin-agarose corneal stroma substitute generated by tissue engineering. *Cornea* **30**, 1428–1435 (2011).

101. Ionescu, A. M. *et al.* UV absorbance of a bioengineered corneal stroma substitute in the 240-400 nm range. *Cornea* **29**, 895–898 (2010).

102. Yang, G. *et al.* Assessment of the characteristics and biocompatibility of gelatin sponge scaffolds prepared by various crosslinking methods. *Sci. Rep.* **8**, 1–13 (2018).

103. Palchesko, R. N., Carrasquilla, S. D. & Feinberg, A. W. Natural Biomaterials for Corneal Tissue Engineering, Repair, and Regeneration. *Adv. Healthc. Mater.* **7**, 1–18 (2018).

104. Ma, Z., Mao, Z. & Gao, C. Surface modification and property analysis of biomedical

polymers used for tissue engineering. *Colloids Surfaces B Biointerfaces* **60**, 137–157 (2007).

105. Katti, D., Vasita, R. & Shanmugam, K. Improved Biomaterials for Tissue Engineering Applications: Surface Modification of Polymers. *Curr. Top. Med. Chem.* **8**, 341–353 (2008).

106. Patrice Tankam, PhD, Jungeun Won, BS, Cristina Canavesi, PhD, MBA, Ian Cox, PhD, A. & Jannick P. Rolland, P. Optical Assessment of Soft Contact Lens Edge-Thickness. *Optom Vis Sci.* **93**, 987–996 (2016).

107. Wang, Y., Ameer, G. A., Sheppard, B. J. & Langer, R. A tough biodegradable elastomer. *Nat. Biotechnol.* **20**, 602–606 (2002).

108. Rai, R., Tallawi, M., Grigore, A. & Boccaccini, A. R. Synthesis, properties and biomedical applications of poly(glycerol sebacate) (PGS): A review. *Prog. Polym. Sci.* **37**, 1051–1078 (2012).

109. Jia, Y. *et al.* Synthesis and characterization of poly(glycerol sebacate)-based elastomeric copolyesters for tissue engineering applications. *Polym. Chem.* **7**, 2553–2564 (2016).

110. Li, Y., Cook, W. D., Moorhoff, C., Huang, W. C. & Chen, Q. Z. Synthesis, characterization and properties of biocompatible poly(glycerol sebacate) pre-polymer and gel. *Polym. Int.* **62**, 534–547 (2013).

111. Loh, X. J., Abdul Karim, A. & Owh, C. Poly(glycerol sebacate) biomaterial: synthesis and biomedical applications. *J. Mater. Chem. B* **3**, 7641–7652 (2015).

112. Quanyong Liu, Ming Tian, Tao Ding, Rui Shi, Yuxing Feng, Liqun Zhang, Dafu Chen, W. T. Preparation and Characterization of a Thermoplastic Poly(Glycerol Sebacate) Elastomer by Two-Step Method. *Appl. Polym. Sci.* **10**, 1412–1419 (2007).

113. Irina Pomerantseva, Nicholas Krebs, Alison Hart, Craig M. Neville, Albert Y. Huang, C. A. S. Degradation behavior of poly(glycerol sebacate). *J. Biomed. Mater. Res. - Part A* **91**, 1038–1047 (2008).

114. Bodakhe, S. *et al.* Injectable photocrosslinkable nanocomposite based on poly(glycerol sebacate) fumarate and hydroxyapatite: development, biocompatibility and bone regeneration in a rat calvarial bone defect model. *Nanomedicine (Lond).* **8**, 1777–95 (2013).

115. Ifkovits, J. L., Padera, R. F. & Burdick, J. A. Biodegradable and radically polymerized elastomers with enhanced processing capabilities. *Biomed. Mater.* **3**, (2008).

116. Pashneh-Tala, S. *et al.* Synthesis, Characterization and 3D Micro-Structuring via 2-Photon Polymerization of Poly(glycerol sebacate)-Methacrylate–An Elastomeric Degradable Polymer. *Front. Phys.* **6**, 41 (2018).

117. Singh, D. *et al.* Additive manufactured biodegradable poly(glycerol sebacate methacrylate) nerve guidance conduits. *Acta Biomater.* **78**, 48–63 (2018).

118. Motlagh, D., Yang, J., Lui, K. Y., Webb, A. R. & Ameer, G. A. Hemocompatibility evaluation of poly(glycerol-sebacate) in vitro for vascular tissue engineering. *Biomaterials* **27**, 4315–4324 (2006).

119. Gao, J., Crapo, P. M. & Wang, Y. Macroporous elastomeric scaffolds with extensive micropores for soft tissue engineering. *Tissue Eng.* **12**, 917–925 (2006).

120. Chen, Q. Z. *et al.* Characterisation of a soft elastomer poly(glycerol sebacate) designed to match the mechanical properties of myocardial tissue. *Biomaterials* **29**, 47–57 (2008).

121. Kemppainen, J. M. & Hollister, S. J. Tailoring the mechanical properties of 3D-designed poly(glycerol sebacate) scaffolds for cartilage applications. *J. Biomed. Mater. Res. - Part A* **94**, 9–18 (2010).

122. Mitsak, A. G., Dunn, A. M. & Hollister, S. J. Mechanical characterization and non-linear elastic modeling of poly(glycerol sebacate) for soft tissue engineering. *J. Mech. Behav. Biomed. Mater.* **11**, 3–15 (2012).

123. Masoumi, N., Jean, A., Zugates, J. T., Johnson, K. L. & Engelmayr, G. C. Laser microfabricated poly(glycerol sebacate) scaffolds for heart valve tissue engineering. *J. Biomed. Mater. Res. - Part A* **101 A**, 104–114 (2013).

124. Zhang, X., Jia, C., Qiao, X., Liu, T. & Sun, K. Porous poly(glycerol sebacate) (PGS) elastomer scaffolds for skin tissue engineering. *Polym. Test.* **54**, 118–125 (2016).

125. Aydin, H. M., Salimi, K., Rzayev, Z. M. O. & Pişkin, E. Microwave-assisted rapid synthesis of poly(glycerol-sebacate) elastomers. *Biomater. Sci.* **1**, 503 (2013).

126. Patel, A. *et al.* Highly elastomeric poly(glycerol sebacate)-co-poly(ethylene glycol) amphiphilic block copolymers. *Biomaterials* **34**, 3970–3983 (2013).

127. Mogosanu, D. E., Verplancke, R., Dubruel, P. & Vanfleteren, J. Fabrication of 3-dimensional biodegradable microfluidic environments for tissue engineering applications. *Mater. Des.* **89**, 1315–1324 (2016).

128. Mahdavi, A. *et al.* A biodegradable and biocompatible gecko-inspired tissue adhesive. *Proc. Natl. Acad. Sci. U. S. A.* **105**, 2307–2312 (2008).

129. Li, Y., Thouas, G. A. & Chen, Q.-Z. Biodegradable soft elastomers: synthesis/properties of materials and fabrication of scaffolds. *RSC Adv.* **2**, 8229–8242 (2012).

130. Li, X., Hong, A. T. L., Naskar, N. & Chung, H. J. Criteria for quick and consistent synthesis of poly(glycerol sebacate) for tailored mechanical properties. *Biomacromolecules* **16**, 1525–1533 (2015).

131. Nijst, C. L. E. *et al.* Synthesis and characterization of photocurable elastomers from poly(glycerol-co-sebacate). *Biomacromolecules* **8**, 3067–3073 (2007).

132. Engelmayr, G. C. *et al.* Accordion-like honeycombs for tissue engineering of cardiac anisotropy. *Nat. Mater.* **7**, 1003–1010 (2008).

133. Ifkovits, J. L. *et al.* Biodegradable fibrous scaffolds with tunable properties formed from photo-cross-linkable poly(glycerol sebacate). *ACS Appl. Mater. Interfaces* **1**, 1878–1886 (2009).

134. Barrett, D. G. & Yousaf, M. N. Design and applications of biodegradable polyester tissue scaffolds based on endogenous monomers found in human metabolism. *Molecules* **14**, 4022–4050 (2009).

135. Zhu, H., Yalcin, T. & Li, L. Analysis of the accuracy of determining average molecular weights of narrow polydispersity polymers by matrix-assisted laser desorption ionization time-of-flight mass spectrometry. *J. Am. Soc. Mass Spectrom.* **9**, 275–281 (1998).

136. Montaudo, G., Garozzo, D., Montaudo, M. S., Puglisi, C. & Samperi, F. Molecular and Structural Characterization of Polydisperse Polymers and Copolymers by Combining MALDI-TOF Mass Spectrometry with GPC Fractionation. *Macromolecules* **28**, 7983–7989 (1995).

137. Podzimek, S. The use of GPC coupled with a multiangle laser light scattering photometer for the characterization of polymers. On the determination of molecular weight, size and branching. *J. Appl. Polym. Sci.* **54**, 91–103 (1994).

138. Cai, W. & Liu, L. Shape-memory effect of poly (glycerol-sebacate) elastomer. *Mater. Lett.* **62**, 2175–2177 (2008).

139. Yang, K. *et al.* β-Tricalcium phosphate/poly(glycerol sebacate) scaffolds with robust mechanical property for bone tissue engineering. *Mater. Sci. Eng. C* **56**, 37–47 (2015).

140. LOSfEAEK, T. G. F. and S. Influence of Molecular Weight and Degree of Crosslinking on the Specific Volume and Glass Temperature of Polymers. *J. Polym. Sci.* **XV**, 371–390 (1955).

141. Viéville, J., Tanty, M. & Delsuc, M. A. Polydispersity index of polymers revealed by DOSY NMR. *J. Magn. Reson.* **212**, 169–173 (2011).

142. Technologies., A. Polymer Molecular Weight Distribution and Definitions of MW Averages. (2015). Available at: https://www.agilent.com/cs/library/technicaloverviews/Public/5990-7890EN.pdf .

143. Liang, S. L., Cook, W. D., Thouas, G. A. & Chen, Q. Z. The mechanical characteristics and in vitro biocompatibility of poly(glycerol sebacate)-Bioglass® elastomeric composites. *Biomaterials* **31**, 8516–8529 (2010).

144. Yang, B., Lv, W. & Deng, Y. Drug loaded poly(glycerol sebacate) as a local drug delivery system for the treatment of periodontal disease. *RSC Adv.* **7**, 37426–37435 (2017).

145. Jaafar, I. H., Ammar, M. M., Jedlicka, S. S., Pearson, R. A. & Coulter, J. P. Spectroscopic evaluation, thermal, and thermomechanical characterization of poly(glycerol-sebacate) with variations in curing temperatures and durations. *J. Mater. Sci.* **45**, 2525–2529 (2010).

146. Yabalak, E., Görmez, Ö., Gözmen, B. & Gizir, A. M. The solubility of sebacic acid in subcritical water using the response surface methodology. *Int. J. Ind. Chem.* **6**, 23–29

(2015).

147. Chatjigakis, A. K. *et al.* FT-IR spectroscopic determination of the degree of esterification of cell wall pectins from stored peaches and correlation to textural changes. *Carbohydr. Polym.* **37**, 395–408 (1998).

148. Manrique, G. D. & Lajolo, F. M. FT-IR spectroscopy as a tool for measuring degree of methyl esterification in pectins isolated from ripening papaya fruit. *Postharvest Biol. Technol.* **25**, 99–107 (2002).

149. Ha, N. T. N. *et al.* Ester formation at the liquid-solid interface. *Beilstein J. Nanotechnol.* **8**, 2139–2150 (2017).

150. Silverstein, R. W. & Bassler, G. C. Spectrometric identification of organic compounds. *J. Chem. Educ.* **39**, 546–553 (1962).

151. Carletti E., Motta A., M. C. Scaffolds for Tissue Engineering and 3D Cell Culture. in *3D Cell Culture* 17–39 (Humana Press, 2011). doi:https://doi.org/10.1007/978-1-60761-984-0_2

152. Kopp, A. *et al.* Influence of design and postprocessing parameters on the degradation behavior and mechanical properties of additively manufactured magnesium scaffolds. *Acta Biomater.* **98**, 23–35 (2019).

153. Zhang, H., Zhou, L. & Zhang, W. Control of scaffold degradation in tissue engineering: A review. *Tissue Eng. - Part B Rev.* **20**, 492–502 (2014).

154. Masterton, S. & Ahearne, M. Mechanobiology of the corneal epithelium. *Exp. Eye Res.* **177**, 122–129 (2018).

155. Shah, A., Brugnano, J., Sun, S., Vase, A. & Orwin, E. The development of a tissue-engineered cornea: Biomaterials and culture methods. *Pediatr. Res.* **63**, 535–544 (2008).

156. Blackburn, B. J., Jenkins, M. W., Rollins, A. M. & Dupps, W. J. A review of structural and biomechanical changes in the cornea in aging, disease, and photochemical crosslinking. *Front. Bioeng. Biotechnol.* **7**, (2019).

157. Garcia-Porta, N. *et al.* Corneal Biomechanical Properties in Different Ocular Conditions and New Measurement Techniques. *ISRN Ophthalmol.* **2014**, 1–19 (2014).

158. Li, H., Choi, Y. S., Rutland, M. W. & Atkin, R. Nanotribology of hydrogels with similar stiffness but different polymer and crosslinker concentrations. *J. Colloid Interface Sci.* **563**, 347–353 (2020).

159. Pukánszky, B. Influence of interface interaction on the ultimate tensile properties of polymer composites. *Composites* **21**, 255–262 (1990).

160. Palomba, D., Vazquez, G. E. & Díaz, M. F. Prediction of elongation at break for linear polymers. *Chemom. Intell. Lab. Syst.* **139**, 121–131 (2014).

161. Atyabi, F. *et al.* Poly (ε-caprolactone) nanofibrous ring surrounding a polyvinyl

alcohol hydrogel for the development of a biocompatible two-part artificial cornea. *Int. J. Nanomedicine* 1509 (2011). doi:10.2147/ijn.s19011

162. Jiang, L. *et al.* Electrospun nanofibrous thermoplastic polyurethane / poly (glycerol sebacate) hybrid scaffolds for vocal fold tissue engineering applications. **94**, 740–749 (2019).

163. Kerativitayanan, P. & Gaharwar, A. K. Elastomeric and mechanically stiff nanocomposites from poly(glycerol sebacate) and bioactive nanosilicates. *Acta Biomater.* **26**, 34–44 (2015).

164. Liang, S., Cook, W. D. & Chen, Q. Physical characterization of poly(glycerol sebacate)/Bioglass ® composites. *Polym. Int.* **61**, 17–22 (2012).

165. Gaharwar, A. K. *et al.* Elastomeric nanocomposite scaffolds made from poly(glycerol sebacate) chemically crosslinked with carbon nanotubes. *Biomater. Sci.* **3**, 46–58 (2015).

166. Lin, D. *et al.* A viscoelastic PEGylated poly(glycerol sebacate)-based bilayer scaffold for cartilage regeneration in full-thickness osteochondral defect. *Biomaterials* **253**, 120095 (2020).

167. Khan, F. & Tanaka, M. Designing smart biomaterials for tissue engineering. *Int. J. Mol. Sci.* **19**, 1–14 (2018).

168. Smith, I. O., Liu, X. H., Smith, L. A. & Ma, P. X. Nanostructured polymer scaffolds for tissue engineering and regenerative medicine. *Wiley Interdiscip. Rev. Nanomedicine Nanobiotechnology* **1**, 226–236 (2009).

169. Liang, S. L. *et al.* In Vitro enzymatic degradation of poly (glycerol sebacate)-based materials. *Biomaterials* **32**, 8486–8496 (2011).

170. Sundback, C. A. *et al.* Biocompatibility analysis of poly(glycerol sebacate) as a nerve guide material. *Biomaterials* **26**, 5454–5464 (2005).

171. Lau, C. C. *et al.* Advanced biocomposites of poly(glycerol sebacate) and β-tricalcium phosphate by in situ microwave synthesis for bioapplication. *Mater. Today Adv.* **5**, 100023 (2020).

172. Quanyong Liu, Ming Tian, Rui Shi, Liqun Zhang, Dafu Chen, W. T. Structure and Properties of Thermoplastic Poly(glycerol sebacate) Elastomers Originating from Prepolymers with Different Molecular Weights. *Appl. Polym. Sci.* **104**, 1131–1137 (2007).

173. Wang, Y., Kim, Y. M., Langer, R. & Truesdell, C. In vivo degradation characteristics of poly (glycerol sebacate). *J. Chem. Phys.* **37**, 2336 (2002).

174. Yoo, E. S. & Im, S. S. Effect of crystalline and amorphous structures on biodegradability of poly(tetramethylene succinate). *J. Environ. Polym. Degrad.* **7**, 19–26 (1999).

175. Gouveia, R. M., Koudouna, E., Jester, J., Figueiredo, F. & Connon, C. J. Template Curvature Influences Cell Alignment to Create Improved Human Corneal Tissue Equivalents. *Adv.*

Biosyst. **1**, 1700135 (2017).

176. A Daxer; K Misof; B Grabner; A Ettl; P FratzlMisof, K., Grabner, B., Ettl, A. & Fratzl, P. Collagen fibrils in the human corneal stroma: structure and aging. *Invest. Ophthalmol. Vis. Sci.* **39**, 644–648 (1998).

177. Foster, J. W., Jones, R. R., Bippes, C. A., Gouveia, R. M. & Connon, C. J. Differential nuclear expression of Yap in basal epithelial cells across the cornea and substrates of differing stiffness. *Exp. Eye Res.* **127**, 37–41 (2014).

178. Chen, B. *et al.* The mechanical properties of amniotic membrane influence its effect as a biomaterial for ocular surface repair. *Soft Matter* **8**, 8379–8387 (2012).

179. Martino, F., Perestrelo, A. R., Vinarský, V., Pagliari, S. & Forte, G. Cellular mechanotransduction: From tension to function. *Front. Physiol.* **9**, 1–21 (2018).

180. Mak, M., Spill, F., Kamm, R. D. & Zaman, M. H. Single-Cell Migration in Complex Microenvironments: Mechanics and Signaling Dynamics. *J. Biomech. Eng.* **138**, 021004 (2016).

181. Ross, T. D. *et al.* Integrins in mechanotransduction. *Curr. Opin. Cell Biol.* **25**, 613–618 (2013).

182. Last, J. A., Thomasy, S. M., Croasdale, C. R., Russell, P. & Murphy, C. J. Compliance profile of the human cornea as measured by atomic force microscopy. *Micron* **43**, 1293–1298 (2012).

183. Wiley, L., SundarRaj, N., Sun, T. T. & Thoft, R. A. Regional heterogeneity in human corneal and limbal epithelia: An immunohistochemical evaluation. *Investig. Ophthalmol. Vis. Sci.* **32**, 594–602 (1991).

184. Hjortdal, J. Regional elastic performance of the human cornea. *J. Biomech.* **29**, 931–942 (1996).

185. Levis, H. J. & Daniels, J. T. Recreating the Human Limbal Epithelial Stem Cell Niche with Bioengineered Limbal Crypts. *Curr. Eye Res.* **41**, 1153–1160 (2016).

186. Kawano, T., Sato, M., Yabu, H. & Shimomura, M. Honeycomb-shaped surface topography induces differentiation of human mesenchymal stem cells (hMSCs): Uniform porous polymer scaffolds prepared by the breath figure technique. *Biomater. Sci.* **2**, 52–56 (2014).

187. Fu, J. *et al.* Mechanical regulation of cell function with geometrically modulated elastomeric substrates. *Nat. Methods* **7**, 733–736 (2010).

188. Dalby, M. J. *et al.* The control of human mesenchymal cell differentiation using nanoscale symmetry and disorder. *Nat. Mater.* **6**, 997–1003 (2007).

189. Maurice, B. Y. D. M. THE STRUCTURE AND TRANSPARENCY OF THE CORNEA. *J. Physiol.* 263–286 (1957).

190. Benedek, G. B. Theory of Transparency of the Eye. *Appl. Opt.* **10**, 15 (1971).

191. Mccally, R. L., Johns, T. & Spring, S. WAVE-LENGTH DEPENDENCIES OF LIGHT SCATTERING IN NORMAL AND COLD SWOLLEN RABBIT CORNEAS AND THEIR STRUCTURAL IMPLICATIONS. *J. Physiol.* **233**, 589–612 (1973).

192. Maurice, D. M. Graft transparency is in the eye of the beholder. *Invest. Ophthalmol. Vis. Sci.* (2001).

193. Mccally, R. L. & Farrell, R. A. Effect of transcorneal pressure on small- angle light scattering from rabbit cornea * Polarizing sheet Cornea holder Spectra physics / Ringer bathing [Viewing screen JsL f ’ Tl ; ~ r Flat gloss window Polarization prism in rotating mount Figure 1 A schem. **18**, 444–448 (1977).

194. Kostyuk, O. *et al.* Transparency of the bovine corneal stroma at physiological hydration and its dependence on concentration of the ambient anion. *J. Physiol.* **543**, 633–642 (2002).

195. Meek, K. M. Corneal collagen-its role in maintaining corneal shape and transparency. *Biophys. Rev.* **1**, 83–93 (2009).

196. Venugopal, B., Madathil, B. K. & Anil Kumar, P. R. *Stem cell-based therapeutic approaches toward corneal regeneration*. *Biointegration of Medical Implant Materials* (Elsevier Ltd, 2019). doi:10.1016/B978-0-08-102680-9.00011-1

197. Orash Mahmoud Salehi, A., Nourbakhsh, M. S., Rafienia, M., Baradaran-Rafii, A. & Heidari Keshel, S. Corneal stromal regeneration by hybrid oriented poly (ε-caprolactone)/lyophilized silk fibroin electrospun scaffold. *Int. J. Biol. Macromol.* **161**, 377–388 (2020).

198. Kong, B. & Mi, S. Electrospun scaffolds for corneal tissue engineering: A review. *Materials (Basel).* **9**, (2016).

199. Mahdavi, S. S. *et al.* Stereolithography 3D Bioprinting Method for Fabrication of Human Corneal Stroma Equivalent. *Ann. Biomed. Eng.* **48**, 1955–1970 (2020).

200. Zhi Chen , Xiao Liu , Jingjing You , Yihui Song , Eva Tomaskovic-Crook , Gerard Sutton, Jeremy M. Crook, G. G. W. Biomimetic corneal stroma using electro-compacted collagen. *Acta Biomater. J.* 5–12 (2020). doi:10.1016/j.jinf.2020.04.010

201. Chen, J. *et al.* Electrospun nanofibrous SF/P(LLA-CL) membrane: A potential substratum for endothelial keratoplasty. *Int. J. Nanomedicine* **10**, 3337–3350 (2015).

202. Tonsomboon, K. & Oyen, M. L. Composite electrospun gelatin fiber-alginate gel scaffolds for mechanically robust tissue engineered cornea. *J. Mech. Behav. Biomed. Mater.* **21**, 185–194 (2013).

203. Ma, L., Zhou, C., Lin, B. & Li, W. A porous 3D cell culture micro device for cell migration study. *Biomed. Microdevices* **12**, 753–760 (2010).

204. Jones, J. R. Observing cell response to biomaterials. *Mater. Today* **9**, 34–43 (2006).

205. Silverstein, M. S. PolyHIPEs: Recent advances in emulsion-templated porous polymers. *Prog. Polym. Sci.* **39**, 199–234 (2014).

206. Lissant, K. J. The geometry of high-internal-phase-ratio emulsions. *J. Colloid Interface Sci.* **22**, 462–468 (1966).

207. Lissant, K. J. & Mayhan, K. G. A study of medium and high internal phase ratio water/polymer emulsions. *J. Colloid Interface Sci.* **42**, 201–208 (1973).

208. Peace, B. W., Wu, S. H. & Mayhan, K. G. Structure of High-Internal-Phase-Ratio Emulsions. **47**, 416–423 (1974).

209. Sergienko, A. Y., Tai, H., Narkis, M. & Silverstein, M. S. Polymerized high internal-phase emulsions: Properties and interaction with water. *Journal of Applied Polymer Science* **84**, 2018–2027 (2002).

210. Zhang, T., Sanguramath, R. A., Israel, S. & Silverstein, M. S. Emulsion Templating: Porous Polymers and beyond. *Macromolecules* **52**, 5445–5479 (2019).

211. Montanino, A., Pandolfi, A. & Milano, P. On the recovery of the stress-free configuration of the human cornea.

212. Cortese, B., Gigli, G. & Riehle, M. Mechanical gradient cues for guided cell motility and control of cell behavior on uniform substrates. *Adv. Funct. Mater.* **19**, 2961–2968 (2009).

213. Charest, J. L., García, A. J. & King, W. P. Myoblast alignment and differentiation on cell culture substrates with microscale topography and model chemistries. *Biomaterials* **28**, 2202–2210 (2007).

214. Lawrence, B. D., Pan, Z., Liu, A., Kaplan, D. L. & Rosenblatt, M. I. Human corneal limbal epithelial cell response to varying silk film geometric topography in vitro. *Acta Biomater.* **8**, 3732–3743 (2012).

215. Kang, K. B. *et al.* The Effect of Micro- and Nanoscale Surface Topographies on Silk on Human Corneal Limbal Epithelial Cell Differentiation. *Sci. Rep.* **9**, 1–8 (2019).

216. Wu, J. *et al.* Corneal stromal bioequivalents secreted on patterned silk substrates. *Biomaterials* **35**, 3744–3755 (2014).

217. Flemming, R. G., Murphy, C. J., Abrams, G. A., Goodman, S. L. & Nealey, P. F. Effects of synthetic micro- and nano-structured surfaces on cell behavior. *Biomaterials* **20**, 573–588 (1999).

218. McHugh, K. J., Saint-Geniez, M. & Tao, S. L. Topographical control of ocular cell types for tissue engineering. *J. Biomed. Mater. Res. - Part B Appl. Biomater.* **101**, 1571–1584 (2013).

219. Freiburg, H. Concise Reviews: The Role of Biomechanics in the Limbal Stem Cell Niche :

New Insights for Our Understanding of This Structure.

220. Geris, L., Lambrechts, T., Carlier, A. & Papantoniou, I. The future is digital: In silico tissue engineering. *Curr. Opin. Biomed. Eng.* **6**, 92–98 (2018).

221. Kloczko, E., Nikkhah, D. & Yildirimer, L. Scaffolds for hand tissue engineering: The importance of surface topography. *J. Hand Surg. Eur. Vol.* **40**, 973–985 (2015).

222. Gallants, N. D., Charest, J. L., King, W. P. & Garcí, A. J. Micro- and nano-patterned substrates to manipulate cell adhesion. *J. Nanosci. Nanotechnol.* **7**, 803–807 (2007).

223. Teixeira, A. I., Abrams, G. A., Bertics, P. J., Murphy, C. J. & Nealey, P. F. Epithelial contact guidance on well-defined micro- and nanostructured substrates. *J. Cell Sci.* **116**, 1881–1892 (2003).

224. Koroleva, A. *et al.* Two-photon polymerization-generated and micromolding-replicated 3D scaffolds for peripheral neural tissue engineering applications. *Biofabrication* **4**, (2012).

225. Silverstein, M. S. & Cameron, N. R. PolyHIPEs - Porous Polymers from High Internal Phase Emulsions. *Encycl. Polym. Sci. Technol.* (2010). doi:10.1002/0471440264.pst571

226. Kulygin, O. & Silverstein, M. S. Porous poly(2-hydroxyethyl methacrylate) hydrogels synthesized within high internal phase emulsions. *Soft Matter* **3**, 1525–1529 (2007).

227. Mert, E. H. & Kekevi, B. Synthesis of polyHIPEs through high internal phase emulsions of β-myrcene. *Colloid and Polymer Science* **298**, 1423–1432 (2020).

228. What Does Resolution Mean in 3D Printing? Pt. 2. Available at: https://formlabs.com/uk/blog/horizontal-resolution-meaning-3d-printing/. (Accessed: 18th June 2020)

229. Formlabs. What Does Resolution Mean in 3D Printing? Pt. 3. Available at: https://formlabs.com/uk/blog/layer-height-meaning-3d-printing/#:~:text=Currently%2C the Form 2 SLA,as high as 25 microns. (Accessed: 18th July 2020)

230. Kim, J. I., Kim, J. Y. & Park, C. H. Fabrication of transparent hemispherical 3D nanofibrous scaffolds with radially aligned patterns via a novel electrospinning method. *Sci. Rep.* **8**, 1–13 (2018).

231. Nam, E., Lee, W. C. & Takeuchi, S. Formation of Highly Aligned Collagen Nanofibers by Continuous Cyclic Stretch of a Collagen Hydrogel Sheet. *Macromol. Biosci.* 995–1000 (2016). doi:10.1002/mabi.201600068

232. Wu, J., Du, Y., Mann, M. M., Funderburgh, J. L. & Wagner, W. R. Corneal stromal stem cells versus corneal fibroblasts in generating structurally appropriate corneal stromal tissue. *Exp. Eye Res.* **120**, 71–81 (2014).

233. Wu, J. *et al.* Bioengineering organized, multilamellar human corneal stromal tissue by growth factor supplementation on highly aligned synthetic substrates. *Tissue Eng. - Part A*

19, 2063–2075 (2013).

234. Wu, J., Du, Y., Watkins, S. C., Funderburgh, J. L. & Wagner, W. R. The engineering of organized human corneal tissue through the spatial guidance of corneal stromal stem cells. *Biomaterials* **33**, 1343–1352 (2012).

235. Salem, A. K. *et al.* Interactions of 3T3 fibroblasts and endothelial cells with defined pore features. *J. Biomed. Mater. Res.* **61**, 212–217 (2002).

236. Romano, A. C. *et al.* Different Cell Sizes in Human Limbal and Central Corneal Basal Epithelia Measured by Confocal Microscopy and Flow Cytometry. *Investig. Ophthalmol. Vis. Sci.* **44**, 5125–5129 (2003).

237. Oxford English Dictionary - Transparency. Available at: https://www.oed.com/view/Entry/204969?redirectedFrom=transparent#eid. (Accessed: 20th August 2021)

238. McLaughlin, C. R. *et al.* Regeneration of functional nerves within full thickness collagen-phosphorylcholine corneal substitute implants in guinea pigs. *Biomaterials* **31**, 2770–2778 (2010).

239. Fagerholm, P., Lagali, N. S., Carlsson, D. J., Merrett, K. & Griffith, M. Corneal regeneration following implantation of a biomimetic tissue-engineered substitute. *Clin. Transl. Sci.* **2**, 162–164 (2009).

240. Ellison Bentley, DVM*, Christopher J. Murphy, DVM, PhD*, Fengfu Li, PhD†, David J. Carlsson, PhD†, and May Griffith, P. Biosynthetic Corneal Substitute Implantation in Dogs. *Cornea.* **29**, 1–14 (2010).

241. Acun, a & Hasirci, V. Construction of a collagen-based, split-thickness cornea substitute. *J. Biomater. Sci. Polym. Ed.* **25**, 1110–32 (2014).

242. Le, X., Poinern, G. E. J., Ali, N., Berry, C. M. & Fawcett, D. Engineering a biocompatible scaffold with either micrometre or nanometre scale surface topography for promoting protein adsorption and cellular response. *Int. J. Biomater.* **2013**, (2013).

243. Massumi, M. *et al.* The effect of topography on differentiation fates of matrigel-coated mouse embryonic stem cells cultured on PLGA nanofibrous scaffolds. *Tissue Eng. - Part A* **18**, 609–620 (2012).

244. Creff, J. *et al.* Fabrication of 3D scaffolds reproducing intestinal epithelium topography by high-resolution 3D stereolithography. *Biomaterials* **221**, (2019).

245. Duarte Campos, D. F. *et al.* Corneal bioprinting utilizing collagen-based bioinks and primary human keratocytes. *J. Biomed. Mater. Res. - Part A* **107**, 1945–1953 (2019).

246. Mansouri, N. & Bagheri, S. The influence of topography on tissue engineering perspective. *Mater. Sci. Eng. C* **61**, 906–921 (2016).

247. Tram, N. K. *et al.* Accommodative tissues influence the shape of the cornea and

potentially drive corneal morphogenesis. *J. Biomech.* **100**, 109582 (2020).

248. Elsheikh, A., Alhasso, D. & Rama, P. Biomechanical properties of human and porcine corneas. *Exp. Eye Res.* **86**, 783–790 (2008).

249. Yang, J., Zeng, Y. J., Huang, K. & Li, Z. H. A comparison of biomechanical properties between human and porcine cornea. *Zhongguo Shengwu Yixue Gongcheng Xuebao/Chinese J. Biomed. Eng.* **20**, 166 (2001).

250. Sitalakshmi, G. *et al.* Ex vivo cultivation of corneal limbal epithelial cells in a thermoreversible polymer (Mebiol Gel) and their transplantation in rabbits: An animal model. *Tissue Eng. - Part A* **15**, 407–415 (2009).

251. Stepp, M. A. *et al.* Wounding the cornea to learn how it heals. *Exp. Eye Res.* **121**, 178–193 (2014).

252. Gwon, A. The Rabbit in Cataract/IOL Surgery. in *Animal Models in Eye Research* (ed. Tsonis, P. A.) 184–187 (2008). doi:10.1017/CBO9781107415324.004

253. G Bozkir, M Bozkir, H Dogan, K Aycan, B. G. Measurements of axial lenght and radius of corneal curvature in the rabbit eye. *Acta Med Okayama* **511**, 9–11 (1997).

254. Hu, J. *et al.* Electrospinning of poly(glycerol sebacate)-based nanofibers for nerve tissue engineering. *Mater. Sci. Eng. C* **70**, 1089–1094 (2017).

255. Luginina, M. *et al.* Electrospun PCL/PGS composite fibers incorporating bioactive glass particles for soft tissue engineering applications. *Nanomaterials* **10**, (2020).

256. Rai, R. *et al.* Bioactive Electrospun Fibers of Poly(glycerol sebacate) and Poly(ε-caprolactone) for Cardiac Patch Application. *Adv. Healthc. Mater.* **4**, 2012–2025 (2015).

257. Salehi, S. *et al.* Poly (glycerol sebacate)-poly (ε-caprolactone) blend nanofibrous scaffold as intrinsic bio- and immunocompatible system for corneal repair. *Acta Biomaterialia* **50**, 370–380 (2017).

258. Zaky, S. H. *et al.* Poly (glycerol sebacate) elastomer supports bone regeneration by its mechanical properties being closer to osteoid tissue rather than to mature bone. *Acta Biomater.* **54**, 95–106 (2017).

259. Redenti, S. *et al.* Engineering retinal progenitor cell and scrollable poly(glycerol-sebacate) composites for expansion and subretinal transplantation. *Biomaterials* **30**, 3405–3414 (2009).

260. Salehi, S., Fathi, M., Javanmard, S., Barneh, F. & Moshayedi, M. Fabrication and characterization of biodegradable polymeric films as a corneal stroma substitute. *Adv. Biomed. Res.* **4**, 9 (2015).

261. Gerecht, S. *et al.* A porous photocurable elastomer for cell encapsulation and culture. *Biomaterials* **28**, 4826–4835 (2007).

262. ATCC. HCE-2 [50.B1] (ATCC® CRL-11135™) Culture method. Available at: https://www.atcc.org/en/Products/All/CRL-11135.aspx#culturemethod. (Accessed: 27th July 2020)

263. ATCC. HCE-2 [50.B1] (ATCC® CRL-11135 ™) cells Flask coating solution. Available at: https://www.atcc.org/Global/FAQs/2/C/Flask coating for HCE-2_SL_50.B1 ATCC CRL-11135 cells.aspx. (Accessed: 27th July 2020)

264. Nordin, N. H. & Ahmad, Z. Monitoring chemical changes on the surface of borosilicate glass covers during the silanisation process. *J. Phys. Sci.* **26**, 11–22 (2015).

265. Guo, W. & Ruckenstein, E. Modified glass fiber membrane and its application to membrane affinity chromatography. *J. Memb. Sci.* **215**, 141–155 (2003).

266. Monticelli, F., Toledano, M., Osorio, R. & Ferrari, M. Effect of temperature on the silane coupling agents when bonding core resin to quartz fiber posts. *Dent. Mater.* **22**, 1024–1028 (2006).

267. Chaijareenont, P., Takahashi, H., Nishiyama, N. & Arksornnukit, M. Effects of silane coupling agents and solutions of different polarity on PMMA bonding to alumina. *Dent. Mater. J.* **31**, 610–616 (2012).

268. Zhang, H. X., Du, G. H. & Zhang, J. T. Assay of mitochondrial functions by resazurin in vitro. *Acta Pharmacol. Sin.* **25**, 385–389 (2004).

269. Perrot, S., Duterte-Catella, H., Martin, C., Rat, P. & Warnet, J. M. Resazurin metabolism assay is a new sensitive alternative test in isolated pig cornea. *Toxicol. Sci.* **72**, 122–129 (2003).

270. Riss TL, Moravec RA, Niles AL, et al. *Cell viability assays*. *Assay Guidance Manual* (2013).

271. Ahn, S. J., Costa, J. & Emanuel, J. R. PicoGreen quantitation of DNA: Effective evaluation of samples pre- or post-PCR. *Nucleic Acids Res.* **24**, 2623–2625 (1996).

272. Thermo Fisher Scientific, U. Quant-iT™ PicoGreen ® dsDNA Reagent and Kits. Available at: https://www.thermofisher.com/document-connect/document-connect.html?url=https%3A%2F%2Fassets.thermofisher.com%2FTFS-Assets%2FLSG%2Fmanuals%2Fmp07581.pdf&title=UXVhbnQtaVQgUGljb0dyZWVuIGRzRE5BIFJlYWdlbnQgYW5kIEtpdHM=. (Accessed: 28th July 2020)

273. Scientific, T. Thermo Scientific™ Pierce™ LDH Cytotoxicity Assay Kit. Available at: https://www.fishersci.co.uk/shop/products/pierce-ldh-cytotoxicity-assay-kit/p-4589213. (Accessed: 24th August 2020)

274. Dinescu, S. *et al.* In vitro cytocompatibility evaluation of chitosan/graphene oxide 3D scaffold composites designed for bone tissue engineering. *Biomed. Mater. Eng.* **24**, 2249–2256 (2014).

275. Norrman, K., Ghanbari-Siahkali, A. & Larsen, N. B. Studies of spin-coated polymer films. *Annu. Reports Prog. Chem. - Sect. C* **101**, 174–201 (2005).

276. Simonsen, A. C. & Bagatolli, L. A. Structure of spin-coated lipid films and domain formation in supported membranes formed by hydration. *Langmuir* **20**, 9720–9728 (2004).

277. Lawrence, C. J. The mechanics of spin coating of polymer films. *Phys. Fluids* **31**, 2786–2795 (1988).

278. Tamada, Y. & Ikada, Y. Fibroblast growth on polymer surfaces and biosynthesis of collagen. *J. Biomed. Mater. Res.* **28**, 783–789 (1994).

279. Welch, W. I. & Suhan, J. P. Morphological study of the mammalian stress response: Characterization of changes in cytoplasmic organelles, cytoskeleton, and nucleoli, and appearance of intranuclear actin filaments in rat fibroblasts after heat-shock treatment. *J. Cell Biol.* **101**, 1198–1211 (1985).

280. Jones, R. R., Hamley, I. W. & Connon, C. J. Ex vivo expansion of limbal stem cells is affected by substrate properties. *Stem Cell Res.* **8**, 403–409 (2012).

281. Yeung, T. *et al.* Effects of substrate stiffness on cell morphology, cytoskeletal structure, and adhesion. *Cell Motil. Cytoskeleton* **60**, 24–34 (2005).

282. Palamà, I. E. *et al.* Cell mechanotactic and cytotoxic response to zinc oxide nanorods depends on substrate stiffness. *Toxicol. Res. (Camb).* **5**, 1699–1710 (2016).

283. Dickens, C. & Dickens, C. Nanomaterials for regenerative medicine: Chapter 22 MECHANICAL GUIDANCE OF CELL MIGRATION. in *Nanomedicine* **6**, 565–578 (2010).

284. Schmidt, R. J., Chung, L. Y., Andrews, A. M. & Turner, T. D. Toxicity of L-ascorbic acid to L929 fibroblast cultures: Relevance to biocompatibility testing of materials for use in wound management. *J. Biomed. Mater. Res.* **27**, 521–530 (1993).

285. Wiegand, C. & Hipler, U. C. Evaluation of biocompatibility and cytotoxicity using keratinocyte and fibroblast cultures. *Skin Pharmacol. Physiol.* **22**, 74–82 (2009).

286. Pizzoferrato, A. *et al.* Cell culture methods for testing Biocompatibility. *Clin. Mater.* **15**, 173–190 (1994).

287. Takayoshi Tokiwa, Miki Miyagiwa, Yusanori Kusaka, A. M. and J. S. EFFECTS OF VARIOUS SUBSTRATES ON HUMAN HEPATOBLASTOMA AND HEPATOMA CELL CULTURE. *Cell Biol. Int. Rep.* **12**, 131–142 (1988).

288. Vrana, N. E. *et al.* EDC / NHS cross-linked collagen foams as scaffolds for artificial corneal stroma EDC / NHS cross-linked collagen foams as scaffolds for artificial corneal stroma. *J. Biomater. Sci. Polym. Ed.* **18**, 1527–1545 (2012).

289. Villalona, G. A. *et al.* Cell-seeding techniques in vascular tissue engineering. *Tissue Eng. - Part B Rev.* **16**, 341–350 (2010).

290. Ma, Z., Gao, C., Ji, J. & Shen, J. Protein immobilization on the surface of poly-L-lactic acid films for improvement of cellular interactions. *Eur. Polym. J.* **38**, 2279–2284 (2002).

291. Uygun, B. E., Bou-Akl, T., Albanna, M. & Matthew, H. W. T. Membrane thickness is an important variable in membrane scaffolds: Influence of chitosan membrane structure on the behavior of cells. *Acta Biomater.* **6**, 2126–2131 (2010).

292. Haifei, S. *et al.* The effect of collagen-chitosan porous scaffold thickness on dermal regeneration in a one-stage grafting procedure. *J. Mech. Behav. Biomed. Mater.* **29**, 114–125 (2014).

293. Ferlin, K. M., Prendergast, M. E., Miller, M. L., Kaplan, D. S. & Fisher, J. P. Influence of 3D printed porous architecture on mesenchymal stem cell enrichment and differentiation. *Acta Biomater.* **32**, 161–169 (2016).

294. Dewez, J. L., Doren, A., Schneider, Y. J. & Rouxhet, P. G. Competitive adsorption of proteins: Key of the relationship between substratum surface properties and adhesion of epithelial cells. *Biomaterials* **20**, 547–559 (1999).

295. Michl, J., Park, K. C. & Swietach, P. Evidence-based guidelines for controlling pH in mammalian live-cell culture systems. *Commun. Biol.* **2**, 1–12 (2019).

296. Wang, M. O. *et al.* Evaluation of the in vitro cytotoxicity of cross-linked biomaterials. *Biomacromolecules* **14**, 1321–1329 (2013).

297. Safrany, A. Radiation processing: Synthesis and modification of biomaterials for medical use. *Nucl. Instruments Methods Phys. Res. Sect. B Beam Interact. with Mater. Atoms* **131**, 376–381 (1997).

298. Neuss, S. *et al.* Assessment of stem cell/biomaterial combinations for stem cell-based tissue engineering. *Biomaterials* **29**, 302–313 (2008).

299. Granja, P. L. *et al.* Cellulose phosphates as biomaterials. In vitro biocompatibility studies. *React. Funct. Polym.* **66**, 728–739 (2006).

300. Atta, A. M. & El-Ghazawy, R. A. M. Effect of chemical crosslinking on swelling parameters of modified poly(vinyl alcohol) hydrogel. *Int. J. Polym. Mater. Polym. Biomater.* **52**, 623–636 (2003).

301. Lopérgolo, L. C., Lugão, A. B. & Catalani, L. H. Direct UV photocrosslinking of poly(N-vinyl-2-pyrrolidone) (PVP) to produce hydrogels. *Polymer (Guildf).* **44**, 6217–6222 (2003).

302. Prina, E. *et al.* 3D Microfabricated Scaffolds and Microfluidic Devices for Ocular Surface Replacement: a Review. *Stem Cell Rev. Reports* **13**, 430–441 (2017).

303. Martínez, E., Engel, E., Planell, J. A. & Samitier, J. Effects of artificial micro- and nano-structured surfaces on cell behaviour. *Ann. Anat.* **191**, 126–135 (2009).

304. Yim, E. K. F. & Leong, K. W. Significance of synthetic nanostructures in dictating cellular response. *Nanomedicine Nanotechnology, Biol. Med.* **1**, 10–21 (2005).

305. Teixeira, A. I. *et al.* The effect of environmental factors on the response of human corneal epithelial cells to nanoscale substrate topography. *Biomaterials* **27**, 3945–3954 (2006).

306. Tocce, E. J. *et al.* The ability of corneal epithelial cells to recognize high aspect ratio nanostructures. *Biomaterials* **31**, 4064–4072 (2010).

307. Kristin J. Pawlowski , Stanley E. Rittgers , Steven P. Schmidt, and G. L. B. ENDOTHELIAL CELL SEEDING OF POLYMERIC VASCULAR GRAFTS. *Front. Biosci.* **9**, 1412–1421 (2004).

308. Roh, J. D. *et al.* Construction of an autologous tissue-engineered venous conduit from bone marrow-derived vascular cells: optimization of cell harvest and seeding techniques. *J. Pediatr. Surg.* **42**, 198–202 (2007).

309. Wright, B., De Bank, P. A., Luetchford, K. A., Acosta, F. R. & Connon, C. J. Oxidized alginate hydrogels as niche environments for corneal epithelial cells. *J. Biomed. Mater. Res. - Part A* **102**, 3393–3400 (2014).

310. Hong, H. *et al.* Compressed collagen intermixed with cornea-derived decellularized extracellular matrix providing mechanical and biochemical niches for corneal stroma analogue. *Mater. Sci. Eng. C* **103**, 109837 (2019).

311. Mi, S., Chen, B., Wright, B. & Connon, C. J. Ex vivo construction of an artificial ocular surface by combination of corneal limbal epithelial cells and a compressed collagen scaffold containing keratocytes. *Tissue Eng. - Part A* **16**, 2091–2100 (2010).

312. Gouveia, R. M. & Connon, C. J. *Collagen scaffolds for corneal regeneration*. *Biomaterials and Regenerative Medicine in Ophthalmology: Second Edition* (Elsevier Ltd, 2016). doi:10.1016/B978-0-08-100147-9.00007-9

313. Wang, H. Y., Wei, R. H. & Zhao, S. Z. Evaluation of corneal cell growth on tissue engineering materials as artificial cornea scaffolds. *Int. J. Ophthalmol.* **6**, 873–878 (2013).

314. Jhala, D. & Vasita, R. A Review on Extracellular Matrix Mimicking Strategies for an Artificial Stem Cell Niche. *Polym. Rev.* **55**, 561–595 (2015).

315. Alamein, M. A. *et al.* Nanospiderwebs: Artificial 3D Extracellular Matrix from Nanofibers by Novel Clinical Grade Electrospinning for Stem Cell Delivery. *Adv. Healthc. Mater.* **2**, 702–717 (2013).

316. Sobral, J. M., Caridade, S. G., Sousa, R. A., Mano, J. F. & Reis, R. L. Three-dimensional plotted scaffolds with controlled pore size gradients: Effect of scaffold geometry on mechanical performance and cell seeding efficiency. *Acta Biomater.* **7**, 1009–1018 (2011).

317. Ma, P. X. Biomimetic materials for tissue engineering. *Adv. Drug Deliv. Rev.* **60**, 184–198 (2008).

318. Mo, X. M., Xu, C. Y., Kotaki, M. & Ramakrishna, S. Electrospun P(LLA-CL) nanofiber: A biomimetic extracellular matrix for smooth muscle cell and endothelial cell proliferation. *Biomaterials* **25**, 1883–1890 (2004).

319. Metze, A. L. *et al.* Gelatin coated 45S5 Bioglass®-derived scaffolds for bone tissue engineering. *Key Eng. Mater.* **541**, 31–39 (2013).

320. Xiaoran Li, Jingwei Xie, Xiaoyan Yuan, and Y. X. Coating Electrospun Poly(ε-caprolactone) Fibers with Gelatin and.pdf.

321. Arafat, M. T. *et al.* Biomimetic composite coating on rapid prototyped scaffolds for bone tissue engineering. *Acta Biomater.* **7**, 809–820 (2011).

322. Goddard, J. M. & Hotchkiss, J. H. Polymer surface modification for the attachment of bioactive compounds. *Prog. Polym. Sci.* **32**, 698–725 (2007).

323. Ashwin, B. *et al.* 3D-poly (lactic acid) scaffolds coated with gelatin and mucic acid for bone tissue engineering. *Int. J. Biol. Macromol.* **162**, 523–532 (2020).

324. Ozcan, C., Zorlutuna, P., Hasirci, V. & Hasirci, N. Influence of oxygen plasma modification on surface free energy of PMMA films and cell attachment. *Macromol. Symp.* **269**, 128–137 (2008).

325. Hsiue, G. H., Lee, S. D., Wang, C. C. & Tsuei Chang, P. C. The effect of plasma-induced graft copolymerization of phema on silicone rubber towards improving corneal epithelial cells growth. *J. Biomater. Sci. Polym. Ed.* **5**, 205–220 (1994).

326. Deplaine, H. *et al.* Biomimetic hydroxyapatite coating on pore walls improves osteointegration of poly(L-lactic acid) scaffolds. *J. Biomed. Mater. Res. - Part B Appl. Biomater.* **101 B**, 173–186 (2013).

327. Intranuovo, F. *et al.* Plasma modification of PCL porous scaffolds fabricated by solvent-casting/particulate-leaching for tissue engineering. *Plasma Process. Polym.* **11**, 184–195 (2014).

328. Terpi, K. & Worzakowska, M. Low-temperature air plasma modi fi cation of chitosan-coated PEEK biomaterials Agnieszka Ewa Wia. **50**, (2016).

329. Yang, J., Bei, J. & Wang, S. Enhanced cell affinity of poly (D,L-lactide) by combining plasma treatment with collagen anchorage. *Biomaterials* **23**, 2607–2614 (2002).

330. Jiao, Y. P. & Cui, F. Z. Surface modification of polyester biomaterials for tissue engineering. *Biomed. Mater.* **2**, (2007).

331. Oehr, C. Plasma surface modification of polymers for biomedical use. *Nucl. Instruments Methods Phys. Res. Sect. B Beam Interact. with Mater. Atoms* **208**, 40–47 (2003).

332. Bettinger, C. J., Orrick, B., Misra, A., Langer, R. & Borenstein, J. T. Microfabrication of poly (glycerol-sebacate) for contact guidance applications. *Biomaterials* **27**, 2558–2565 (2006).

333. Masoumi, N., Johnson, K. L., Howell, M. C. & Engelmayr, G. C. Valvular interstitial cell seeded poly(glycerol sebacate) scaffolds: Toward a biomimetic in vitro model for heart valve tissue engineering. *Acta Biomater.* **9**, 5974–5988 (2013).

334. Poplawski, T. *et al.* Cytotoxicity and genotoxicity of glycidyl methacrylate. *Chem. Biol. Interact.* **180**, 69–78 (2009).

335. Matsumura, S. *et al.* Stability and Utility of Pyridyl Disulfide Functionality in RAFT and Conventional Radical Polymerizations. *J. Polym. Sci. Part A Polym. Chem.* **46**, 7207–7224 (2008).

336. Kedjarune, U., Charoenworaluk, N. & Koontongkaew, S. Release of methyl methacrylate from heat-cured and autopolymerized resins: Cytotoxicity testing related to residual monomer. *Aust. Dent. J.* **44**, 25–30 (1999).

337. Yoshii, E. Cytotoxic effects of acrylates and methacrylates: Relationships of monomer structures and cytotoxicity. *J. Biomed. Mater. Res.* **37**, 517–524 (1997).

338. Maroudas, N. G. Adhesion and spreading of cells on charged surfaces. *J. Theor. Biol.* **49**, 417–424 (1975).

339. Kishida, A., Iwata, H., Tamada, Y. & Ikada, Y. Cell behaviour on polymer surfaces grafted with non-ionic and ionic monomers. *Biomaterials* **12**, 786–792 (1991).

340. Sugimoto, Y. Effect on the adhesion and locomotion of mouse fibroblasts by their interacting with differently charged substrates. A quantitative study by ultrastructural method. *Exp. Cell Res.* **135**, 39–45 (1981).

341. Wachem, P. B. Van, Hogt, a H., Beugeling, T., Bantjes, A. & Aken, W. Van. Adhesion of cultured human endothelial cells onto methacrylate polymers with varying surface wettability and charge. *Biomaterials* **8**, 323–328 (1987).

342. Li, B., Ma, Y., Wang, S. & Moran, P. M. Influence of carboxyl group density on neuron cell attachment and differentiation behavior: Gradient-guided neurite outgrowth. *Biomaterials* **26**, 4956–4963 (2005).

343. Lee, J. H., Jung, H. W., Kang, I. K. & Lee, H. B. Cell behaviour on polymer surfaces with different functional groups. *Biomaterials* **15**, 705–711 (1994).

344. Smetana, K., Vacík, J., Součková, D., Krčová, Z. & Šulc, J. The influence of hydrogel functional groups on cell behavior. *J. Biomed. Mater. Res.* **24**, 463–470 (1990).

345. Isaacson, A., Swioklo, S. & Connon, C. J. 3D bioprinting of a corneal stroma equivalent. *Exp. Eye Res.* **173**, 188–193 (2018).

346. Kutlehria, S. *et al.* High-throughput 3D bioprinting of corneal stromal equivalents. *J. Biomed. Mater. Res. - Part B Appl. Biomater.* **108**, 2981–2994 (2020).

347. Tang, L., Thevenot, P. & Hu, W. Surface Chemistry Influences Implant Biocompatibility. *Curr. Top. Med. Chem.* **8**, 270–280 (2008).

348. Keselowsky, B. G., Collard, D. M. & García, A. J. Surface chemistry modulates focal adhesion composition and signaling through changes in integrin binding. *Biomaterials* **25**, 5947–5954 (2004).

349. Ertel, S. I., Ratner, B. D. & Horbett, T. A. Radiofrequency plasma deposition of oxygen-containing films on polystyrene and poly(ethylene terephthalate) substrates improves

endothelial cell growth. *J. Biomed. Mater. Res.* **24**, 1637–1659 (1990).

350. Lan, M. A., Gersbach, C. A., Michael, K. E., Keselowsky, B. G. & García, A. J. Myoblast proliferation and differentiation on fibronectin-coated self assembled monolayers presenting different surface chemistries. *Biomaterials* **26**, 4523–4531 (2005).

351. Liu, L., Chen, S., Giachelli, C. M., Ratner, B. D. & Jiang, S. Controlling osteopontin orientation on surfaces to modulate endothelial cell adhesion. *J. Biomed. Mater. Res. - Part A* **74**, 23–31 (2005).

352. Keselowsky, B. G., Collard, D. M. & García, A. J. Integrin binding specificity regulates biomaterial surface chemistry effects on cell differentiation. *Proc. Natl. Acad. Sci. U. S. A.* **102**, 5953–5957 (2005).

353. Faucheux, N., Schweiss, R., Lützow, K., Werner, C. & Groth, T. Self-assembled monolayers with different terminating groups as model substrates for cell adhesion studies. *Biomaterials* **25**, 2721–2730 (2004).

354. Li, X. *et al.* Improved biocompatibility of poly (styrene-b-(ethylene-co-butylene)-b-styrene) elastomer by a surface graft polymerization of hyaluronic acid. *Colloids Surfaces B Biointerfaces* **102**, 210–217 (2013).

355. Yu, X. *et al.* Collagen/chitosan/heparin complex with improved biocompatibility for hepatic tissue engineering. *J. Bioact. Compat. Polym.* **20**, 15–28 (2005).

356. Wang, Y., Cui, F. Z., Jiao, Y. P., Hu, K. & Fan, D. D. Modification of bone graft by blending with lecithin to improve hydrophilicity and biocompatibility. *Biomed. Mater.* **3**, (2008).

357. Zhang, M., Li, X. H., Gong, Y. D., Zhao, N. M. & Zhang, X. F. Properties and biocompatibility of chitosan films modified by blending with PEG. *Biomaterials* **23**, 2641–2648 (2002).

358. Flaig, F. *et al.* Design of Functional Electrospun Scaffolds Based on Poly(glycerol sebacate) Elastomer and Poly(lactic acid) for Cardiac Tissue Engineering. *ACS Biomater. Sci. Eng.* **6**, 2388–2400 (2020).

359. Shilpa Sant, Chang Mo Hwang, S.-H. L. and A. K. Hybrid PGS–PCL microfibrous scaffolds with improved mechanical and biological properties. *J. Tissue Eng. Regen. Med.* **5**, 283–291 (201AD).